Buncefield Explosion Mechanism Phase 1

Volumes 1 and 2

Prepared by the **Steel Construction Institute**
for the Health and Safety Executive 2009

Buncefield Explosion Mechanism Phase 1

Volume 1

Steel Construction Institute
Silwood Park
Ascot
Berks SL57QN

The Buncefield explosion (11 December 2005) resulted in tremendous damage to the outlying area and huge fires involving 23 large oil fuel tanks. One important aspect of the incident was the severity of the explosion, which would not have been anticipated in any major hazard assessment of the oil storage depot before the incident. The Buncefield Major Incident Investigation Board (MIIB) invited explosion experts from academia and industry to form an Advisory Group to advise on the work that would be required to explain the severity of the Buncefield explosion. This MIIB Advisory Group carried out a preliminary assessment of the forensic evidence obtained following the incident and of the results of experiments carried out by the Health and Safety Laboratory – HSL. The objectives of this assessment were:

■ to determine whether a sequence of events could be identified that would explain why such severe explosion pressures were generated; and

■ if this was not possible, to recommend to the Board what further actions would be required to explain the explosion severity.

The Advisory Group attempted to explain the explosion event at Buncefield using deflagration, detonation or a combination of both. It also examined other possible means of flame acceleration. However, it was not possible to identify a single scenario that could explain all aspects within the time available.The Advisory Group therefore recommended that a joint industry research project be initiated that would, in its first phase, have the objectives of completing the assessment started by the Advisory Group and, on the basis of this, of defining the requirements for further research. The research undertaken, both experimental and theoretical, and has lead to a better understanding of likely explosion mechanisms and explanation of the observed damage.

HSE Books

ACKNOWLEDGEMENTS

FOREWORD

by

Judith Hackitt, CBE

Chair of the Health and Safety Executive

I am pleased to be able to introduce this report as it marks a significant development in our understanding of the reasons for both the magnitude and the extent of damage caused by the explosion at the Buncefield fuel storage site. This incident was unusual in that it was possible to collect a vast amount of data from the incident site in the form of photographs, CCTV video footage and first hand accounts.

This project, co-ordinated by HSE and supported by industry, follows on from the excellent work undertaken by the Buncefield Major Incident Investigation Board. The complex nature of analysing all the data gathered from site required the input from many different organisations and disciplines; I applaud the way in which industry and government agencies have worked together to achieve the project objectives.

There still remain some scientific and technical issues to be resolved, and I sincerely hope that industry and other interested parties will now embrace the recommendations for further research proposed in this report in order to improve the understanding of the underlying mechanisms and the best ways of designing out and mitigating such incidents.

CONTENTS

EXECUTIVE SUMMARY

This project was undertaken on the recommendation of the Buncefield Major Incident Investigation Board (MIIB) Advisory Group[1]. Its main objectives are to provide an understanding of the explosion mechanism in the Buncefield incident, to provide interim guidance where this proves possible and to define the scope of further work that may be necessary based on the findings of Phase 1.

A vast amount of data in the form of witness statements (using extracts from anonymised witness statements), photographs, CCTV and video footage were studied and catalogued. Careful examination of this data enabled the explosion source terms and characteristics to be inferred.

The area covered by the vapour cloud was estimated to be around $120,000m^2$ and the average height of the cloud was around 2m giving a volume of $240,000m^3$. There is a weight of evidence to suggest that the source of ignition was in the emergency pump house.

Overpressures within the area of the cloud were found to be consistently high. From a combination of damage assessment and comparative testing and analysis it was concluded that the overpressure within the cloud was generally greater than 200kPa; the maximum overpressure was probably much higher. These high levels of overpressure were seen in all areas; there was no distinction between different terrain (car parks, tank farms, open grassland and belts of trees).

Overpressure diminished rapidly with distance away from the edge of the cloud; evidence suggests overpressures in the region of 5-10 kPa within ~150m. Another distinctive feature was the direction of net impulse; within the cloud this acted in the opposite direction to the direction of propagation of the explosion whereas outside the cloud it acted in the direction of propagation of the explosion.

The two most commonly known explosion mechanisms, deflagration and detonation, were assessed for their consistency with the observed explosion characteristics. Deflagration was found to be inconsistent with the near-field significant damage to objects and cars. It was also inconsistent with the net impulse as shown by directional damage to lamp posts, trees and posts within the flammable cloud. Detailed modelling of the area immediately surrounding the emergency pump house supports the proposition that the trees and undergrowth along Three Cherry Trees Lane caused flame acceleration to a velocity of several hundred m/s; at such high flame speeds a transition to detonation is considered possible. It should be borne in mind that the deflagration model had been validated for use with pipe racks as obstacles, rather than vegetation as in this case.

Detonating vapour clouds are known to generate high overpressures. Modelling confirmed the direction of net impulse both within and outside the cloud and the rapid decline in overpressure with distance from the edge of the cloud. However, the magnitude of the loading predicted by the model would have caused significantly greater damage to Northgate and Fuji buildings. This discrepancy needs further investigation; it might be explained if, for example, the detonation was confined to part of the cloud depth (*e.g.* if only part of the cloud depth was at a

---

[1]   Explosion Mechanism Advisory Group Report, Buncefield Major Incident Investigation Board, Crown copyright, published 08/2007.

concentration within detonability limits or if the cloud in some parts was not deep enough to sustain a detonation).

A preliminary examination of alternative mechanisms (that are not as well understood as detonations and deflagrations) was also undertaken. Of these, a mechanism involving unsteady combustion with forward radiation warrants further research.

From the work undertaken, the most likely scenario can be summarised as follows:

- Dense vapour dispersion in very low wind speed conditions leading to a cloud build-up over an area of $120,000m^2$;
- Ignition at the emergency pump house; failure of the pump house structure followed by a deflagration outside the pump house and flame propagation to the undergrowth and trees.
- Flame acceleration in the undergrowth and trees along Three Cherry Trees Lane up to flame velocities to several hundred m/s, followed by a transition to detonation near the junction between Three Cherry Trees Lane and Buncefield Lane.
- Detonation of part of the remaining gas cloud.

This phase of the project has also defined experimental and analytical work to be completed in a second joint industry funded phase of the project. The aim of the proposed work (which is expected to take 24 months to complete) is to improve the understanding of low wind speed dispersion and large shallow vapour cloud explosions and the response of varios forms of construction to such explosions.

This phase has also identified areas for fundamental research of a longer term nature suitable for academic institutions and specialist technical organisations. It is suggested that this should be progressed through the normal funding channels for academic research (e.g. EPSRC, European Framework, etc.).

1 INTRODUCTION

1.1 BACKGROUND

The Buncefield explosion (11 December 2005) resulted in tremendous damage to the outlying area and huge fires involving 23 large oil fuel tanks. One important aspect of the incident was the severity of the explosion, which would not have been anticipated in any major hazard assessment of the oil storage depot before the incident. The Buncefield Major Incident Investigation Board (MIIB) invited explosion experts from academia and industry to form an Advisory Group to advise on the work that would be required to explain the severity of the Buncefield explosion[2]. This MIIB Advisory Group carried out a preliminary assessment of the forensic evidence obtained following the incident and of the results of experiments carried out by the Health and Safety Laboratory – HSL. The objectives of this assessment were:

- to determine whether a sequence of events could be identified that would explain why such severe explosion pressures were generated; and
- if this was not possible, to recommend to the Board what further actions would be required to explain the explosion severity.

The Advisory Group attempted to explain the explosion event at Buncefield using deflagration, detonation or a combination of both. It also examined other possible means of flame acceleration. However, it was not possible to identify a single scenario that could explain all aspects within the time available. The Advisory Group therefore recommended that a joint industry project be initiated that will, in its first phase, have the objectives of completing the assessment started by the Advisory Group and, on the basis of this, of defining the requirements for further research. This research – experimental and theoretical – would then be completed in a second phase of the project with guidance to industry and HSE being a primary deliverable of the work.

1.2 OBJECTIVES OF THIS PROJECT

The objectives of Phase 1 of this project are:

- to provide as definitive a record as possible of the characteristics of the Buncefield incident relevant to the formation and dispersion of the vapour and to the explosion, including the distribution of damage to nearby items and structures;
- where possible, to provide industry and the regulator with guidance for the operation of oil fuel storage sites based on this record of information and current knowledge of vapour cloud formation, dispersion and explosions;
- to define the research that would be required in Phase 2 to confirm in greater detail the explosion mechanism involved in the Buncefield accident and to provide improved guidance for both oil storage facilities and facilities storing other flammable liquids.

---

[2]   Explosion Mechanism Advisory Group Report, Buncefield Major Incident Investigation Board, Crown copyright, published 08/2007.

1.3 SCOPE OF PROJECT

Data collection and assimilation

A summary of evidence (collected after the Buncefield accident) that is relevant to the analysis of the explosion mechanism was compiled. Available data included a multitude of photographs, video and CCTV footage, extracts from anonymised witness statements on the character of the explosion, seismic records and repair records. It also included evidence relating to the magnitude of overpressure (*e.g.* extent of damage to various objects) and directional indicators (*e.g.* final deformed orientation of simple structures such as lamp posts).

Explosion characteristics

The characteristics of the explosion were derived from the data collected. The explosion was characterised by reference to:

- the size of the vapour cloud;
- the position of the ignition point;
- the timings of the various phases of the explosion;
- the magnitude of overpressure;
- the variation of overpressure across the site (both within and outside the cloud);
- the magnitude and direction of drag forces (net dynamic pressure impulses);
- the variation of dynamic pressure impulses across site (both within and outside the cloud);
- similarities to previous incidents.

Ability of explosion mechanisms to explain the evidence

A number of explosion scenarios were analysed to investigate those characteristics of the Buncefield explosion and associated evidence that can (or cannot) be explained by such scenario. The scenarios considered were:

- A deflagration scenario
- An initial deflagration scenario in which the flame accelerates leading to transition to detonation
- A preliminary examination of a range of alternative explosion mechanisms including: hydrocarbon aerosol explosion, stratified explosion, multiple ignition sources, multiple detonations, self-sustaining episodic explosion (without radiative effects) and ignition of suspended debris (dry leaves) by forward radiation from the flame front, *etc*.

The scenarios were tested against the Buncefield explosion characteristics.

Proposals for further research

The project has defined the requirements for future research. The proposed work includes both analytical and experimental work which aim to identify a range of design implications. It is recommended that this work is undertaken as a joint industry project over a period of 24 months.

The project has also identified a number of areas requiring fundamental academic research (e.g. alternative explosion mechanisms) and it is suggested that this should be progressed through the normal funding channels for academic research (e.g. EPSRC, European Framework, etc.).

2 OBSERVATIONS AND OVERPRESSURE ASSESSMENT

The information available from the Buncefield accident is vast. This project has focused on the data that could provide the most information on the nature and characteristics of the explosion based on earlier studies by the Health and Safety Laboratory and the MIIB Explosion Mechanism Advisory Group Report. Witness statements, CCTV camera records and evidence of damage to a range of structures and objects were considered. These are discussed below. The explosion characteristics derived from this information are summarised in Section 3.

Figure 1 shows a schematic of the site and provides a key to those buildings and locations that are referred to in this report and its appendices.
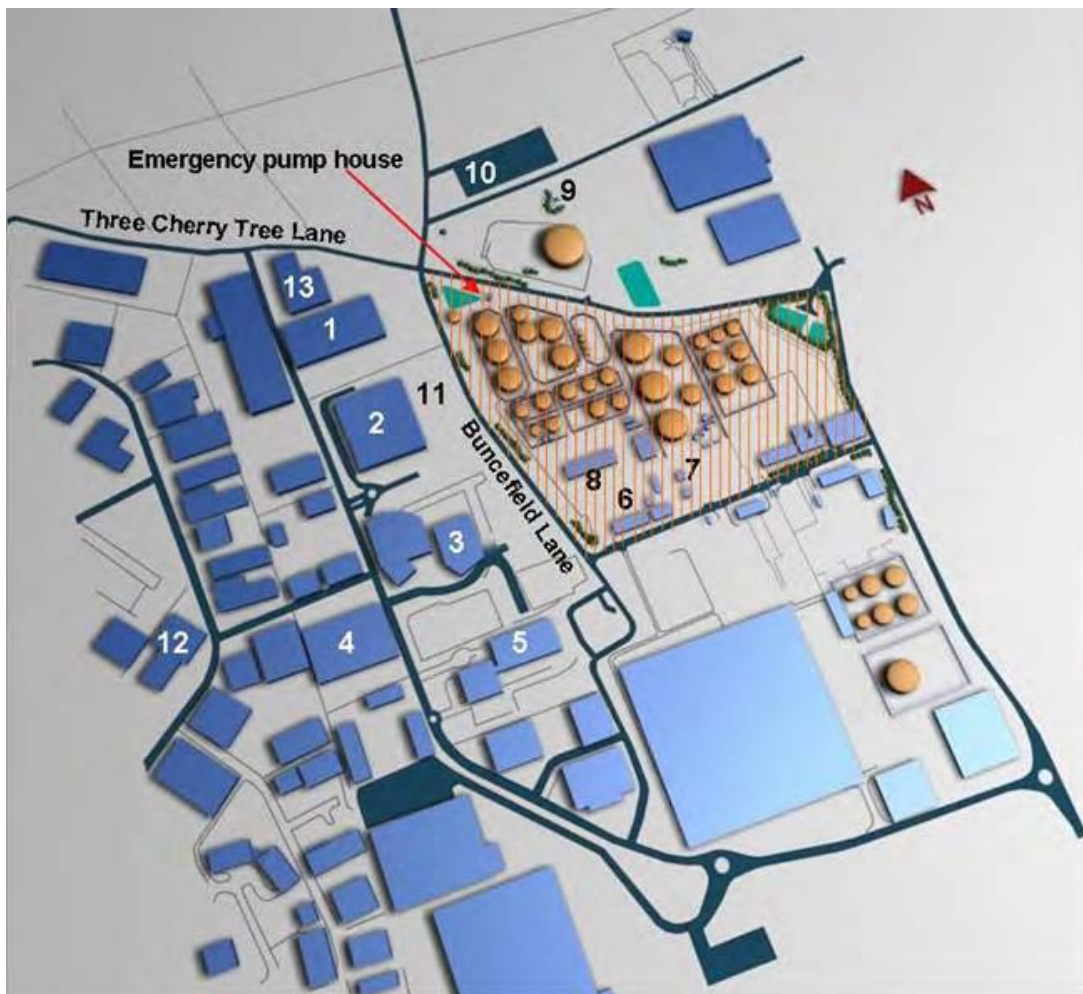
1.	Fuji Building	6.	Control room	11. Northgate Building car park
2.	Northgate Building	7.	Mess room	12. Furnell Building
3.	RO Building	8.	Tanker loading bay	13. Catherine House
4.	Avica Building	9.	The Cottages	Shaded area is Hertfordshire Oil Storage Ltd (HOSL)
5.	Alcon Building	10.	Fircones	and British Pipeline Agency (South)

Figure 1   Schematic of the Buncefield site and surrounding area

2.2   WITNESS STATEMENTS

The location of witnesses is shown in Figure 2. Based on extracts from anonymised witness statements that describe what happened, there were reports of a "noise", "drag forces" or other pressure effects prior to the arrival of the most powerful blast wave. The noise is variously described as a "vacuum noise", a "jet engine noise", a "very loud crackling noise", "thunder" or "a whoosh". The initial drag was described as a "strong wind". The arrival of the most intense blast wave was characterised by destruction of buildings and witnesses being thrown around. It was described variously as 'a terrific bang', 'a massive and loud explosion', 'an almighty explosion', 'a very loud bang' and 'a tremendous crash'. A 'flash' was also reported during this sequence of events.

All the witnesses within a few tens of metres of the cloud describe sustained pressure effects and/or sounds prior to the most violent phase of the blast.
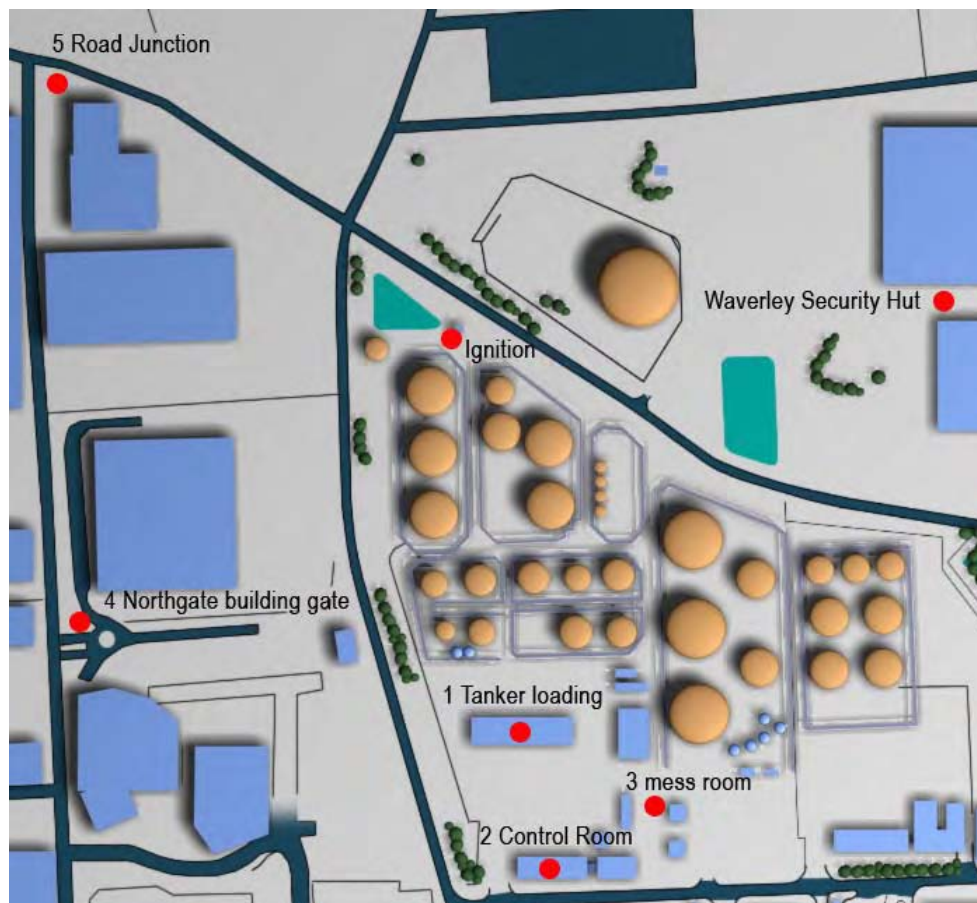
Figure 2   Location of witnesses

The approximate overpressure at each witness location as might be deduced from the observed effect of the explosion in their locale is given in Table 1.

Table 1 Overpressure estimates based on witness locations

Witness location	Observations	Estimated overpressure[1]
Tanker loading	Tankers were shaken. Witnesses were blown from their feet to the ground	~ 10 kPa
Control Room	Witness was blown across the room	~ 10 kPa
Mess room	Ceiling of room damaged and objects blown around the room	~ 5 kPa
Northgate building gatehouse	Door and windows were blown in	~ 7 kPa
Junction of Boundary Way and Three Cherry Trees Lane	Witnesses were blown from their feet to the ground	~ 10 kPa
Waverley security hut	Witnesses were blown from their feet to the ground	~ 10 kPa
1 Note: there is uncertainty associated with these estimates. However, as none of the witnesses suffered any hearing damage, it can be concluded that the overpressure at the witness locations is < hearing damage threshold (The threshold for eardrum rupture is 35kPa, with a 50% chance of rupture at 100kPa.).		

2.3   CCTV RECORDS

The video and CCTV cameras acted as sensors and the analysis of their output was used to construct a time line (see Appendix A). Their locations and directions are shown in Figure 3.
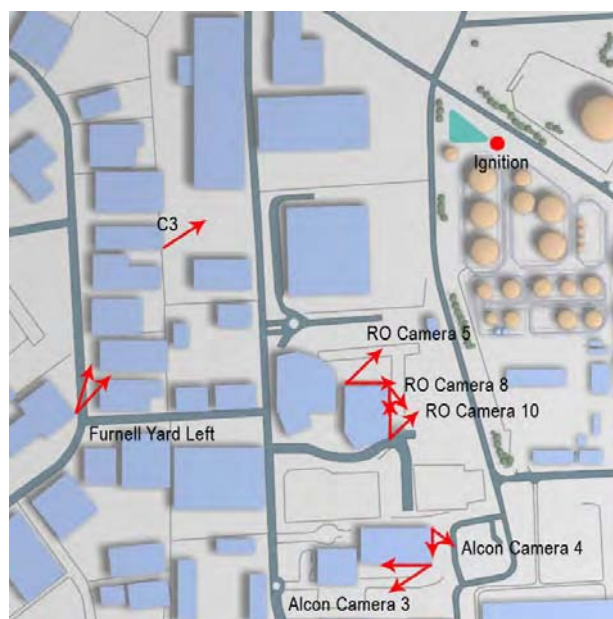
Figure 3   Location and direction of CCTV cameras

The explosion was recorded by a number of cameras and this helped confirm the location of the ignition point. The cameras also provided information on illumination from the explosion, the arrival of shock waves generated by the event, the possible appearance of condensation of water vapour (evidencing the arrival of rarefaction) and the end of the rarefaction phase. In particular the timing of the arrival of the first shockwaves was very well defined by the onset of camera shake. These are summarised in Table 2.

Table 2 Camera shake and rarefaction timings

Time[1] at which:	*RO Cameras*	*Furnell YL Camera*
Camera shake starts (denotes arrival of overpressure wave front/start of positive phase)	666 - 1000 ms	1600 – 1640 ms
Rarefaction starts (denotes start of the negative phase of overpressure)	1333 - 1666	2280 - 2400
Rarefaction ends[2]	2333 - 3000	3000 - 3360

1   Measured from when the camera first detected a change in light conditions

2   As evidenced by the pictures becoming clear again – this is not a definitive indicator of the end of the rarefaction phase. Rarefaction may have ended before the mist clears. Dust thrown up into the atmosphere and originating from damaged objects also introduces uncertainty.

2.4   DAMAGE TO OBJECTS (OTHER THAN BUILDINGS)

There were a number of objects (*e.g.* switch boxes, oil drums, cars) distributed across the site and immediate surrounding areas. The condition of these objects after the explosion provided an indication of the overpressure magnitude at the location of these objects (shown in Figure 4). A more detailed assessment of damaged objects can be found in Appendix B.

Figure 4 identifies cars, drums and a range of other metal enclosures which exhibited damage consistent with overpressures in excess of 200 kPa. Table 3 shows images of typical damage to a number of these objects and a brief description is provided in the following sections.

2.4.1   Lightweight metal boxes

There were a number of lightweight steel junction boxes on the site located within the area covered by the gas cloud (Table 3 – items 2 and 5). These were compared with similar boxes tested under a range of different loading conditions using hydrostatic pressure, gas explosions and High Explosive charges (HE).

Analysis of these results has shown that the magnitude of overpressure required to cause damage comparable to that sustained by junction boxes on the Buneceflield site is of the order of 200 kPa with duration ~ 50 ms.   At shorter durations that are more representative of overpressure within a detonating gas cloud (~10 ms), an overpressure of 500 kPa would be required.

2.4.2   Steel drums

An empty steel drum sustained inward plastic deformation (crushing) to its walls (Table 3 – picture 1) and buckling of the drum end (Table 3 – picture 4). A similar damage pattern was caused in a hydrostatic pressure test at pressures of between 150 and 200 kPa. A gas explosion with a maximum overpressure of 180 kPa on an empty drum produced a smaller magnitude but similar deformation patern in the end plate of the drum.

There were also similar but partially filled drums on the site. These were damaged by fire following the explosion, with a resultant convex deflection (dishing out) of the end plates due to internal pressure caused by expansion of the drum content (Table 3 – picture 3). However, the buckling pattern caused by the explosion near the top of the wall of the drums remained visible. Comparable damage to a similar drum was caused in a hydrostatic pressure test at pressures of

between 200 and 300 kPa. The above observations suggest that the overpressure at the location of the drums in Buncefield was around 200 kPa.
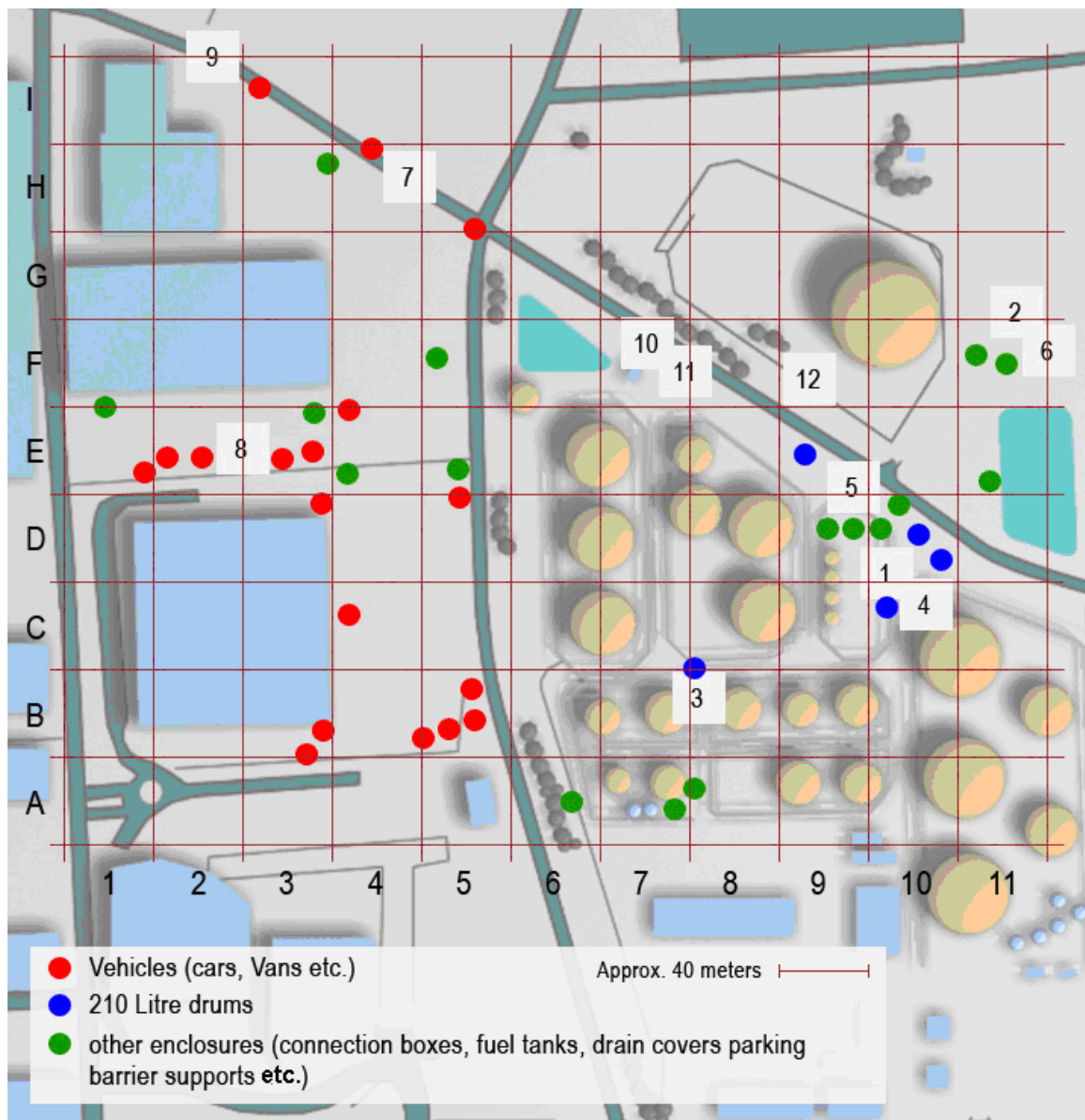
Figure 4 Location of vehicles, drums and other enclosures which exhibited damage consistent with overpressures in excess of 200 kPa (for images of selected objects identified by numerical tags in this figure, see Table 3)

Table 3 Objects identified by numerical tags in Figure 4

1. Crushed drum	2. Crushed hydraulic switch box	3. Creased drums (buckled walls)
4. Drum with plastic end deformation	5. Crushed electrical connection box	6. Crushed oil filter
7. Crushed car	8. Crushed car	9. Line of crushed cars
10 Diesel tank in pump house	11. Water tank in pump house	12. Deflected lamp post

2.4.3 Oil filter

An oil filter on the Buncefield site sustained significant inward plastic deformation (Table 3 – picture 6). In comparative gas explosion tests, no permanent visible plastic deformation occurred to a similar oil filter at pressures up to 180 kPa.

2.4.4 Cars

Over 20 cars were in the area covered by the gas cloud and all were badly crushed. Comparative tests using HE have shown that overpressures of the order of 1000 kPa were required to cause the level of damage observed at Buncefield (see Table 3 – pictures 7 and 8). Comparative gas explosion tests in a strong steel enclosure in which cars were subjected to overpressures of 100 kPa resulted in significantly less damage that observed at Buncefield. It is concluded from examining all the data available that the overpressures experienced by cars at Buncefield exceeded 200 kPa for durations ~ 50 ms.

Damage to cars also provided useful evidence on the decline in overpressure magnitude outside the cloud. A good example can be seen in Table 3 – picture 8. It shows the extensive damage to the cars furthest from the camera which were clearly within the gas cloud as they have been crushed and set alight. Damage to the light coloured car nearest the camera is slight, whereas the black hatchback behind it shows significant crush damage. This suggests a very rapid decrease in overpressure magnitude with distance away from the edge of the cloud.

2.4.5 Objects in the emergency pump house

The emergency pump house, where the explosion is thought to have started, contained a number of lightweight metal objects that sustained minimal damage (Table 3 – pictures 10 and 11). This suggests that in its initial phase, the explosion overpressure was modest.

2.4.6 Directional evidence

A number of objects on site were susceptible to drag forces (*e.g.* lamp posts, fence posts, camera masts, trees). An example can be seen in Table 3 – picture 12. The deformation exhibited by such objects provided information on the net drag impulse sustained by these objects. Other directional evidence was provided by the directional abrasion found on one side or one part of painted surfaces and tree bark. There was also evidence of large objects such as cars and skips being displaced in a particular direction.

Study of this evidence (Appendix B) provided data on the direction of the explosion propagation across the Buncefield site and enabled an overall picture of propagation of the explosion front to be constructed. This is shown in Figure 5. Over the area covered by the cloud the direction of net impulse is inwards – towards the origin of the explosion (in the opposite direction to explosion propagation). Immediately outside the cloud the direction reverses and objects are blown outward.
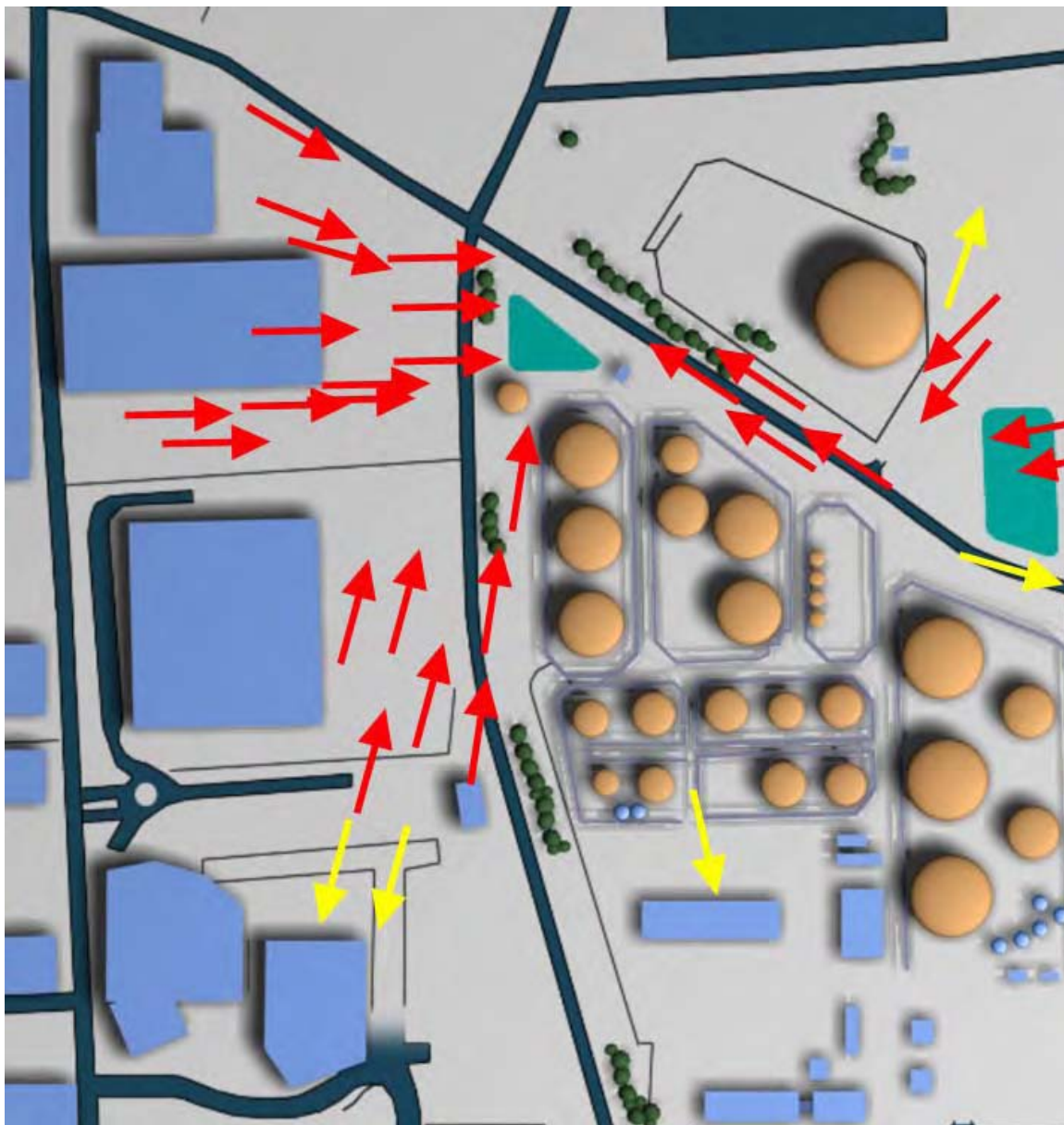
Figure 5   Direction of net drag impulse across the Buncefield site

2.5   OVERALL ASSESSMENT OF BUILDING DAMAGE

2.5.1   Near and mid-field damage

An assessment of near and mid-field building damage is reported in Appendix F. Typical overpressures from a TNT charge near the centre of the gas cloud which would be expected to cause the observed damage to a number of buildings within a 0.5km radius of the emergency pump house are shown in Figure 6.

The charge size near the centre of the cloud found to give these overpressure values is 7500kg of TNT. Although derived from conventional military explosives scaling, the overpressures are reasonably consistent with the observed damage. However, it is well known that a single value

of TNT equivalence will not predict both the far field and near field damage for a vapour cloud explosion.   The charge size of 7500 kg TNT therefore does not generate the required pressures to cause the far-field damage to the residential areas (see Section 2.5.2).
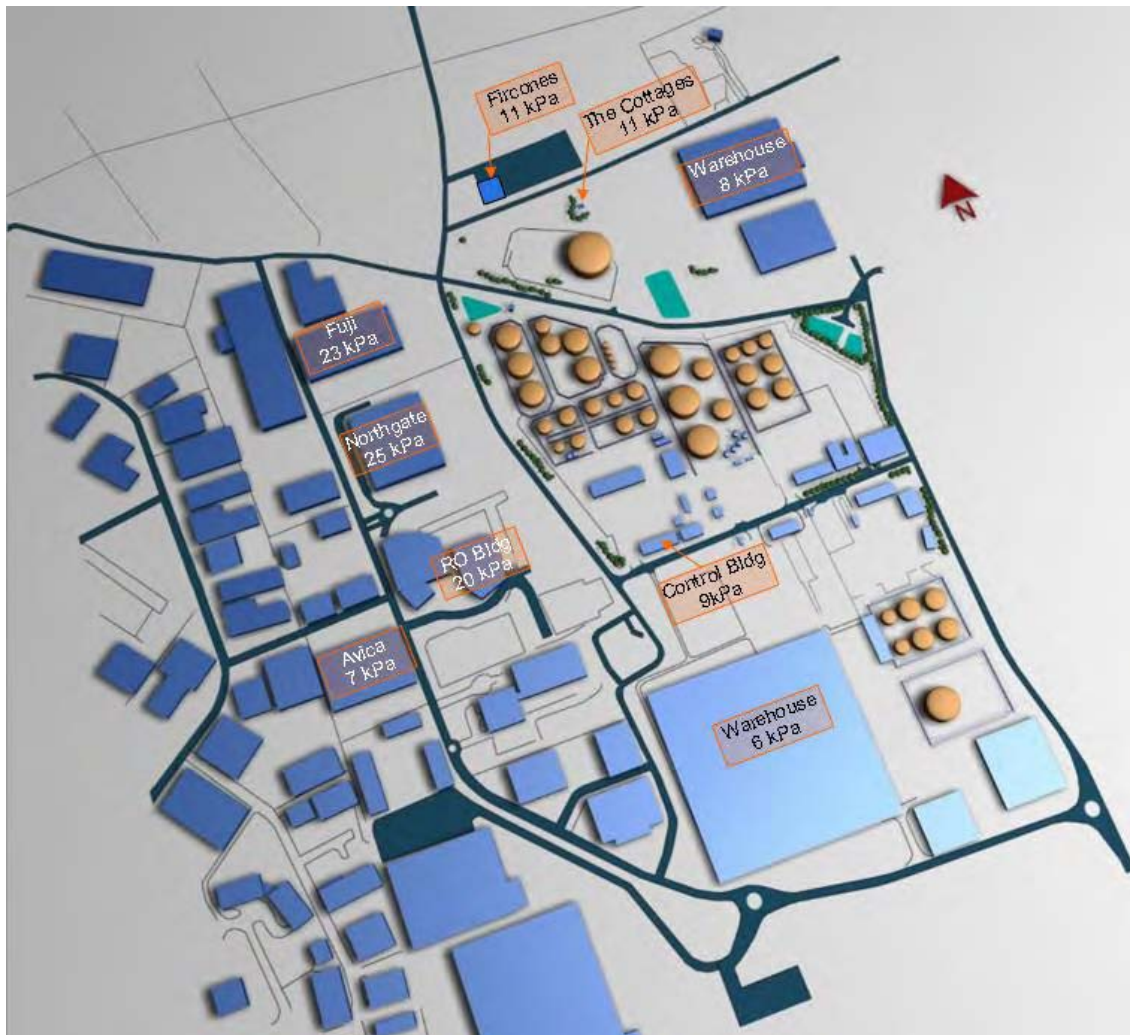
Figure 6   Overpressures from a TNT charge expected to cause the observed level of damage to buildings in the near and mid-field

2.5.2   Far-field damage to buildings

Domestic housing estates exist to the North, West and South of the industrial area surrounding the Buncefield site. Based on information from insurance claims, the damage was frequent within a distance of 2 km from the site and sporadic building damage extended to a distance of more than 4km. There was a higher concentration of damage to the North and South of the site compared to the West (Figure 7).

Damage to domestic dwellings has been well characterised through analysis of wartime building damage, specific testing undertaken by the MoD and international collaboration. Zones where multiple cases of light damage occurred were identified at distances of between 1 and 1.5 km from the emergency pump house. It included damage to glazing, door frames, roofing

materials, lightweight structures *etc*. and this can be associated with peak overpressures of the order 5kPa. It can therefore be concluded that the overpressure at these locations was in the region of 5 kPa.
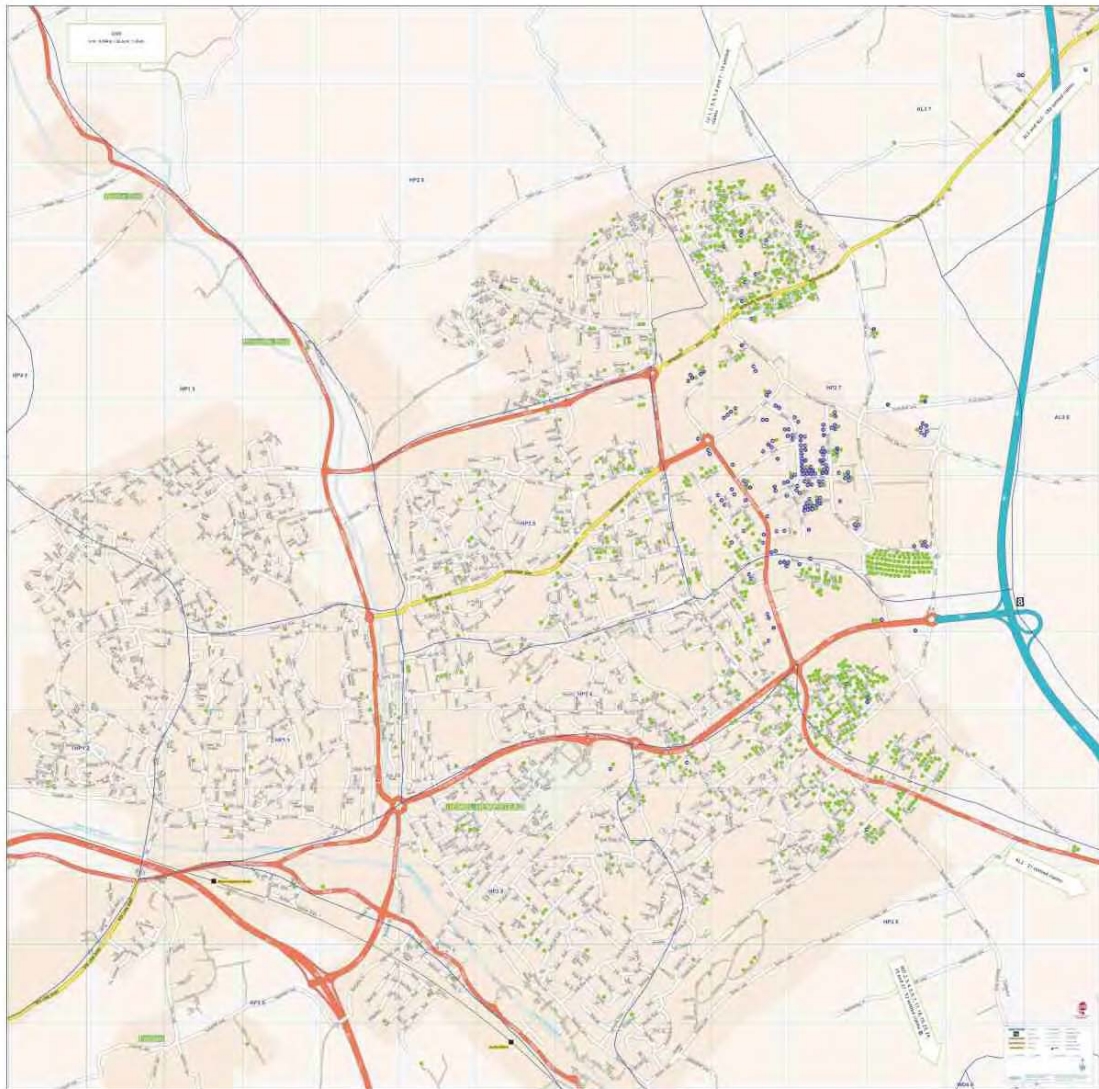
Figure 7   Property damage (shown as green and blue dots) Courtesy of Kennedys Law

Using military scaling rules (see Appendix F), the charge size at the ignition source that would be required to cause such damage at these distances is estimated to be between 105,000 and 250,000 kg TNT. Such a charge size would have caused significantly greater damage in the near and mid-field than that observed.

2.6   DETAILED ASSESSMENT OF BUILDING DAMAGE

2.6.1   Assessment of Damage to RO Building

An assessment of damage to the RO Building concluded that there was:

- Severe (80-100%) glazing pane damage to the east and north elevations with frame damage on the north elevation.
- Minimal damage to the perimeter masonry cladding.
- Minimal or no damage to the building structural frame.

The assessment concluded that an over-pressure of 20kPa at the North East corner of the building was capable of generating the observed levels of damage.

2.6.1   Assessment of damage to Northgate Building cladding

The Northgate Building had been built in two phases at different times. The cladding panels used in the two phases were architecturally identical. However, examination of failed panels revealed that the earlier phase panels contained less reinforcement than those used in the second phase. This difference manifested itself in the response of these panels to the explosion. Two adjacent panels at the top floor level – one on the earlier phase and the other on the later phase were found to have deflected by 200mm and circa 30mm respectively (Figure 8).

Figure 8   "strong" (left hand side) and "weak" (right hand side) cladding panels on East face of the Northgate Building

A finite element structural analysis of these two panels was carried out to derive the single load profile that is consistent with the levels of damage to the two panels. A range of generic load profiles (typical of gas deflagrations, detonations and combinations of deflagration and detonation) were examined. The peak overpressure and the impulse were also varied. In total, some 160,000 analysis were performed and this enabled iso-damage diagrams to be constructed for both panels.

The load profile found to cause damage consistent with that observed in both panels has a rise time equal to 30% of the overall duration and a decay equal to 70% of the overall duration. Assessment of the sensitivity of the response to variation in the properties of the reinforcing bar yielded a peak pressure of 16kPa when using design values for the steel strength and 30kPa when using measured steel strength (from samples taken from site after the accident). The associated load durations were 1.6s and 0.6s respectively. Figure 9 shows these load profiles. Furthermore, it was found that the damage caused is very sensitive to the magnitude of peak pressure but much less sensitive to the magnitude of the impulse.
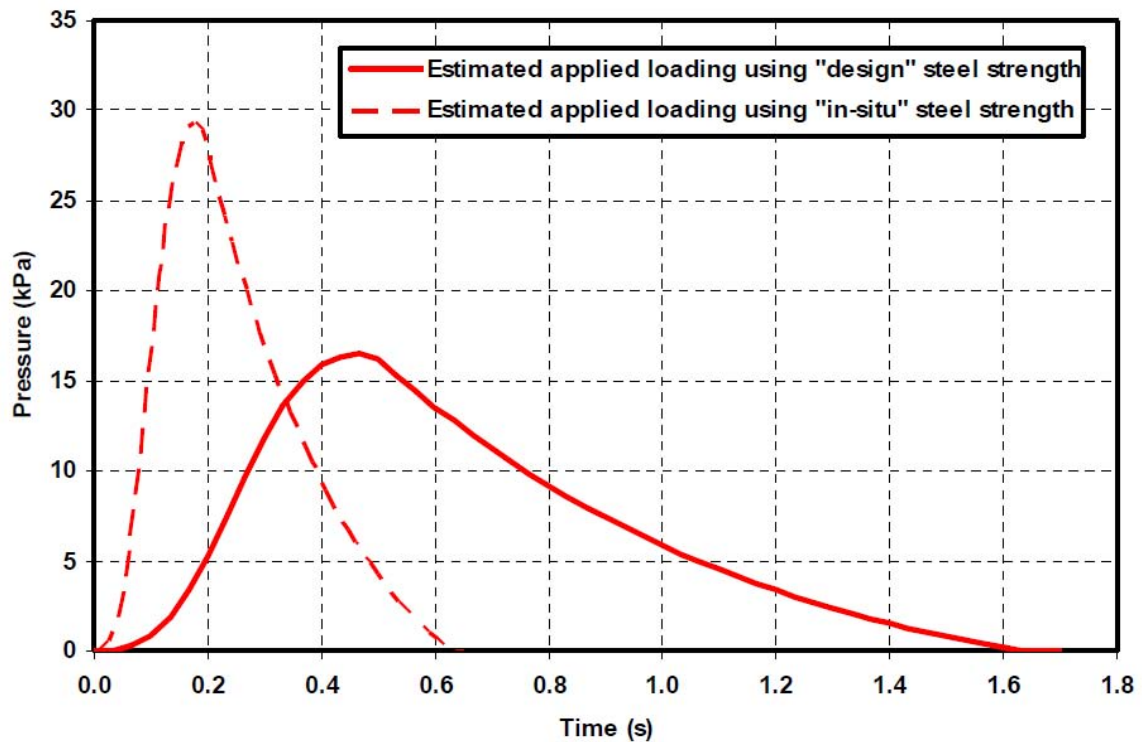
Figure 9   Load curves that were found to cause the observed structural response (the curves correspond to the response calculated using "design" strength and "in-situ" (measured) strength of the reinforcing steel

3 CHARACTERISATION OF THE BUNCEFIELD EXPLOSION

The key characteristics of the Buncefield explosion can be deduced from the observations and analysis of Section 2. They are summarised in this Section.

3.1   CLOUD CHARACTERISTICS

Burnt areas that were consistent with the thermal effects from the combustion of the vapour cloud enabled the cloud's location to be estimated (Figure 10). The area covered by the cloud is approximately 120,000 m^2. CCTV images enabled the average depth of the cloud to be estimated as 2 m (assuming that the flammable limit corresponds closely to the top of the mist). The volume of the cloud with a concentration above the lower flammable limit (LFL) is therefore in the region of 240,000m^3.

Based on inventory information, the chemical composition of the cloud is similar to butane or propane in terms of reactivity[3].
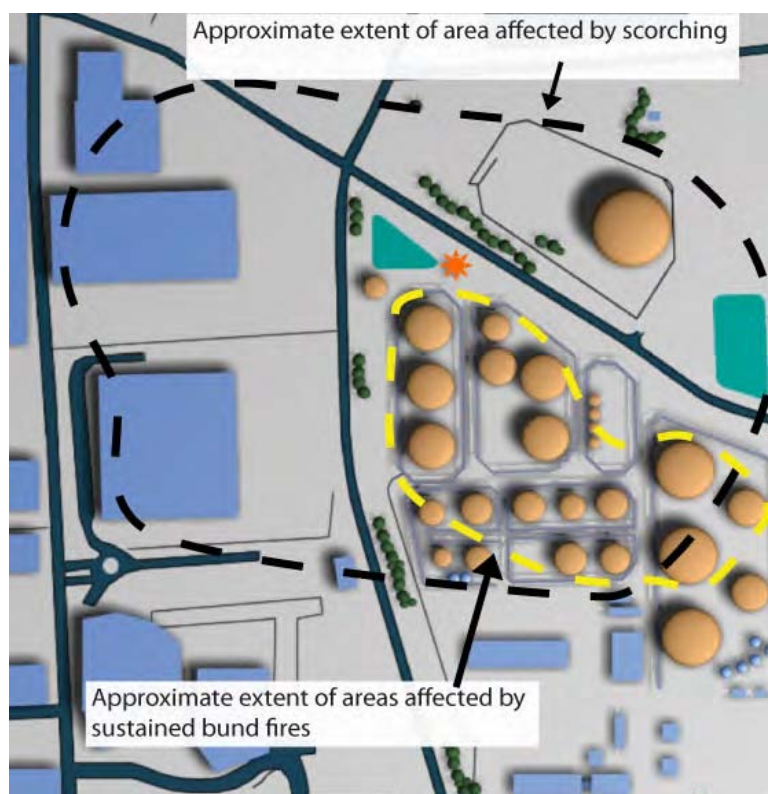
Figure 10   Extent of flammable cloud (ignition location denoted by ✷)

---

[3]   For more information on the characteristics of vapour produced by a cascade of winter petrol see Atkinson G., Gant S., Painter D., Shirvill L. and Ungut A., "Liquid dispersal and vapour production during overfilling incidents", Hazards XX: Process Safety and Environmental Protection, Harnessing Knowledge, Challenging Complacency (Symposium Series 154), 14-17 April 2008, Published by the Institution of Chemical Engineers.

3.2   IGNITION LOCATION

There is a weight of evidence to suggest that the source of ignition was in the emergency pump house. This includes witness statements, CCTV records, evidence of an internal explosion at the emergency pump house (it is believed that the pumps should have started when the emergency fire alarm was activated just before the explosion occurred) and directional indicators. The location of the ignition point is shown in Figure 10.

The scenarios considered in Section 4 have therefore assumed ignition at the emergency pump house.

3.3   TIMING OF EXPLOSION PHASES

It should be noted that the RO building cameras recorded at 3 frames per second and the Furnell cameras recorded at variable speed; the images used in the analysis of the Furnell camera records were typically at 25 frames per second. The accuracy of the analysis of timings is therefore limited by the time resolution of the cameras.

Indications of the start of the positive phase of the explosion at camera locations are evidenced by the start of camera movement. The appearance of a mist in the picture is likely to denote the start of the negative phase. The cameras at the RO buildings (Figure 3) therefore suggest that the time between the start of the positive phase and the start of the negative phase at that location lasted for 666 ($\pm$333) ms. The corresponding time period derived from the Furnell YL camera is around 700 ms.

In both the RO building and the Furnell cameras, the mist cleared 1000 ms after it first appeared. The disappearance of the mist is not necessarily coincident with the end of the negative phase as the atmosphere may remain misted beyond the end of rarefaction. Furthermore, the dust caused by the explosion is difficult to distinguish from the mist in some of the pictures and this causes some uncertainty.

3.4   OVERPRESSURE MAGNITUDE AND DISTRIBUTION

Assessment based on damage to objects suggests that the overpressure within the area covered by the cloud was around 200 kPa; local maximum overpressures were probably much higher. High overpressures ($\geq$ 200kPa) were not confined to small areas of the site but applied in every part of the burned cloud. There also appeared to be no distinction in damage level between objects that are in different types of surroundings e.g. car parks, tank farms, open grassland and belts of trees. The only exception is the interior of the emergency pump house (where the explosion started); here pressures were lower. The area with overpressure indicators which suffered damage consistent with overpressures of 200 kPa or more is highlighted in Figure 11.

Another feature of the explosion is the rapid drop in overpressure with distance from the edge of the gas cloud. This is confirmed by car and buildings damage and the lack of any serious injury to witnesses. Spot values of estimated overpressure are shown in Figure 11 based on these indicators. It is also worth noting that low values of overpressure (~5 kPa) extend to distances in excess of 2 km from the ignition source, as evidenced by domestic and commercial property damage.

3.5   EXPLOSION PROPAGATION

The net drag impulse was towards the general direction of the emergency pump house within the gas cloud, and away from the pump house outside the gas cloud (Figure 5). This indicated that the explosion propagated away from the emergency pump house.

Figure 11   Overpressure indicators (the area where damage suggests overpressures   > 200 kPa is shown shaded)

3.6   HOW BUNCEFIELD COMPARES WITH PREVIOUS INCIDENTS

Eight previous significant incidents (Table 4) for which detailed data are available were reviewed to assess whether key features of the Buncefield explosion have been reported in those incidents. More details can be found in Appendix G.

On the basis of directional evidence and evidence of overpressure distribution over the area covered by the vapour cloud it is concluded that both Port Hudson and Ufa are very similar to

Buncefield in terms of the characteristics of the explosion, whereas Flixborough, Texas City and Beek are very different.

Both Port Hudson and Ufa resulted from ignition of a gas release whereas Buncefield resulted from a liquid release but all three occurred following extended releases. Dispersion of the heavy vapours over most of the area would have been by slow gravity currents in low wind conditions. Flow speeds would have been low with the potential for very low (or zero) entrainment rates. Substantial volumes of gas would have been created with low concentration gradients in at least two-dimensions. It is possible that a high level of homogeneity in the cloud is a prerequisite for a Buncefield type explosion.

Table 4 Previous incidents

Accident	*Date*	*Type of fuel and release*
Flixborough	1974	Cyclohexane – Process leak
Port Hudson	1970	Propane – Pipeline failure
Ufa	1989	LPG - Pipeline failure
Naples	1985	Petrol - Tank overfill
Saint Herblain	1991	Petrol - Process leak
Newark (NJ)	1983	Petrol - Tank overfill
Beek	1975	Propylene- Process leak
Texas City	2005	C5-C7 Process leak

Buncefield, Ufa and Port Hudson also covered a wide range of terrain types; they included dense forest, lightly wooded areas, arable land, tarmac parking, rough grassland, hedging/roads, tank farm. At Buncefield, in particular, it was possible to show that the severity of the explosion was maintained over at least the last four types of terrain. Another common feature is the cloud size; Buncefield, Port Hudson and Ufa all involved vapour clouds with a maximum dimension >300m. However, clouds of a similar size were also a feature of Flixborough and Newark (NJ).

There is good evidence that the initial explosion at Port Hudson occurred in a storage building made from concrete blocks. The initial explosion would have been confined, with a corresponding increase in the pressure. The original investigation report for the Port Hudson incident identified this as a potential mechanism of triggering detonation. The Buncefield explosion started in the emergency pump house; it was therefore confined and with some congestion. However, the evidence suggests that the overpressure associated with the explosion within the emergency pump house was low (see Section 2.4.5). The high overpressure at Buncefield is thought to be a result of flame acceleration outside the pump house.

4 COMPARISON OF POTENTIAL SCENARIOS WITH THE BUNCEFIELD EXPLOSION

A number of potential scenarios were examined. They differed primarily in the mechanism by which overpressure is generated. Each was tested against evidence from the Buncefield explosion and the explosion characteristics derived from that evidence to demonstrate the likelihood or otherwise of each of these scenarios. In this section, a brief description of each scenario is presented, followed by a comparison with the observed evidence. More details can be found in Appendices C - E.

All the scenarios considered assumed ignition to occur at the emergency pump house.

4.1 DEFLAGRATION SCENARIO

The deflagration scenarios were modelled using the CFD code EXSIM. Details of the geometry modelled can be found in Appendix C. Modelling simplifications had to be made to the congestion offered by tree branches and undergrowth – these were modelled as rigid pipe elements and blockage ratios had to be estimated. The cloud shape and the geometry of the domain of interest were also outside those for which the model is validated and normally used. Nevertheless, the model results are instructive when used for comparative purposes. Three models were studied as described below.

4.1.1 Large domain simulation

The physical size of the domain in this model was such that the modelling of congestion in the trees and shrubs bounding Three Cherry Trees Lane and Buncefield lane had to be simplified in order to allow the large-scale gas cloud to be modelled. Trees and shrubs were modelled as rigid pipe elements and a range of blockage ratio. This allowed a coarse mesh size to be used, and so permitted the modelling of the very large cloud and associated domain. However, this simplification has the tendency to under-predict the flame velocity and overpressure. The model is illustrated in Figure 12. A stoichiometric propane gas cloud extending over the square region shown was modelled.
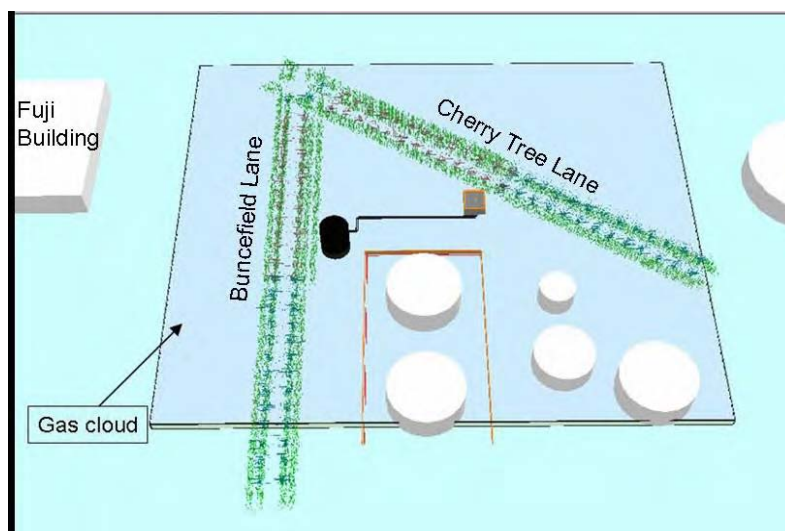
Figure 12   Large domain deflagration model and gas cloud

The peak overpressure reached at the junction of Buncefield lane with Three Cherry Trees Lane was 200 kPa. Other pressure spikes of around 200 kPa were predicted along Buncefield Lane at points of high local congestion, but the pressure generally dropped to around 100 kPa and dropped significantly in open areas either side of the lanes. The peak overpressure as it arrives at the Fuji Building is 15 kPa. Flame speed in Buncefield Lane is around 280 m/s but peaks at 500m/s.

## 4.1.2 Small domain simulation

In order to consider the effect of small obstacles that are more representative of the form of congestion presented by the trees and shrubs in Three Cherry Trees Lane, a smaller geometric domain that included the emergency pump house (acting as the ignition location) and parts of Three Cherry Trees Lane adjacent to it was modelled (Figure 13).
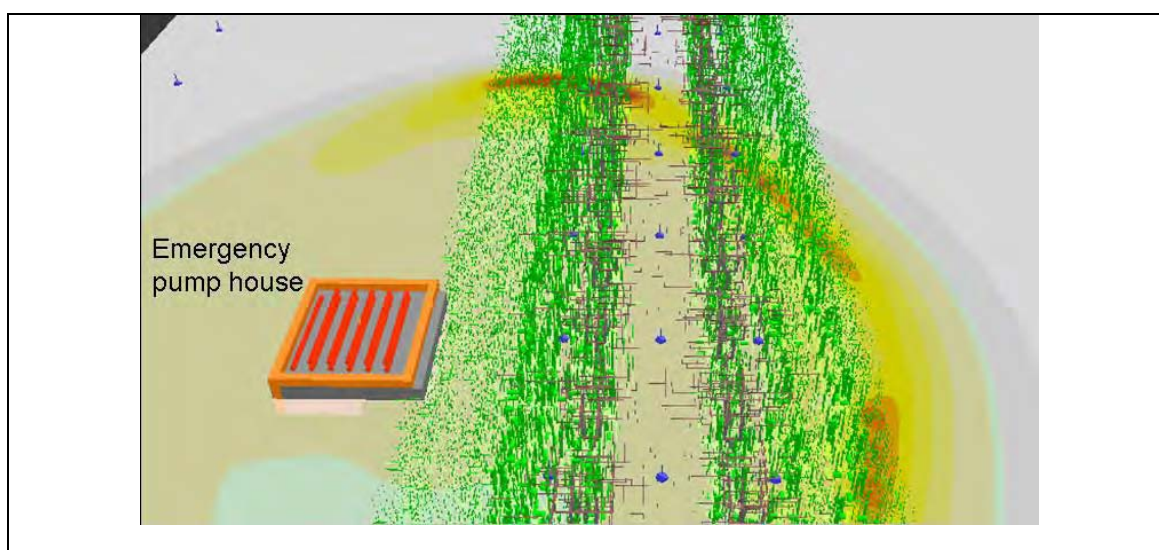
Figure 13   Finely resolved model of vegetation

The overpressure predicted close to the junction with Buncefield Lane was around 400 kPa and the flame speed was 714 m/s. There is experimental evidence to show that a deflagration to detonation transition (DDT) can occur at flame speeds of around 600 m/s for fuels with a similar reactivity to that at Buncefield (see Appendices C and D). There is therefore a possibility that DDT occurred close to the junction with Buncefield Lane. The analysis estimated that this would have happened some 230ms after initial ignition.

4.1.3 Large domain simulation using a more reactive fuel (Ethylene)

In order to examine the effect of enhanced burning (due to fine obstacles) over a large domain, ethylene (which has a higher burning rate than propane) was used in conjunction with the domain and congestion model referred to in Section 4.1.1. The higher reactivity of ethylene is intended to compensate for the enhanced burning of propane in the regions of fine obstacles. This is merely an analytical device to overcome the computational difficulties that would arise with modelling the fine scale obstacles over such a large domain. The results of this analysis are therefore only relevant in the areas of high congestion.

The results in the congested areas were consistent with those obtained using propane with fine obstacles in the smaller domain. They therefore confirm that DDT may have occurred at the Junction of Three Cherry Trees Lane with Buncefield Lane.

4.2 DETONATION SCENARIO

The detonation scenario examined in Appendix D comprises the following sequence of events:

- Ignition in the emergency pump house resulting in a confined explosion venting into the external cloud.
- Flame propagation into the tree line to the north of the emergency pump house along Three Cherry Trees Lane.
- Flame acceleration in the tree line in the same manner as described in the deflagration scenario (Section 4.1).
- Transition to detonation somewhere near the junction of Buncefield Lane and Three Cherry Trees Lane.

Analysis of the timing of events based on witness statements, time of arrival of first shock wave at the cameras and luminosity of camera images showed that the evidence was not inconsistent with a detonation but has insufficient certainty to be a conclusive means of proving the scenario.

4.2.1 Small scale numerical simulations

Numerical simulations of an idealised rectangular gas cloud were performed to investigate the overpressure decay outside the cloud and the net impulse both within and outside the cloud. These showed that the overpressure outside the edge of the cloud decays rapidly with horizontal distance from the cloud's edge. The overpressure decay in a vertical direction from the top of the cloud was also found to be rapid, although the rate of decline was slightly less than in the horizontal direction. For example, at a point 7 m above a 20m x 2m cloud, the overpressure was calculated to be 300kPa, whereas at a similar distance in the horizontal direction, the overpressure was 300kPa just 4 m from the cloud edge. The net impulse throughout the cloud calculated in these simulations was found to be negative (*i.e.* in the opposite direction to the propagation of the detonation).

4.2.2 Large scale numerical simulations

Large scale simulations of axisymmetric pancake shaped clouds of 400m diameter and 2m height were performed. They enabled the overpressure decay from the edge of the cloud and the net impulse (both outside and within the cloud) to be calculated. Additionally, an obstructed scenario was simulated by placing a solid object at the edge of the cloud. This was used to estimate the overpressure that might have acted at the face of the Northgate Building if the cloud detonated up to face of the building.

Overpressures within the cloud comprised a short duration (10 – 20 ms) shock wave with an overpressure in excess of 1000 kPa followed by a positive duration phase that lasted > 100 ms. A similar phenomenon is observed outside the cloud. At 30 m from the edge of the cloud, a short duration of shock wave of around 70 kPa is followed by a long duration low overpressure phase that lasts over 300 ms.

The simulations showed a net impulse in the opposite direction to the propagation of the explosion within the cloud and in the direction of the explosion outside the edge of the cloud.

4.2.3 Consistency with damage to objects and structures

Far-field damage

The volume of the vapour cloud at Buncefield was estimated to be around 250,000 m^3. A simple multi-energy calculation method was used to estimate the relationship between the cloud volume and the overpressures produced at distance from a detonating vapour cloud (see Appendix D). If a cloud volume of 100,000 m^3 had detonated, this would have resulted in overpressures of 4 kPa and 2 kPa at about 900m and 1700m respectively. These distances are dependent on the cube root of the cloud volume, thus a doubling or halving of the cloud volume will alter these distances by approximately 25%. The observed far field damage is consistent with these values of overpressure.

Near to mid-field damage

The level of damage to items such as cars and boxes within the cloud is consistent with the detonation scenario.

In the case of Northfield Building, a load profile comprising a slow rise time was found to provide a solution that was consistent with the damage to the cladding panels (see Section 2.6.1). This is clearly not consistent with the detonation scenario, which would generate high shock loadings on the building if the detonation reached the building. On the other hand, a detonation that involved a thinner section of the cloud than that modelled might be consistent with the damage. Additional detonation simulations are therefore required to explore the loading regimes that might be generated at the face of the Northgate Building.

No structural analysis has been conducted of the Fuji Building. However, it is notable that there was severe damage all around the perimeter of this building in areas where the vapour cloud had been present. This included complete demolition of the one bay of the building along most of the southern side of the building where the cloud was present. The rapid decay of the overpressure as it propagated into the building might be expected to limit how far the high level of damage would extend. The south east corner of Catherine House, which suffered complete collapse, was either very close to or within the vapour cloud.

The damage to the RO building is consistent with an incident overpressure of 20kPa (see Section 2.5.1). This building was about 60-80 from the cloud edge. The small scale simulations indicate that a 20m x 2m high cloud would give overpressures of 21-14kPa at these distances from the cloud edge whereas the large scale simulations indicate an overpressure of about 30kPa at these distances. There is therefore reasonable agreement between the level of overpressure estimated from the observed damage and those obtained from the detonation simulations. Reasonable agreement is also found in the case of the buildings on the North side of the site.

4.3   COMPARISON OF DEFLAGRATION AND DETONATION WITH THE EVIDENCE

Table 5 provides a summary of how the deflagration and detonation scenarios compare with the evidence and characteristics of the Buncefield explosion.

Neither scenario was found to be inconsistent with either the witness evidence or the CCTV camera evidence relating to arrival of first shock wave or luminosity. This is due to the fact that there is sufficient uncertainty in this evidence and the assumptions that may be made about the different stages of each scenario.

Table 5 Testing the deflagration and detonation scenarios against the evidence

Evidence	Agreement or disagreement with the observed evidence	
	Deflagration	Detonation
Timing of events based on witness evidence	The witness evidence consistently describes an explosion event over a period of time lasting up to a few seconds. It is not possible from this evidence to distinguish between the scenarios, but neither scenario is inconsistent with this evidence.	
Arrival of first shock wave at CCTV camera locations	The evidence of arrival of the first shock is clear within the timing resolution of each camera (333ms and 40ms). Uncertainties and assumptions about the stages of each scenario enable a range of timings to be accommodated and either scenario to fit the timings. Neither scenario is therefore inconsistent with the timing of the arrival of the first shock at the CCTV cameras.	
Time from start of positive phase to start of negative phase (determined by misting on CCTV camera pictures)	The deflagration simulation does not provide results at the positions of the cameras. Results at locations closer to the ignition source than the cameras indicate a shorter time period before the negative phase begins than was observed from camera pictures. Simulations of a larger domain are required to investigate further.	Numerical simulations of a detonating pancake shaped cloud support a period of hundreds of milliseconds before the start of the negative phase.
Luminosity records in CCTV camera pictures	The luminosity records allow for a sufficiently wide interpretation not to be inconsistent with either the deflagration or the detonation scenarios. As such, the camera records do not provide definitive evidence.	
Directional indicators	The deflagration scenario is only consistent with directional evidence within the tree lines. It is not consistent with directional evidence in the open areas within the cloud where directional indicators point towards the ignition source.	Numerical simulations of a detonating pancake shaped cloud are consistent with directional evidence both within and outside the cloud.
Near and mid-field damage to objects	The deflagration scenario cannot explain the damage to objects that are within the cloud but separated by some distance from congestion.	The detonation scenario explains the damage to objects within the cloud. It is also consistent with the rapid change in damage patterns across the edge of the cloud.
Near and mid-field damage to buildings	The deflagration is consistent with the near to mid-field building damage.	Detonation of a vapour cloud where the detonation extends up to the face of the building is not consistent with damage to the Northgate Building. A detonation that fails some distance from the face of the building may be consistent with the observed damage. Analysis of scenarios that do not involve detonation of the full cloud is required to verify.
Far-field damage to buildings	Consistency of a deflagration with the far-field building damage depends on the amount of fuel consumed in the deflagration and the presence and effect of an atmospheric inversion.	Detonation of a significant proportion of the cloud is consistent with the far-field damage (e.g. simple calculations show that detonation of 100,000m^3 would give overpressures of 2 kPa at a distance of 1.7 km).
Similarity to previous incidents	Previous incidents that most closely matched Buncefield were not consistent with a deflagration.	Previous incidents that most closely matched Buncefield were consistent with a detonation.

(pink)	Scenario is not consistent with the evidence
(yellow)	Not possible to be conclusive (due to nature of evidence or extent to which a scenario was studied)
(green)	Scenario is consistent with the evidence

A strong deflagration reaching 400 – 500 kPa (just short of DDT), could have produced overpressures of the order of 100 kPa in the Northgate Building car park. This is short of the lower limit of 200 kPa derived from the damage analysis of the cars in the car park.. It may have been sufficient to damage the Northgate and Fuji Buildings as observed. However, the overpressures predicted from this scenario would be lower than those necessary to cause the observed damage to the switch boxes and drums on the HOSL and British Pipeline Agency (South) sites (see Figure 1). Furthermore, an explosion consisting only of deflagration is not consistent with the directional indicators outside the congested area, which point towards the source of the explosion, not away from it.

Acceleration of the flame up Three Cherry Trees Lane to DDT near the junction with Buncefield Lane, was indicated by the simulation with propane and fine congestion (Section 4.1.2). The overpressure profile outside the cloud (a long duration from the start of the positive phase before the start of the negative phase) that was well defined by CCTV records was found to be consistent with the detonation simulations. Damage patterns support the simulated overpressure decay from the edge of the cloud and the directional indicators are consistent with a detonation.

Near-field damage to objects on the HOSL and British Pipeline Agency (South) sites and far-field damage to buildings are also consistent with a detonation. The main uncertainty associated with the detonation scenario relates to the damage of the Northgate Building. This would have been considerably more severe if the cloud detonated through its full depth up to the face of the building. However, a detonation that fails before reaching the building, or one that is limited to part of the cloud depth near the building (or both) may provide an explanation that is consistent with the observed damage levels.

Further support may be found in past incidents. The accidents at Port Hudson and Ufa were described by the accident investigators as detonations. These explosions had a number of features that were in common to the Buncefield explosion. Of particular interest are the nature of the terrain and the presence of a very large quiescent cloud. Also of significance is directional evidence at Port Hudson.

4.4   ALTERNATIVE EXPLOSION MECHANISMS

A number of alternative mechanisms and characteristics are considered in more detail in Appendix E and their merits are discussed. These are:

- Mist explosion
- Multiple detonations
- Strong ignition
- Multiple ignitions
- Stratified explosion
- Flame acceleration due to dust particles
- Unsteady deflagration accelerated by forward radiation from the flame front
- Unsteady deflagration without radiative effects
- Cellular flames
- Chemistry effects
- Pancake shaped cloud
- Inhomogeneous fuel concentration

- Internal tank explosion
- Localised high overpressure
- Precursor event

At least one of these alternative mechanisms (unsteady deflagration accelerated by forward radiation from the flame front) warrants further research. This mechanism, along with its hypothesis in relation to the evidence, are summarised below.

Timings from CCTV, structural analysis and witness reports may be interpreted to show that the total duration of the explosion was 1600 ms. Given the maximum radius of the cloud was 240m this indicates an average velocity of 150 m/s. If flame propagation is episodic, *i.e.* comprises short periods of intense combustion (which generate the high overpressures) punctuated by pauses, then the apparent the low average flame speed can be reconciled with the high overpressures within the cloud.

Such a variation in burning rate may arise through a combination of thermal radiation and adiabatic compression. If forward radiation initiates combustion in suspended particulates the pressure will rise close to the flame front. If the particle density is sufficient, the resulting compression will initiate further ignition (in preheated particulates) further away form the flame front. This results in the initiation of ignition in an extended range. Still further out from the flame front particulates and gas are not pre-heated sufficiently to be ignited by adiabatic compression. When the pressure subsides gas associated with these more distant particles simply cools and is left at a temperature well below that required for spontaneous ignition. There is an extended delay until forward radiation brings gas and particles to the temperature required for ignition and the next cycle of rapid combustion can start. The distance scale over, which the flame progresses in each cycle is determined by the range of thermal radiation i.e. the length scale of the burned cloud.

The episodic character of the explosion also explains how appropriate particulates could be numerous and suspended in the gas cloud. Since the average speed is sub-sonic, relatively strong shock waves progress ahead of the flame and these can disperse and fragment objects such as dried leaves.

5   PROPOSALS FOR FURTHER WORK

The work undertaken in this project represents a major advance in the understanding of the Buncefield explosion. The work has also identified a number of areas that require further research. A few of these, although specific to the Buncefield explosion, will lead to a greater understanding of explosions of large unconfined vapour clouds and associated structural response.

The aim of the work is to provide a better understanding of:

- the characteristics and modelling of low wind speed dispersion;
- the characteristics of pancake shaped vapour cloud explosions;
- the effect of tress/vegetation on vapour cloud explosions; and
- the response of different forms of construction to vapour cloud explosions;

A series of work packages are proposed to achieve the above aim. These are:

WP1 - Explosion and structural response modelling

WP1.1 Modelling of pancake shaped clouds

- Extension of the initial work described in Appendix H;
- Pre-prediction of the proposed pancake shaped vapour cloud explosion tests to aid the test design;
- Parametric studies to consider the decay in overpressure from the edge of the cloud;
- Study of the effects of cloud geometry, ignition location, effects of obstacles such as buildings (treated as solid obstacles – i.e. excluding interaction with structural response) on the overpressure pattern.

WP1.2 Structural modelling

- Re-analysis of Northgate Building cladding panels using load profiles generated from WP1.1. This could include a range of cladding panels as well as overall structural response;
- Generation of PI diagrams for a range of forms of construction (e.g. multi-storey steel framed buildings, multi-storey concrete framed buildings, steel (portal) framed industrial buildings, brick/masonry residential buildings).

WP2 – Characteristics of pancake shaped vapour cloud explosions

A test programme will be conducted to study the characteristics of pancake shaped vapour cloud explosions. A cloud radius of 25m is envisaged. Alternatively, by using a 90° wedge, a radius of 50m can be tested.

Overpressures will be measured and high speed video recordings will be made. A range of objects will be subjected to the overpressure generated at a range of locations within and outside the cloud. These would include metal boxes and drums, cars, painted posts and smoked plates.

WP3 – Effect of trees on vapour cloud explosions

This work package comprises a series of tests to study the effect of trees on gas explosions. The following parameters are envisaged:

- Length of row of trees (to include undergrowth): circa 60 m;
- Height of trees: 3m.
- Width of undergrowth: to be varied between 1 and 4 m;
- Density of undergrowth;
- Type of trees: based on a survey of what is currently used – allow for up to 5 different types;
- Fuel type: 3 different fuels

In addition to high speed video records of the tests, instrumentation will be provided to measure the following parameters:

- Overpressure
- Flame speed
- Fuel composition and concentration
- Gas velocity

WP4 – Characteristics and modelling of low wind speed dispersion

HSL are currently conducting experimental work to study the effect of aerodynamic break-up of dense liquid cascades and of the impact of liquid streams on a wind girder and/or the ground the behaviour of the vaporising cascade. The results of the HSL work will provide the source term for this Work Package. Using this data, dispersion modelling will be carried out to investigate the following:

- Effect of the cascade on the development of large vapour clouds;
- Effect of bund design on the development of large vapour clouds.

WP5 – Design implications

Design implications will be identified based on Work Packages 1 – 4. In particular, the following aspects will be addressed:

- Modelling low velocity vapour cloud dispersion
- Modelling of congestion caused by trees and undergrowth
- The effect of storage tank layout on explosion characteristics
- The effect of trees on explosion characteristics
- Structural damage associated with vapour cloud explosions

It is proposed that the above work is undertaken within a joint industry project over a period of 24 months.

In addition, the project has identified a number of areas which may play a part in large vapour cloud explosions where fundamental research is needed. These are:

- The response to high intensity thermal radiation of porous particulates (especially dry leaf fragments) that have been immersed in flammable vapours for an extended period;
- Data on burning velocities and Markstein numbers of key explosive mixtures at higher temperatures and pressures;

- Data on ignition delay times of key explosive mixtures at lower temperatures and pressures and on deflagration to detonation transition;
- Nature of premixed turbulent combustion in boundary layers.

This fundamental research is suitable for academic institutions and specialist technical organisations and is of a longer term nature. It is suggested that this should be progressed through the normal funding channels for academic research (e.g. EPSRC, European Framework, etc.).

6 CONCLUSIONS

The Buncefield Explosion Mechanism Project (Phase 1) has focused on the data available from the accident that could provide the most information on the nature and characteristics of the explosion. Examination and comparative analysis and testing have shown that overpressures within the gas cloud were uniformly high (in the region of 200 kPa or more). There appeared to be no distinctions between objects in different terrain (car parks, tank farms, open grassland and belts of trees). The only exception was the interior of the emergency pump house, where the explosion started and where the evidence suggests significantly lower overpressures.

Another feature of the explosion was that overpressures decreased very rapidly outside the edge of the vapour cloud. However, low overpressures (~5 kPa) were evident at significant distances (up to 4 km) from the explosion. It is thought that a large cloud size as the source and an atmospheric inversion contributed to this. The net drag impulse on objects susceptible to drag was towards the general direction of the ignition source within the gas cloud, and away from the ignition source outside the gas cloud.

Deflagration and detonation mechanisms were studied to ascertain how either might explain the evidence and characteristics of the Buncefield explosion. Based on the near-field damage to objects and the directional indicators, it is concluded that Buncefield required more than a deflagration in which congestion provides the mechanism for flame acceleration.

Detonation was found to be consistent with:
- the long duration between the start of the positive phase and the start of the negative phase;
- the high near-field overpressures and associated damage to objects;
- the rapid drop in overpressure across the cloud boundary;
- the directional indicators both within and outside the cloud; and
- the far-field damage to property.

A detonation scenario in which the cloud detonates up to the face of the building is not consistent with the near to mid-field structural damage. However, a detonation which is limited to part of the cloud depth may be consistent with the observed damage. Further work is needed to confirm this.

A preliminary examination of alternative mechanisms (that are not as well understood as detonations and deflagrations) was also undertaken. Of these, a mechanism involving unsteady combustion with forward radiation warrants further research.

On the basis of the work undertaken in this project, it is concluded that the most likely scenario at Buncefiled was a deflagration outside the emergency pump house that changed into a detonation due to flame acceleration in the undergrowth and trees along Three Cherry Trees Lane. The detonation extended to a significant part of the remaining vapour cloud.

Experimental and analytical work to be completed in a second joint industry funded phase of the project has been defined. The aim of the proposed work is to improve the understanding of low wind speed dispersion, large shallow vapour cloud explosions and the response of various forms of construction to such explosions.

Buncefield Explosion Mechanism Phase 1

Volume 2

Steel Construction Institute
Silwood Park
Ascot
Berks SL57QN

The Buncefield explosion (11 December 2005) resulted in tremendous damage to the outlying area and huge fires involving 23 large oil fuel tanks. One important aspect of the incident was the severity of the explosion, which would not have been anticipated in any major hazard assessment of the oil storage depot before the incident. The Buncefield Major Incident Investigation Board (MIIB) invited explosion experts from academia and industry to form an Advisory Group to advise on the work that would be required to explain the severity of the Buncefield explosion. This MIIB Advisory Group carried out a preliminary assessment of the forensic evidence obtained following the incident and of the results of experiments carried out by the Health and Safety Laboratory – HSL. The objectives of this assessment were:

■ to determine whether a sequence of events could be identified that would explain why such severe explosion pressures were generated; and
■ if this was not possible, to recommend to the Board what further actions would be required to explain the explosion severity.

The Advisory Group attempted to explain the explosion event at Buncefield using deflagration, detonation or a combination of both. It also examined other possible means of flame acceleration. However, it was not possible to identify a single scenario that could explain all aspects within the time available.The Advisory Group therefore recommended that a joint industry research project be initiated that would, in its first phase, have the objectives of completing the assessment started by the Advisory Group and, on the basis of this, of defining the requirements for further research. The research undertaken, both experimental and theoretical, and has lead to a better understanding of likely explosion mechanisms and explanation of the observed damage.

HSE Books

CONTENTS

APPENDIX A   RELEVANT DATA COLLECTED FOLLOWING THE BUNCEFIELD ACCIDENT

A.1.   INTRODUCTION

This appendix provides a summary of evidence relevant to the analysis of the explosion mechanism, including:

- The size of the flammable cloud.
- Witness statements
- CCTV records
- Ignition location

Evidence related to overpressures and directional indicators are not included in this appendix, but are discussed separately in Appendix B.

In general, the evidence is provided with limited interpretation. Where interpretation is provided it is the view of the Technical Group that it is not contentious.

A.2.   CLOUD SIZE

Investigation carried out following the incident identified burned areas that were consistent with the thermal effects from the combustion of the vapour cloud and not thermal radiation produced by the liquid pool fire following the explosion. Though these areas were not contiguous, it was possible to interpolate between them to provide an estimate of the extent of the flammable cloud.

Figure A.1 shows the estimated flammable cloud extent (black dashed line). The area covered by the cloud would have been approximately 120,000 m^2.
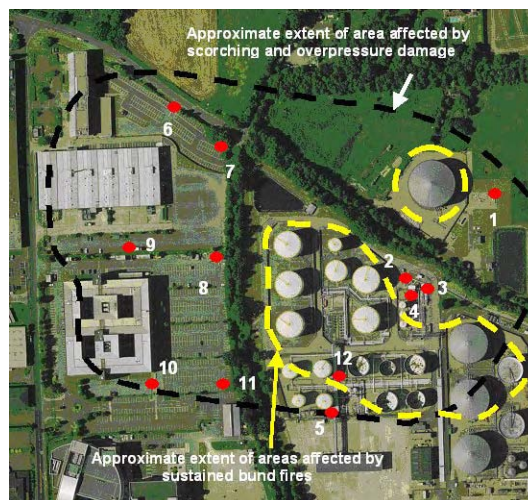
Figure A.1 Extent of the Flammable Cloud as Interpreted from Burned Areas

The cloud depth can be estimated from the CCTV records on the assumption that the flammable limit corresponds closely to the top of the mist observed as the cloud developed. Not all areas of the cloud were recorded; however an estimate of an average depth of about 2 metres would not be unreasonable.

This suggests that the volume of the cloud with a concentration was above the lower flammable limit was approximately 250,000 m^3 (to the nearest 50,000 m^3).

A.3. WITNESS EVIDENCE

There were a relatively large number of people very close to the edge of the vapour cloud who were consequently well placed to see and feel the effects of the explosion. There were nine witnesses who described the explosion. Eight of these were interviewed by the Police within a few days of the incident and provide useful descriptions. At the time of these interviews the incident was being investigated by the Police as a possible bomb explosion. The interviewers had no knowledge of, or interest in, vapour cloud explosions. A further witness was interviewed by HSE several weeks after the incident, as part of a series of interviews of people in the vicinity who had been affected by the explosion. Again the interviewer had no specific knowledge of vapour cloud explosions and the questions focussed on the witness's experiences.

The locations of witnesses are shown in Figure A.2. It can bee seen that witnesses were located at various points around the edge of the vapour cloud.
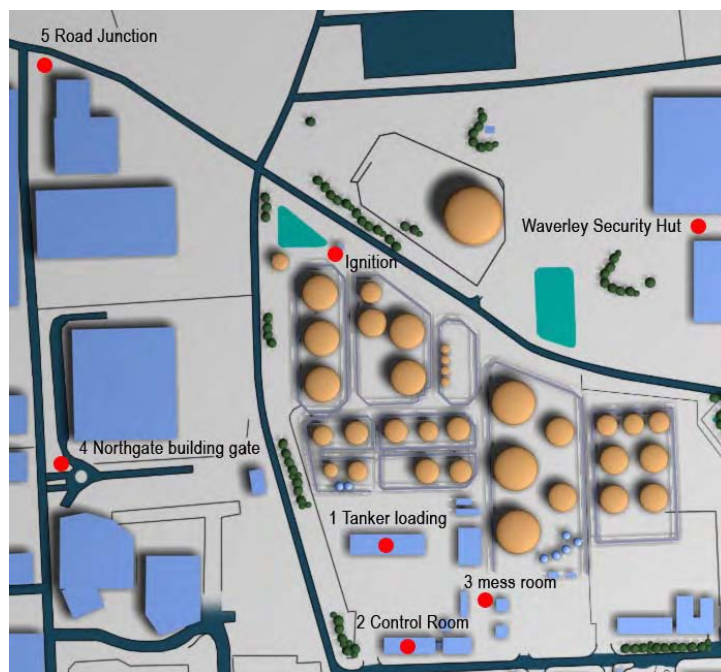
Figure A.2 Locations of Key Witnesses at the Time of the Explosion

The witnesses uniformly describe an explosion that consisted of a sequence of events. They all indicate that this lasted for a period of time. This is described variously as a few moments or several seconds. They also describe seeing or hearing the initial stages of the explosion event before they were affected by the overpressure. The initial stages are described as rushing or roaring noises, some of the witnesses saw the spreading out of the ignited vapour cloud. The witnesses then describe hearing a very loud bang. Effects of the explosion depend on where the witnesses were located; some were blown to the ground, others describe damage to the rooms they were in. None of them mention any temporary or permanent damage to their hearing.

A.4.   EFFECT ON WITNESSES

A number of witnesses clearly describe physical effects of the explosion, which is summarised in Table A.1.

Table A.1 Physical Effects of Explosion on Witnesses

Witness location	*Observations*
Tanker loading	Tankers were shaken. Witnesses were blown from their feet to the ground
Control Room	Witness was blown across the room
Mess room	Ceiling of room damaged and objects blown around the room
Northgate building gatehouse	Door and windows were blown in
Junction of Boundary Way and Three Cherry Trees Lane	Witnesses were blown from their feet to the ground
Waverley security hut	Witnesses were blown from their feet to the ground

None of the witnesses suffered hearing damage. Information supplied by the UK MOD indicates that rupture of eardrums can occur at overpressures above 35 kPa and there is a 50% chance of eardrum rupture at 100 kPa. Some of the witnesses were inside buildings and this would have provided some attenuation of the overpressures.

A.5.   CCTV RECORDS

The development of vapour cloud (made visible by a water vapour condensation aerosol) was shown in detail by numerous cameras on the Buncefield site and in the car parks of buildings closest to the site (Northgate and Fuji Buildings). These images are of great interest in confirming the cloud extent and depth but were surrounded by the vapour cloud and destroyed by the explosion – the last images recorded correspond to the seconds prior to the blast or a few hundred milliseconds after ignition (prior to the arrival of the shock wave).

Fortunately, the explosion itself was recorded by a number of cameras located outside the vapour cloud. These provide a record of illumination throughout the explosion and the arrival of pressure waves with frame rates of 3-25Hz).

The locations of the CCTV cameras used in the analysis of the explosion are shown in Figure A.3 below.
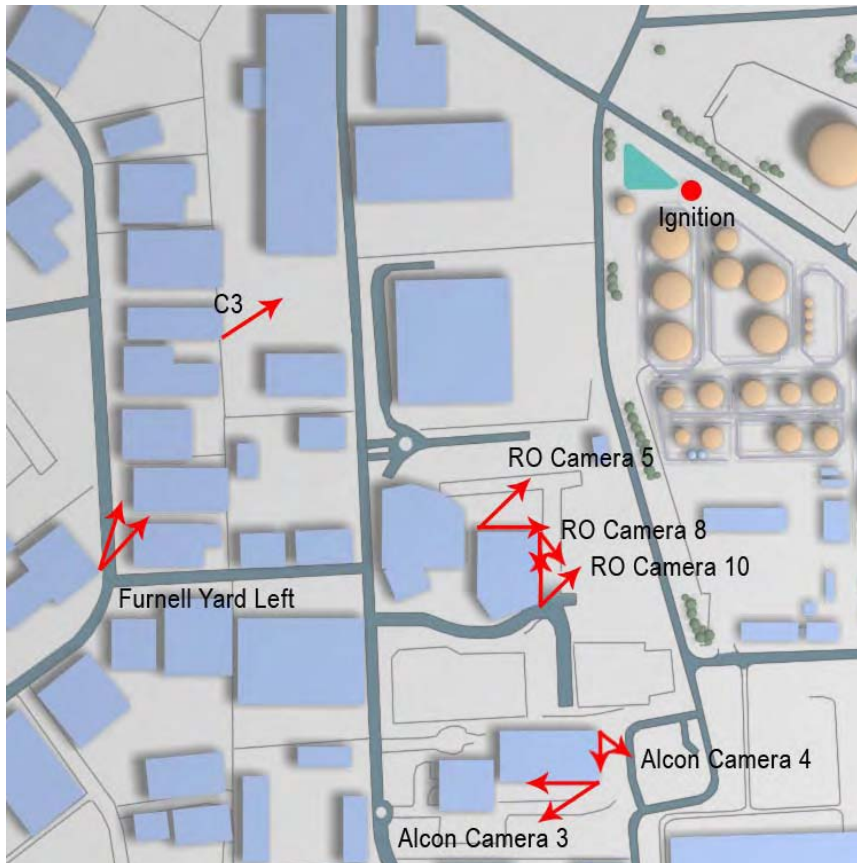
Figure A.3 Location of CCTV Systems

Once triggered, the RO images were recorded at 3Hz. The images shown in the appendix are labelled with the time. For Cameras 5 and 10, the early stages of the explosion are underway in the first image. Camera 8 triggered earlier and had been recording for some seconds prior to the explosion. Frames recorded by the RO cameras 5, 8 and 10 are given in Table A.2 along with comment on the changes being seen at each stage.

The Furnell images were recorded at variable intervals. Images shown in Table A.3 are from Furnell yard left camera (YL) and are labelled with the 25 Hz replay frame number. The analysis refers to images by this number and/or by the time after the initial image where an increase in light is observed.

The Alcon images were recorded (in groups of 4) at a rate of up to 20 Hz. This CCTV system is more sophisticated than the others in that significant quantities of data are stored in RAM prior to writing to disc. The system can therefore increase the framing rate of the record slightly in advance of (as well as during) a significant event. Frames from the Alcon cameras are not provided in this appendix.

In all cases the cameras provide information not only on illumination from the explosion, but also on the shock waves generated by the event. In particular the timing of the arrival of the first shockwaves is very well defined by the onset of camera shake.

Table A.2 Camera Frames taken from RO Cameras C5, C8 and C10

Time (ms)	Camera C5	Camera C8	Camera C10	Commentary
-666	Not recorded		Not recorded	Camera C8 was the only camera of the three that recorded at this time. Video frames before this point are all the same.
-333	Not recorded		Not recorded	Although not certain, there is possibly some increase in the light from the preceding frame.
0				Brightness at the top of C5 and C10 views. Increase in brightness at C8. Indicates that the event is definitely underway at this point. Cloud can be seen in Northgate park on C10.

Time (ms)	Camera C5	Camera C8	Camera C10	Commentary
333				Significant increase in brightness in all views. Lighting suggests an event happening to the north of these camera locations. No evidence of overpressure at the camera location at this time.
666				Camera C10 gives the impression of reducing light levels, whereas C5 and C8 show increasing light levels. Camera C5 suggests view suggests that flame has propagated to the cloud edge, though this is by no means certain. No evidence of overpressure at the camera location at this time.
1000				Increased light levels on C8 and C10. Evidence of overpressure arrival at all three cameras. C5 blurred and seems to suggest damage to building. Chair and paper have moved at bottom right of C8 frame along with other small items. C10 camera has moved upwards.

Time (ms)	Camera C5	Camera C8	Camera C10	Commentary
1333				Items falling off building in C10. There appears to be some dust produced by the explosion hitting the building. Possible that C10 shows the start of the rarefaction at the top of the frame
1666				General obscuration of view. If this is condensation of water vapour in the atmosphere, it indicates that the rarefaction phase has arrived at the building.
2000				Continuation of rarefaction phase. Bright flame or combustion products still evident on C10.

Time (ms)	Camera C5	Camera C8	Camera C10	Commentary
2333				Fog seems to be clearing, evidence of continuing bright flame on both C5 and C10.
2666				Fog has definitely cleared on C10. C5 has moved, possibly hit by debris. Still bright flame on both C5 and C10.
3000		Not included		Brightness of flame on C10 seems to be diminishing.

Table A.3 Camera YL at Furnell

View	Frame Number/Time (ms)	Comment
	45-47	No change in light levels
	48/0	First change in light levels, times below measured relative to this point
	53/200	Light level increasing
	55/280	Light levels continue increasing
	57/360	Light levels apparently drop though this may be due to the camera adjusting its sensitivity
	71/920	Light levels increasing

Table A.3: Camera YL at Furnell (continued)

View	Frame Number/Time (ms)	Comment
	73/1000	Light levels continue to increase and image eventually whites out.
	75/1080	
	78/1200	
	82/1360	Light levels apparently start to drop (though it may again be the camera self adjusting). As the camera has not moved, overpressure from the explosion has not reached this location yet.
	84/1440	
	87/1560	
	89/1640	Overpressure from explosion causes camera to move.

Table A.3: Camera YL at Furnell (continued)

View	Frame Number/Time (ms)	Comment
	96/1920	Camera continues movement with some streaking of the image.
	98/2000	
	100/2080	
	103/2200	Movement of camera reduces
	105/2280	Debris apparent in field of view
	107/2360	Dust and possible mist from rarefaction

View	Frame Number/Time (ms)	Comment
	109/2440	Continuation of possible rarefaction.
	121/2920	
	123/3000	Atmosphere clears, dust cloud extends across view.
	125/3080	
	128/3200	
	132/3360	

Camera C3, located on a building to the west of the Northgate building appears to have captured the early phases of the explosion in a single frame. Figure A.4 shows two frames from this camera with frame numbers 180 and 204. With 40 ms between each frame this equates to a time difference of 960 ms between the two pictures.

Figure A.4 View from Camera C3

It can be seen that on the second frame flame can be seen to the left of a building. Figure A.5 shows two lines of sight from this camera to the left of the Northgate building, which must be the building casting the shadow in the second frame. The flame must be within these two lines of sight and if it is assumed it is within the tree line on Three Cherry Trees Lane, then the red dot shows the flame location.

Figure A.5 Line of Sight for Flame Recorded by Camera C3

The camera appears to have captured the very beginning of the event. Unfortunately the next frame recorded was some time after the explosion. However, the images captured strongly suggest that in a time period of less than 1 second, ignition occurred and the flame was propagating along the tree line.

A.6.   CAMERA SHAKE ON FURNELL YL CAMERA

It is possible to analyse the movement of the Furnell YL camera to determine the displacement of the camera (by displacement of the image) and the speed of the movement of the camera by the degree of the streaking on the image.

Figure A.6 shows the results of this analysis, with the colour coding indicating the degree of streaking on the camera.
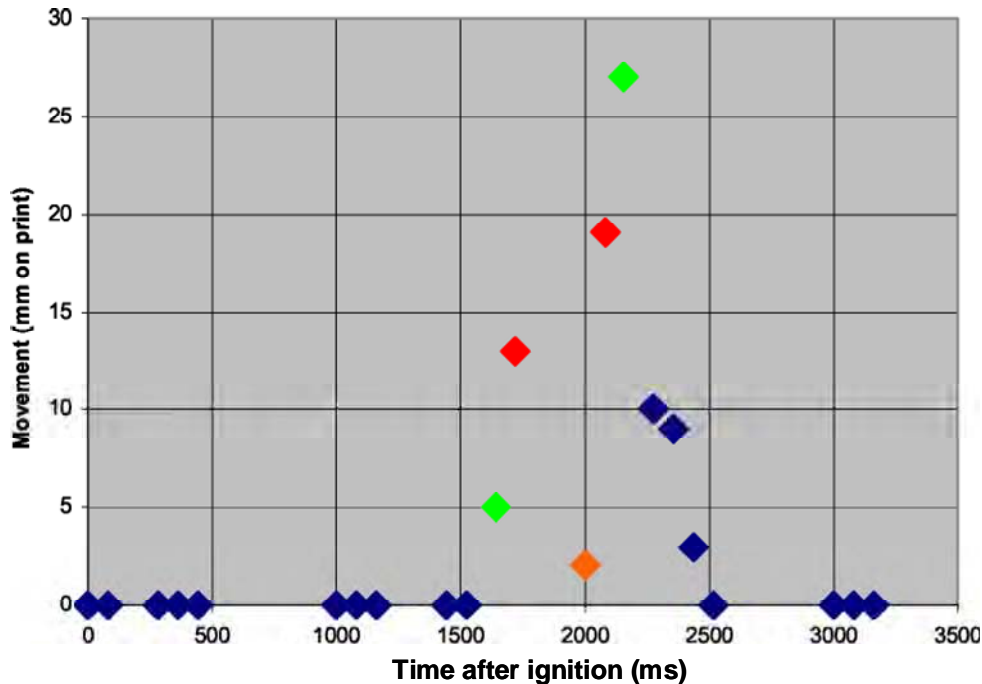
Figure A.6 Displacement and Speed of Movement of Camera YL (Coloured by extent of streaking of bright points on image, Blue <2 mm, Green 2-5 mm, Orange 5-10 mm, Red >10 mm)

A.7. IGNITION LOCATION

A witness was at the Waverley Building security hut and reported seeing the explosion start to the left of the water tank on the HOSL site. He reported seeing a flash of light. Figure A.7 shows the line of sight this witness had (yellow line). The Pump House is to the right of this tank as seen by this witness. The evidence from this witness is therefore consistent with ignition occurring in the Pump House.

The CCTV records from Camera C3 also indicate ignition occurred at the north end of the HOSL site.

In addition to this evidence, it is also known that:

• The Pump House suffered an internal explosion.
• The explosion occurred immediately after the fire water pumps were started.
• The Pump House had been within the vapour cloud for some time. This would allow time for a flammable mixture to build up within the building.

There is, therefore, a weight of evidence pointing towards the Pump House being the source of ignition. As will be seen in Appendix H the directional evidence also supports an event that started at the north end of the HOSL site.

It was therefore concluded that the analysis of the Buncefield explosion would be based on ignition within the Pump House.
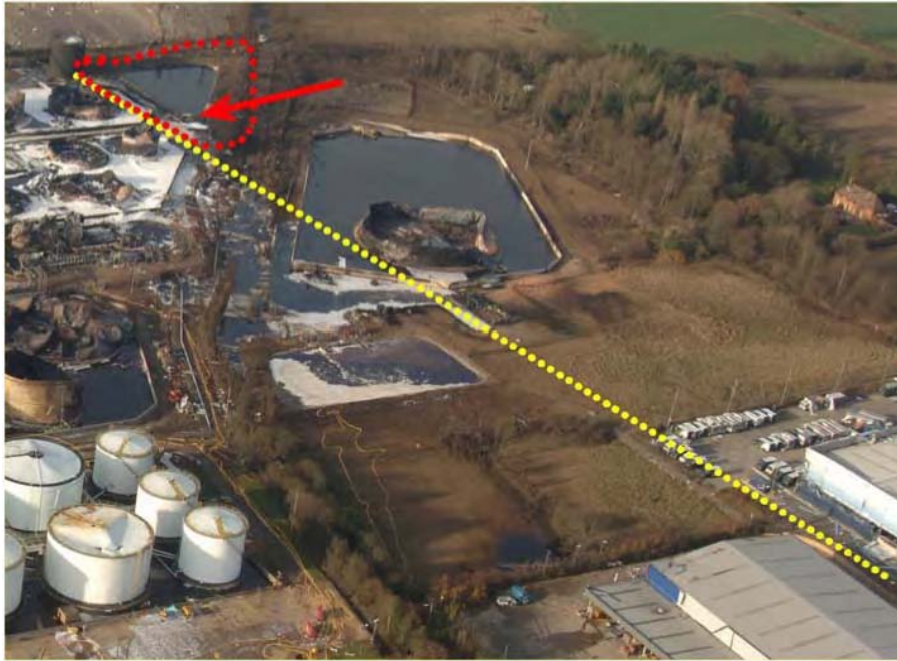
Figure A.7 Witness view of the surviving (water) tank. Locations on the site to the right of this tank are indicated by the red dotted line. The Pump House is indicated by the red arrow

APPENDIX B   REVIEW OF EVIDENCE ON OVERPRESSURES

B.1.   INTRODUCTION

The objective of this work package is to provide overpressure and explosion propagation direction information across the Buncefield site and immediate surrounding area such as the car park. This information is needed in the determination of explosion mechanisms which are described in other appendices (deflagration, detonation and novel mechanisms) in this report.

In the body of the gas cloud, there were very few large objects and they were located towards the edge of the gas cloud, e.g. the Northgate Building. A closer study of the site revealed that there were small objects, e.g. switch boxes distributed across the site and immediate surrounding areas. These objects could be used as overpressure indicators. The final state of these objects, after the passage of the explosion, whether undamaged or deformed, provides indication of probable overpressure in their localities. Figure B.1 gives an example of crushed objects which were found to be distributed widely across the site. We did not find any uncrushed objects except inside the pump house.

There were also objects which were exposed directly or indirectly to drag forces, e.g. abrasion on lamp post, fence post, etc. Study of these objects provided data on explosion propagation direction across the Buncefield site. The focus of this appendix is to quantify the overpressure and direction distribution based on these small objects. The assessment of buildings is the subject of a separate appendix (APPENDIX G).

Theoretical analysis, laboratory testing and field experiments were carried out to establish a lower bound of overpressure in various parts of the Buncefield site. Field experiments included tests on objects in a gas explosion chamber and in the open (subjected to a High Explosive (HE) blast wave). There were limitation to what could be achieved in these experiments; they were not commissioned by the Phase 1 Project specifically to address this issue but funded and conducted for other purposes by bp and UK MOD. Yet, they provided very useful data which were not available otherwise. This is a testament of the high level of cooperation offered by these organisations. Likewise the FE analysis reported in this Appendix was part of a separate ongoing project at Kingston University. The Phase 1 Project acknowledges the assistance given by bp, Kingston University, and the UK MOD in accommodating Phase 1 requirements, and the UK HSE for providing additional funding to purchase test pieces (cars and switch boxes).

B.1.1. Overpressure indicators:

The most useful types of object that directly showed the effects of raised side-on overpressure were lightweight, ductile metal enclosures. The following types of object were studied and they were found within the area covered by the cloud at Buncefield: steel junction boxes, cars and vans, steel drums, tanks, and drain covers.

The assessment of these objects is described in more detail later. An album of objects showing damage of this kind has been compiled – with location information some of these are reproduced here for illustration.

B.1.2.   Directional indicators

In addition to overpressure distribution, work was also carried out to determine the direction of propagation of the explosion. Gas explosion produces drag forces. The direction of this gives an indication of direction of propagation of the explosion front.

There were objects that are primarily susceptible to drag forces at Buncefield; they include trees, lamp posts, CCTV camera masts and fence posts.

It is possible for objects to be exposed to high overpressures but low drag forces – for example a small area near the centre of a symmetric explosion. But in the case of damage caused by exposure to a progressive explosion front, the degree of drag related damage is a useful indicator of the flame speed and hence overpressure.

B.1.3.   Potential Impact of Overpressure on Lightweight Metal Enclosures

A large steel sheet restrained at the edge, of 1-2 mm thickness is expected to deflect of order 1 m in an explosion with overpressure of about 100 kPa. For small metal enclosure, the expected permanent deflection is much less due to (a) compressive resistance due to the strength of the box, (b) resistance of solid objects inside the enclosure and (c) adiabatic compression which counters the compressive force exerted by an explosion.

The assessment of pressure from deformed object is not straightforward as the objects deformed by gas explosion could recover some of its original volume, e.g. the oil drum in Figure B.1 which recovers most of its original shape after the passage of the explosion. In the following chapter, each of the object types was assessed to provide estimate of overpressures.

The following sections in italics provide further explanations on the use of light weight metal enclosure as overpressure indicators, and can be skipped.

B.1.4.   Inertia effects – what counts as a lightweight metal enclosure?

Most of the objects listed above are fabricated from steel sheet with a thickness of around 1 mm. The typical value of overpressure within the cloud was at least 200 kPa (see sections below). If unrestrained a 1 mm sheet will respond to a pressure differential of 200 kPa by accelerating at an average rate of (linear rate of pressure increase is assumed):

a = 0.5 * 200,000 /7.5 = 13,300 m/s2

(The density of steel is taken as 7500 kg/m3)

Assuming a typical duration of the overpressure pulse is approximately 20-30 ms, the resulting maximum velocity U and displacement (during pressurisation) S of an unrestrained piece of sheet steel can be estimated as:

U = at = 0.025 × 13,3000 = 330 m/s

S = ½ at2 = ½ × 13,300 × (0.025)2 = 4.2 m   (note deflection will continue)

(a thicker steel of a few mm still give significant deflection of order 1 m)

These figures are approximate (as the movement will eventually affect the pressure applied) but it is clear that the inertia of such sheet material will not prevent very large movement (if the sheet is not restrained). In fact extremely large displacements of various cladding sheets were observed around the site.

The deflection of a metal sheet forming part of an enclosure is influenced by a number of factors; these include:

1.   The overall plan dimensions of the sheet. Generally, the larger the dimensions of the sheet, the greater the deflection. For a sheet simply supported on two sides and acting as a simple beam strip subjected to a uniformly distributed load per unit length, the deflection increases in proportion to the span to the power 4. The same is true for a square plate simply supported on all sides and subject to a uniformly distributed pressure causing small deflections. However, as the deflection increases, nonlinear effects due to membrane stretching come into play thereby casing the plate to exhibit stiffer behaviour. This effect comes into play once deflections have exceeded the thickness of the plate and continues until plasticity causes a softening in behaviour.

2.   Boundary/support conditions. The edge fixity of each face of the enclosure contributes to reducing the deflection of that face under applied loading. For example, in the case of a steel box enclosure, a steel sheet supported on all four sides (by other sides of the box) will deflect less than one supported on three sides (e.g. as in the case of an open sided box).

3.   The compressive strength of objects within the enclosure. The faces of the enclosure deform until they come into contact with strong or heavy objects within the enclosure. Examples of such restraining objects include terminal strips in a junction box, support framework in a car door, liquid in a drum, etc.

4.   The pressure rise associated with adiabatic compression of the enclosed gas - the internal pressure rise partially offsets the external overpressure. Comparing the ratio of volumes before and after compression allows an estimate to be made of the internal pressurisation. For example, a box reduced in volume to 40% of its original volume indicates an internal overpressure of approximately 200 kPa.

B.1.5. Shape recovery

Some caution has to be exercised in deriving estimates of the maximum overpressure from the final (deformed) shape of enclosures because of the possibility of continuing deformation and shape recovery (e.g. due to energy released from adiabatic compression) after the external pressure declined.

The drum in Figure B.1 showed almost a complete volume recovery when the external pressure falls – although the creasing associated with severe plastic deformation remain. Fortunately most electrical or hydraulic junction boxes have large hinged fronts that provide a good seal during rapid compression but fly off or leak rapidly and relieve the internal pressure during the (typically slower) phase of external depressurisation. Many such steel enclosures were found where close forming of the shell around objects within indicated that venting had been rapid enough to prevent significant volume recovery (right picture in Figure B.1).

Figure B.1 Examples of object which recover its volume after the passage of overpressure (drum on the left) and one which deformed with little sign of volume recovery (switch box on right).

Similarly, broken windows rapidly and effectively vent most vehicles, as the pressure falls. There are many examples where (for example) door panels remain closely formed around the underlying framework or car roofs remain pressed into seats; in these cases the maximum extent of plastic deformation has been preserved.

B.2.   OVERPRESSURE ESTIMATES

B.2.1. Introduction

A range of studies have been carried out to allow the observed damage to be interpreted in terms of overpressure.

B.2.2. FE analysis

FE analysis was carried out using ANSYS. The analysis was first used to predict the results from the gas explosion test. Then the analysis was extended to include higher overpressures and different durations for switch boxes and oil drums. The results of this assisted in the interpretation of gas explosion tests and the planning of the HE tests.

B.2.3. Static hydraulic tests to assess static load response

Static hydraulic tests were carried out using the diving equipment test chamber at HSL. One of these is shown in the Figure B.2.

Figure B.2 A diving equipment test chamber used for hydraulic testing of switch boxes. The grey box in the centre of the chamber is the switch box. The yellow gas cylinder provides the pressure source.

B.2.4. Testing in semi-enclosed gas explosions

A short programme of gas explosion tests was carried out at GexCon, Norway using the medium scale offshore test rig Figure B.3. This test rig is a scale model of a compression module on an offshore platform. The rig is 8 m long. Three tests were carried out generating maximum overpressure of 60 kPa, 110 kPa and 180 kPa. The first test was at the lowest overpressure, and the last was at the highest.

Figure B.3 The medium scale gas explosion test rig operated by GexCon, Norway.

In each of these tests, one empty oil drum, two 600 mm by 600 mm switch boxes and one engine oil filter were placed inside the test rig.

Figure B.4 Test objects exposed to explosion overpressure loads: an empty oil drum (left) and two switch boxes at different locations (right)

B.2.5. Testing of response to blast wave from HE

High Explosion charges of about 77 kg and 170 kg of TNT equivalent were used to generate blast waves to test the response of switch boxes. The larger charge size was used to test cars. Test objects (cars and boxes) were placed at distances known to produce specific overpressures required for the tests. Overpressure sensors were placed close to test objects for actual pressure measurement and at various distances to capture the far field pressures.

B.3. SMALL OBJECTS FOR PRESSURE INDICATORS

The rest of this section describes the observed state of small crushed objects (e.g. switched boxes, cars, etc.), and work to estimate overpressures required to deformed these objects.

These objects were widely distributed across the Buncefield site. This is shown in Figure B.5 below. In addition to locations of objects (given by colour dots), location of items illustrated in figures in this Appendix is also given (white box with number). The locations of these figures are given below:

Number 1:   Figure B.1   Crushed drum
Number 2.   Figure B.1   Crushed hydraulic switch box
Number 3.   Figure B.6   Creased drums
Number 4.   Figure B.8   Drum with inward plastic deformation
Number 5.   Figure B.10   Crushed electrical connection box
Number 6.   Figure B.17   Crushed oil filter
Number 7.   Figure B.19   Damage car and close up of tyre
Number 8.   Figure B.19   Crushed car
Number 9.   Figure B.27   Line of crushed cars
Number 10. Figure B.28   Diesel tank in pump house
Number 11. Figure B.28   Water tank in pump house
Number 12. Figure B.31   A directional indicators (left most figure)

A version of Figure B.5, using schematic site drawing, is also produced in Figure 4 in the main report
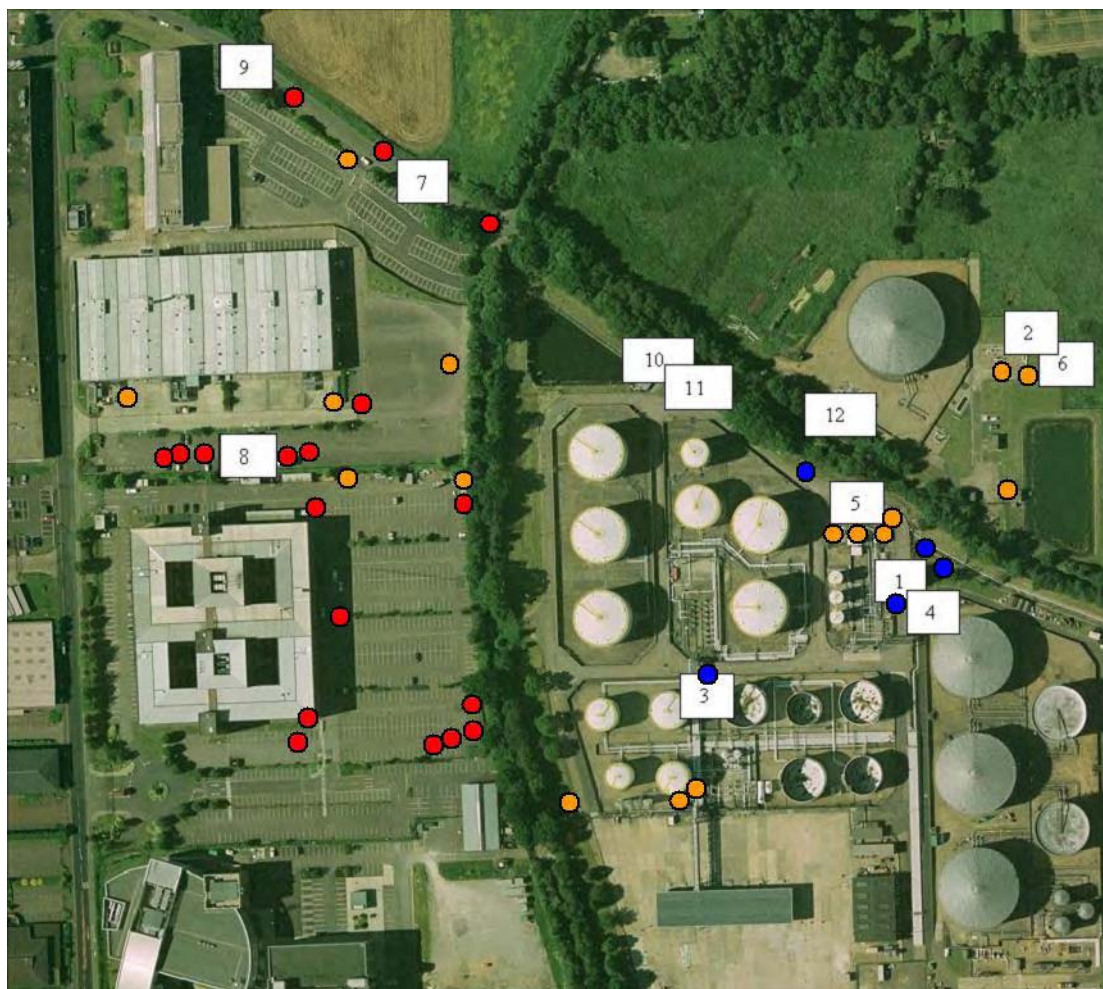
Figure B.5 Distribution of small objects across the Buncefield site.
Locations of small objects are given by colour dots: red for vehicles (cars and vans), blue for drums and orange for other enclosures (switch boxes, fuel tanks, drain covers, oil filters, parking barrier supports, etc.). Locations of objects illustrated in figures in this appendix are also given (see text).

B.4. STEEL DRUMS

B.4.1. Observations:

Steel drums were located in various parts of the site. These included full, partially empty and empty examples. In many cases the prior location of the drums could be determined. Overall translational displacements during the explosion were small (<5 m) which mirrors the behaviour of cars.

A typical group of drums from near the centre of the site is shown in Figure B.6. The fill level can be judged from the fire damage to the exterior. These drums were compressed during the explosion (when they were vertical) and then subjected to severe and prolonged heating. Internal pressurisation during fire engulfment has domed out the end caps but clear signs of severe plastic deformation of the sidewall in the ullage remain.

Figure B.6 A group of nearly full drums near the centre of the site. Prior location (left) and final form (right).

B.4.2. Assessments

The deformation characteristic of the top of the drum is a good overpressure indicator; this includes the end plate and the section of side wall near the end plate.

Similar deformation of the top of a drum can be reproduced in a static hydraulic test. Figure B.7 shows the result of an HSL test at an imposed pressure of 300 kPa. A pressure of 200 kPa caused no deformation of the sidewall.

Figure B.7 Fully plastic longitudinal sidewall buckling in the ullage. This was observed at above 200 kPa but less than 300 kPa.

In these tests, drums were filled with concrete up to the liquid level indicated by the drum in Figure B.7. This is necessary in a static test because the slow pressurisation allows movement of a liquid charge and inward buckling of the whole sidewall (at a pressure of around 100 kPa). This type of failure is not observed in an explosion because of the liquid inertia.

These results clearly indicate a static overpressure in excess of 200 kPa in this location.

A deformed empty drum from the northern edge of the site is shown in Figure B.8. In this case, the drum escaped damage by the bund fires.

HSL tests showed that the onset plastic deformation of the top is observed at a static overpressure of 200 kPa (Figure B.8); no such deformation was observed up to 150 kPa. This result indicates a static overpressure of (at least) 150 kPa.

24

Figure B.8 Plastic deformation of drum end cap: (left) a drum in Buncefield and (right) after a static pressure test at 200 kPa.

Gas explosion tests carried out on empty oil drums did not produce the level of deformation observed in both the static tests and objects in Buncefield at overpressure of up to 180 kPa. As expected, the oil drum was deformed to a greater degree as overpressure was increased. However, the deformation was largely restricted to the side, see Figure B.9. At the highest pressure test, the end plates of the drum exhibited a limited amount of distortion seen in Figure B.8 - it did not extend the whole circumference and the amount of deformation was small. The gas explosion test results on end plate distortion indicated an overpressure of over 180 kPa (~ 50 ms) and are consistent with those from hydraulic tests.
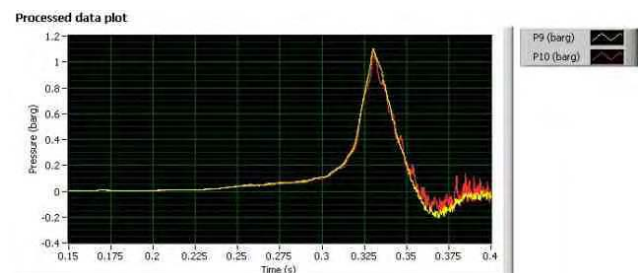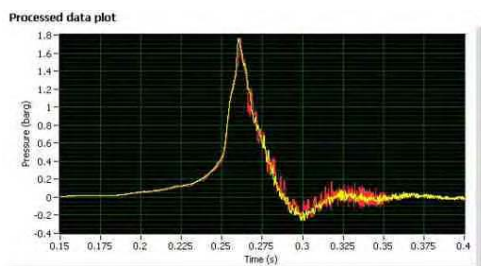
Figure B.9 Plastic deformation of an empty oil drum exposed to 120 kPa (left top) and 180 kPa (right top) in a gas explosion test.

B.5.   BOXES

The album of overpressure indicators includes a number of examples of crushed junction boxes. An example is shown in the Figure B.10.

Figure B.10 A crushed junction box, close to the northern edge of the HOSL site.

B.5.2. Testing of boxes in enclosed gas explosions

The switch boxes showed no sign of deformation or any damage except in the last test where the maximum overpressure was 180 kPa (Figure B.11). The damage suffered by the box was relatively minor, when compared with those observed in Buncefield. The maximum deformation on the front panel was measured to be 11 mm.

Figure B.11 View of the only switch box which had been deformed in the gas explosion test.

B.5.3. Exposure of boxes to shock waves from HE

A number of switch boxes were exposed to blast overpressure from HE in a number of tests. Two box sizes were used: 300 mm by 300 mm and 600 mm by 600 mm. The majority of these boxes were carbon steel; some of the 600 mm by 600 mm boxes were made of stainless steel.

HE produce pressure waves of different characteristics to those from gas explosions - blast wave from a HE has a much shorter duration compared with a gas explosion and the wave profile is also different. The impulse from this series of tests is expected to be much lower than those in the gas explosion tests described above. Even so, the results of these tests supplement those from other tests described in this appendix to provide indications of the magnitude of overpressure needed to cause the deformation observed in Buncefield.

In each test, boxes of the two sizes were placed at locations to receive specific overpressure loading for the explosive charge used. Figure B.12 gives a typical general arrangement; it can be

seen that for each of the box sizes, one box had the front face facing the charge; one had its side wall facing the charge.

Figure B.12 Typical arrangement of switch boxes in a explosive test.
(a) Two sets of boxes (600 mm by 600 mm and 300 mm by 300 mm) were set at a specified distance from the charge (left), and (b) one set in front of a wall (right). Pressure gauges were located close by and at the same distance as the boxes to the charge measuring side-on overpressure (centre of (b)) and reflected overpressure (right side of (b)).

Peak side-on overpressures in the tests ranged from 100 kPa to 800 kPa. The reflected pressure (pressure experienced by the side of the box that faced the charge) ranged from 320 kPa to 4 MPa. Both of these overpressure values are given in discussions below. The duration of the highest peak side-on overpressure was around 8 ms and the lower ones around 17 ms for the positive phase of the blast wave. These are within the range of pressure durations that are to be expected in detonations, and are shorter than what would be expected in a deflagration.

The characteristic damage was predominantly by crushing of the 'front' face. This is different from the damage observed in Buncefield where boxes were crushed on all faces (Figure B.10).

One of the characteristics of these HE tests is that pressure decayed rapidly at these levels of overpressure. Thus, the peak side-on pressure on the face closer to the charge is larger than that at the 'back' face. It is noted that in some cases, the 'back' face was pushed outwards (rather than crushed inwards). This is due to the effect of adiabatic compression. The crushing of the 'front' face caused an increase in internal pressure which deformed the 'back' face outwards.

These factors contributed to the difference in observed damage pattern between the boxes tested and those in Buncefield. The deformation suffered by the front face of boxes provided indicative overpressures required to crush boxes observed in Buncefield.

The following analysis focuses on the face closest to the charge.

B.5.4. 600 mm by 600 mm by 250 mm switch boxes

The larger front face is more susceptible to deformation (deflection) than the smaller side face. Consequently, the front face deformed more. Reason for this is already given in Appendix B.1.4.

Front of the box facing incoming blast: At peak side-on pressure of 100 kPa (reflected pressure of 320 kPa), the 600 mm box suffered very minor deformation. At 200 kPa (reflected pressure of 650 kPa), deformation increased to about 6 cm. At pressure higher than 470 kPa (reflected pressure of > 2.7 MPa), deformation of the front panel is similar to the depth of the box.

27

Side of the box facing incoming blast: the side of the box suffered less deformation. Deformation only started to occur at peak side on overpressure greater than 470 kPa (reflected pressure of 2.7 MPa).

Figure B.13 shows the deformation of the panels which faced the blast wave. These 4 boxes were exposed to 100 kPa, 200 kPa, 470 kPa and 800 kPa peak side on overpressure for the front face and the side face. The maximum deformations measured were 28 mm, 95 mm, 150 mm and 130 mm respectively for the front face. The deformation for the 100 kPa and 200 kPa tests were higher than those measured in the gas explosion test (11 mm) in which the impulse (and duration) was much larger. This indicates that the overpressure that caused this deformation could be closer to the reflected overpressure (320 kPa to 5.3 MPa).

Figure B.13 The final shape of 600 mm by 600 mm by 250 mm switch boxes exposed to overpressures from 100 kPa to 960 kPa peak side-on pressure (low pressure on left and high pressure on right in the picture). The left picture shows the deformation of the front panel which faced the explosive charge. The right picture shows the deformation of the side panel which faced the explosive charge.

B.5.5. 300 mm by 300 mm switch boxes

No significant deformation occurred until peak side-on overpressure exceeded 470 kPa (reflected pressure of 2.7 MPa) on the front face. The response of the side panel of the box was similar. The smaller deflections are due to the smaller dimensions of these boxes (which use the same thickness of metal as the larger boxes).

Figure B.14 The final shape of 300 mm by 300 mm by 150 mm switch boxes exposed to overpressures from 100 kPa to 960 kPa peak side-on pressure (low pressure on left and high pressure on right in the picture). The left picture shows the deformation of the

front panel which faced the explosive charge. The right picture shows the deformation of the side panel which faced the explosive charge.

B.5.6. Static hydraulic testing

Some static hydraulic testing of 300 mm × 300 mmm × 150 mm boxes has been carried out in a diving equipment test chamber at HSL (see Figure B.2). Pressurisation used air in a cylinder reservoir and was complete in approximately 2 seconds.

An applied overpressure of 100 kPa caused minimal pressure damage to the box as shown in Figure B.15.

Figure B.15 Two views of damage to the 300 mm by 300 mm switch box by 100 kPa overpressure: slight bowing of back but no plastic deformation of the front panel.

Figure B.16 Views of damage to box caused by application of 400 kPa overpressure – over a period of around 2 seconds. Large deformation of back and side – tearing of weld between back and sides. Some plastic deformation of front (final volume to initial volume ratio of 50%).

Application of a pressure of 400 kPa over a period of 2 seconds caused substantial plastic deformation of the box back and sides –Figure B.16. The front was only slightly deformed.

The pressurisation is slow enough to allow very large amplitude deformation via the first observed failure. This causes an internal pressure rise and tears welds - allowing rapid inflow of water. The lack of high amplitude deformation of the front of the box in Figure B.16 does not necessarily mean that this would not have occurred if the box had been exposed to a pressure rising rapidly to 400 kPa.

B.5.7. Overall interpretation of box data

The switch boxes were found to be unexpectedly strong. The smaller (300 mm by 300 mm) boxes were much stronger than the larger boxes (600 mm by 600 mm) in resisting overpressures. Static pressure tests showed that the box can withstand 100 kPa overpressure with minor damage. A 400 kPa static loading was capable of crushing a 300 mm by 300 mm switch box.

Both the gas explosion and the HE tests indicated that damage at around 200 kPa for a range of explosion duration (~ 50 ms) is minor; it causes the onset of plastic deformation. This is supported by results FE analysis.

At high pressure range, there was only data from HE tests for which the duration is much shorter.

Results and analysis indicated the overpressure required to cause the level of damage at Buncefield exceeds 200 kPa. Further FE analysis and/or gas explosion tests covering both detonation and deflagration would be required in order to provide the overpressure experienced at Buncefield using pressure characteristics matching those of explosion scenarios.

B.6. OIL FILTER

An oil filter was badly crushed in Buncefield. This is shown in Figure B.17:

Figure B.17 A crushed oil filter in Buncefield.

In the gas explosion test described above (Appendix B.2.4), the oil filter did not suffer any damage or deformation in all the tests at overpressures up to 180 kPa (see Figure B.18).

Figure B.18 An oil filter which had been exposed to an gas explosion test of 180 kPa was not damage.

This indicates that the pressure that produced the type of damage in Buncefield was well over 180 kPa.

B.7. TYRES

Approximately half of the tyres on vehicles exposed to the cloud were deflated by the explosion. Figure B.19 shows a typical example.

Figure B.19 Car tyre pushed off the rim during the explosion.

The tyre side wall and bead has been pushed inwards over the inner rim of the wheel. Pressure applied slowly in a hydraulic test does not have this effect – even at pressures in excess of 1 MPa. In this case, all faces of the tyre (and especially the load bearing face with tread) collapse inwards balancing the internal and external pressure. There is never sufficient net force to stretch the tyre bead over the inner rim. When the pressure is removed in a static test the tyre re-inflates to the original pressure.

In an explosion, inward deflection of all faces of the tyre occurs with the lightweight sidewall moving particularly rapidly. As the sidewall and bead contact the inner rim there is still sufficient pressure difference to stretch the bead over the rim. This difference is illustrated in Figure B.20.

These observations clearly indicate the overpressure was well in excess of the inflation pressure of the tyres involved which is around 200 kPa.
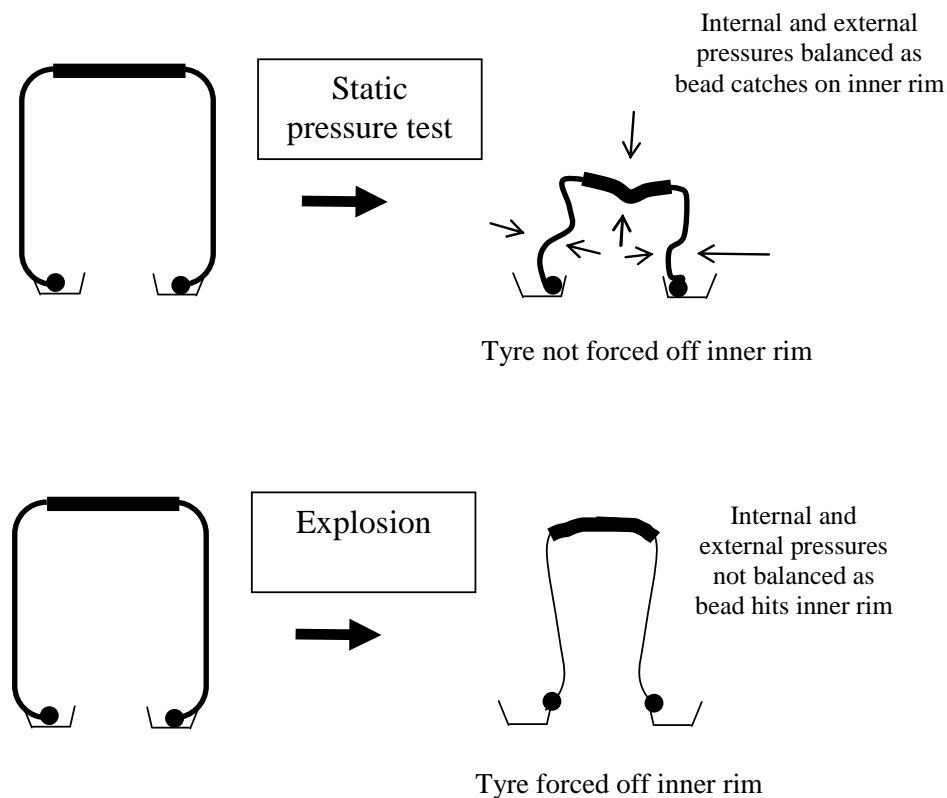
Figure B.20 Schematic diagram showing the response of tyre to static and explosive pressures.

B.8. CARS

Around 20 cars were in the area covered by the vapour cloud. All of them were badly crushed – a wide range of images is available in the Buncefield archive. One typical and representative example is shown in Figure B.21.

Figure B.21 Typical car damage, with rear tyre blown off inner rim.

B.8.2. HSL enclosed gas explosion tests

Figure B.22 shows views of cars exposed to gas explosions in a large strong steel enclosure. Corresponding pressure records are also shown. Full details can be found in HSL Report EC-06-69.
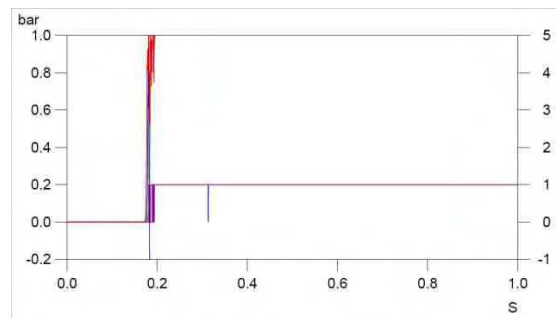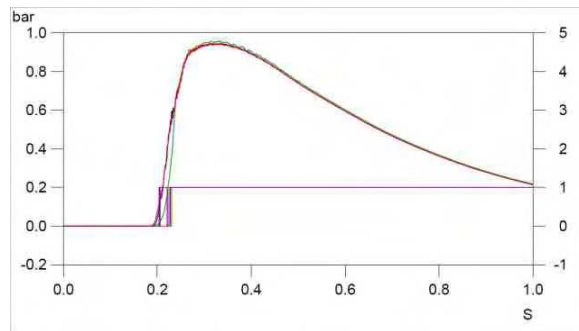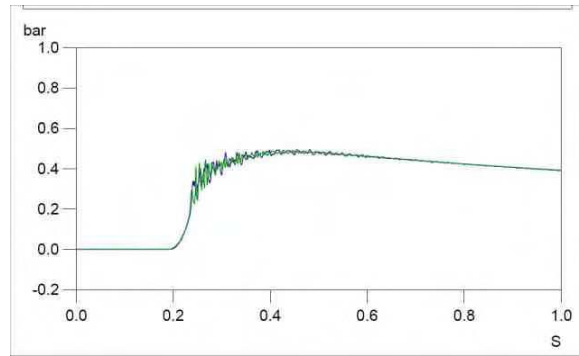
Figure B.22 View of cars after exposed to overpressures. The cars are shown in order of overpressure exposed. Pressure time curves are shown to the right of the cars.

The results of these tests show that pressures of well over 100 kPa and a rapid rise in overpressure are required to cause anything like the damage observed at Buncefield. Unfortunately the pressure transducers hit the top of their range in the final test (lowest picture of Figure B.22). Even in this case the damage did not fully match some of the severe car damage observed at Buncefield but no better estimate can be made of the minimum overpressure.

B.8.3.   bp/MOD Explosive tests

A test was carried out with 5 cars positioned at various distances and various orientations from a HE charge of about 170 kg equivalent of TNT. They were positioned to expose the cars to overpressure ranging from 170 kPa to 1 MPa peak side on pressure (reflected pressure ranged from 500 kPa to 5 MPa) and various orientations (e.g. nose orientation for Figure B.23, side orientation for Figure B.24 and rear orientation for Figure B.25). The duration of the positive phase was between 10 ms to 12 ms.

Figure B.23 Arrangement of cars before the test explosion. There were 5 cars arranged at various distance to the explosive charge which was located between the white car near the centre of the picture and the red car at a distance behind it.

The Figure B.23 shows the arrangement of cars. One car was positioned in front of a wall which provided a more even pressure load on the vehicle as well as increasing the pressure impulse the car experienced.

Figure B.24 Picture of a car (nose oriented) after exposed to blast overpressure. Panels were deformed, but there was no significant structure deformation on this side of the car.

The damage observed in many cases was limited to panel damage while the underlying supporting structure remained intact. Figure B.24 showed the side of cars which had been exposed to a peak side-on overpressure of 200 to 300 kPa. Similar pattern of damage was observed for other cars. The figure below shows a Ford Sierra after exposure to a peak side-on overpressure of 400 kPa.

Figure B.25 Picture of a car (side oriented) exposed to a side-on overpressure of 500 kPa. Panels were deformed, but there was no significant damage to underlying supporting structure.

Figure B.26 Picture of the end view of the Peuguet car (rear oriented) after exposed to blast overpressure. Severe damage occurred to both panels and underlying structures.

Major structural damage was observed at peak side-on overpressure of 1 MPa . Figure B.26 showed the damage caused by a peak side-on overpressure of about 1 MPa, with a positive phase of 11 ms.

B.8.4. Other data

Tests had been carried out by Centre for the Protection of National Infrastructure (CPNI) in the UK and Engineering Research Development Centre (ERDC) in the USA on vehicles exposed to high blast overpressures from a range of explosive charges including ANFO. Details of these tests are classified. But we can say that the results of the bp/MOD tests described in this report are consistent with those by CPNI and ERDC. Their data showed that for significant structural damage similar to those observed in Buncefield, peak side-on overpressure of well over 200 kPa is required.

There was an accident involving ammonium nitrate (AN) explosion in 2001 in the Total site in Toulouse. This accident was extensively studied. It was estimated that between 40 t and 110 t of AN was involved. The Total study concluded that the pressure required to crush vehicles was in the range of 100 kPa and 150 kPa. This conclusion is at variance with test data that we have access to and requires further investigation. If the Toulouse study is correct, the overpressure threshold would be reduced to 100 kPa rather than the 200 kPa as indicated by the bp/MOD, CPNI nd ERDC data.

B.8.5. Overall interpretation of car data

The test results showed that fairly high explosion explosion overpressure is required to deform a vehicle causing its structure to collapse (as was observed in Buncefield). The bp/MOD tests described here were only able to deform the vehicle predominantly on one side, whereas, the Buncefield vehicles were uniformly crushed indicating that the pressure loading was uniform around the vehicles.

From damage observed in the bp/MOD tests, the overpressure required to cause the level of damage observed in Buncefield was estimated at over 1 MPa with duration of the positive phase of 11 ms. However, due to different overpressure characteristics between gas explosion and HE, from examining other available test data, it is very likely that overpressures experienced by cars at Buncefield exceeded 200 kPa for durations typical of a gas explosion in the open (~ 50 ms as indicated in Appendix C).

Cars are complex structures, the response of which to explosion loads could be different for HE, AN, ANFO and the two types of gas explosions (deflagration and detonation). There could be merit in the Toulouse accident assessment. It is suggested that specifically designed gas explosion tests are carried out to verify the results described here.

B.9.   OVERPRESSURES OUTSIDE THE CLOUD - RAPID DECAY WITH DISTANCE

The explosion overpressures declined very rapidly outside the cloud. A number of photographs of indicative objects are included in the overpressure "album". One example is reproduced in the Figure B.27. The cars furthest from the camera were clearly exposed to the gas explosion as they have been crushed and set alight. The black hatchback has been significantly crushed – as has the rear portion of the light coloured vehicle in the foreground. Pressure damage to the front and sides of this vehicle is slight.

Figure B.27 A line of parked cars shows high level of damage at the far end and relatively low level at the front.

This and other images show that the high (>200 kPa) overpressures decline extremely rapidly with distance – on a scale comparable to the cloud depth.

B.10.   OVERPRESSURES IN THE EMERGENCY PUMP HOUSE

The only place where uncrushed boxes and tanks were observed was in the HOSL emergency pump house – where the explosion started. Figure B.28 shows some examples.
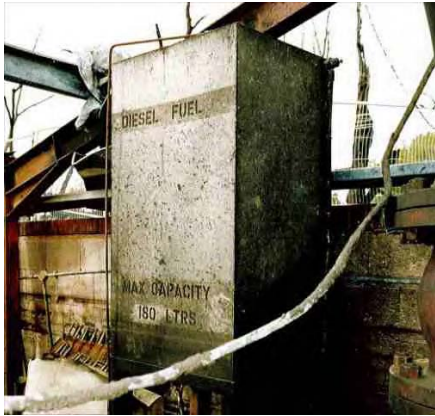
Figure B.28 Minimally damaged lightweight tanks and housings in the pump house where the explosion started.

This is interesting because of the potential light it casts on the earliest stages of the incident; the explosion clearly increased in intensity after the initial phase in the pump house. This evidence is inconsistent with pressure waves from a localized source.

B.11.   OVERPRESSURES AT A DISTANCE FROM BUNCEFIELD

There were numerous incidents of damage to domestic and public buildings in the surrounding area to the Buncefield site.

Figure B.29 shows the distribution of building damage on a map of the Hemel Hempstead area, including the Buncefield site. This map is provided by courtesy of Kennedys Law and was prepared to support the civil litigation cases. Each green or blue dot corresponds to a claim for building damage, with the colour difference only representing whether the claim had been settled or not at the time the map was prepared. The level of damage to each of the buildings is not known.

It can be seen that there is frequent building damage within a distance of 2 km of the HOSL site (which is marked with a star in the figure) and that sporadic building damage extends to a distance of more than 4 km. There were also claims that lie outside the boundary of the map in the figure.
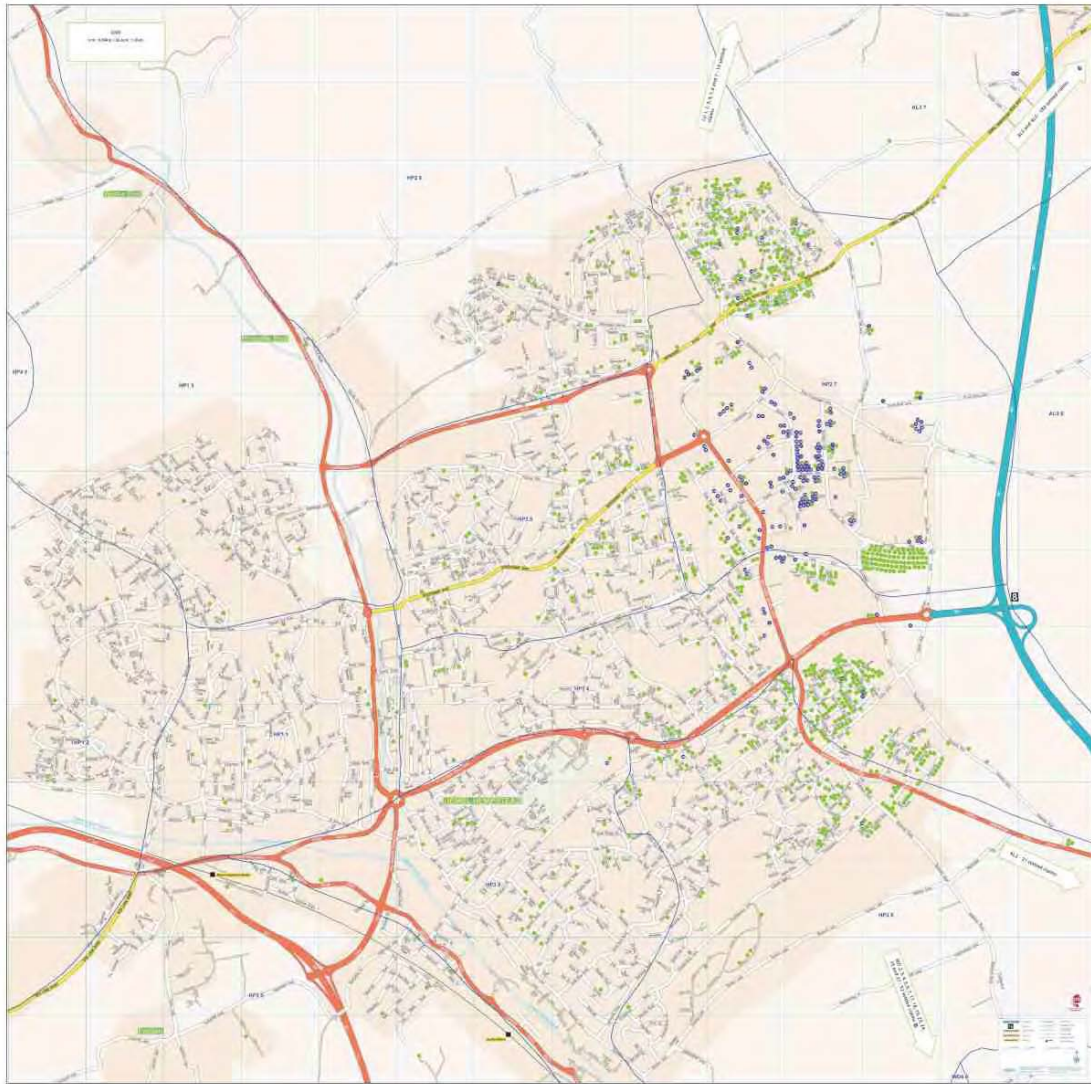
Figure B.29 Distribution of property damage as indicated by insurance claims. Each colour dot indicates a claim, green for settled claim and blue for claim in progress. Each grid is 0.5 km square and there are claims outside the boundary of this map
(Produced with permission from Kennedys Law).

B.12. DIRECTION ESTIMATES

In addition to overpressure distribution, work was also carried out to determine the direction of propagation of the explosion. Gas explosion produces drag forces. The direction of this gives an indication of direction of propagation of the explosion front.

Objects that are primarily susceptible to drag forces at Buncefield include: Trees, lamp posts, CCTV camera masts and fence posts. This was manifested in the following:

Deformation:
Objects were typically bent at points of weakness or close to the ground. In many cases, the impulse of drag forces was not sufficient to completely displace the broken part and the final shape indicates the direction of the net drag impulse (the cumulative effect of drag forces exerted on an object over the duration of the explosion).

Abrasion:
Many standing objects were abraded by debris driven by the explosion. The effect was most noticeable in surfaces covered by paint but was also apparent in tree bark and other types of surface. The pattern of abrasion was highly directional; only one side or part of one side was affected.

Displacement:
Some objects such as vehicles and skips were moved by drag forces during the explosion. They also typically suffered high level of compression as a result of increases in overpressure. In a number of cases, the location of the objects prior to the explosion is known (typically from CCTV images). In these cases, the displacement of the object can be determined and gives an approximate indication of the direction of the net drag impulse.
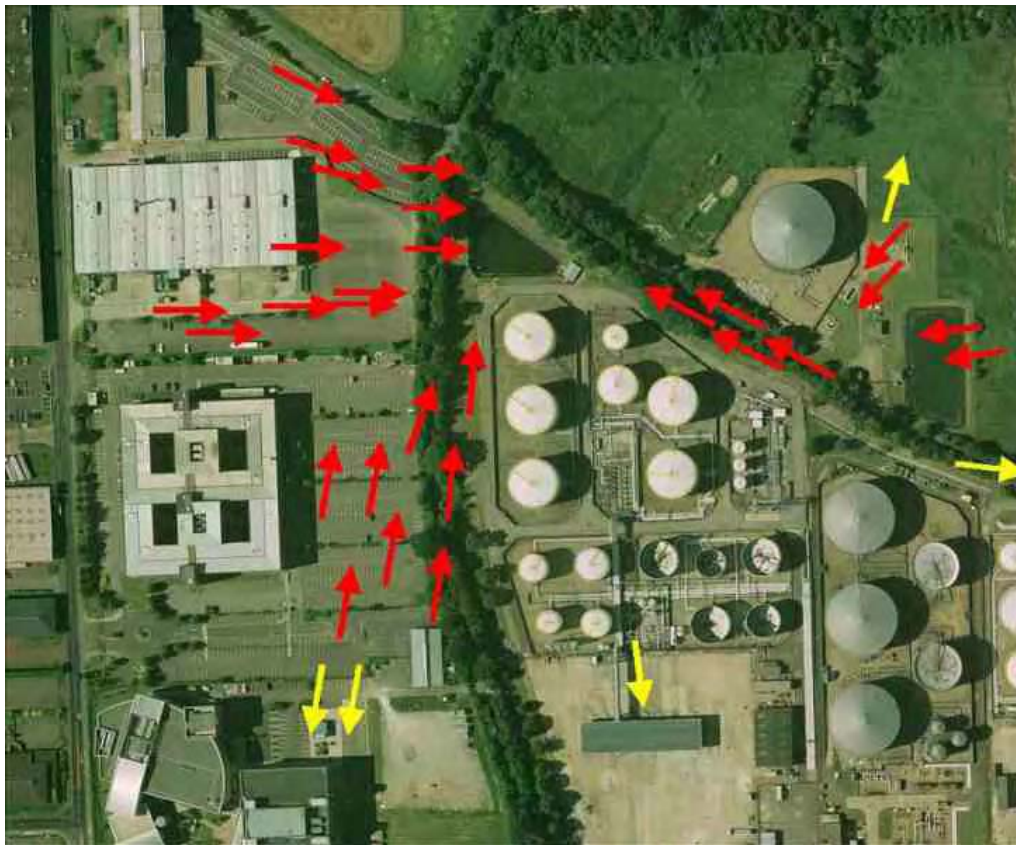
Figure B.30 Direction of net drag impulse across the Buncefield site.

Results of a site survey of directional information are summarised in Figure B.30. Each arrow represents an object which provided directional information. An example of a photograph showing directional evidence is shown Figure B.31 below.

Over the area covered by the cloud the direction of net impulse is inwards – towards the origin of the explosion and in the opposite direction to explosion propagation (shown by the red

arrows in the figure). Immediately outside the cloud the direction reverses and objects are blown outward (indicated by the yellow arrows).

The outward movement is well understood but inward deflections have not been clearly highlighted before or have been ascribed to the convective inflow driven by a fire plume.

Figure B.31 Effect of drag forces on a lamppost (left), and abrasions to objects in the car park: the base of a tree (middle) and on a steel post on its south face (right).

B.13. CONCLUSIONS

The results of overpressure and drag impulse direction distribution provides the data with which predictions from explosion mechanisms are compared.

B.13.1. Overpressure Distribution at or close to HOSL site

Overpressure within the gas cloud in the Buncefield site was found to be uniformly high, at least 200 kPa, see Figure B.32.
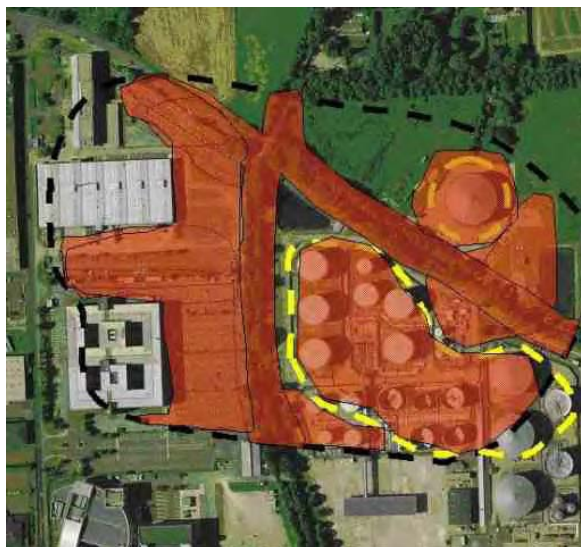
Figure B.32 Coloured areas contained different types of overpressure indicators. They showed that overpressure in these regions exceeded 200 kPa.

There are detailed photographs of almost every area of the site, and all objects at ground level appear to have been exposed to such extremely high overpressures. There appear to be no

distinctions between objects that are in different types of surroundings e.g. car parks, tank farms, open grassland and belts of trees. The only exception is the interior of the emergency pump house (where the explosion started); here pressures were lower.

Our assessment was based on damage suffered by cars, switch boxes, drums and other small objects which were distributed widely across the Buncefield site. Explosion tests gave consistent results indicating overpressure of greater than 200 kPa for the damage observed. No definite limit on the maximum overpressure could be established – the true figure probably could be much higher than 200 kPa.

Further test work would be necessary to quantify the maximum overpressure; and to validate the assessment described here (to eliminate effects due to different load characteristics of AN, ANFO, HE and different types of gas explosions). Load characteristics would need to be matched to those predicted for deflagration or detonation scenarios.

The low level of damage at the pump house and high overpressure over an extensive area shows that damage cannot be caused by pressure waves from a localized source.

Evidence collected on site suggests that overpressures fall off very rapidly outside the edge of the vapour cloud (a few metres).

B.13.2. Overpressure distribution at a distance

Information from insurance claims for property damage indicated that there was frequent building damage within 2 km and sporadic building damage to 4 km from the HOSL site.

B.13.3. Directional Indicators

The study of objects susceptible to drag forces shows that the net drag impulse was towards the general direction of the pump house within the gas cloud, and away from the pump house outside the gas cloud. This indicated that the explosion propagated away from the pump house.

B.14.   ABBREVIATION

HE   High Explosives
AN   Ammonium nitrate
ANFO Ammonium nitrate fuel oil

APPENDIX C   POTENTIAL FOR HIGH SPEED DEFLAGRATION

In this Appendix we shall study the processes of deflagration in the Buncefield gas cloud. We shall attempt to model such a deflagration and examine whether there is a credible development of the explosion, involving only deflagration, that is consistent with observed damage.

C.1.   INTRODUCTION- GAS CLOUD EXPLOSION MECHANISMS

The burning of a vapour cloud in the absence of confinement or congestion does not generate significant overpressure. In order to generate what may be regarded as an explosion, there must be either confinement of the gas cloud, or congestion, i.e. obstacles in the path of the flame, or both.

In the absence of turbulence, the (laminar) burning velocity of a hydrocarbon flame is quite low, around 0.5 m/s. As the flame ball grows this can increase owing to instabilities, but only by a factor of two to three. However, the expansion pushes gas ahead of the flame. If the resulting flow passes obstacles (e.g. in petrochemical plant vessels or pipework), turbulence will be generated. The flame speed in a turbulent flow is much greater than the laminar flame speed, principally because the turbulence wrinkles the flame, creating a much greater area for reaction. Therefore, when the flame reaches the turbulent region downstream of the obstacles, it burns faster. This faster burning in turn creates faster flow and so a higher level of turbulence downstream of the next group of obstacles. The more intense turbulence results in even faster burning, and so on. This process is known as the Shchelkin mechanism

The obstacles also have another major effect on the burning. As the flame passes between the obstacles it becomes distorted. An initially nearly flat flame can become very convoluted by this process, which therefore also increases flame area and burning rate. Thus, even where there is little confinement, high flame speeds may be generated by congestion. The high velocities associated with the rapid burning are sufficient to generate high pressure, i.e. an explosion.

As the combustion progresses beyond the congested region of plant and into the open, a deflagration flame slows down soon after leaving the congested region, as the turbulence decays.

At Buncefield, the density of pipework and other small obstructions was very low compared with complex petrochemical plant, and was not at a level that would be expected to generate high explosion overpressures. However, the two lanes adjacent to the depot were bordered by wide verges containing trees and very dense undergrowth. The undergrowth of bushes had not been cleared over a period of many years, and was very dense. Indeed, the branches constituted a network of flow obstructions considerably denser than that presented by pipes and vessels in highly congested plant. Thus, it is reasonable, with hindsight, to consider that they could have as strong, or stronger, influence in generating explosion overpressure as such plant.

C.2.   DETONATION

It should be noted that the flames discussed above consist of the normal type of burning known as a deflagration. Almost all gas cloud explosions are deflagrations. In a deflagration, the burning velocity is limited by the diffusion of heat and species through the flame front. In a detonation, by contrast, the gas mixture ahead of the flame is heated by a shock wave coupled to the flame. A detonation is supersonic and self-sustaining, and, once initiated, will continue to propagate at the same speed even through an unconfined, uncongested cloud. The pressure generated by detonation in a typical hydrocarbon/air mixture is about 1800 kPa, with velocity around 2000 m/s.

In less severe cases, there may still be explosion effects that go beyond deflagration. The strong flow ahead of the flame in a severe explosion may be sufficient to trigger auto-ignition near obstacles ahead of the flame.

Detonation is the subject of a later Section of this report. However, the concept is introduced here because we shall consider in this Section the possible role of high-speed deflagration in the run-up to "deflagration-to-detonation transition" (DDT).

C.3.   COMPUTATIONAL FLUID DYNAMICS – THE EXSIM MODEL

The overpressure that would be generated by a gas explosion in a congested environment as discussed above can be calculated using computational fluid dynamics (CFD)

It is not possible to use a computational grid in such models that is fine enough to resolve all the small obstacles that can have an effect on the explosion overpressure. To do so would need computers many thousands of times larger than the largest we currently have available. To get round this problem, Hjertager (1993, 199) devised the porosity/distributed-resistance (PDR) approach, which represents the effect of obstacles smaller than the computational grid by an equivalent porosity and resistance to flow. Allowance can also be made for the effect of the sub-grid obstacles in increasing the flame area. Several models using the PDR technique have been developed. One of these is EXSIM.

The essence of the PDR approach is that there are obstacles smaller than the computational cell size that have a significant effect on the flow and/or combustion. Thus subgrid modelling is included to take account if the effect of these obstacles. In the original PDR approach [1] there are added terms for subgrid drag, turbulence generation and the reduced fluid volume in the cell. For example in the momentum equation:

$$\frac{\partial}{\partial t}\left[\beta_v \rho u_i\right] + \frac{\partial}{\partial x_j}\left[\beta_j \rho u_j u_i\right] + \beta_v \frac{\partial p}{\partial x_i} - \beta_v \rho g_i = \frac{\partial}{\partial x_j}\left[\beta_j \sigma_{ij}\right] + R_i$$

where β_v and β_j are volume and area porosities respectively, and R_i is the subgrid drag term.

The additional source term for turbulence kinetic energy is taken as proportional to the subgrid drag; the turbulence integral scale is forced to approach the scale of the subgrid obstacles.

However, it must be emphasised that the effect of the subgrid obstacles on the combustion is equally important, and this is included in the subgrid modelling. As an initially planar flame passes through a group of obstacles, it becomes distorted, generating additional flame area. This effect is allowed for by enhancing the combustion rate in the cell. If there are many obstacles in a cell, there is also the potential for continuing acceleration of the flame through successive groups of obstacles, and the model attempts to allow for this also. This introduces a dependence on the number of obstacles in the cell, and may be overestimated for large numbers of subgrid obstacles - hence the need to limit the number of subgrid obstacles by not going to too large a cell size. The model validates well, provided this restriction is observed.

C.3.1. Laminar flames and laminar flame instabilities

Before any turbulence is generated, the model calculates an initially spherical laminar flame around the ignition point. Laminar flame instabilities are also included, in an empirical way, by accelerating the flame as it progresses. Such instabilities might become significant in an unobstructed cloud that is large in all three dimensions, but much less so where the vertical extent of the cloud is small.

C.3.2. Other processes

Some physical processes are not explicitly modelled in the EXSIM code. Two of these are flame quench effects at high turbulence levels, and the influence of pressure wave/flame interactions in accelerating the burning rate. The former of these would reduce overpressure, and the latter increase it.

While we would prefer that we would be able to model such processes, at present we note that:

(a) The validation of the model continues up to the highest pressures experienced in the Spadeadam Phase 2 and 3a experiments with no systematic deviation. The empirical model behaviour seems reasonable at these levels, if not entirely for the right reasons.

Modelling the combustion of a large diameter but relatively shallow gas cloud in a fairly open area is rather challenging, even using one of the CFD models specifically designed for plant explosion simulations, in this case EXSIM.

C.4.   EXSIM SIMULATION OF THE BUNCEFIELD INCIDENT

Because the Buncefield plant had little or no congestion, attention is concentrated on the two wooded avenues to the North and West of the plant: Three Cherry Trees Lane and Buncefield Lane. This approach is supported by the results of experiments (van Wingerden and Wikens, 2008), which showed that bushes could indeed have a major effect of flame acceleration.

Modelling vegetation with a code intended for process plant is rather difficult. For example:

i)   Vegetation extends down to extensive small-scale twigs and leaves, whereas process plant tends to have much less fine detail. Both the volume blockage presented by the congestion and the number density of obstacles are important in the generation of overpressure. The latter was higher in the vegetation than in process plant.

ii) Vegetation moves to accommodate airflow, whereas process plant is stiff. Such compliant objects would generate less turbulence than stiff one, but may still have a significant influence in flame area generation.

EXSIM has been designed and validated for explosions in typical process plant, and we are careful to run it within the range of conditions for which it has been validated. An important aspect of this is the relationship of the cell size to the density of the congestion. Essentially, as the number density of the congestion increases, the required cell size decreases. This causes difficulties for the Buncefield case. To meet the cell size restrictions within the congested regions (the lanes) and also to cover the whole region of interest with a suitable Cartesian mesh would require many more computational cells than can be handled by the current (32 bit) code.

In order to gain an understanding of the possible nature of the flame generation and pressure wave propagation across the region of interest, it was decided to perform the initial runs with reduced congestion. A consequence of this was that these computations would be likely to under predict the actual levels of overpressure. Later runs studied the effect of more realistic obstacle densities, albeit over a more restricted computational domain.

C.4.1. Large-scale simulation – low-density congestion

A restriction of EXSIM is also that congestion must have a Cartesian representation, and so the equivalent to a tree is rather unusual (see Figure C.1).
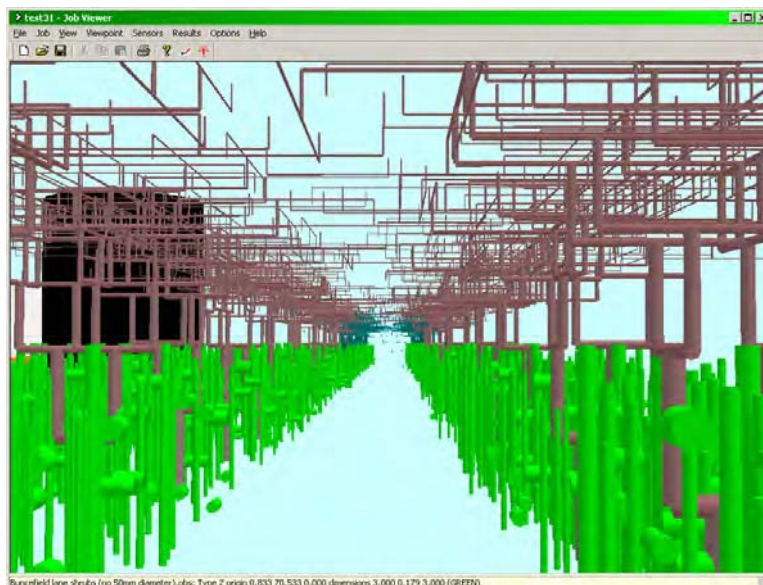
Figure C.1 Representation of vegetation in Buncefield Lane

In Figure C.1 the bright green 'vegetation' extends up to three metres high, and above that the trees are represented (assumed deciduous and with no foliage). The two rows of trees are 6 metres apart. The correct level of congestion is difficult to determine. However, owing to computer limitations, it was found necessary to use a coarse form of low-level blockage in order for the model to utilise a sufficiently large mesh size to accommodate a significant gas cloud.
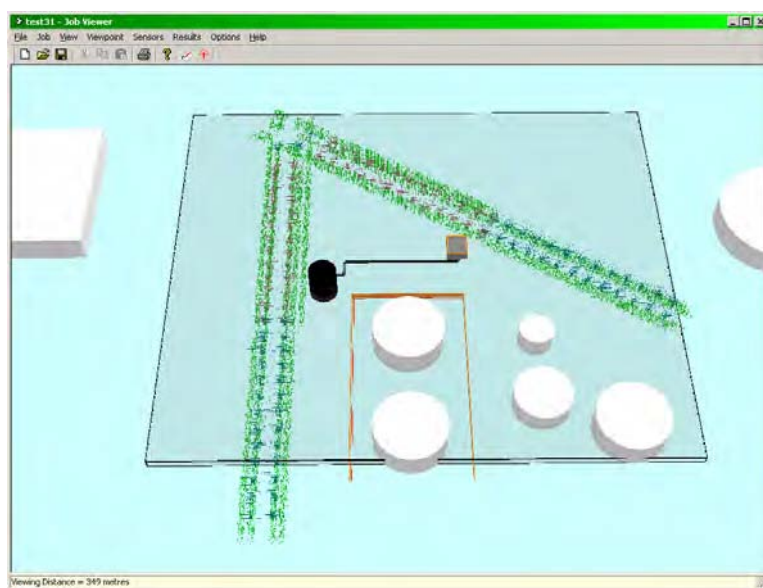
Figure C.2 Final simulation gas cloud and wooded lanes

Approximately 30 explosion simulations were run before reaching the final form seen in Figure C.2, where the grey slab region represents the flammable gas cloud (modelled as a stoichiometric propane cloud – which is usually considered a conservative assumption when modelling alkanes due to its higher burning velocity than other alkanes).

A large number of point monitors were located in the model along each of the wooded lanes, and in the direction of the Fuji building (building not shown). As can be seen, there was very little detail modelled of congestion within the plant. However, aerial photographs seem to

suggest very little congestion in the region of interest, the top corner being occupied by a firewater pond, and the area within the modelled bund also being quite open. The auxiliary pump house was included so that the effect of an explosion within it could be modelled as an initiating event. It had internal congestion added and walls set to fail at 500 mbar overpressure.

It should be noted that the EXSIM explosion model must be run with an appropriate mesh size determined by the sub-grid statistics, and this was done in all cases (unless explicitly stated otherwise), and with the type of congestion shown this was generally with a mesh size of circa 0.9 metres.

C.4.2. Results

Of the two suggested ignition locations, we have chosen to simulate ignitions at the pump house. This is based primarily on the fact that there is a region of Three Cherry Trees Lane near the pump house with little damage to the trees; this is consistent with the flame starting to accelerate from this location, initially having too low a speed to cause much damage.

Early simulations assumed either an ignition inside the pump house, with the roof failing at 500 mbar, or a simple ignition in the lane close to the pump house. In the former, vented explosion case, significant rapid combustion and overpressure generation occurs in the jet of fuel/air ejected through the vent (roof). This is driven by the intense turbulence generation in the shear layers around the jet. This phenomenon is often termed the "external explosion" (Harrison & Eyre 1987). This might be expected to "kick-start" the explosion but there were few obstacles between the pump house and the lane, so the turbulence kevels and burning rate rapidly decayed with distance from the vented explosion. Simulations using either ignition in the pump-house or near the lane produced very similar results, so they are considered here together.

As is expected for any deflagration, the presence of congestion increases the burning rate and so the flame front expands faster along the direction of the lane, the image below showing the fuel in red being consumed by the advancing combustion.
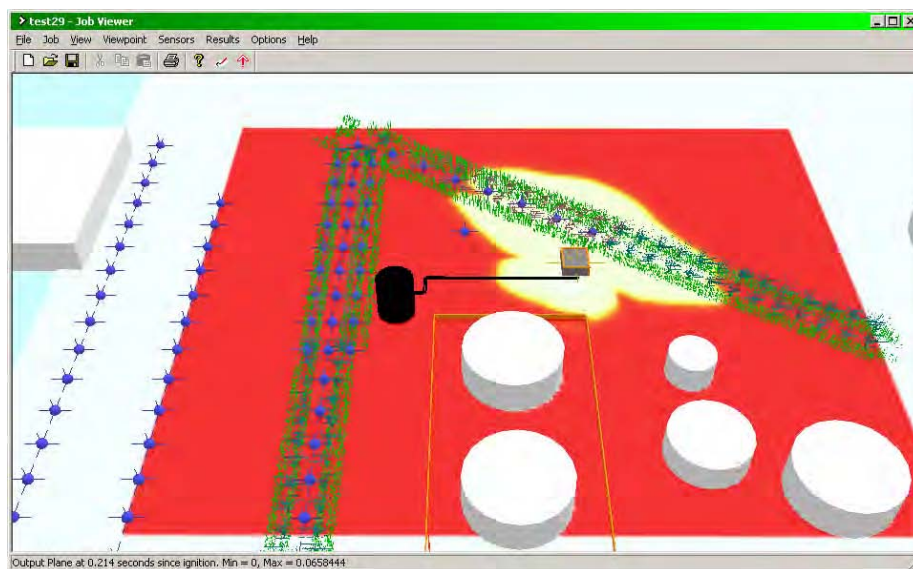
Figure C.3 Fuel cloud 214 ms after combustion initiated by pump house

The North lane has been modelled with sufficient length so that the pressure drives the cloud equally in either direction. The pressure is of course free to relax upwards but at this stage has had little time to do so.

In Figure C.4 the corresponding horizontal pressure plane is shown scaled so that red = 300 mbar or above. The pressure wave is expanding as an elongated hemisphere, and in regions where there is no congestion or no gas, the pressure is already decaying.

In regions where there is gas but no congestion, the burning rate slows progressively until it approached the laminar burning rate, while the pressure pulse continues on at the speed of sound.
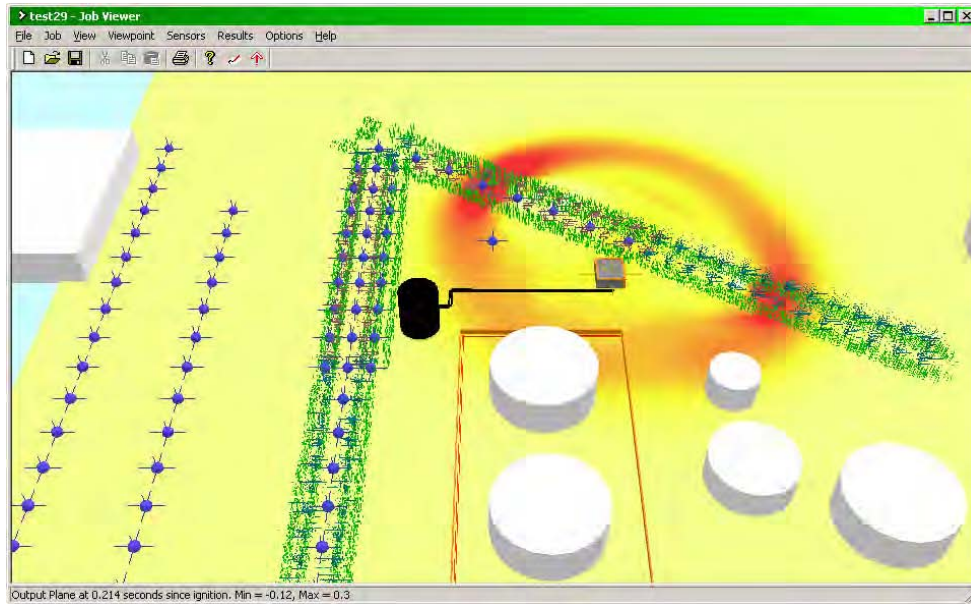
Figure C.4 Overpressure plane scaled to red = 300 mbar (peak = 660 mbar)
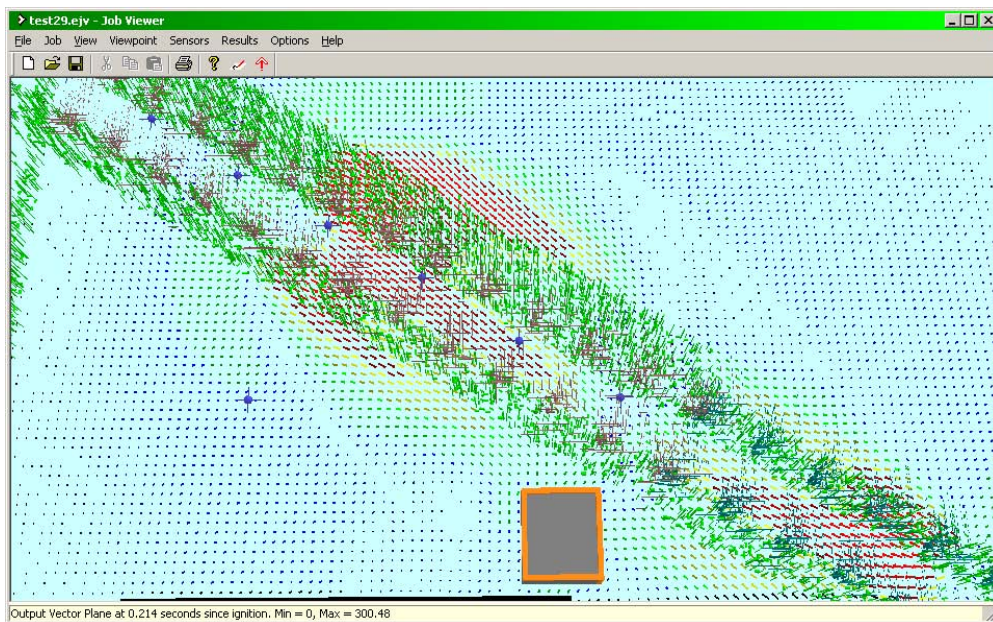
Figure C.5 Reverse flow behind the flame front is high velocity but low density (red is > 300 m/s)

It is worth noting that the blast behaviour is different from an expanding hemisphere as we might predict for a single explosion source, e.g. the pump house on its own. The three Cartesian directions all behave differently. The shallow depth of the cloud means that there is no combustion or expansion above the lane allowing vertical pressure relief only hindered by the

leafless branches of the tree canopy. Along the road direction we have rapid combustion accelerated by the congestion generating the pressure that must be relieved, and normal to the direction of the road we have rapidly slowing combustion, as there is negligible congestion to generate turbulence, so the rate of volume generation is very low.

It is noticeable that ahead of the flame front we see the uncombusted gas pushed ahead by the pressure wave at 150 m/s, but behind the flame front we see a reverse flow of 300 to 400 m/s in the hot combustion products (Figure C.5). The density of these gases is however about a tenth of that of the unburned fuel/air cloud and the drag load is proportional to both the density and the square of the velocity. So the drag load would appear to be lower in the reverse direction. A further difference might be the duration of the drag loads and the net displacement (as vegetation is flexible), both of which are available from the model.

If we use a massless tracer that travels with the flow we can see the maximum displacement that the passing explosion front would cause. This involves displacement in the direction of travel of the flame front due to the compressive blast wave, followed by reverse flow once the flame front has passed accompanied by vertical motion due to the expansion upwards of the hot combustion products. (See Figure C.6).
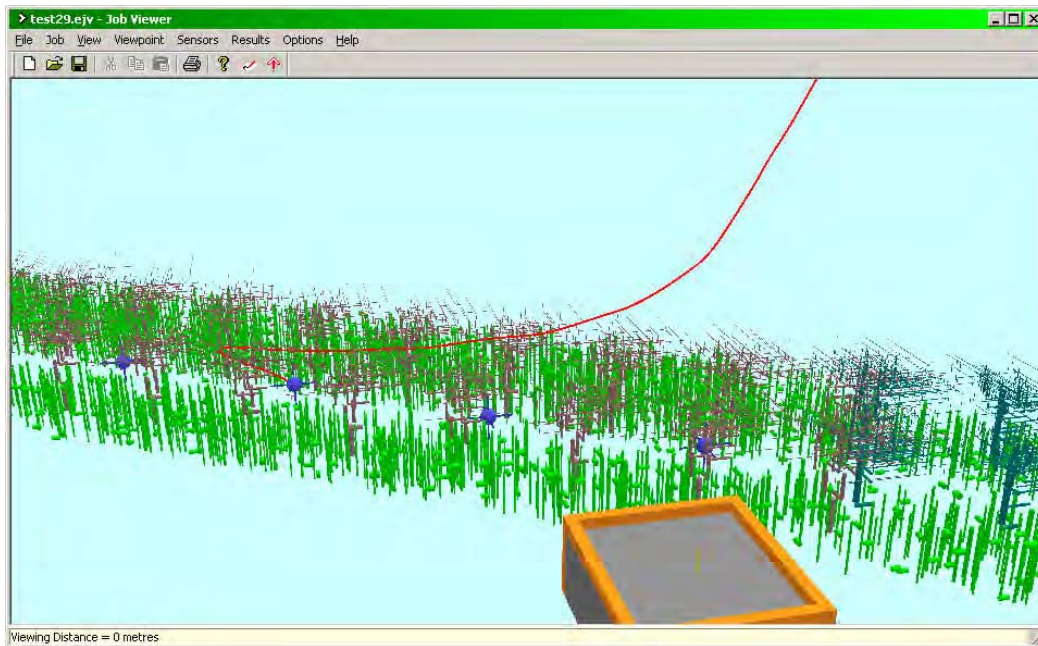
Figure C.6 Massless tracer

For the particular tracer shown the initial forward displacement was 5 metres before the flame front passed and the motion was reversed. For the trees and shrubs in the lane the displacement would clearly be less, as the air has to flow past them before any drag load is experienced, and then the acceleration is dictated by the inertial mass of the object and in some cases by elastic forces from any fixed parts, e.g. from the root of a tree.

Another output from the model is the dynamic pressure at any of the monitoring points, recorded at every time-step. The dynamic pressure enables us to calculate the drag load that would be experienced by anything in the path of the flow, and importantly it takes into account the density change due to the combustion, which is vital in this instance (simply using velocity and assuming air density would massively overestimate the drag load due to the reversed flow behind the flame front).

The dynamic pressure has to be multiplied by the drag coefficient (in this case we have assumed cylindrical geometry and so the C_d is about 1), and the cross sectional area. The force per unit length on a cylinder can thereby be calculated. Assuming a typical density for wood we can also calculate the mass per unit length, and the acceleration is force/mass. By integrating the acceleration over time we obtain the velocity, and a further integration gives the displacement.

The first location considered is in the middle of Three Cheery Trees Lane 20 metres away from the pump house, as the deflagration accelerates through the congestion. The sensor location is that chosen for the massless tracer plot in Figure C.6. Three sizes of cylinder are considered – 0.1 m (4 inch), 0.025 m (1 inch), and 0.006 m (1/4 inch).

The density of the wood is chosen as $650\,\text{kg/m}^3$ – which, given it is green wood, may be erring on the light side, as most textbook figure are quoted for dried wood. This gives the mass of 1 metre of each size as 5 kg for the 0.1 m, 300 g for the 0.025 m, and 21 g for the 0.006 m.

The maximum overpressure seen by this sensor was 1.5 bar; however, pressure is not as important as drag load when considering damage to trees, as the instantaneous pressure gradient across a small cylindrical object such as a branch is very small.

The dynamic pressure in Pascals (Figure C.7) is shown for the sensor previously studied, and here the flame front is propagating in a negative x direction, so the initial compressive blast pulse is in the negative direction (this is the vector dynamic pressure in the West-East direction). The initial dynamic pressure is therefore in the negative x direction before the reverse flow behind the flame front, which is in the positive x direction, gives rise to a dynamic pressure acting in the positive x direction.
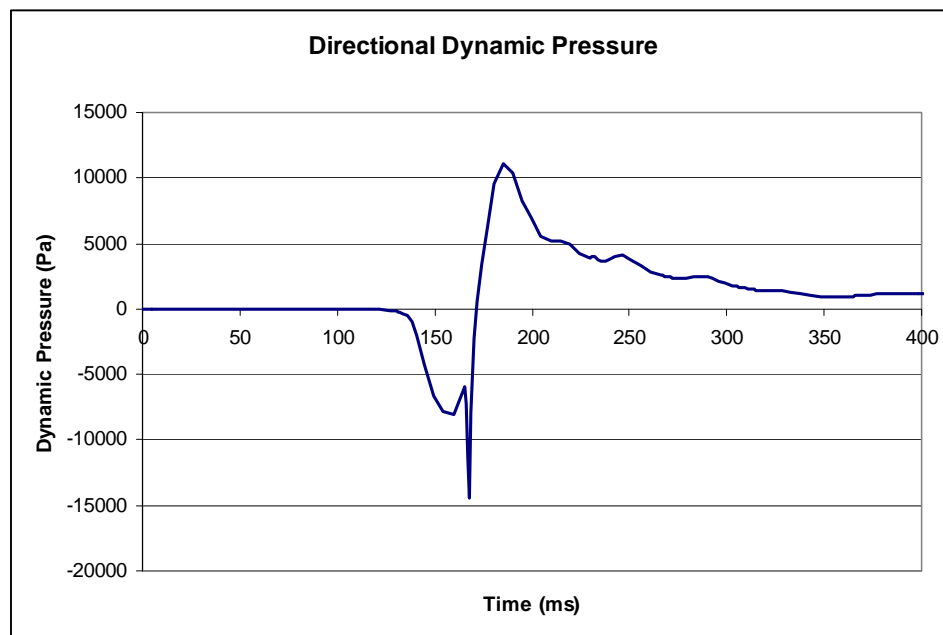
Figure C.7 Dynamic Pressure on sensor 70 (example)

The corresponding velocity and displacement of the three 1 m long branches defined above are shown in Figure C.8 and Figure C.9.
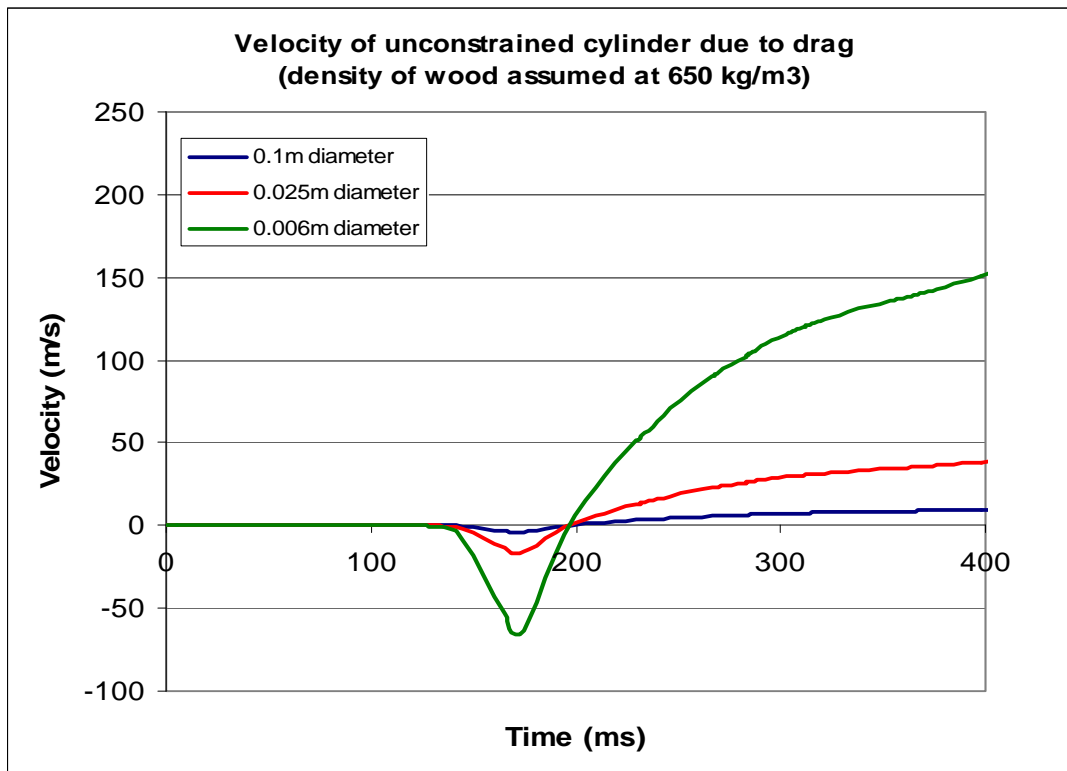
Figure C.8 Velocity caused by drag on unconstrained cylinder
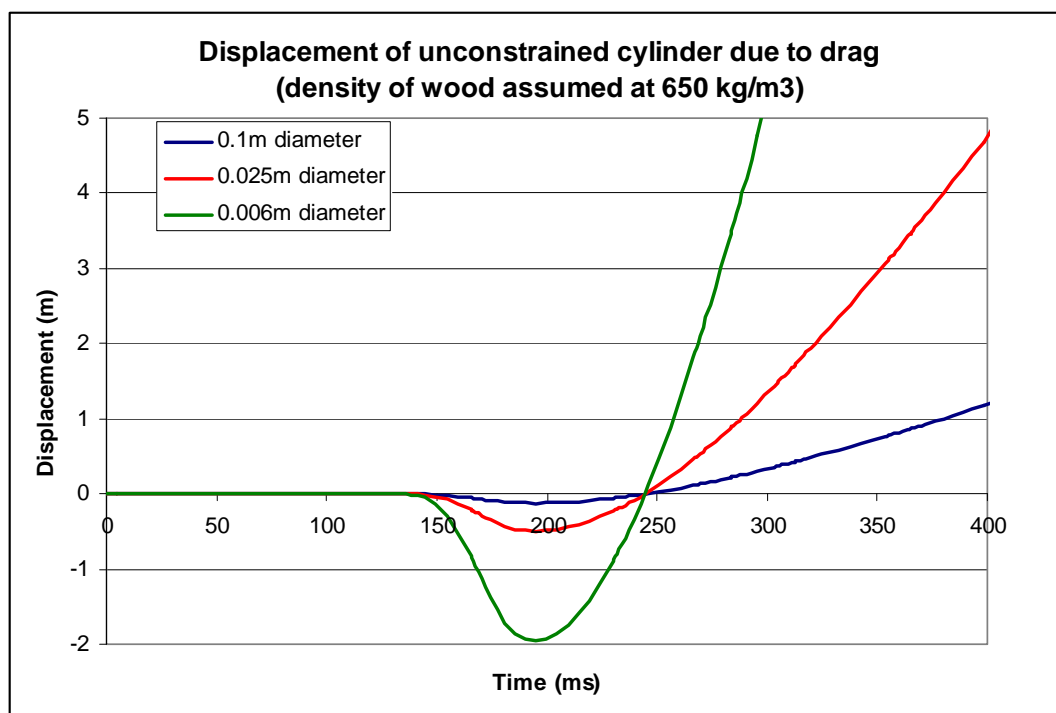
Figure C.9 Displacement of unconstrained cylinder

The results suggest that the forward pulse of the explosion at this early stage would probably damage smaller twigs and branches, but that larger branches would suffer a sufficiently small displacement that they would survive the compressive pulse, and have more problems with the reversed flow which is observed behind the flame front.

The results so far were for an early sensor, in the middle of Three Cherry Trees Lane, not far from the selected point of ignition, which was in this case the pump house.

If we follow the simulation to a later stage the flame front continues at a rapid pace through the most congested regions, which includes entering and following the congestion in Buncefield Lane. The combustion rate in the areas of low congestion slows considerably.
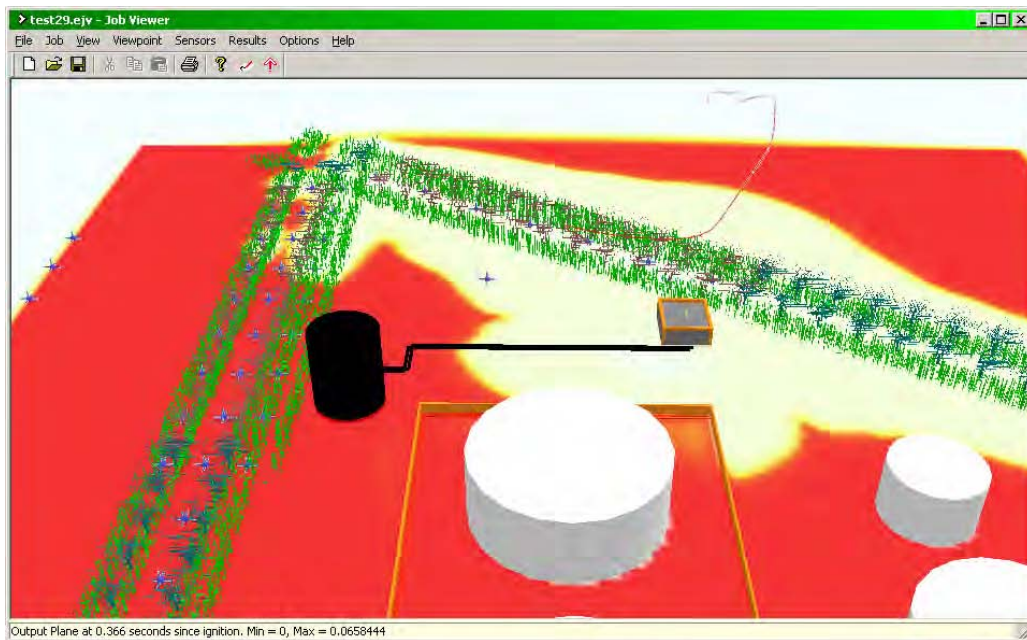
Figure C.10 Unburnt fuel shown in red, as flame front enters Buncefield Lane (366 ms after ignition)
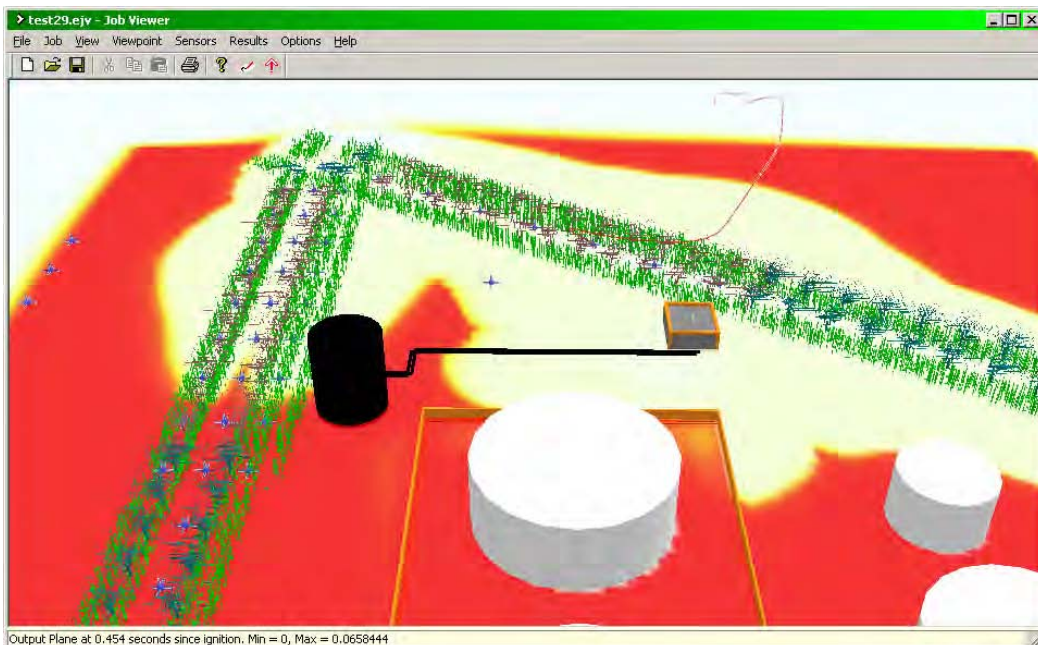
Figure C.11 Fuel cloud as combustion follows Buncefield Lane (454 ms after ignition)
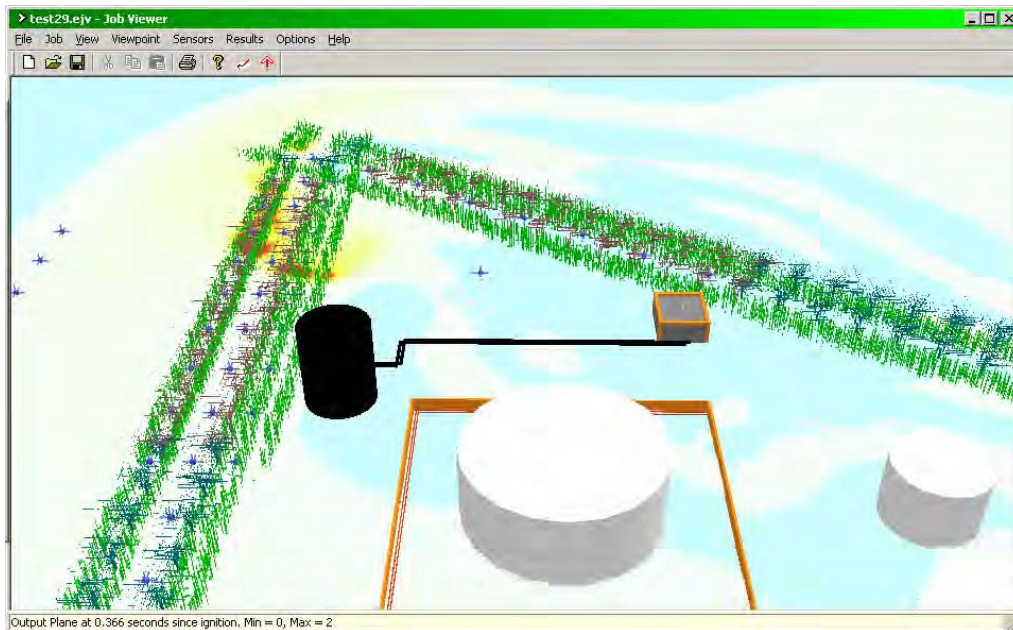
Figure C.12 Overpressure as flame-front enters Buncefield Lane
(366 ms, red = 200 kPa)
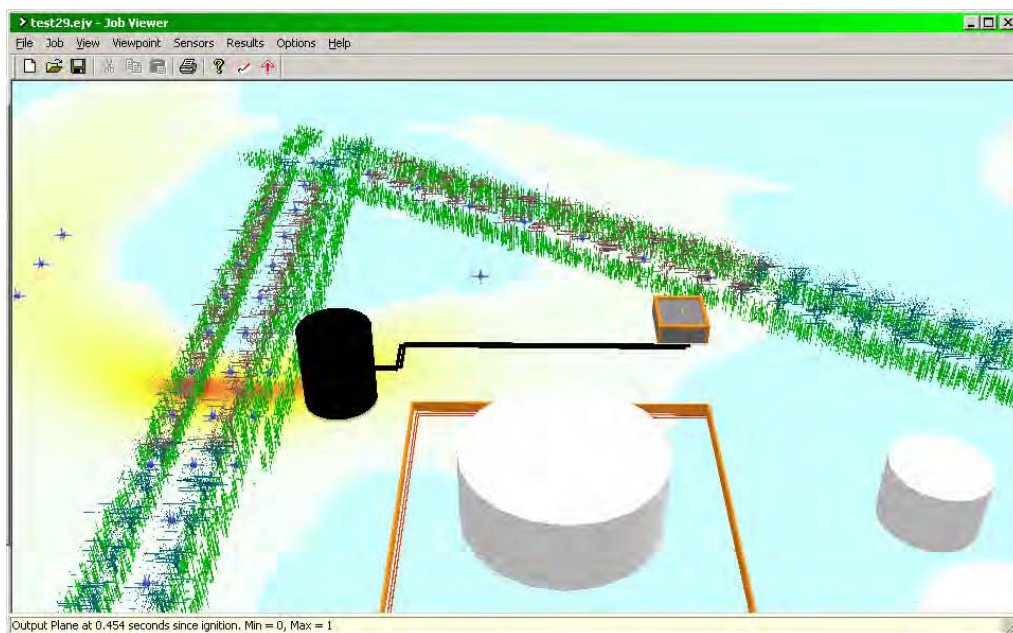
Figure C.13 Overpressure as combustion follows Buncefield Lane
(454 ms, red = 1 bar)

As can be seen from Figure C.12 there are localised higher pressure spots as the flame front turns into Buncefield Lane, but as time progresses the flame front appears to drop back to about 100 kPa overpressure with occasional spikes to 200 or more kPa associated with local congestion (the congestion has a random distribution, so has localised pockets of higher blockage).

Figure C.14 shows the results from successive sensors located in the congestion on the East side of Buncefield Lane.
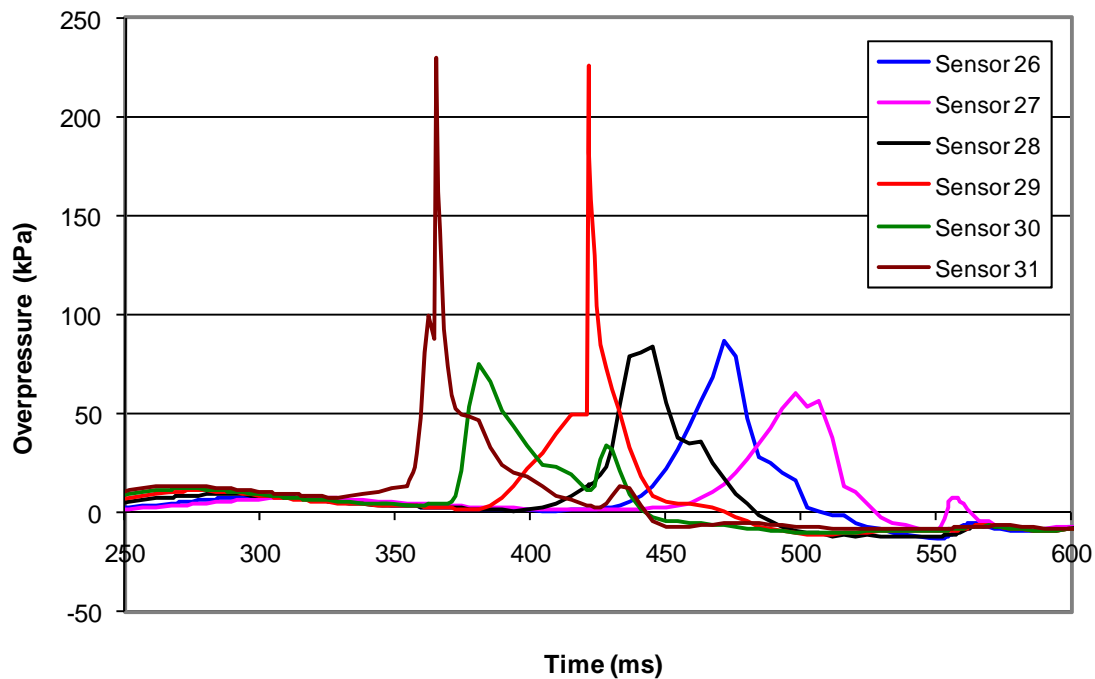
Figure C.14 Pressure sensors on East side of Buncefield Lane

There are a number of interesting issues revealed by Figure C.14. One is that the explosion appears to reach a steady state pressure of approximately 0.75 bar, though there are occasional localised pressure spikes. These may in part be due to the fact that the flame front is moving quickly through the congestion on either side of the road, and there is interaction between the pressure waves generated by the two flame fronts. There also may be some pressure waves from continuing combustion elsewhere in the model with the resulting pressure waves approaching Buncefield Lane from the East side. As mentioned before, the congestion on either side of the road has a random element, and so the rate of combustion may also speed up and slow down according to the local congestion levels.

It is also notable that there is very little rarefaction behind the pressure wave, whereas for a normal explosion resulting in a hemispherical expanding pressure wave it is normal to see rarefaction. Maybe this arises due to the symmetry of the hemispherical wave, and does not evolve for this form of rather two-dimensional combustion where pressure is relieved vertically.

The speed of the pressure wave can be deduced from the separation of the sensors (10 metres apart). The peak pressure covers the 50 metres in 132 ms, giving a speed of 378 m/s.

The flame front can be tracked in a similar way by plotting the combustion products (or unburnt fuel) at each of the sensors – see Figure C.15. This takes 180 ms to travel the 50 metres, so the flame speed is 277 m/s. It does vary, and the peak is 500 m/s between sensors 28 and 29. However the fact that combustion is occurring in parallel along two congested areas does complicate the issue (Figure C.16). Velocity vectors are shown in Figure C.17.

54
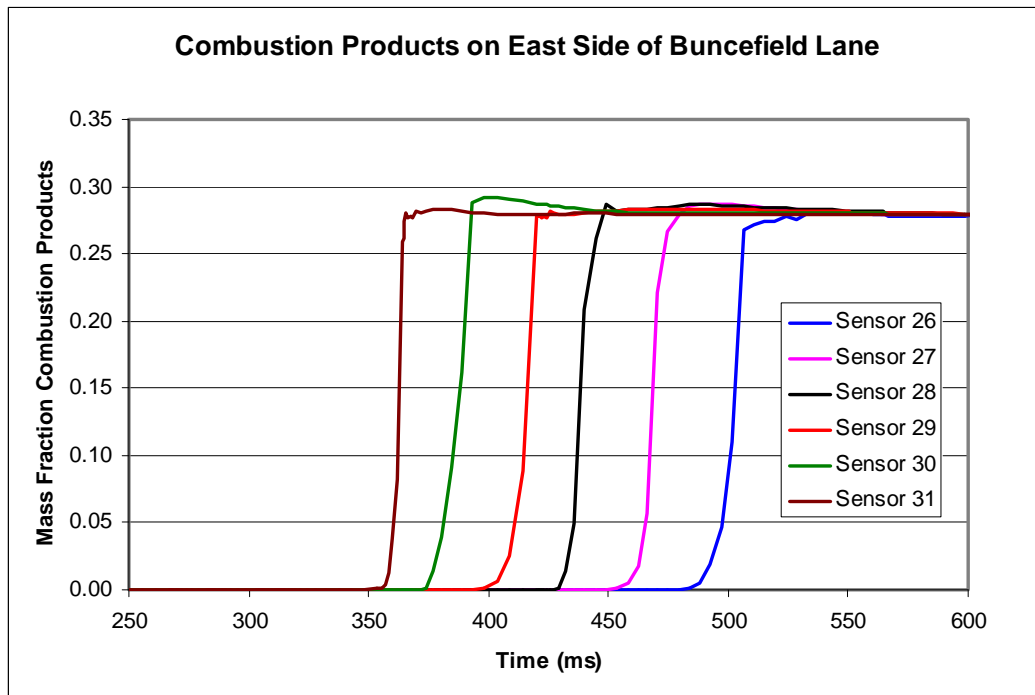
Figure C.15 Tracking flame front by combustion products
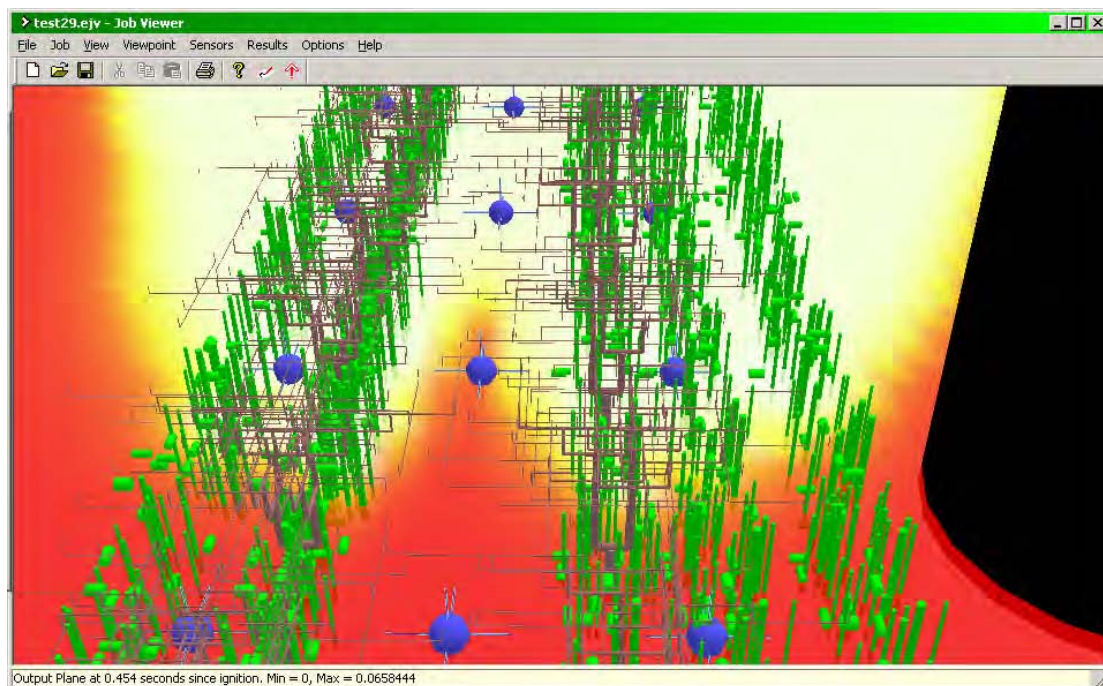
Figure C.16 Parallel combustion on either side of the lane

55
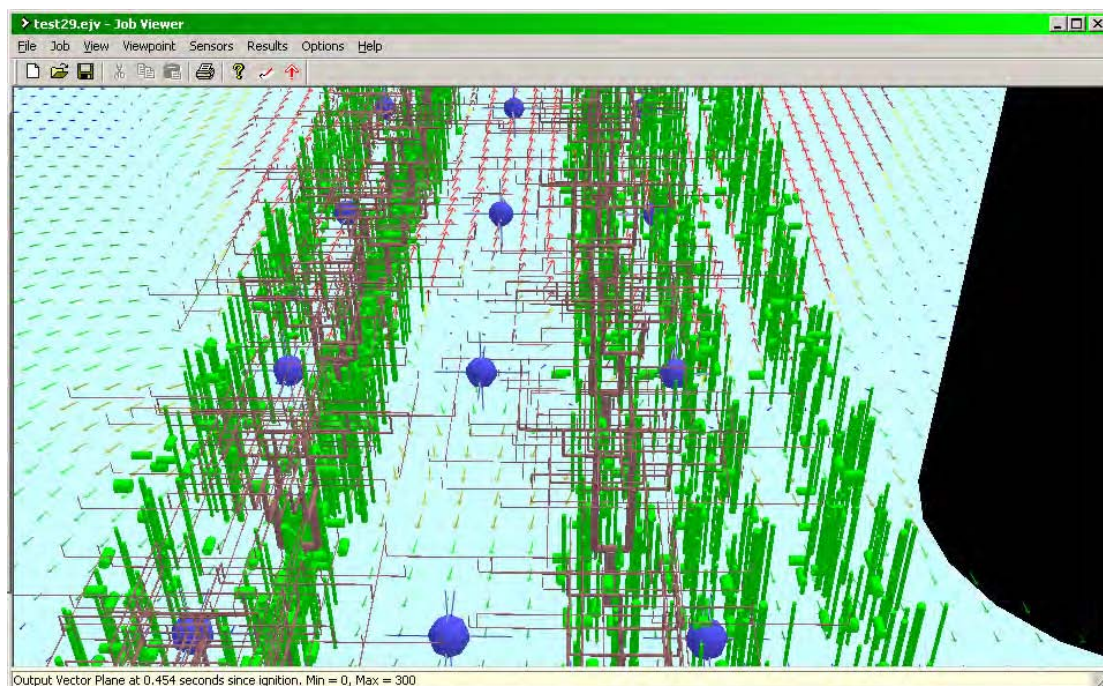
Figure C.17 Velocity vectors showing reversed flow behind combustion front

Returning to the damage and calculation of the drag load, Figure C.18 shows the dynamic pressure loading in the direction of Buncefield Lane for sensors 26 to 31.
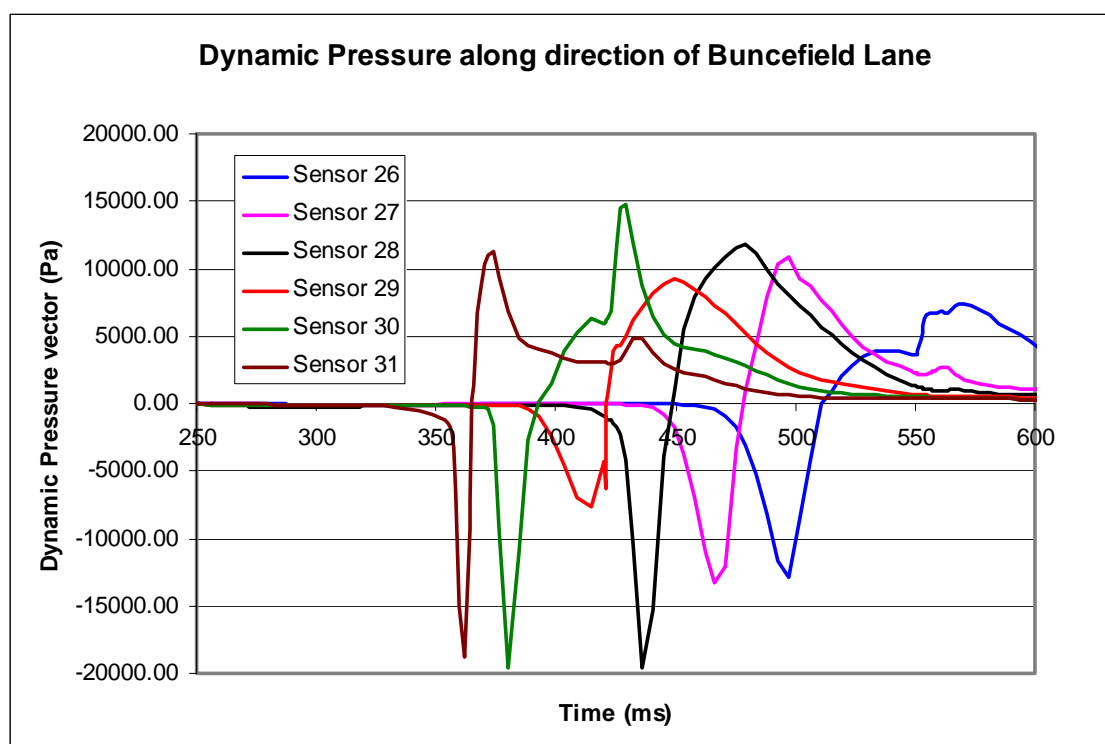
Figure C.18 Dynamic Pressure tracer for sensors on East side of Buncefield lane

By comparison with the earlier sensor in Three Cherry Trees Lane (Figure C.7), we see that the duration of the drag is rather shorter, although the maximum value is higher, thus representing a more rapid combustion.
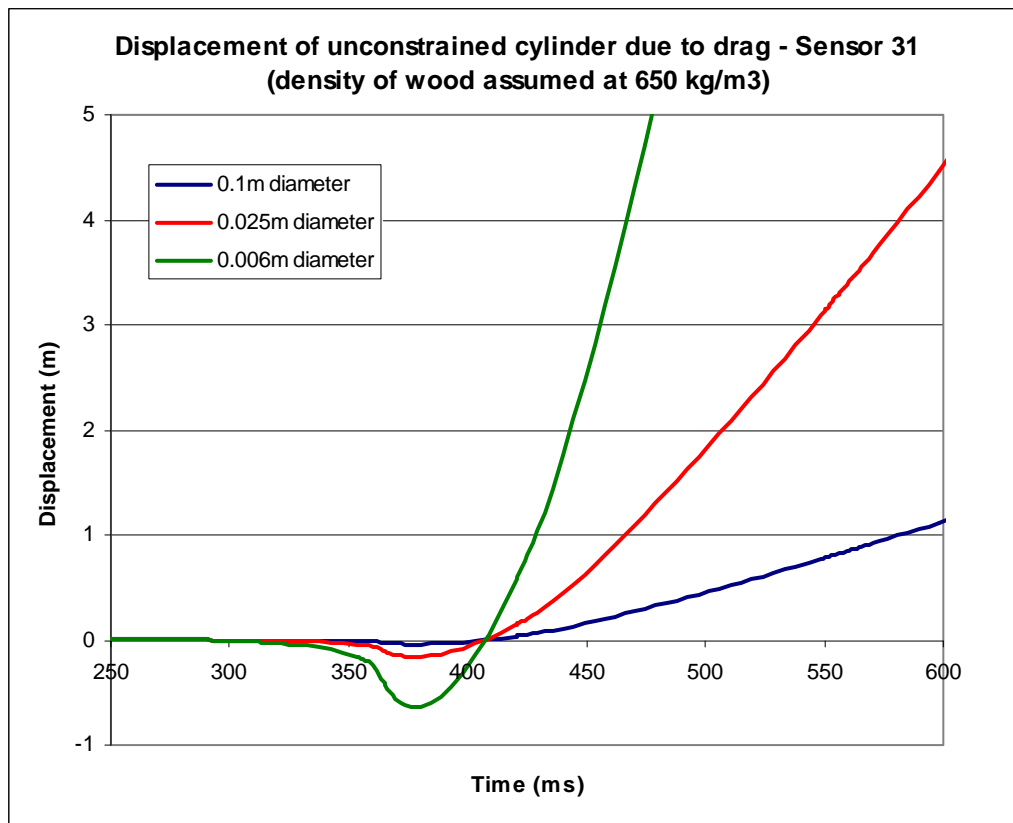
Figure C.19 Displacement calculations due to drag load at Sensor 31

When we calculate the displacement, the short duration of the drag load means the inertial mass significantly damps the displacement, and it therefore appears that for increasingly strong explosions the drag load effect on damage will get smaller in the forward direction, while staying large in the reverse direction. Thus the damage vectors due to branches, poles etc, will tend to point towards the source of the explosion rather than away from it.

Note that drag load is the load arising on an object inserted in a steady-state flow field, whereas in a blast there are additional loads arising from transient pressure gradients. A pressure gradient can exist with zero flow, so we generally consider drag load and pressure gradient load to be separate components.

For an example of pressure gradient load, consider a rate of pressure change on the leading edge of a blast wave of 1 bar in 1 ms - the blast wave will propagate at the speed of sound (340 m/s), so the gradient is 100 kPa in 0.34 metres. So the net force on a square post 0.34 m wide normal to the pressure gradient will be 34 kN per metre, which is 5 times bigger than the dynamic pressure values in Figure C.18.

As the dimensions of the object get bigger, so the pressure gradient force scales with volume, as does the mass of the object, so induced acceleration stays the same, whereas drag load scales with area, and so acceleration due to drag load increases at smaller length scales. The duration of the pressure gradient load lasts only as long as the pressure gradient persists, whereas the duration of the drag load persists as long as flow exists - usually far longer. For this reason we normally concern ourselves with pressure when considering damage to larger structures such as buildings and blast walls, but when considering the displacement of smaller items, such as branches and posts, the drag load is often the dominant factor in causing damage.

C.4.3. In the Car Park

As would be expected for a deflagration, the flame front emerging into the open car park area slows appreciably as there is no longer any congestion to generate turbulence. The blast wave continues as a pressure wave at the speed of sound, and takes the form of a more normal pulse with rarefaction following the initial pressure pulse. The peak pressure as it meets the Fuji building is 150 mbar, with an impulse of 1300 Pa.s.

Note that the correct modelling of the progress of the flame front as it enters the open space of the car park could be important in determining the time delay between the blast wave arriving at the far side, and the arrival of the flame front. The level of turbulence arising due to the blast wave interacting with the surface of the car park and anything in the car park could have a significant effect on the flame speed.

C.5.   MODELLING THE EFFECTS OF MORE FINE-SCALE CONGESTION

As described earlier, the modelling of congestion in the trees and shrubs bounding Three Cherry Trees Lane and Buncefield lane had to be simplified in order to allow the large-scale gas cloud to be modelled. The form of this simplification was to replace many small-scale items with fewer large-scale items with equivalent drag and blockage. This allows a coarse mesh size to be used, and so permitted the modelling of the very large cloud.

A large number of analyses were subsequently run with smaller domains in order to test the effect of using a more finely resolved model of the vegetation, and also using a more reactive gas (ethylene). Both approaches were expected to increase the speed of the deflagration, and hence the pressure build-up.

These simulations modelled an explosion travelling along Three Cherry Trees Lane with congestion on either side. The explosion was initiated from the auxiliary pump house. The results from two of these simulations are presented here; the first is a propane explosion with more detailed congestion, and with the width of the congestion slightly increased (see Figure C.20).

The anticipated effect of more congestion is to increase the amount of flame folding and turbulence and thereby increase flame area and hence the rate of fuel consumption. In addition the extra congestion provides more drag and so reduces the ability of pressure to be relaxed away upwards and to the sides of the road. The two effects combined mean the deflagration follows a positive feedback loop, building pressure and burning rate as it progresses down the lane.

Observation of similar simulations with variations in the width of the congestion, show that the outcome of a long run through congestion is very sensitive to these parameters, and it needs stressing that we are not only attempting to estimate a suitable equivalent level of congestion, but we are having to model the congestion as 100% stiff – so that it doesn't move with the blast.
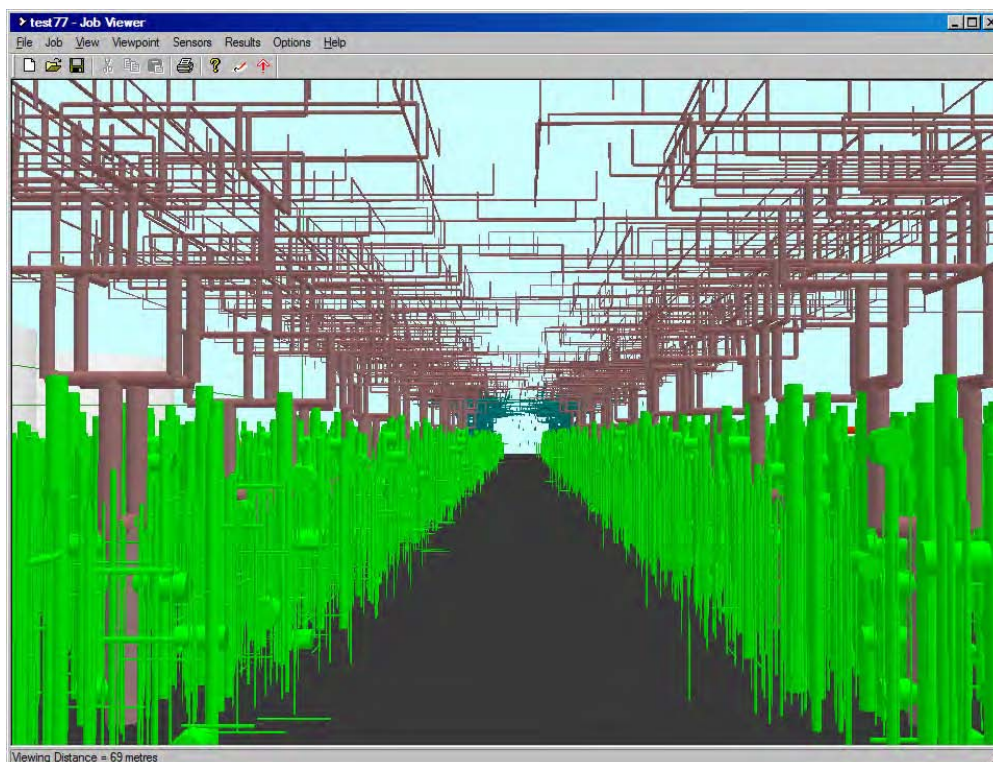
Figure C.20 More finely resolved congestion

The development of the explosion proceeds much as before, with the flame front initially expanding hemi-spherically from the pump house, and accelerating along the congestion in the lane.
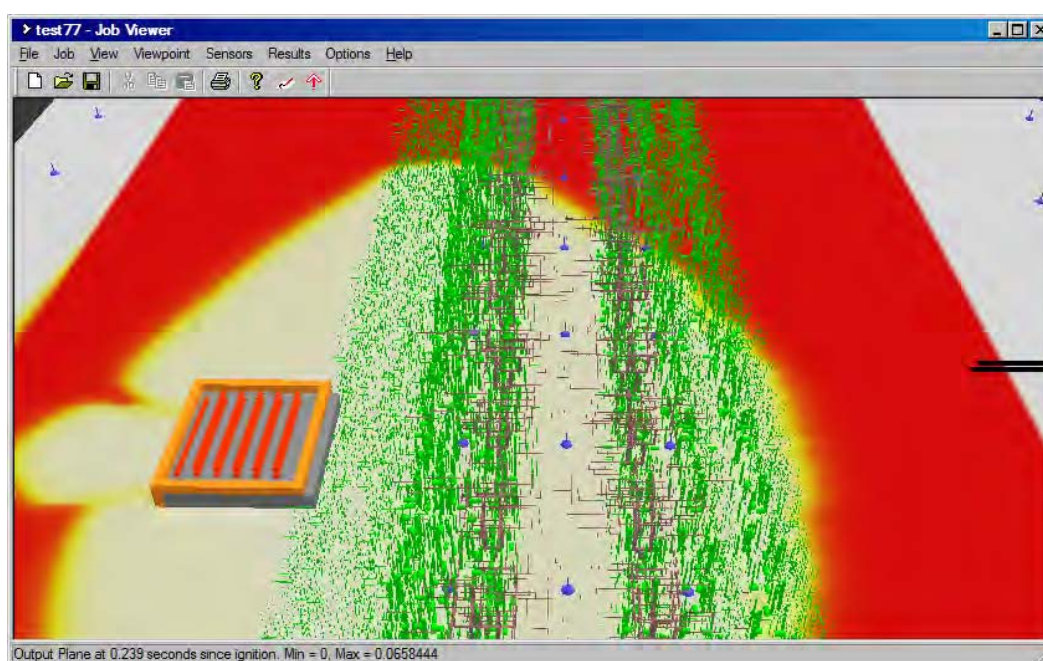
Figure C.21 Fuel cloud 239 ms after ignition

In this instance we have three rows of pressure sensors and if we plot the pressure along the left hand side of the lane (as viewed above), then we can see the pressure building and the flame front accelerating.
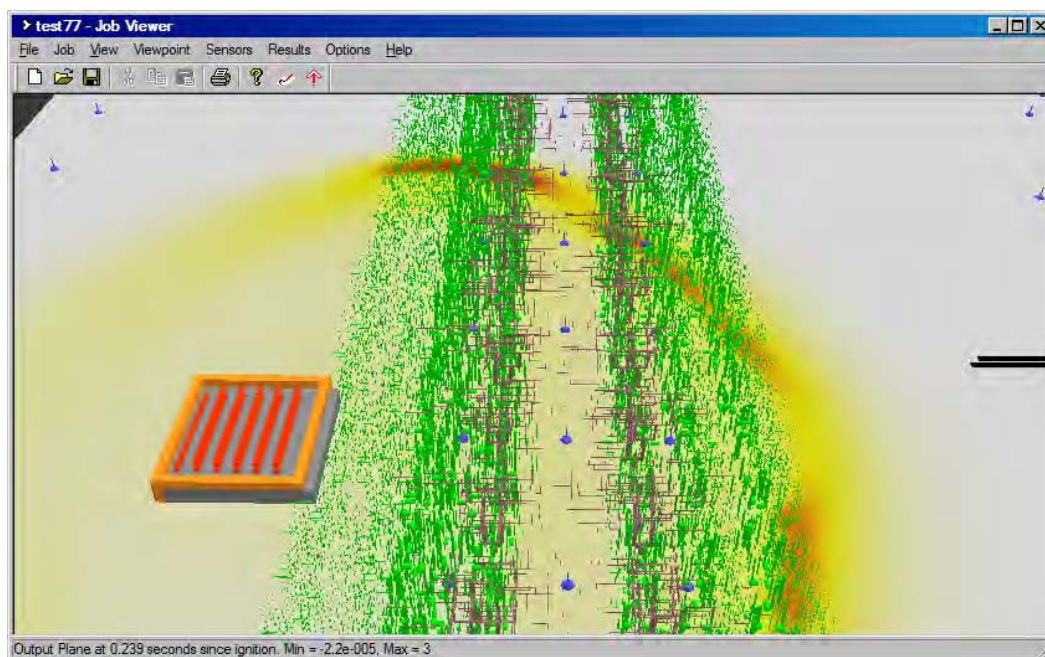
Figure C.22 Pressure at 239 ms after ignition, red = 3 bar overpressure
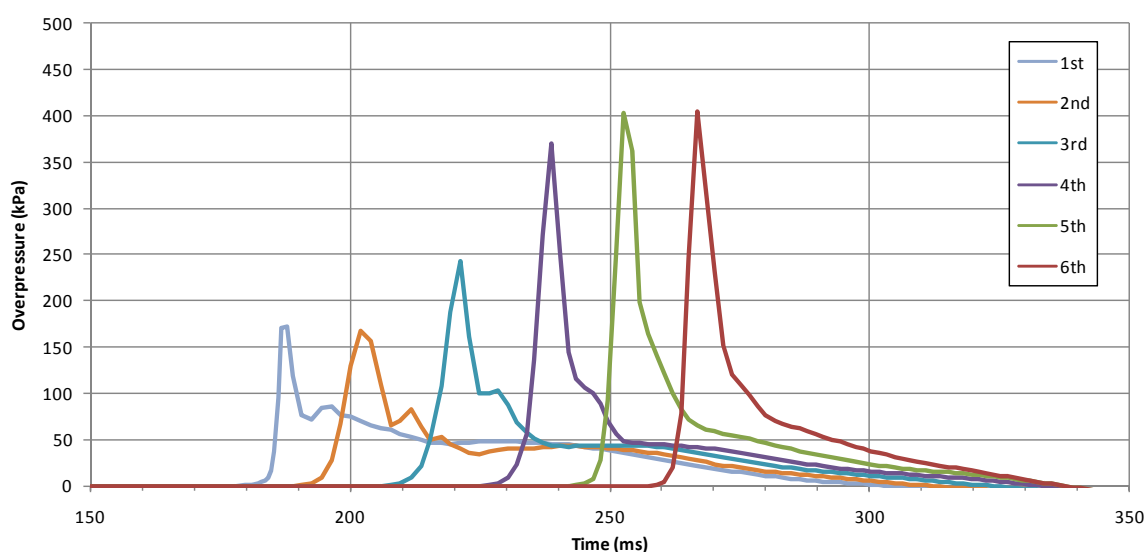
Figure C.23 Explosion pressure building along the lane

Analysis of the corresponding traces for fuel and product formation confirm that the pressure peaks above coincide with the flame front propagation, and given the 10 metres separation of the pressure sensors this gives a flame speed over the ground of 714 m/s.

It should be noted that the increase in predicted overpressure in this run is a result of the greatly increased number of obstacles included in the simulation. Approximately 2.4 times as many (61000) obstacles were used here as in the previous coarse-mesh runs.

In the 1980s British Gas carried out experiments on flame acceleration in a long region of pipe congestion with dimensions comparable to the verges on Three Cherry Trees. When the flame speed reached 600 m/s, there was a transition to detonation. As the Buncefield fuel has similar

reactivity to propane, there is a clear possibility that a deflagration to detonation transition (DDT) occurred close to the junction with Buncefield Lane.

C.6. LARGE SCALE SIMULATION USING ETHYLENE AS AN ALTERNATIVE TO FINE SCALE CONGESTION

As described earlier, the large domain has prevented modelling the vegetation in detail due constraints on current computing power. The descriptions of fine congestion above correspond to a mesh size in the congested region of 0.43 m, compared to the original propane simulation at 0.9 m. As the mesh is 3-dimensional this corresponds to an order of magnitude increase in the number of computational cells between coarse and fine congestion definitions, which was more than could be accommodated as the simulation of such a large cloud was already close to the limits of the model.

An alternative way to simulate the enhanced burning due to the small scale congestion is to use a faster burning gas instead of propane – in this case ethylene. It is not suggested that a more reactive gas was involved at Buncefield, it is purely used to overcome a limitation of the maximum mesh size permitted in the EXSIM model, and to explore what might happen if fine scale congestion was able to enhance the turbulent burning rate.

We ran some simulations with ethylene and a medium level of congestion, initially only in Three Cherry Trees Lane. The resulting flame acceleration was very similar to that found with propane and fine congestion shown previously. Extending the computational domain for this case resulted in overpressures rising to over 1100 kPa, well outside the validity of the model, and well beyond where DDT would be expected.

The results below are for an ethylene explosion simulation with the lower (original) level of congestion (0.9 m mesh); they are therefore quite likely an underestimate of what occurred, but allow us to explore the progress of the pressure if the explosion did reach about 400 kPa peak overpressure. It shows the development of the explosion as it travels along Three Cherry Trees Lane to the junction with Buncefield Lane.

Figure C.24 Large-scale simulation using ethylene showing cropped gas cloud
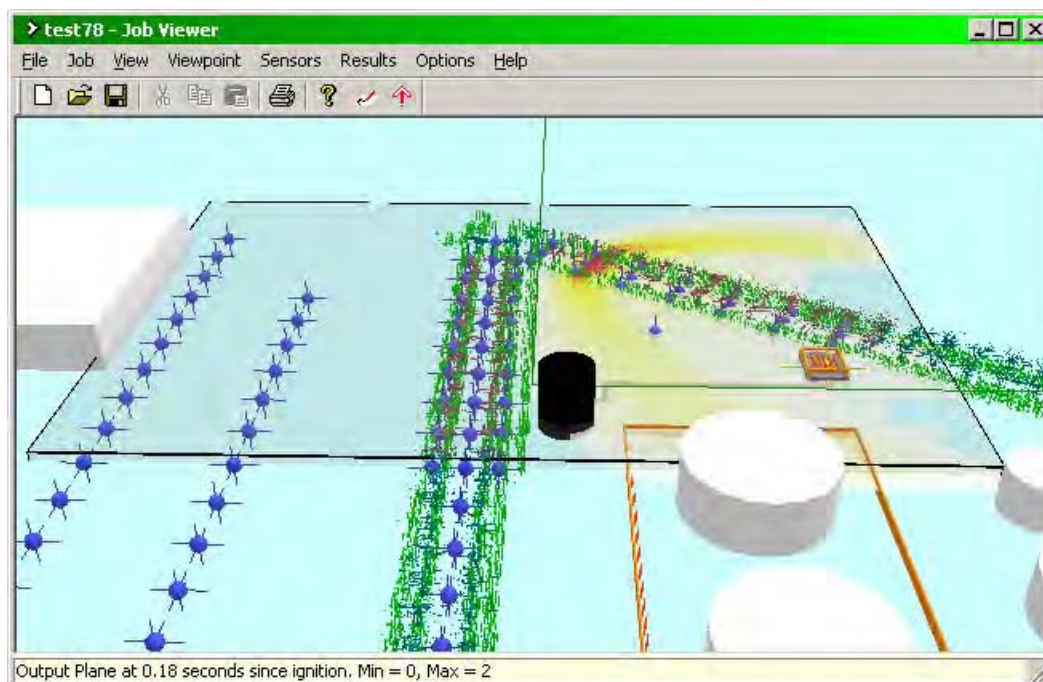
Figure C.25 Pressure trace from developing ethylene simulation

The more reactive gas significantly affects the explosion build up, and in the plot above red is 2 bar overpressure or over (peak overpressure is 2.7 bar at this point), and it is clear that the blast front is about to interact with the vegetation along Buncefield Lane.

At about 225 ms after ignition the explosion crosses the Buncefield Lane vegetation and the flame front would be expected to slow rapidly as it emerges into the uncongested car park, though the blast wave continues to travel on an almost planar front. Peak pressures reported within the model as the explosion crosses Buncefield Lane are about 2.9 bar.
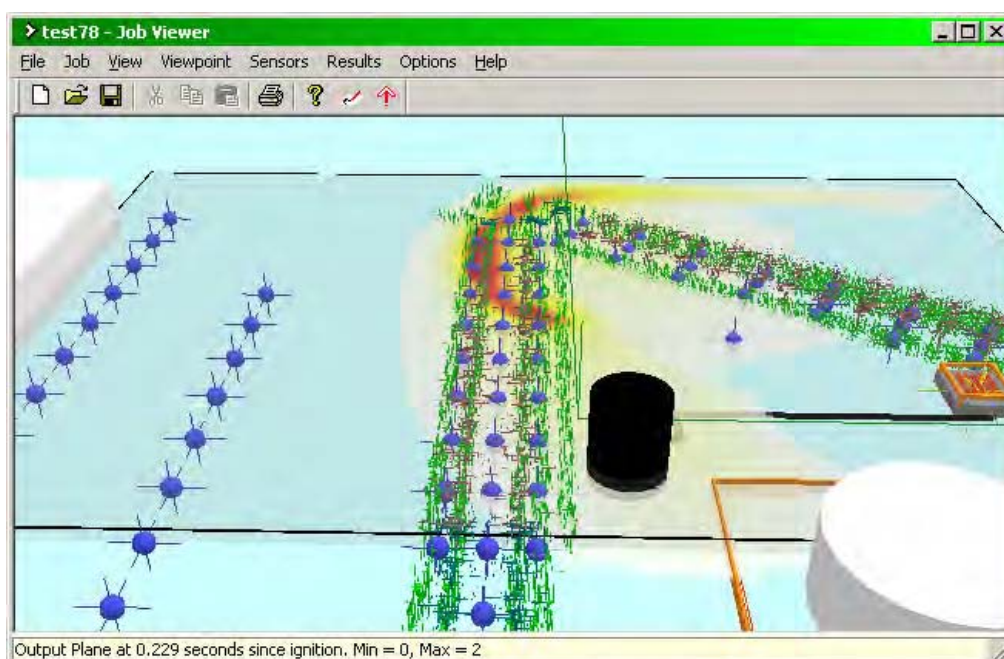
Figure C.26 Explosion front crossing Buncefield Lane (ethylene simulation)

The blast wave continues to accelerate down Buncefield Lane, but the blast wave travelling across the car park decays as significantly as the burning rate slows due to the lack of congestion.
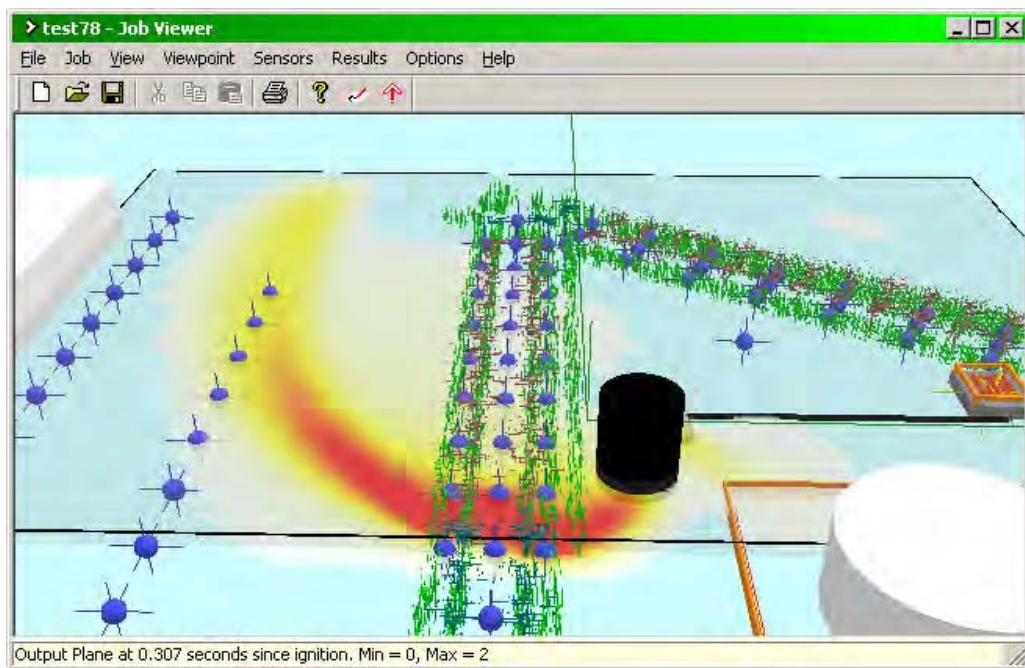
Figure C.27 Explosion front in car park and travelling south on Buncefield Lane
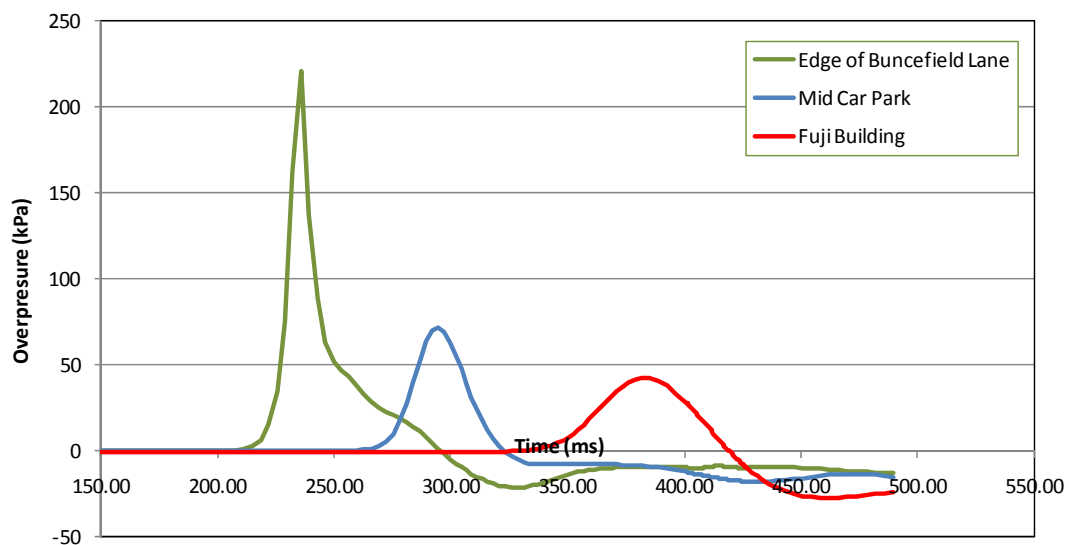
Figure C.28 Pressure Traces for Ethylene Simulation

The pressure traces in Figure C.28 have been compared with the flame front arrival, and there is no separation of the flame front from the blast wave, which is the sort of behaviour expected for propane deflagration as it leaves the congestion and enters the car park. As we only introduced ethylene as a way of simulating the effect of small-scale congestion in the wooded lane on burning rate, it is inappropriate to analyse in detail effects such as drag load outside the congested area where the burning rate of ethylene could significantly distort the results. However it seems reasonable that a 2.5 bar blast wave emerging from the edge of Buncefield

Lane might decay significantly across the car park, but be increased by reflection as it impacted the Fuji building.

C.6.2. Peak overpressure contours

The simulations we have shown were particularly focussed on the interaction of the deflagration with the trees and shrubs in the lanes, but the study can be expanded to look at the effects over the wider area. As discussed before, we used ethylene to simulate the effect of additional turbulence generation and explosion development in the congestion, however this is not appropriate for modelling the explosion in the open areas, as the combination of the low level turbulence from shear over the ground, and the high laminar burning rate of the ethylene tends to keep the flame front speed higher than we observe for simulations using propane.

Furthermore we did not attempt to model the entire gas cloud, especially to the East and South of the site, neither have we simulated the congestion present in those parts of the site in any detail. This is in part due to reaching the limitations of the memory requirements for the model. For these reasons the information we can give on maximum pressures is restricted to the region encompassed by Three Cherry Trees Lane and Buncefield Lane, and the car park to the West of this area.

The contour map below is for the simulation using ethylene, and the grey square bounded by a dark line shows the extent of the flammable cloud in the model. The contours are made from the maximum pressure seen at each of the pressure sensors – blue circles. As would be expected the maximum pressures are seen in the vegetation in the lanes, and the maximum pressure drops off rapidly as the blast wave crosses the car park. The contours are 20 kPa apart, and by halfway across the car park the maximum overpressure has dropped to 80 kPa. It continues to fall, though comes up again slightly at the building due to the effect of reflection.
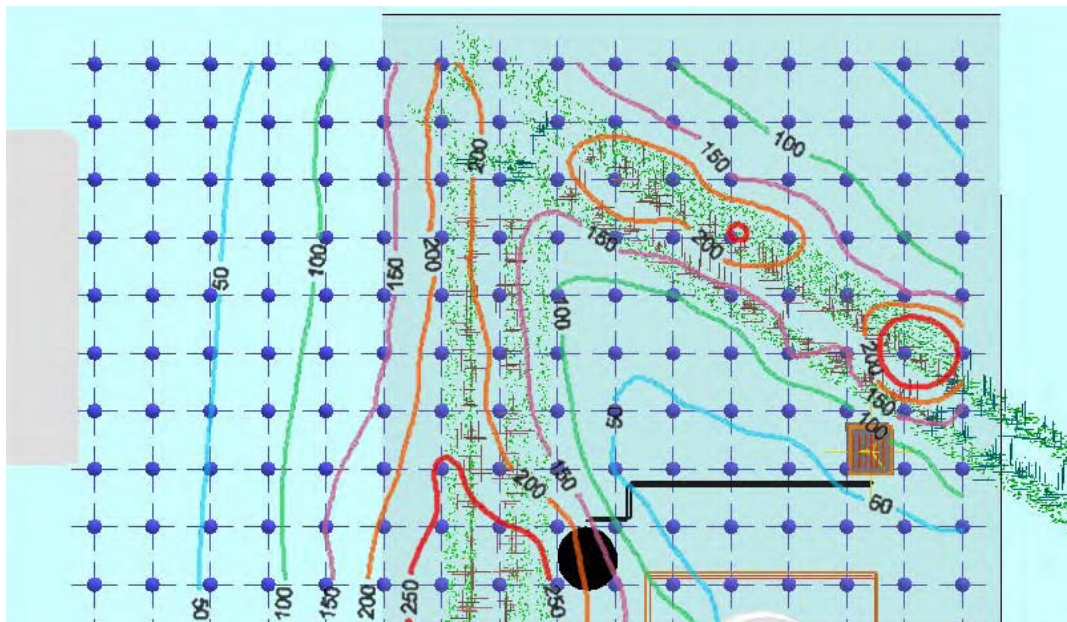
Figure C.29 Contours of peak overpressure

C.6.3. Negative pressure phase

In the rapid combustion of a spherically symmetric cloud ignited at the centre, volume is being generated all the time combustion takes place. When the fuel is exhausted, and combustion stops, the momentum of the radially outward flow of the air surrounding the flame continues. This outward flow eventually causes an underpressure at the centre that slows the flow; a

significant rarefaction wave then results. In the case of a pancake-shaped cloud, overpressure and underpressure can both be relieved vertically and so the effect is less pronounced. In Figure C.28, the overpressure is of the order of 200 kPa, and the underpressure is about 50 kPa, which seems entirely reasonable in the circumstances. Our experimental experience is that negative pressure waves tend to have longer duration than the preceding positive. Thus the ratio of the positive and negative impulses may well be less than 4. However, the simulation was not continued long enough to show this.

From these studies it is clear that the long runs through the congestion make the resulting overpressure and flame speed difficult to predict, as the outcome is very sensitive to the balance between the process of flame acceleration due to congestion and the ability to vent the pressure. This determines whether the pressure reaches a steady level, or whether the pressure continues to build.

C.7.   NET IMPULSE IN OPEN AREAS

The last simulation allows us to draw conclusions about the deflagration-induced damage vectors outside the congested area in a similar way to the earlier calculations of the drag load within the trees in one of the lanes.

Results are shows for sensor 51 (circled in Figure C.30)
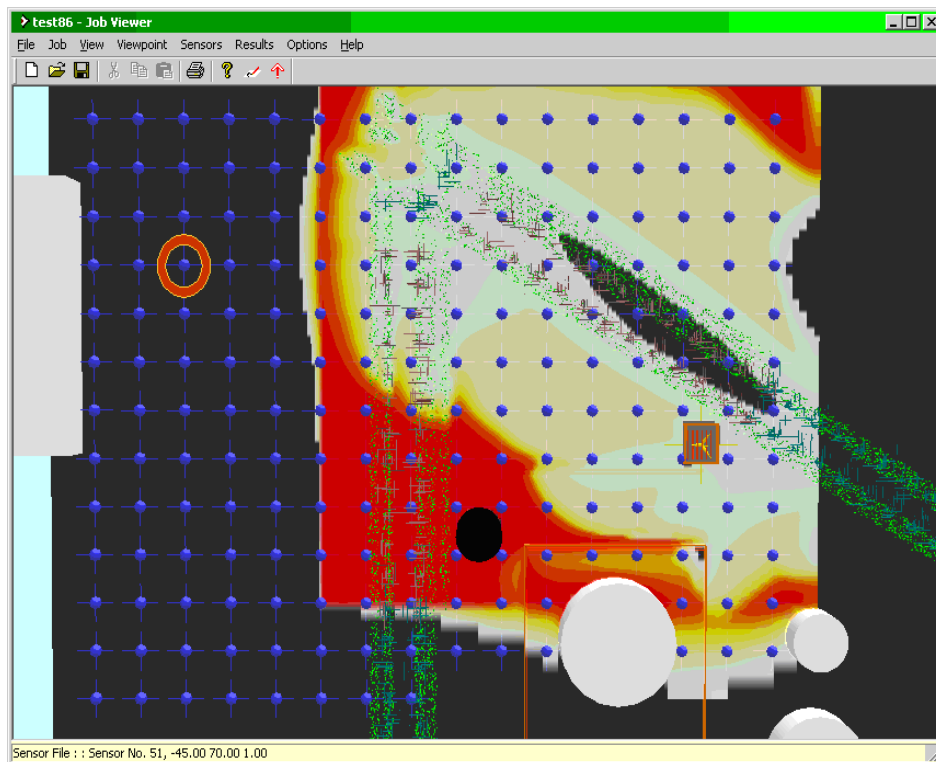
Figure C.30 Location of sensor 51
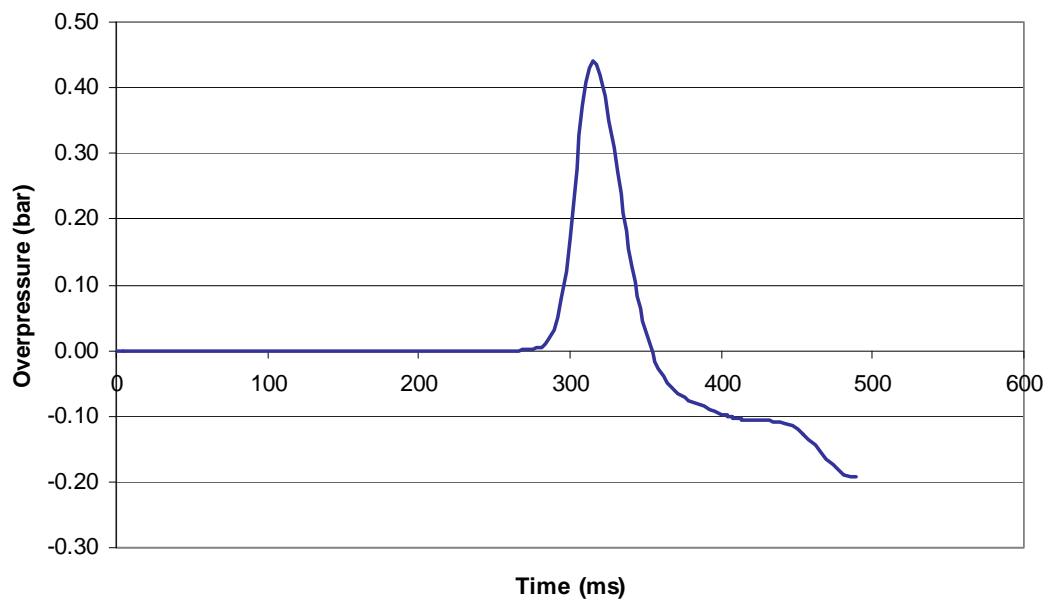
Figure C.31 Overpressure
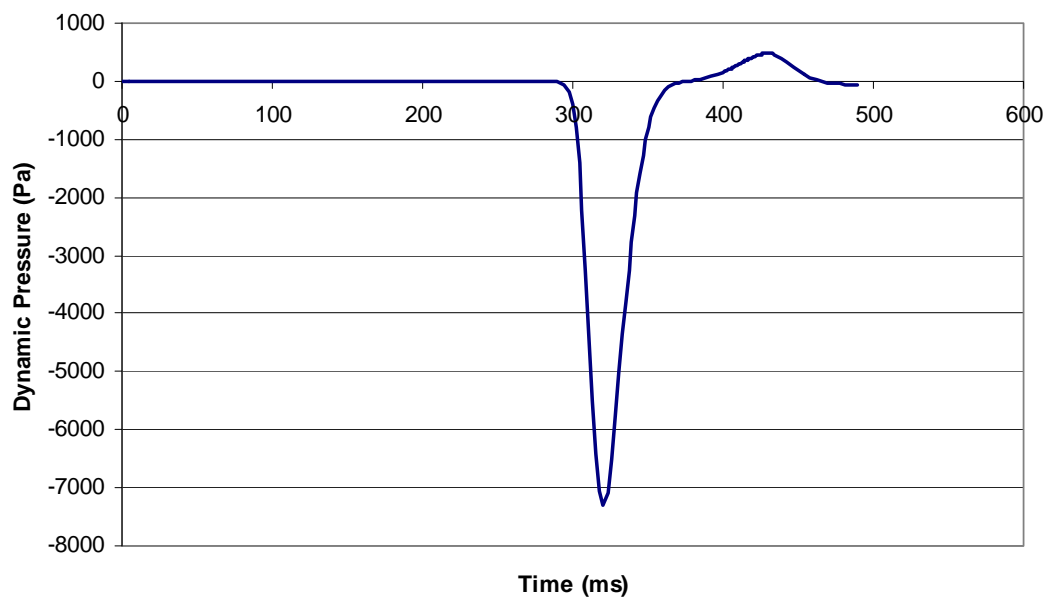
Figure C.32 Directional dynamic presure
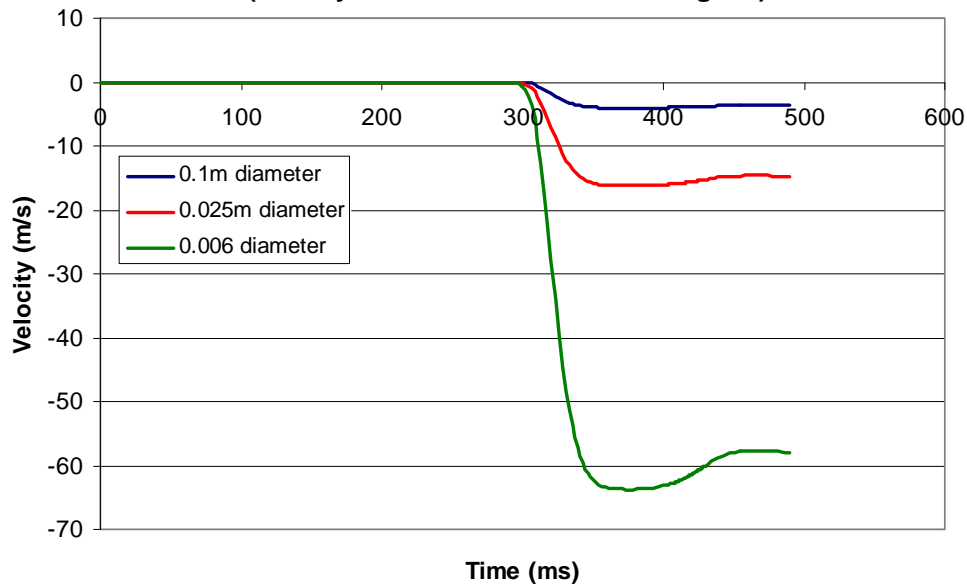
Figure C.33 Velocity of an unconstrained cylinder due to drag (density of wood assumed at 650 kg/m^3)
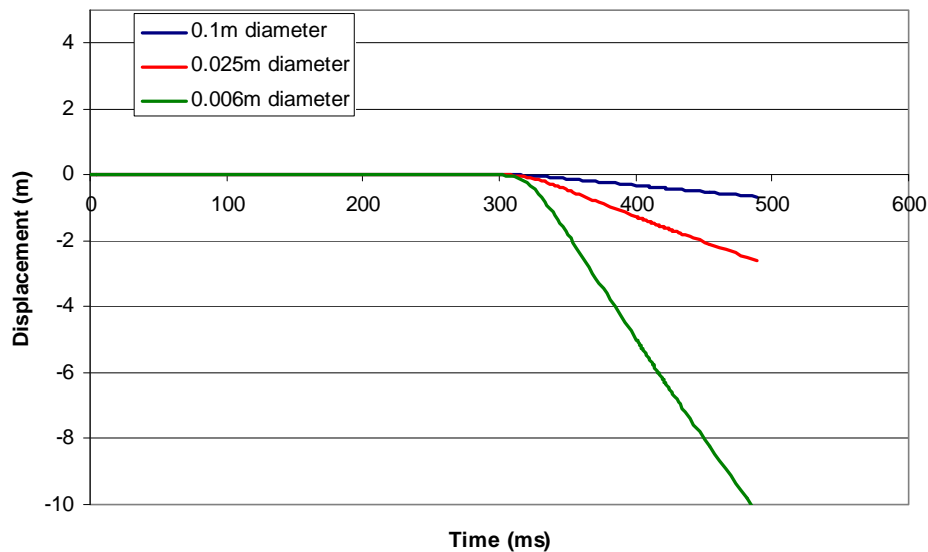
Figure C.34 Displacement of an unconstrained cylinder due to drag (density of wood assumed at 650 kg/m^3)

As can be seen from the graphs above, the predictions for the loading due to the blast wave alone are that the damage vectors will be away from the source of the explosion. It appears that the reverse flow behind the combustion front observed when the same analysis was carried out within the gas cloud is generated by the combustion process. Without combustion the main effect is in the direction of the blast wave. Note that combustion in the car park was suppressed in this simulation by truncating the cloud. For a propane cloud extending into the car park, the flame front is expected to follow the blast wave at much reduced velocity with very limited pressure generation, and this will tend to reduce the rarefaction following the blast wave, but is unlikely to have a significant effect on the results above.

C.8. EXPANSION OF GAS CLOUD DURING EXPLOSION

We have investigated whether there is a significant difference between the original un-ignited cloud size and the cloud size as revealed by evidence of direct burning. In fact the horizontal expansion is minimal. The reasons are are two-fold. First is the flat shallow nature of the cloud, which being unconfined vertically, relaxes upwards rather than outwards. The second is that the interaction with the congestion in the lane has accelerated the deflagration, so that the time between the communication of pressure outwards (which occurs at the speed of sound), and the arrival of the flame-front is quite short, so there is little time for the gas cloud to be accelerated away from the flame-front before it arrives.

Results from the model are shown in the following Figures. Figure C.35 shows the initial gas cloud (rectangular in the simulation), red showing the full initial concentration. Figure C.36 and Figure C.37 show its extent at two later times; the change of colour shows that some dilution has taken place at the edge. Thus the gas cloud might expand five metres or more in the direction south from the pump house where the slow rate of burning (due to low congestion), gives the unburned gas more time to respond. In the direction of the car park, where the feedback mechanism increases the flame speed, the gas is only moved a few metres before the flame front arrives.

The actual gas cloud was, of course, not rectangular, but the order oof magnitude of the expansion should not be dependent of the cloud shape.
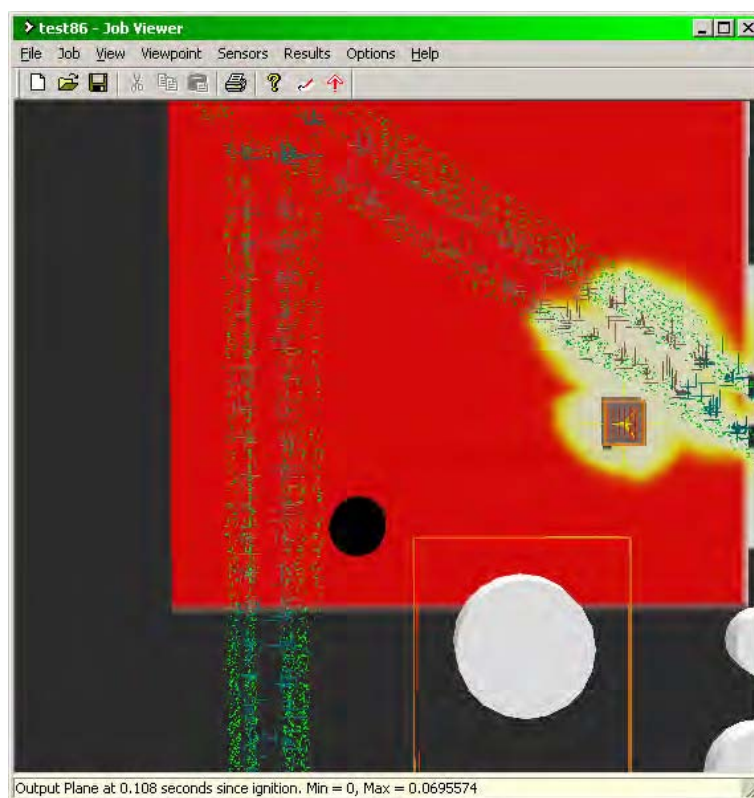
Figure C.35 initial gas cloud
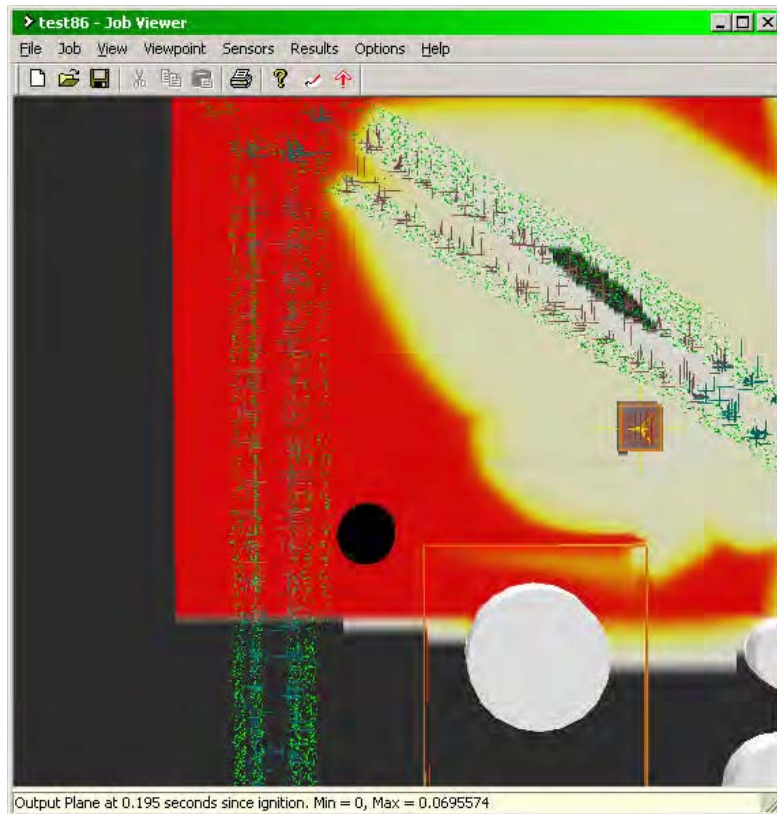
Figure C.36 Gas cloud extent during combustion
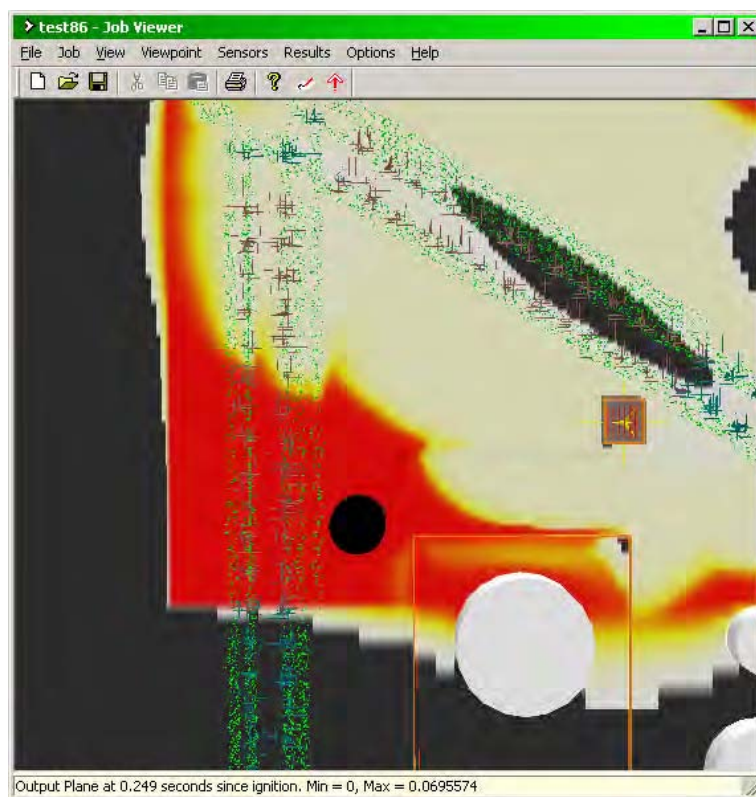
Figure C.37 Gas cloud extent during combustion

C.9. CONSISTENCY WITH DAMAGE OBSERVATIONS

A strong deflagration reaching 400 or 500 kPa, just short of DDT, could have produced overpressures of the order of 100 kPa in the car park. This is short of the lower limit of 200 kPa derived from the damage analysis on the cars in the car park. It may have been sufficient to damage the buildings as observed. The overpressures predicted from this scenario on the HOSL site are generally lower, showing a greater discrepancy with the peak pressures necessary to cause the observed damage to the switch boxes. Furthermore, an explosion consisting only of deflagration is not consistent with the direction markers outside the congested area, which point towards the source of the explosion. We have shown that the net impulse outside the congested region would be in the outward direction for a deflagration.

However, acceleration of the flame up Three Cherry Trees Lane to DDT near the junction with Buncefield Lane, as indicated by the simulation with propane and fine congestion, removes this inconsistency. This scenario is consistent with the overpressure estimates and the directional damage found in the deflagration region in Three Cherry Trees Lane and in the open areas.

C.10. SUMMARY AND CONCLUSIONS

The explosion model EXSIM has been developed and validated against experimental data obtained for simulated petrochemical plant. When applied to a large shallow cloud intersecting large open areas as well as trees and hedgerows, it is taking the model outside its validation range. We would not be able to use the model as a predictive tool for this sort of scenario until we have adequate data obtained from explosion experiments involving dense vegetation.

However, it has been possible to simulate the vegetation by arrays of pipe elements. Initially the small-scale details were ignored, to enable us to simulate all of the main region of interest. The effect of this is likely to be a considerable reduction of the overpressures predicted.

This was followed by localised studies with finer congestion. However the finer congestion requires a finer mesh size and so modelling of the full problem domain in this way was not feasible owing to computational limitations.

The simulations indicate that a deflagration will tend to accelerate through the congestion represented by the trees and shrubs, and may locally reach overpressures of several hundred kPa. A number of factors limit this build-up:

- The cloud is shallow allowing rapid pressure relief upwards above the flammable region
- The trees and shrubs are mainly round in section, so do not generate as much drag and turbulence as square sections of the same width.

The following factors would generally be judged as conservative (i.e. may lead to over-prediction):

- We have assumed a uniform stoichiometric propane cloud of 3.0 metres depth; it is more likely that the cloud has varying composition with depth.
- We cannot allow for the fact that vegetation is less stiff than engineering plant, and will move thereby reducing drag.

The following factors are concerns with applying the model to this sort of problem:

- The process of congested explosion development depends on a feedback mechanism, and for very long runs in congested regions it may be very sensitive to the level of feedback.

- The appropriate level of blockage to use for the vegetation is unknown, especially with regard to the fact that the model uses stationary congestion, whereas vegetation is increasingly free to move in response to the blast wind as it gets smaller.

The simulation that appears to match the conditions at Buncefield most closely included representation of all scales of the congestion and used propane fuel. This led to acceleration of the flame to a speed that has been observed experimentally to result in transition to detonation. This occurred in Three Cherry Trees Lane near to the junction with Buncefield Lane.

The results were, however, found to be very sensitive to the amount of congestion. In a run with somewhat lower width of the vegetated verges, the feedback mechanism was not strong enough to maintain flame acceleration, and much lower overpressures were generated.

In order to compensate for the reduced flame acceleration when simulating a larger domain (because of the inability to include the effects from small obstacles), some further simulations were performed using ethylene as the fuel. Ethylene with a medium level of congestion matched the propane run with a high level of congestion (smallest obstacles included) mentioned above. Over the larger domain this gave further acceleration to overpressures up to 1300 kPa, but this is well beyond where the model is valid, and beyond where a transition to detonation is probable.

With all the uncertainties, the above simulations might be an overestimate of the flame acceleration and resulting pressure. It was possible to study how the pressure wave would develop from an explosion that reached 400-500 kPa in the lanes by using ethylene and a lower level of congestion. A significant blast wave was predicted travelling across the car park over a wide front, leading *to free-field* overpressures of no more than100 kPa over most of the car park and at the Fuji building. Predicted pressures on the Buncefield site were lower. These values are inconsistent with the overpressures estimated from damage to cars and switch boxes.

The model does indicate a strong reverse flow behind the flame front as it propagates along the Lanes, and use of drag load suggests that the larger vegetation may be able to move sufficiently to accommodate the forward pressure pulse, but may fail when exposed to the longer duration reverse flow. Thus the direction damage of the trees in the two lanes is generally consistent with these calculations. By contrast, for the deflagration wave travelling across the open areas the calculated net impulse is forward; this is again inconsistent with the observations.

Such inconsistencies lead us to consider the scenario of acceleration in Three Cherry Trees Lane up to DDT, with a detonation travelling through the remainder of the gas cloud. This is discussed further in the following Appendix.

C.11.   REFERENCES

Harrison, A. J. and J. A. Eyre. "External explosions as a result of explosion venting." Comb.Sci.Tech. 52 (1987): 92-106.

Hjertager, B. H. "Computer modelling of turbulent gas explosions in complex 2D and 3D geometries." J.Hazardous Materials 34 (1993): 173-97.

Hjertager, B. H., T. Solberg, and K. O. Nymoen. "Computer modelling of gas explosion propagation in offshore modules." J.Loss Prev.Process Ind. 5 (1991): 165-74.

van Wingerden, M and Wilkens, B. "Experimental Investigation of the Effect of Flexible Obstructions on Flame Propagation in Vapour Cloud Explosions", Ref. No.: GexCon-08-F44110-RA-1, 31/10/2008.

APPENDIX D   POTENTIAL FOR DETONATION

D.1.   INTRODUCTION

Damaging overpressures can be produced when a flammable gas mixture undergoes a detonation. Detonations have been studied widely, though mostly in relation to the generation and propagation of detonations in tubes. In relation to Buncefield, however it is the possibility of detonation of in an 'unconfined' vapour cloud that is of interest. In these circumstances, detonation can be initiated by high speed flames and the associated overpressures and can therefore be a development of the high speed deflagration discussed in Appendix H.

The assessment given here in relation to detonation provides:

- A description of the basic physical processes involved in a detonation
- The detonation scenario being considered in relation to the Buncefield incident
- Details of modelling work carried out as part of this project
- Comparison of the understanding of detonations and the modelling results with the evidence from both the incident and subsequent experiments, to determine if detonation provides a possible explanation.

For the purposes of this analysis, detonations are considered in the context of hydrocarbon-air mixtures at atmospheric pressure, unless otherwise stated. It should also be noted that this analysis is not intended as a thorough review of detonation understanding and research.

D.2.   MECHANISM

D.2.1.   General Factors

Although the detailed description of detonation propagation is relatively complex, the basic physical processes involved can be stated relatively simply. A detonation involves:

- An initial shock wave with a typical magnitude of over 2000 kPa.
- Compression of the hydrocarbon-air mixture by the shock wave such that it raises its temperature above the auto-ignition temperature of the mixture, initiating combustion.
- Energy transfer from the combustion maintains the magnitude of the shock wave.

The part of the shock wave associated with the auto-ignition will have a very short duration of typically just a few tens of microseconds. The overall shock wave may have a duration of a few milliseconds.

This coupling of the shock wave and combustion can be self sustaining and, unlike a deflagration, is not dependent upon the presence of obstacles for its continued propagation. The detonation front typically travels at speeds of 1500 to over 1800 ms^{-1}, depending on the fuel concentration [1], i.e. it can exceed five times the ambient speed of sound.

Whilst the characteristics of established detonation (e.g. pressure and flame speed) in most fuel-air systems are broadly similar, different fuels have different propensities for undergoing detonation (the detonability of the mixture). This latter property is governed by the rate of the high temperature oxidation reaction of the system when subject to the detonation shock front and thus depends on the fuel reactivity.

The detonability of any specific fuel, common hydrocarbon fuels can be considered in three general classes [2]:

- High reactivity fuels that readily detonate: such as hydrogen, acetylene and ethylene.
- Normal reactivity fuels where there is evidence to indicate that detonation is possible in practical situations but less likely: such as propane and butane.
- Low reactivity fuels that are very difficult to detonate: such as natural gas and its main constituent methane.

The vapour cloud formed at Buncefield probably comprised mainly butane and pentane [3] and would therefore fall into the normal reactivity category.

The ability of a detonation to be sustained also depends on the concentration of the hydrocarbon in the air. Whilst in practice the limits to fuel/air detonation are similar to the flammability limit, they are governed by quite different physical and chemical factors. The influence of both fuel type and concentration is illustrated in Figure D.1, reproduced from Bull [4].
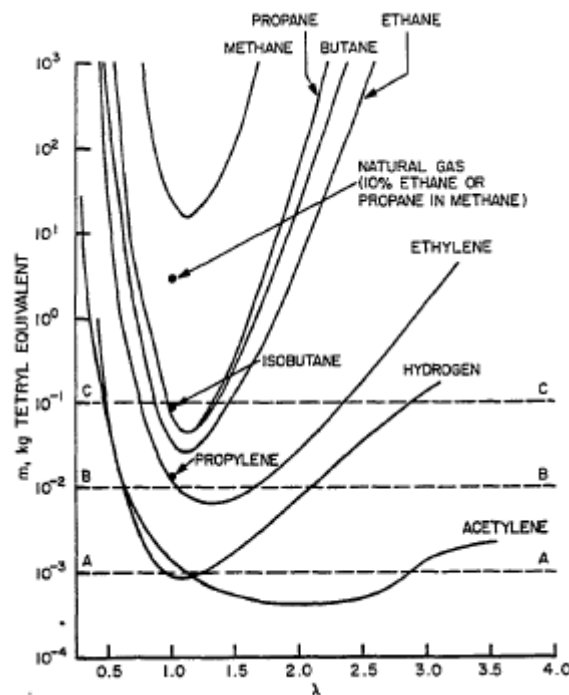
Figure D.1 Detonability of Fuel-air Mixtures as a Function of Concentration

The detonability in Figure D.1is measured by the mass of High Explosives required to initiate detonation. In this figure, λ on the x-axis indicates the concentration of the fuel relative to stoichiometric. It can be seen that many fuels are most detonable (i.e. require the least amount of explosives) at concentrations just above stoichiometric ($\lambda \approx 1.1$) and the detonability of propane and butane are very similar.

74

D.2.2. Initiation of a Detonation

Detonation of flammable mixtures within pipes or tubes has been studied in some detail but is not directly relevant to the potential for a detonation to occur at Buncefield. It is necessary to turn to the much more limited information related to detonation in unconfined hydrocarbon-air clouds to assess the possibility of a detonation occurring in the vapour cloud at Buncefield.

In general, transition to detonation requires that pressures of sufficient magnitude are generated within a volume that is large enough for auto-ignition to occur and be sustained in a propagating detonation. This concentration of pressure energy can be produced in a number of ways, including:

- Direct initiation by a high explosive charge within the cloud.
- A detonation venting from a pipe or duct into an external cloud.
- An explosion venting from a confined volume, such as a building, into the cloud.
- A deflagration to detonation transition ("DDT").

The evidence from the site investigation and that described Appendix A does not support the possibility of either of the first two mechanisms being involved at Buncefield. In addition, as will be discussed later, initiation by venting from a building is not supported by the evidence. However, Appendix H shows that a high speed deflagration could have been generated at Buncefield and the possibility of deflagration to detonation transition therefore needs to be considered.

The initial question to be asked, therefore, is whether DDT could be considered, at least in some way credible, for 'intermediate' type fuels given the deflagration predicted for Buncefield.

One particularly relevant large scale experimental study of flame acceleration and DDT in open clouds is described in Harris & Wickens [5]. The experiments were carried out in a 3 m square test rig measuring up to 45 m in length and containing repeated obstacle arrays. Ignition was at one end of the test rig either by a low energy spark or vented explosion. A picture of the test rig is shown in Figure D.2. In this configuration ignition was by a vented explosion on the left hand side of the picture. The figure also shows the pipework congestion used in most of these experiments.

Figure D.2 45 m long Test Rig

The long flame acceleration path provided in the experiments has similarities with the tree lines at Buncefield. In addition, the congestion in the tree line appears to be more 'severe'[1] than that present in the experimental work. Experiments were mostly conducted with natural gas-air mixtures, however a smaller number were conducted with ethylene, propane and cyclohexane. The propane and cyclohexane tests are particularly important as these fuels fall in the normal reactivity group of fuels, similar to the Buncefield cloud.

The experiments showed that flame acceleration to high flame speeds was possible with propane and cyclohexane-air mixtures and that once flame speeds of 200-300 ms^{-1} had been achieved, continued flame acceleration could lead to DDT within a distance of a few metres, typically at flame speeds in excess of 600 ms^{-1}. This detonation was then sustained through the remaining length of the test rig, even if no pipework obstacles were present. It is worth noting that it would be expected that a DDT would involve a discontinuity in the speed of the flame. Detonations do not occur as a result of continuous flame acceleration up to 1500 or 1800 ms^{-1}. If a transition to detonation is to occur, it will happen at speeds well below this, resulting in a sudden increase in the speed of the flame.

Other experimental work has shown that when flame speeds approach the ambient sound speed and generate shock waves, then shock reflections appear to initiate a transition to detonation [6, 7]. It is likely that this mechanism was also involved in the DDT observed in the 45 m rig tests.

D.2.3. Detonation Propagation

Detonation propagation in flammable gas clouds in the open atmosphere can be less certain compared to that in experimental work. In experiments, the fuel mixture is almost always at a single homogeneous concentration, whereas in a flammable cloud dispersing in the atmosphere, there will be fluctuations in the fuel concentration. If these fluctuations take the concentration outside the detonable range and the size of the fluctuation is large enough, then the detonation will stop.

However, there are reasons why this may not prevent propagation of a detonation in the cloud produced in the Buncefield incident:

- The Buncefield incident involved dispersion of denser than air petrol vapours in quiescent conditions and over an extended period. These conditions are less likely to produce concentration fluctuations than, for example, the sudden release of a pressurised liquid fuel at a temperature well above its atmospheric boiling point.
- The vapour cloud would have had a range of concentrations both through its height and in the horizontal plane. As a result, there would probably have been some path for the detonation to take to get around any region where the concentration was outside the detonable limits.
- Detonations can jump relatively small fluctuations, as indicated in Bull et al [8].

It is worth noting that if DDT were to occur, it would probably require something close to a stoichiometric mixture in the region where the transition takes place, as indicted by the data presented in Figure D.2. However, once detonation has been initiated it is less sensitive to concentration variations than a deflagration, assuming the detonation can find a path that is within the detonable limits. Deflagrations, particularly those propagating in high aspect ratio congested regions, with venting of combustion products behind the flame, can be highly sensitive to concentration variations.

---

[1] In that it will give greater flame acceleration under otherwise identical conditions.

D.2.4. Previous Incidents

Previous incidents are discussed in Appendix H. Two of these, Port Hudson and Ufa, involved explosions of propane-air clouds that were subsequently described by the accident investigators as detonations. As is shown in Appendix H, these explosions had a number of features that were common to the Buncefield explosion.

Detonation may have occurred in other incidents. However, as the majority of vapour cloud explosions involve ignition of a cloud that is mostly contained within a congested process area, it would be difficult to distinguish between a high flame speed deflagration and a detonation in these circumstances.

D.2.5. Summary in Relation to the Detonation Mechanism

It is recognised that there are many technical factors that affect the potential for a particular fuel mixture to detonate. In addition, just because an accident investigator has reported a previous incident as a detonation, it does not therefore follow that the Buncefield explosion involved a detonation. However, at the highest level; the experimental work combined with the incident record shows that the occurrence of a detonation in the Buncefield incident is credible and should be examined to see if it is consistent (or at least not inconsistent) with the available evidence.

D.3. DETONATION SCENARIO AT BUNCEFIELD

D.3.1. Aspects that Might Suggest a Detonation

Before conducting any detailed analysis of the evidence, it is first worth considering those aspects of the incident for which a detonation of a significant part of the vapour cloud provides a potentially attractive explanation. These are:

- **High Overpressures** – A detonation would explain the widespread high overpressure damage within the cloud. The damage is described in Appendix H and suggests pressures of many times atmospheric pressure.
- **Directional Indicators** – Those inside the cloud point inwards, those outside the cloud point outwards (as discussed in Appendix HThis strongly suggests that whatever mechanism generated the high flame speeds and overpressures, it propagated through the majority of the cloud, including the open areas. A detonation can extend throughout the cloud, whereas a deflagration of the type discussed in Appendix H is limited to the regions of congestion provided by the tree lines.
- **Pressure Decay** – There was rapid fall off in the level of pressure damage from the edge of the vapour cloud. A detonation propagating though a low lying vapour cloud could be expected to produce rapid pressure decay from the boundary of the detonable cloud.

Further examination of the last two aspects is presented in the following sections along with comparison with other evidence taken from the incident site.

D.3.2. Detonation Scenario

In order to assess the potential for detonation to explain the evidence it is preferable to consider a single simple scenario and test this against the evidence.

As discussed in Appendix A, the evidence supports ignition in the Pump House. However, given that the roof and walls would have failed at relatively low overpressures within the building and the lack of any congestion immediately outside the Pump House, it is highly unlikely that this

explosion could have directly initiated a detonation. In addition, direct initiation would not be consistent with the witness statements discussed in Section D.4.

The analysis detailed in Appendix H clearly shows that flame acceleration within the trees and bushes along Three Cherry Trees Lane is credible. The simplest detonation scenario that therefore suggests itself involves ignition in the Pump House, flame acceleration in the trees and, at some point, DDT.

The directional indicators are particularly useful in suggesting a location for the DDT. The directional indicator evidence is described in Appendix H and a summary is reproduced Figure D.3.
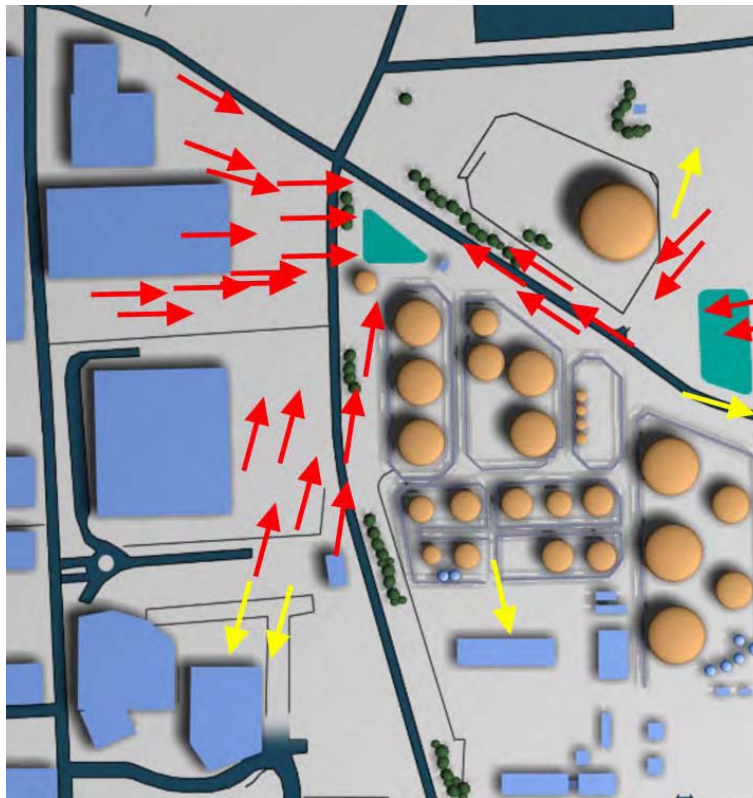
Figure D.3 Summary of Directional Indicators

The forces imposed on items within a detonating cloud are considered in Section D.6. However, if the assumption is made at this stage that a detonation propagating through the Buncefield cloud would give directional indicators in a direction opposite to the direction of propagation, then the directional indicators strongly suggest that the detonation initiated in the area of the junction of Buncefield Lane with Three Cherry Trees Lane.

Taken in combination with the analysis given in Appendix H, this suggests the following detonation scenario:

- Ignition in the Pump House resulting in a confined explosion venting into the external cloud.
- The flame propagates into the tree line to the north of the Pump House.
- The flame accelerates in the tree line in the same manner as described in Appendix H.

- Instead of continuing as a deflagration, transition to detonation occurs somewhere near the junction of Buncefield Lane and Three Cherry Trees Lane and this detonation propagates through a substantial proportion of the cloud.

It is recognised that there are many variations on this detonation scenario, for example DDT could have occurred more than once in the tree line. However, to allow initial comparison with the evidence to uncover possible discrepancies, this simple scenario has formed the basis of the assessment described in the following sections.

D.3.3. What Needs to be Explained

Before embarking on a comparison of the evidence with the detonation scenario described above, it is worth stating the aspects of the incident that need to be explained (or at the very least, it needs to be shown that the detonation scenario is not inconsistent with the evidence):

Timing of events – the evidence, in terms of both the CCTV records and the statements made by witnesses who were close to the explosion, places constraints in terms of timing of the events.

Duration of positive (non-negative) phase – CCTV records show arrival of overpressure (in the form of moving objects and cameras) at a number of locations followed by a 'misting' of the atmosphere of the order of half a second later. As described in Appendix A, this misting has been interpreted as being due to condensation of water vapour in the atmosphere as a result of below ambient pressures being generated. This 'negative phase' of the overpressure loading, often called the rarefaction, generally follows the 'positive phase'. However, the long period of time before the rarefaction phase begins needs to be explained for the detonation scenario, where timescales of the detonation front are generally measured in tens of milliseconds or less.

Directional indicators – selection of the detonation scenario involved the assumption that a detonation could produce the pattern of directional indicators observed. This assumption needs to be tested and, in particular, it needs to be shown that there is a net negative impulse on items present within a detonating cloud.

Pressure Decay from the edge of the cloud – it needs to be confirmed that a detonation scenario will reproduce the apparent rapid decay in overpressure from the edge of the vapour cloud.

Lack of ear damage to witnesses in the vicinity of the cloud – this is clearly related to the rapid pressure decay from the edge of the cloud, but is worthy of separate consideration as it places limits on the overpressure at the witness locations.

Damage to buildings in the near and mid-field – the overpressure loading predicted for buildings at the boundary of the cloud, primarily to the Northgate and Fuji buildings, should be consistent with the damage observed. In addition, damage to buildings in the mid-field (a few 100 metres from the cloud) should be consistent with the scenario.

Far field damage – the far field overpressure predicted for the scenario will need to be consistent with the damage observed (building damage extended to distances of several kilometres)

No further consideration is given to the overpressure damage to items such as cars and instrument boxes located within the cloud. The overpressures required to cause this damage are discussed in Appendix H and, though the overpressure levels are not defined precisely, it is clear that the overpressures produced by a detonation could be expected to cause the damage

observed. Unlike the deflagration scenario, the detonation scenario can explain the occurrence of this damage at many locations throughout the cloud.

D.4.   ANALYSIS OF EVENT TIMINGS

D.4.1. Timings

The first part of the analysis is to compare the proposed detonation scenario against the events recorded in on the CCTV cameras and reported in witness statements. This analysis is relevant as:

- The witness statements can be used to determine a minimum time interval, T_{min}, between the initial explosion and the DDT.
- By working back from the first arrival of overpressure at each CCTV camera, the records can be used to estimate a maximum time interval, T_{max}, between the initial explosion and the DDT.

The approach taken for the analysis of the witness and CCTV evidence has been to determine if the records are inconsistent with the detonation scenario (ie give $T_{min}>T_{max}$), rather than attempt to prove the scenario. Falsification of assumptions is generally easier than proof. Calculations have only been carried out to the nearest 5 ms to avoid giving the impression of great precision when there are clear uncertainties.

The CCTV camera records used in this analysis are those from the RO cameras C5, C8 and C10 and the Furnell Yard Left (YL) camera, with reference being made to CCTV camera C3. The locations and approximate viewing angles are reproduced in Figure D.4 for ease of reference.

Most of the cameras were tilted downwards and therefore did not provide a view of more distant areas.
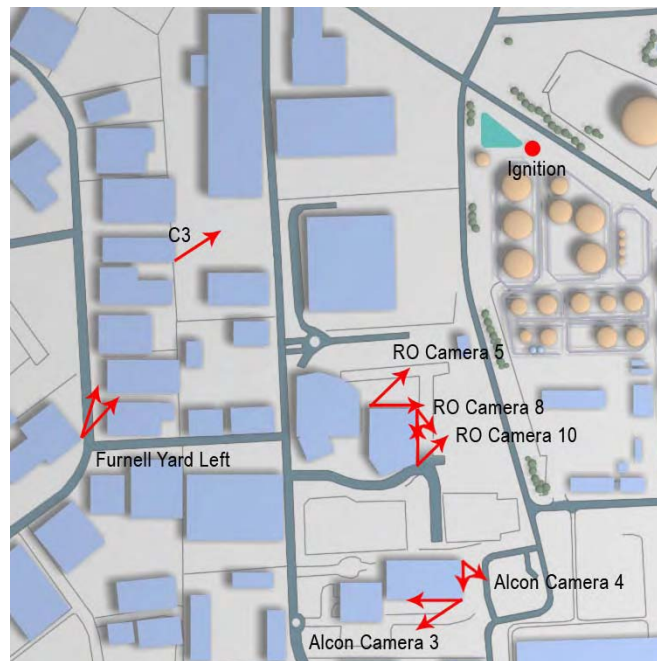
Figure D.4 Location and Approximate Viewing Angle of CCTV Cameras

It would be possible to use the deflagration analysis reported in Appendix H to calculate the time interval from the Pump House explosion to DDT. However, the values predicted by the

analysis will have considerable uncertainty without in any way invalidating the conclusions of the deflagration study, as:

- The construction of the Pump House and the way it was set into the ground would tend to prevent the venting of flame in the direction of the tree line along Three Cherry Trees Lane. The flame speed in this direction may have therefore been relatively low. In the extreme, if laminar flame speeds were assumed, given that the north face of the Pump House was about 10 metres from the tree line, then it could take 2-3 seconds for the flame to reach the tree line.

- Flame acceleration in the tree line is again very dependent on the exact circumstances and fuel concentration at the point where the flame entered the tree line. Non-stoichiometric concentrations or lower levels of congestion at this point would have lengthened the time taken for flame acceleration and could easily add another half to one second to the time scale.

The deflagration modelling has therefore not been used in the analysis of timings given here.

D.4.2. Witness Statements

A number of key witness statements are provided in Appendix A. Although not entirely consistent, the important features that can be drawn from these statements are:

- There was an initial event that witnesses to the east, west and south of the cloud reported seeing, hearing and, in some cases, feeling. The sound of this event was described variously as 'a whoosh', 'a loud crackling noise', 'a huge pressure sound, like a jet engine', 'a sound similar to thunder', 'two distinct echoing tapping noises'.

- A subsequent explosion event that was much more severe, described variously as 'a terrific bang', 'a massive and loud explosion', 'an almighty explosion', 'a very loud bang', 'a massive explosion', 'a tremendous crash'.

- Some witnesses reported seeing a 'flash' during this sequence of events.

From the view point of the detonation scenario, these features can be interpreted as follows:

- The initial event is the explosion in the Pump House followed by flame acceleration in the trees. As indicated in Appendix A, the evidence from the witness at the Waverly Security Hut is consistent with ignition occurring in the Pump House.

- The much larger explosion event is the overpressure generated by detonation of the vapour cloud. It should be noted that as the first part of the scenario includes the deflagration, there would be continuous 'noise' perceived by witnesses up to the time the detonation blast arrives.

- The flash is the propagation of the detonation through the vapour cloud, which would take approximately one tenth of a second.

Caution needs to be employed in the interpretation of witness statements. However, taking the combined weight of this evidence, it is clear that there was sufficient time for the initial explosion event to be heard at various locations prior to the main explosion being experienced. This places constraints on the detonation scenario as the detonation wave travels faster than the speed of sound. Unless there is sufficient time between the initial explosion event and the transition to detonation the detonation will overtake the pressure wave and the initial explosion will not be heard.

Given the unusual and unexpected circumstances, it would not be prudent to use the witness statements to postulate time intervals between the initial event and the larger explosion event.

The greatest constraint is provided by the statements from witnesses to the south of the cloud in the area of the HOSL tanker loading bay. The greater distance from the Pump House gives the maximum opportunity for the detonation to overtake the initial event. The statements from this location dictate a minimum time interval, T_{min}, between the initial explosion event and the transition to detonation.

In order to estimate this minimum time, the following approximate distance estimates have been used:

- The distance from the Pump House to the tanker loading bay – 230 m.
- The distance from the junction of Buncefield Lane and Three Cherry Trees Lane to the southern edge of the vapour cloud – 230 m
- The distance from the southern edge of the cloud to the tanker loading bay – 40 m.

The time taken for the sound of the initial explosion to travel from the pump house to the tanker loading bay is given by 230/340 = 680 ms (assuming an ambient sound speed of 340 ms^{-1})

The time taken for a detonation to propagate from the junction of Buncefield and Three Cherry Trees Lanes to the southern edge of the vapour cloud is dependent upon the speed of the detonation front, which is also dependent upon the concentration of the fuel in the vapour cloud, with the range of possibilities is between approximately 1500 and over 1800 ms^{-1}. The faster the detonation, then the greater the test placed on the detonation scenario and a speed of 1800 ms^{-1} has therefore been assumed. The time taken for the detonation to reach the southern edge of the cloud will therefore be 120 ms.

The speed of the detonation pressure wave once it is outside the vapour cloud will depend on the magnitude of the shock wave. However, given the rapid decay of the pressure wave this effect is likely to be small. For simplicity, if it is assumed that the pressure wave travels at the ambient speed of sound, 340 ms^{-1}, then the detonation pressure will travel from the edge of the cloud to the tanker loading bay in approximately 120 ms. An estimate of the total time for the pressure wave to reach the tanker loading bay is therefore 240 ms.

Consequently, for the initial explosion event to be heard by people at the HOSL tanker loading bay, the minimum time interval between the initial explosion in the Pump House and the DDT is:

$$T_{min} = 680\text{-}240 = 440 \text{ ms}$$

It should be noted that if the detonation stopped prior to reaching the cloud boundary closest to the tanker loading bay, then T_{min} would be reduced. For example, if the detonation stopped some 80 m from the tanker loading bay then T_{min} would be reduced by approximately 100 ms.

D.4.3. Analysis of RO CCTV Evidence to Estimate Time of DDT

The RO cameras only recorded at a rate of three frames a second and therefore do not provide good temporal resolution. Also, frames were only recorded by the system when there was sufficient change in the view. As a consequence, the records for cameras C5 and C10 start only when it appears there is already light from the explosion event.

It has been assumed for the purposes of this analysis that frames from the three cameras are all recorded at the same time. The distance from the edge of the vapour cloud to camera C5 was about 60-80 metres. The distance from the cloud to camera C10 was about 100 metres.

It is noted that none of these cameras have a direct line of site of the Pump House. Figure D.4 shows that the tanks on the HOSL site would have obscured the view of this area even had the cameras been pointing in that direction. Camera C10 had a direct view of the vapour cloud in the car park of the Northgate building.

For the detonation scenario, the arrival of overpressure at a time of 1000 ms (at all three cameras) is taken to be the arrival of the detonation pressure wave. Given the distance from the Pump House and the tree line along Three Cherry Trees Lane, it is considered that the Pump House explosion and subsequent deflagration could not have caused the effects observed at 1000 ms (which includes movement of a chair on the C8 record).

There are a number of options for analysing the timing of these video frames depending on whether it is considered that light emanating from the initial explosion in the Pump House is recorded and, if so, which frame captured this event. The following analysis explores these options with a view of determining the maximum time interval they allow between the initial explosion and DDT, T_{max}. This can then be compared with minimum time of detonation interpreted from the witness statements, as discussed in Section D.4.2.

Pump House Explosion Detected by RO CCTV Cameras

It is clear that at time zero (as given in Appendix A), the light levels have increased and the explosion event is under way. The initial explosion in the Pump House must therefore have happened before this time.

If it is assumed that the light from the Pump House explosion would have resulted in a detectable change in lighting at the RO cameras, then the Pump House explosion would have to have happened between -666 ms and -333 ms or between -333 ms and time zero, depending on whether it is considered that there is a change in light level between the -666 ms and -333 ms frames on camera C8.

The time taken for the overpressure from the detonation to reach the cameras varies, but is greatest for camera C10 as it is furthest away from the cloud boundary. Again, although the speed of the pressure wave from the cloud boundary would be dependant upon the magnitude of the shock wave, given the apparent rapid decay of overpressure from the cloud edge and the distance to the camera, the ambient speed of sound (340 ms^{-1}) is assumed. This indicates a time of travel from the edge of the cloud of $100/340 \approx 295$ ms to the C10 camera location.

The time of travel of the detonation wave from the junction of Buncefield and Three Cherry Trees Road and the southern edge of the cloud has already been calculated to be approximately 120 ms. The time interval between DDT and arrival of overpressure at camera C10 is therefore 415 ms.

This overpressure arrived at a time between 666 ms and 1000 ms (using the timescale employed in Appendix A). This means that DDT would have to occur at a time that was between 666-415 ms and 1000-415 ms, or approximately 250 ms to 585 ms, using the same timescale.

Given this, if it is assumed that the initial explosion in the Pump House was detected by the cameras, then it is possible to estimate the maximum time, T_{max}, between the Pump House explosion and DDT for the range of possibilities.

Table D.1 Time to DDT for RO Cameras Assuming they Capture the First Explosion

| | Maximum Time Between Pump House Explosion and DDT | | | |
| | Pump House Explosion between -666 ms and -333 ms | | Pump House Explosion between -333 ms and 0 ms | |
	Min	**Max**	**Min**	**Max**
Range for T_{max}	250+333 = 585 ms	585+666 = 1250 ms	250+0 = 250 ms	585+333 = 920 ms

It can be seen that if the Pump House explosion took place between -333 and 0 ms, then the range of possibilities for T_{max} is between 250 ms and 920 ms. If it were assumed that the explosion occurred between the previous CCTV frames, then T_{max} would be between 585 ms and 1250 ms. In the first case T_{max} can be greater than T_{min}, in the second case T_{max} is always greater than T_{min}. The detonation scenario is therefore not contradicted by the evidence.

Pump House Explosion was not Detected by RO CCTV Cameras

An alternative assumption is that the Pump House explosion could not be detected by the RO cameras due to the shielding of the storage tanks on the HOSL site and the field of view of the cameras. This is not unreasonable, as the height of the vapour cloud was significantly less than the height of the storage tanks. The increase in light level at the RO cameras could instead be due to the flame extending beyond the point where the cameras were in the shadow of the storage tanks. The records from CCTV Camera C3 strongly suggest that the time period between the Pump House explosion and flame propagating along the tree line of Three Cherry Trees Lane was at most 960 ms. However, this would still allow the possibility that the RO cameras did not record the early part of the event.

Under these conditions, T_{max} to be greater still and there would clearly be no contradiction of the detonation scenario.

D.4.4. Analysis of Furnell Yard CCTV Evidence to Estimate Time of DDT

The YL and YR cameras were located in the Furnell Yard, with YL shown on Figure D.4, and were pointing downwards in order to view vehicles in the yard. They had an even poorer view of the initial explosion in the Pump House than the RO cameras.

The YL and YR cameras are relatively consistent in what they show, so the analysis has been based on the YL camera. Comparison with the detonation scenario has been carried out in the same manner as the RO cameras. That is, the timings will be calculated under the assumptions that either the first light change corresponds to the Pump House explosion or that this event is not recorded. The relevant images from the YL camera are given in Appendix A.

The YL camera could record a video frame every 40 ms if changes occurred between video frames. It can therefore provide greater temporal resolution than the RO cameras. Table D.2 shows a summary of what was recorded by the YL camera.

Table D.2 Summary for Camera YL

Time (ms)	Observation
0	First sign of increase in brightness. This continues to increase until 360 ms, when it dims
920-1200	Light level increases continuously and eventually cause the camera to 'white out'
1360-1560	Light level gradually dims until the vehicles in the yard can be seen.
1640	Pressure effects observed

In the case of the YL camera, the overpressure from the explosion can arrive either from the cloud between the Fuji and Northgate buildings or from the cloud edge just south of the Northgate building. Although the latter location was slightly closer (say 10 metres) to the camera than the cloud in the gap between the buildings, it is significantly further away from the point of DDT. Given the different speeds of the detonation front and the pressure wave outside the cloud, it makes little difference which source of the overpressure is used. The timings have therefore been based on the arrival of overpressure from the part of the cloud located between the Fuji and Northgate buildings. The following information has therefore been used:

- The distance between of the cloud edge and the camera was approximately 320 metres.
- The distance of the cloud edge from the point of DDT was approximately 190 metres.

Given the distance between the cloud edge and the camera, it is reasonable to assume the pressure wave travels from the edge of the cloud to the camera at the ambient speed of sound of 340 ms^{-1}. The time taken is therefore $320/340 = 940$ ms.

The time for the detonation to travel from the point of DDT to the edge of the cloud is between $190/1800$ or 105 ms. The time between DDT and arrival of pressure at camera YL would therefore be 1045 ms.

If it is assumed that the first sign of any change in light levels at the YL camera corresponds to the Pump House explosion, then the arrival of the detonation pressure at the YL camera is somewhere between 1600 ms and 1640 ms after the Pump House explosion. This indicates that the maximum time between the Pump House explosion and DDT, T_{max}, would be between 555 and 595 ms. Again T_{max} is greater than the value for T_{min} estimated from the witness statements and the scenario is not contradicted.

As with the RO cameras, greater time differences between the arrival of the initial explosion pressure and the detonation pressure wave would be allowed if camera YL did not detect any light from the initial Pump House explosion.

D.5. ASSESSMENT OF OTHER ASPECTS OF THE CCTV RECORDS

D.5.1. Luminosity

The luminosity of the explosion event cannot be taken directly from the CCTV camera records without some interpretation, as the cameras will adjust to the changing light levels. In addition, their sensors may be overloaded by the sudden change in light levels and take time to recover.

In general, as it would be expected that the event would initially involve an increasing luminosity, increasing luminosity on the CCTV records probably does correspond to a greater degree of illumination from the explosion event. However, during this stage, a decreasing luminosity does not necessarily mean a reduction in light levels but may indicate that the camera has made some adjustment to its sensitivity.

In addition, cameras where the image has become completely white, such as YL on the Furnell building, may not correctly indicate the time at which light levels drop as they may take some time to recover from the high light levels.

However, a number of comments can still be made be made regarding the luminosity:

1. The RO camera records shown in Appendix A indicate a relatively long lasting period of bright flame and/or combustion products. This lasts throughout the whole record from 333 ms to 3000 ms, though there are some times when the light level is more intense. This illumination continued through the rarefaction phase of the explosion, suggesting that much of it is not associated with the explosion process itself but the combustion of fuel not involved in the explosion. There could, for example, be areas of high fuel concentration closer to the source of the vapour cloud. If there is a vertical variation in concentration, this may also represent the combustion of a rich (above the upper detonable limit) layer in the cloud, or ignition of the liquid pool in bund A.

2. The RO camera C5 gives the impression at 666 ms that the source of the illumination is close to the southern edge of the cloud. Though there is some uncertainty regarding this interpretation, this would be consistent with the proposed detonation scenario as it would be expected that by the next frame, the shock wave from the detonation would have hit the RO camera location, which is the case.

3. The time taken for pressure information to reach camera YL indicates that the DDT would have occurred at a time of 555 to 595 ms and the detonation would have spread through the cloud in little more than 100 ms. (Note that this is not dependent upon whether the camera recorded the Pump House explosion or not.). In the detonation scenario therefore, all of the light increase from 920 ms onwards, as described in Table D.2, would have been after the detonation had propagated through the cloud. The changing light levels at camera YL (and YR) would therefore have to be associated with how much of the combustion process can be 'seen' from the camera location. Increasing light levels may, for example, correspond to flame rising above the building line and thus being able to illuminate a wider area. Again, combustion of parts of the cloud with concentrations outside the detonable limits, particularly on the rich side, may have played a part in this.

D.5.2. Time Period to the Start of the Rarefaction

The RO CCTV records in Appendix A show the arrival of pressure at this location in the 1000 ms frames. The rarefaction phase, characterised by the general fogging of the atmosphere, does not arrive until 1666 ms, though there is some hint of it at 1333 ms on C10. This indicates that the rarefaction phase was not entered until an interval of at least about one third of a second and possibly up to one second had elapsed.

A detonation wavefront is a very short duration event, typically lasting just a few milliseconds. The long period between the arrival of the initial pressure wave and the commencement of the rarefaction phase therefore requires some explanation.

The long duration before the rarefaction phase begins could be due to the time taken for the expansion of combustion products and some contraction. As this process is not driven by the detonation shock wave, it is reasonable to assume that the onset of the rarefaction phase would

have a significantly longer timescale than that associated with the detonation wavefront. In fact, the detonation scenario probably maximises the time this expansion process would take as it converts the vapour cloud to hot combustion products within a short timescale (about one tenth of a second). In a slower event, there would be more time for the hot combustion products to expand backwards and upwards and there would therefore be less outward expansion once the flame reaches the edge of the cloud.

This issue will be addressed in more detail by the modelling work described in Section D.6. However, at this stage an example can be provided from the experimental work described in reference 5 and carried out in the test rig shown in Figure D.2. As already described, these experiments included DDT of propane and cyclohexane-air mixtures. Figure D.5 shows overpressure profiles measured inside the test rig and 20 m outside the test rig, in a direction of the long axis of the test rig.

The time interval plotted is approximately the same in both plots (this time base is measured from the time of ignition and includes the run up to DDT). It can be seen that the duration of the positive (i.e. not below ambient pressure) appears significantly longer at the external location, with about 30 ms elapsing before the pressures drop consistently below ambient.

In the case of the Buncefield cloud, this effect would be expected to be greater, partly due to the much larger scale but also due to the differences in the way the combustion products can expand. In the experimental work, the combustion products were free to expand sideways as well as upwards and backwards. In the case of the Buncefield cloud, this sideways expansion is not possible and this could be expected to increase the time interval before the rarefaction phase begins. This issue is addressed by the modelling work described in the following section.
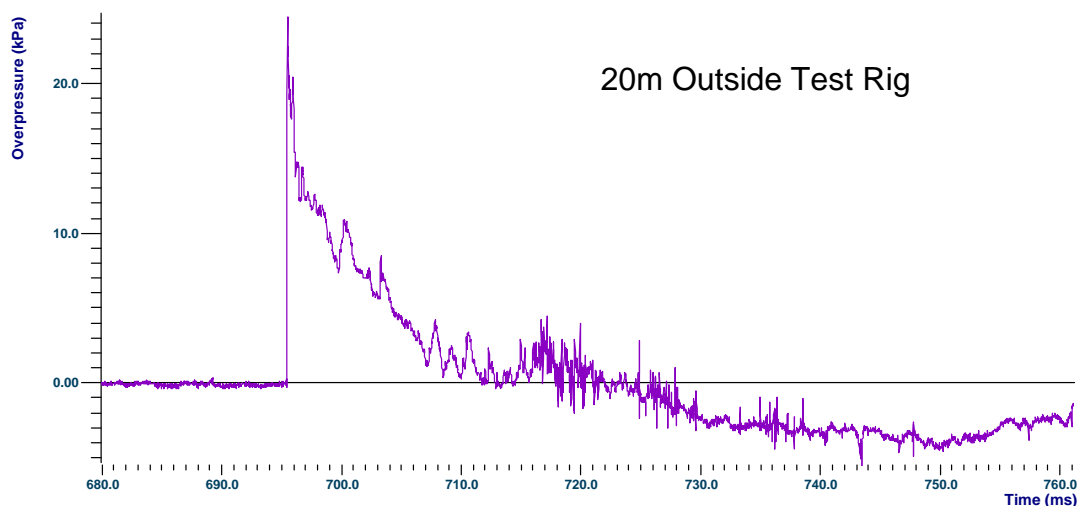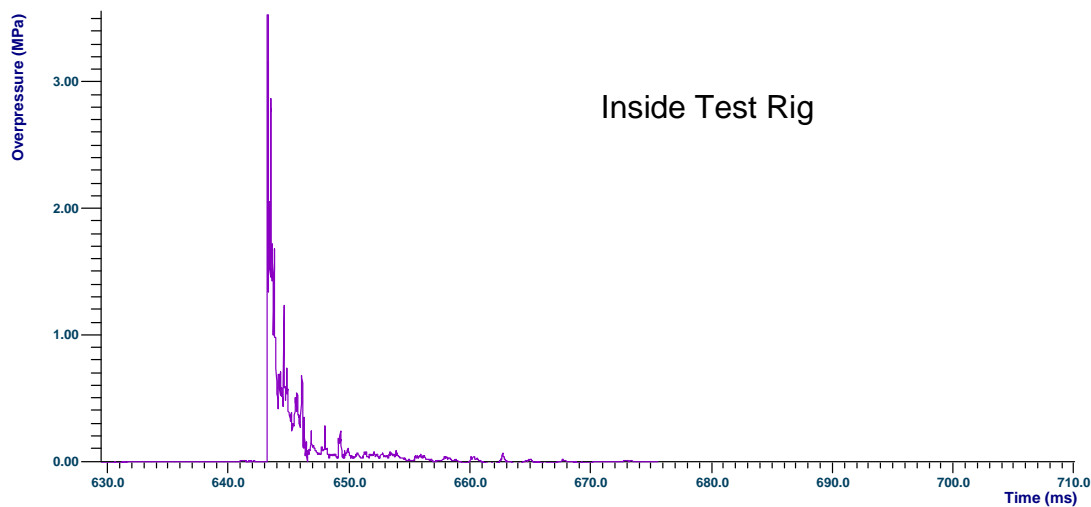
Figure D.5 Overpressure Profiles Inside and Outside Large Scale Detonation Experiment

D.6.   MODELLING

Modelling work has been carried out to support the comparison of the detonation scenario with the evidence obtained from the Buncefield site. This modelling work has been carried out by Kingston CFD Ltd and Fluid Gravity Ltd.

D.6.1. Modelling by Kingston CFD Ltd

This modelling was commissioned primarily to understand the overpressure decay from the edge of the cloud (both horizontally and vertically). However, as the importance of the directional indicators became more evident, this work was also used to provide an initial assessment of the direction, magnitude and duration of gas flows impacting on any item located within the vapour cloud. This modelling was not intended to represent the actual cloud present at Buncefield.

Simulations were conducted for 2-D cloud of stoichiometric propane-air mixture. Given that the cloud at Buncefield was much larger than those being simulated and the interest was in the near field overpressures, cylindrical symmetry was not used for these simulations. However, it should be noted that this, combined with the smaller cloud size, would mean that the far field overpressures would not be representative of Buncefield.

Four rectangular shaped cloud profiles have been considered. The aspect ratio was systematically varied to investigate the effect of height to length ratio on the resulting pressure, velocity fields and the net impulse. The cloud sizes modelled were 10×7, 10×2, 20×2 and 20×1.5 metres.

The total domain size in all cases was 160 by 70 metres. The origin of the domain was placed 60 metres from the left boundary so the 4 corners of the domain were (-60 0), (-60 70), (100, 0) and (100, 70). The cloud started from the origin and extended towards the right hand side of the domain. Figure D.6 shows the set up for the 20 m by 2 m high cloud, where the red region represents the cloud and the blue region is filled with air.
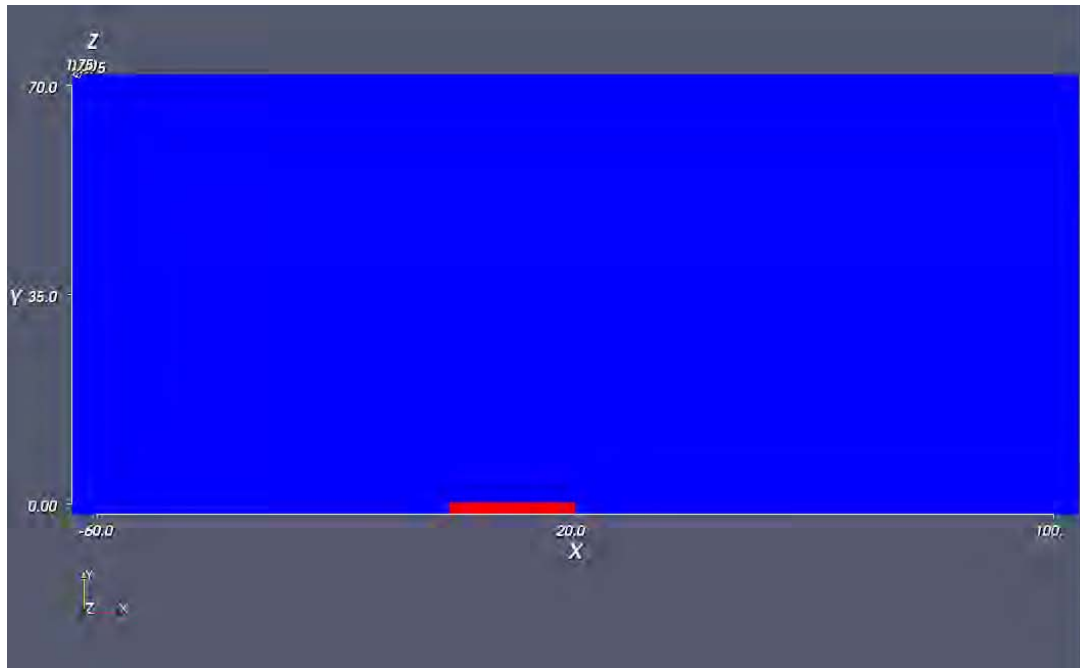
Figure D.6 Domain and Cloud (Red) for 20 x2 m Cloud

Further details of the modelling approach are given in Section D.12.

Pressure Decay

The decay of the peak overpressure from the edge of the cloud is shown in Figure D.7for the 20×2 m cloud case. In this case, it can be seen that within a distance of 5 m from the edge of the cloud the overpressure is below 300 kPa and by 10 m from the edge of the cloud it is about 100 kPa. At a distance of 20 m from the cloud edge, the overpressure is about 50 kPa. At distances of 30, 40, 60 and 80 m from the cloud, the overpressures were 37, 29, 21 and 14 kPa respectively.
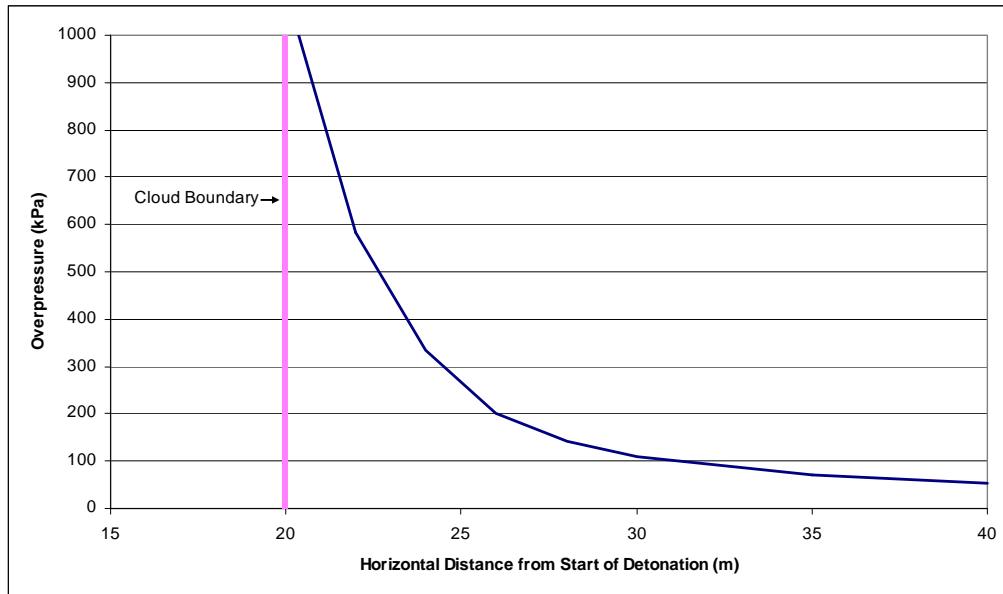
Figure D.7 Decay in Peak Pressure from Edge of the Cloud (X=20 m) for the 20x2 m Cloud Simulation

The experimental work described in Appendix H indicates that overpressures of over 200 kPa are required to cause the type of damage observed to cars located within the cloud. The decay of overpressure shown in Figure D.7 indicates that this type of damage would not extend much more than five metres beyond the cloud boundary.
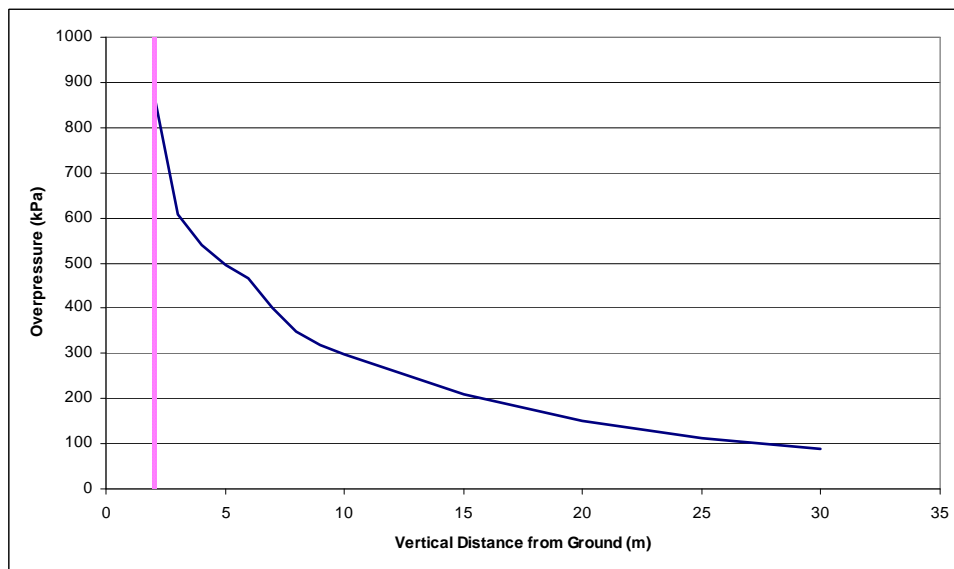
Figure D.8 Decay in Peak Pressure Vertically from Top of 20x2 m Cloud (at 20 m point)

Figure D.8 shows the pressure decay in a vertical direction from the top of the 20×2 m cloud. This vertical line was located at the 20 m point, that is, at the boundary of the cloud furthest from the point of initiation. Again the pressure decay is rapid, but in this case not as rapid as the decay in a horizontal direction. For example, at a point 7 metres above the cloud the overpressure is 300 kPa, whereas at a similar distance in the horizontal direction, the overpressure is 300 kPa just 4 metres from the cloud edge.

Gas Velocities and Densities

The gas velocities were calculated at many locations within the cloud. Figure D.9 shows an example of the horizontal gas velocities calculated at a point half way across the cloud and at mid height in the 20×2 m detonation simulation. A positive velocity represents gas moving in the direction of propagation of the detonation.
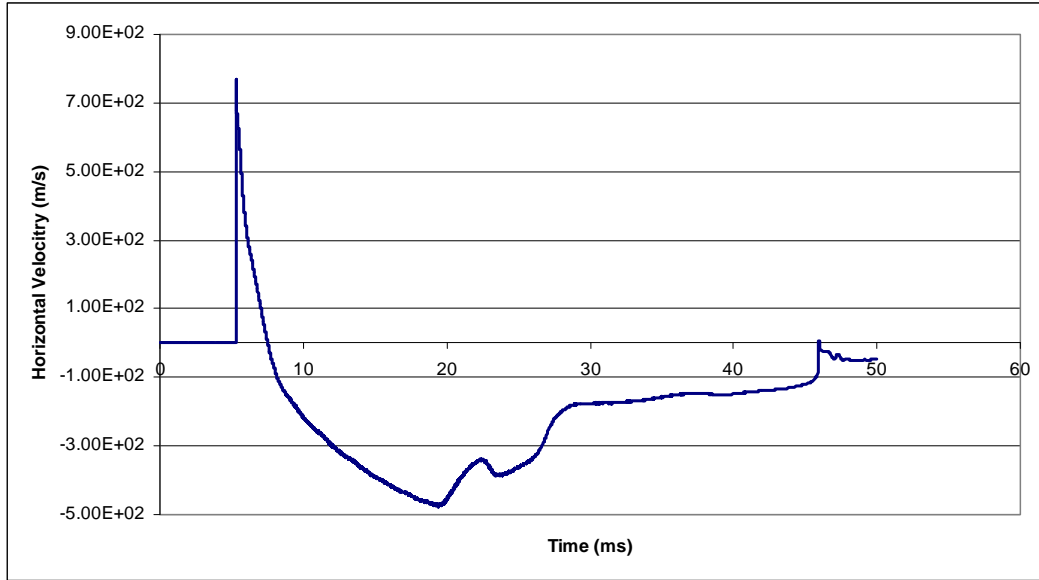
Figure D.9 Gas Velocities in 20×2 m Cloud Simulation at Mid Point in the Cloud (10,1)

It can be seen that there are short duration positive velocities followed by a longer duration phase where the velocities are negative. The velocity in this negative phase has a lower magnitude than that in the positive phase.

The forces imparted by these high gas velocities also depend on the density of the gas. During the positive velocity phase, the density rapidly increases from the ambient 1.2 kgm^3 to 2.9 kgm^3, corresponding to the passage of the shock front, and then falls as the pressure reduces. The density then falls to values well below the ambient density, representing the stage where the hot combustion products are present.

Net Impulse

In order to calculate the net effect of these positive and negative forces, the net impulse was calculated in the simulation. This was calculated at a fixed point assuming no movement of the target. The net impulse was calculated using the horizontal velocities U_x and a simplified Morrison equation with a cumulative total for each time step, as shown below.

$$I = \int f.dt = \int_{0}^{t_i} \left(\frac{1}{2} C_d.\rho.A.U_x.|U_x| \right) dt$$

For the purposes of the simulations, the drag coefficient C_d and the target area A were taken to be unity.

An example of the calculated net horizontal impulse is shown in Figure D.10. This is for the same central point as the velocities shown in Figure D.9.
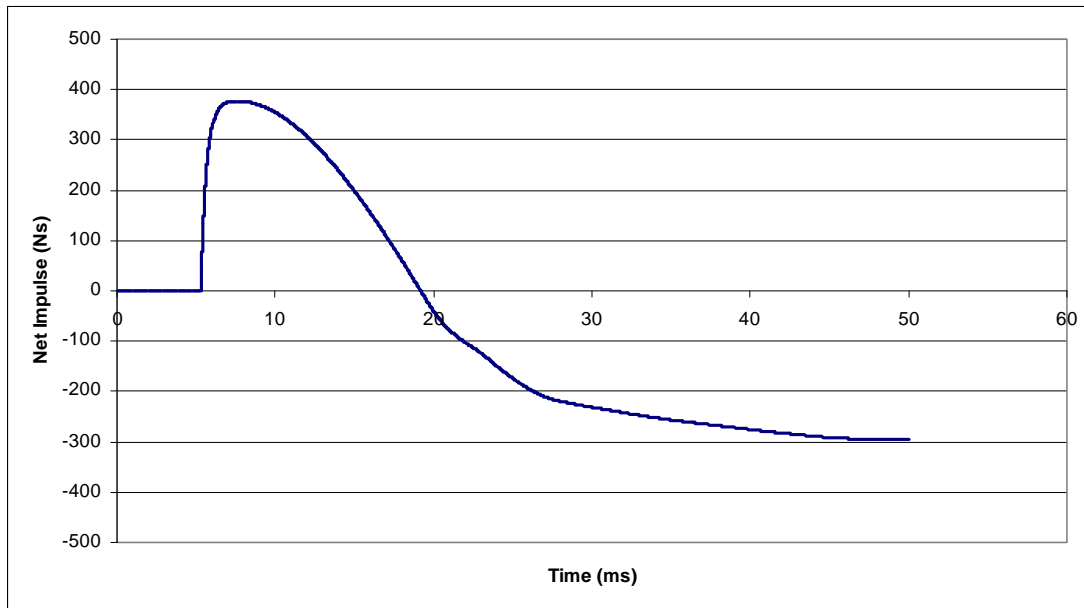
Figure D.10 Net Impulse at Mid Point of 20 × 2 m Cloud Simulation

It can be seen that there is a short duration phase (about 2 ms) where a positive impulse is applied (i.e. the curve is going up). This is then followed by a longer duration (over 40 ms) phase where the forces are in a negative direction (opposite to the direction of the detonation propagation) and ultimately the overall net impulse is negative.

These results were not restricted to this mid point in the cloud. Similar results were obtained throughout the cloud.

It should be noted that the calculations take no account of the response of the target. If the natural period of response of the target structure is significantly more than 2 ms, then the target will be influenced far more by the negative forces than the short duration positive ones.

The directional indicators at Buncefield include structural deformation, movement of large items and pitting on one side of items such as lampposts. The results described above indicate that the propagation of a detonation throughout the cloud at Buncefield provides an explanation for the observed effects.

D.6.2. Modelling by Fluid Gravity Ltd

The modelling work carried out by Kingston CFD Ltd involved an idealised cloud that was significantly smaller than that involved in the Buncefield explosion. As the investigation of the detonation scenario progressed, it became apparent that modelling of a much larger cloud geometry would be required in order to investigate the time period to the rarefaction phase and also interactions with buildings. Additional modelling was therefore commissioned with Fluid Gravity Ltd to investigate a cloud with a 200 m radius and a height of 3 m. This was modelled assuming cylindrical symmetry (i.e. equivalent to a 400 m diameter cloud). It should be noted that this probably exceeds the size of the actual cloud in both the overall diameter and the depth. The full report from Fluid Gravity is given in Appendix H.

Two scenarios were examined:

- Scenario 1: an open unobstructed cloud
- Scenario 2: an obstructed cloud where a rigid obstacle, simulating a building was present at the edge of the cloud.

Figure D.11 illustrates the simulation of the open cloud, showing the velocities 100 ms after the detonation was initiated.
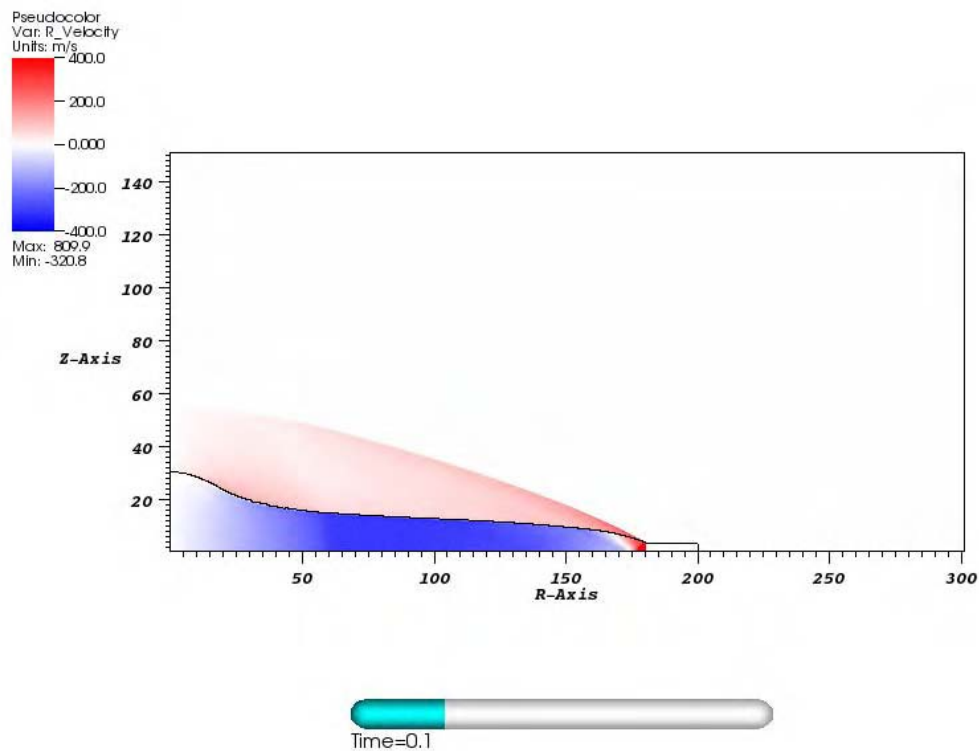
Figure D.11 Illustration of Open Cloud Simulation Showing Gas Velocities

Figure D.12 provides an illustration of the overpressures generated in the obstructed cloud case (Scenario 2).
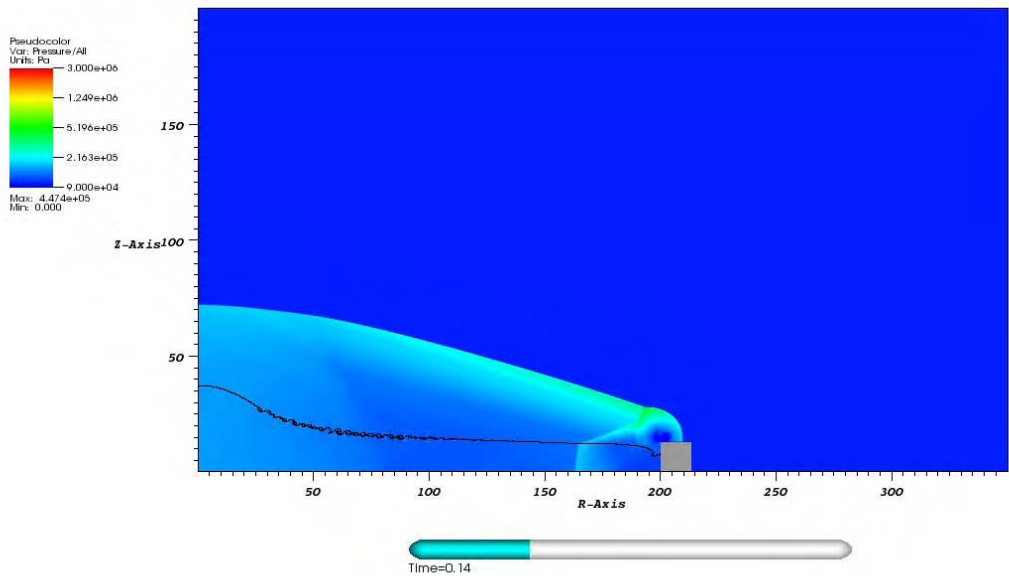
Figure D.12 Illustration of Obstructed Cloud Simulation Showing Pressures

Gas Velocities and Net Impulse

The predicted gas velocity profiles inside the cloud have similar magnitudes to those calculated by Kingston, as might be expected. However, comparison of the Fluid Gravity calculations in Figure D.13 with the Kingston predictions in Figure D.9 shows that the increase in cloud size increases the duration of the negative phase from about 40 ms to over 150 ms.
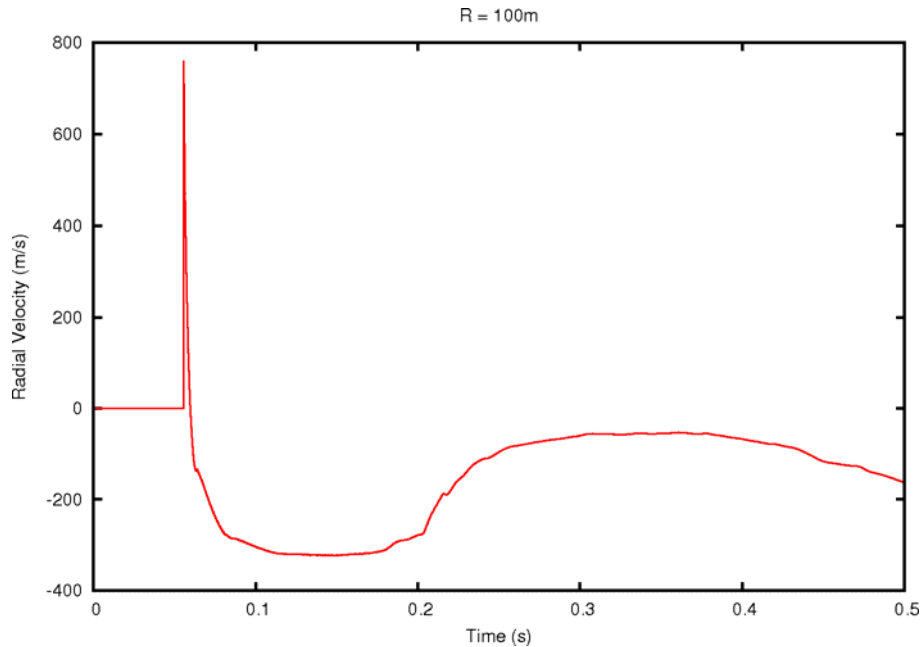
Figure D.13 Gas Velocities at 100 m from the Point of Detonation Initiation

The predicted net impulse (cumulative impulse) inside the cloud was again opposite to the direction of the detonation, though with a much greater magnitude than obtained in the Kingston modelling. This is due to the much longer period in which negative velocities are present compared to the Kingston simulation.

The simulations also confirmed that outside the open cloud, directional indicators would be pointing away from the cloud, as observed.

Overpressures Inside the Cloud

The overpressures inside the cloud and 100 m from the point of initiation are illustrated in Figure D.14 with various adjustments to both the pressure and time axes. It can be seen that the main part of the shock wave has a duration of about 30 ms, by which time the overpressure has fallen to about 50 kPa. The overpressure then falls to about 20 kPa and holds at this level for a period, this second stage lasting over 100 ms. The pressure then falls again until it enters the rarefaction phase.
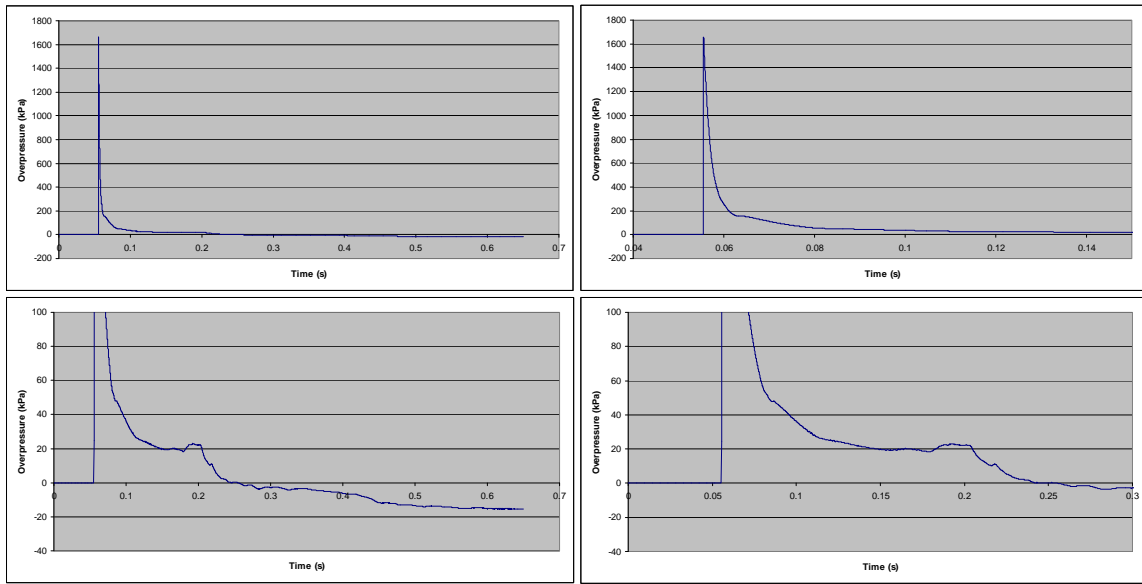
Figure D.14 Overpressure Inside the Cloud (100 m from the point of initiation)

Overpressures Outside the Open Cloud

Overpressures have also been predicted at distance 30 m and 100 m outside the free cloud. Figure D.15 shows the predicted overpressure at these location. A key aspect of the Buncefield explosion is the apparent long duration of the positive phase of the explosion. It can be seen that the neither of the overpressure profiles drop below ambient for the duration of the simulation.

This is an important result as it suggests that one very well defined aspect of the Buncefield explosion, the long time period between the arrival of overpressure and the start of the rarefaction phase, can be explained by the detonation scenario.
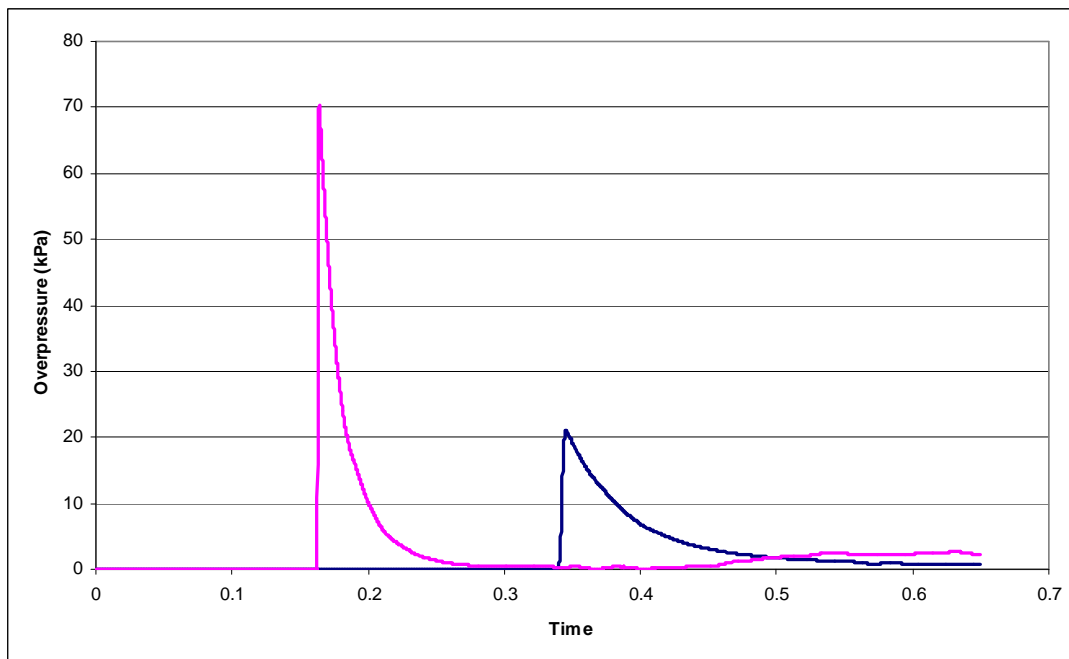
Figure D.15 Overpressure 30 m and 100 m Outside the Cloud Boundary

95

The simulations also provide a plot of the decay in peak pressure and impulse with distance from the edge of the cloud (Figures 12 and 13 in the Fluid Gravity report). The decay in peak overpressure, though still rapid, is slower than that obtained in the Kingston simulations due to the larger cloud size. At 30 m from the cloud edge, the overpressure predicted by Fluid Gravity is 70 kPa, as illustrated in Figure D.15, whereas Kingston predicted 36 kPa. Thin Kingston simulations only went to a distance of 80 m from the cloud boundary, where the predicted overpressure was 14 kPa, whereas at 100 m, Fluid Gravity predict 21 kPa. Thus even though the cloud sizes differ considerably between the two simulations, the overpressure outside the cloud only varies by a factor of about two[2].

Loading on the Obstruction

Figure D.16 shows plots of the predicted overpressure profiles on the front face of the obstacle at a range of heights from the ground. It can be seen that very high loadings are experienced on the obstruction, with the loading remaining over 500 kPa at a height of 12 m. As might be expected given the presence of the obstruction, the loadings are greater than the equivalent calculated in the Kingston analysis and shown in Figure D.8.
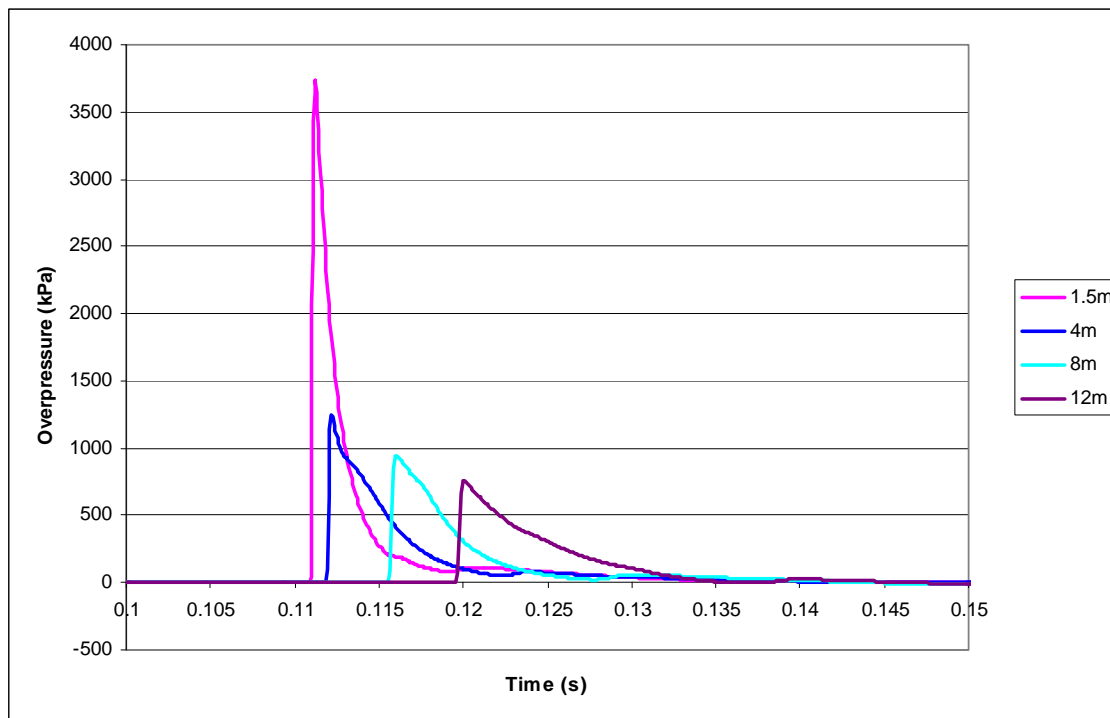
Figure D.16 Overpressure Loading on Obstruction

D.6.3. Comments on Results of Modelling

The modelling of the detonation cloud has necessarily been simplified within this project. In effect two extremes have been modelled, one with a cloud much smaller than that in the

---

[2] It could be expected that the overpressures at distance would depend on the cube root of the cloud volume, however it should be noted that it was decided that the Kingston simulations would not employ cylindrical symmetry and as such the overpressure decay at distance would be less than if cylindrical symmetry had been employed, as was the case in the Fluid Gravity simulations.

Buncefield incident and one that is most probably bigger. The following comments can be made in relation to the results:

1. The direction of the net impulse inside the cloud is consistent across both sets of simulations, indicating that the directional indicators found inside the cloud can be explained by the detonation scenario.

2. The detonation scenario could result in relatively long periods between the first arrival of overpressure at points outside the cloud and the start of the rarefaction phase. This is consistent with the CCTV records.

3. The rate of decay of the overpressure with distance varies depending on the size of the cloud simulated, though overpressures at distance where not highly sensitive to this factor. The Fluid Gravity simulation represents a cloud size that exceeds that actually present at Buncefield and there are factors that would reduce the effective size of the cloud, including:

    a. Part of the cloud would have been consumed by the initial deflagration.

    b. The cloud was not a simple cylindrical pancake; it was subdivided by the buildings and other obstacles. For example, on the west side of the cloud the detonation would propagate in part to the north of the Fuji building, in part between the Fuji and Northgate buildings and in part to the southern edge of the cloud. It is notable that the size of the cloud to the north of the Fuji building was relatively small and this is where the rapid change in overpressure damage to cars was observed at the cloud edge. It is likely that in this area, the overpressure decay would be closer to that given in the Kingston analysis.

    c. The detonation may not have propagated through the full cloud height as a result of vertical concentration variations. It may have propagated around regions of the cloud that contained fluctuations that took the concentration outside the detonable range.

The simulations provide valuable insight to the behaviour of a detonation in the Buncefield cloud. They demonstrate that the directional indicators and the long time period before the start of the rarefaction can be explained by a detonation. Both sets of simulations also confirm rapid overpressure decay outside the cloud.

D.7. PRESSURE DAMAGE

The pressure damage to items such as cars and boxes within the cloud is discussed in Appendix H and, as already stated, is consistent with the detonation scenario and is not discussed further.

There are, however, other aspects of the pressure damage that do warrant some consideration. The far field damage to properties is variable and can be affected by factors such as the presence of atmospheric inversion layers; however it is worthwhile to make some comparison between the detonation scenario and the damage at some distance from the cloud.

In addition, the damage to the Northgate and Fuji buildings and buildings in the near field should be considered given the high peak overpressures that would be incident on these buildings if a detonation propagated though the vapour cloud.

D.7.1. Damage to the Near Field Buildings

Northgate Building

Weidlinger Associates have analysed four loading profiles in order to determine the conditions that would lead to the observed damage to panels on the face of the Northgate building. Three of these included shock loading within the profile and one involved a relatively slow rise time and decay for the loading (described as Vapour Cloud Explosion Load A). The conclusion of this analysis was that the profiles that included shock loading do not explain the panel damage observed on the Northgate building. The slow rise time loading could provide a solution that was consistent with the damage. This is clearly not consistent with the detonation scenario, which would generate high shock loadings on both the Northgate and Fuji buildings if the detonation was assumed to reach these buildings. In addition, the loading predicted by Fluid Gravity, shown in Figure D.16, would have been expected to cause much more severe damage to the Northgate building.

It may be considered that this suggests that the 'deflagration only' scenario is a better fit to the observed damage. However, it should be noted that even the loading from the 'deflagration only' scenario will be a shock given that supersonic flame speeds are predicted in Appendix H.

Alternatively, if the overpressure were generated in the car park as well as the tree line (which the damage to the cars suggests) by some means of non-detonative fast flame propagation, the flame speed would need to be in excess of the ambient sound speed in order to generate the magnitude of the overpressures estimated (>200 kPa). Again this would produce a shock loading on the Northgate building.

There is no known combustion mechanism that can provide the loading profile that Weidlinger have found achieves a solution and would also be consistent with full range of pressure damage discussed in Appendix H. Therefore, either a major change is required in the understanding of vapour cloud explosions or there are aspects of the actual loading the detonation scenario may produce on the Northgate building that have not, as yet, been represented in the combination of the Weidlinger analysis and detonation simulations. Though this would require further work, the aspects that could be assessed (some of which have already been identified in Section D.6.3) for their effect include:

- The detonation propagates through a relatively thin cloud layer by the time it reaches the Northgate building.
- The effect of overpressure propagating through the windows into the building and loading the inside of the panels examined by Weidlinger.
- The overhang of the floors above the ground floor (the detonation would propagate into a more confined space.

The discrepancy between the damage and predicted loading cannot be answered by the idealised detonation simulations carried out to date and may well require 3D simulations with a greater parameter variation. Such analysis was not possible within the scope of the current project.

Fuji Building and Catherine House

No structural analysis has been conducted for the Fuji building; however it is notable that there was severe damage all around the perimeter of this building in areas where the vapour cloud had been present. This included complete demolition of the one bay of the building along most of the southern side of the building where the cloud was present. It should be noted that other than in this area, the roof of this building was basically intact, suggesting that there had been no significant internal explosion. The rapid decay of the overpressure as it propagated into the

building might also be expected to limit how far the high level of damage would extend, which corresponds to what was observed on the south side of the building.

Similarly, no analysis has been carried out for Catherine House, however it is noted that the south east corner of this building suffered complete collapse. This part of the building would have either been very close to or within the vapour cloud.

D.7.2. Mid Field Damage

Damage to buildings outside the cloud and within a radius of approximately 500 m is assessed in Appendix H. The ability to explain the overpressure damage depends very much on the rate of decay in pressure assumed from the cloud edge. As indicated in Section D.6.3, the rate of decay from the cloud edge is somewhat dependent on the actual cloud size involved in the detonation, but this does not preclude a comparison with the simulations.

For example, it has been estimated in Appendix H that the damage to the RO building is consistent with an incident overpressure of 20 kPa. This building was about 60-80 from the cloud edge. The Kingston simulations indicate that a 20 m × 2 m high cloud would give overpressures of 21-14 kPa at these distances from the cloud edge. The Fluid Gravity simulation indicates an overpressure of about 30 kPa at these distances. There is therefore reasonable agreement between the level of overpressure estimated from the observed damage and that obtained from the detonation simulations.

To the north of the cloud, given the reduced extent of the cloud and that some of it would have been consumed in the deflagration, it might be expected that the level of overpressure would be closer to the Kingston simulation rather than that of Fluid Gravity (i.e. lower). This is what was observed, as the damage levels suggested lower overpressures at given distances from the cloud in this direction.

Many of the other buildings are outside the range of the simulations; however it is considered that the observed damage levels are consistent with the detonation scenario given the variability that is possible within this scenario.

D.7.3. Far Field Damage

Geiger [9] investigated the overpressures generated by detonation of a gas cloud of radius 73.7 m and height 1.2 m and also compared them to those produced by a hemispherical cloud of the same volume (radius 21.4 m). The 2-D simulations showed that beyond a distance of about 100 m from the centre of the cloud, the peak overpressures generated by the two clouds converged onto the same curve, as illustrated in Figure D.17.
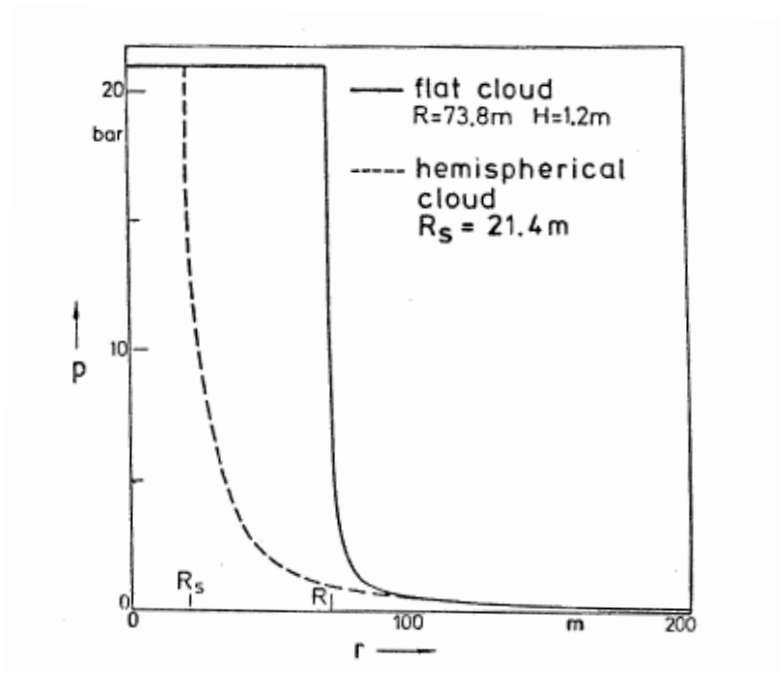
Figure D.17 Comparison of Pressure Decay from Flat and Hemispherical Clouds with the Same Volume (reproduced from Geiger [9], 1 bar = 100 kPa)

This suggests that for the purposes of the far field damage, a simple comparison based on a hemispherical cloud located centrally on the Buncefield cloud would provide a reasonable indication of the consistency between the detonation scenario and the far field damage that actually occurred.

Appendix H shows that damage occurred to many properties out to distances of 2 km or more and that sporadic property damage occurred to distances of over 4 km.

The TNO Mutli-Energy Method [10] has been used to estimate the relationship between the cloud volume and the overpressures produced at distance given a detonation of the cloud. Figure D.18 plots this relationship for three overpressure values.
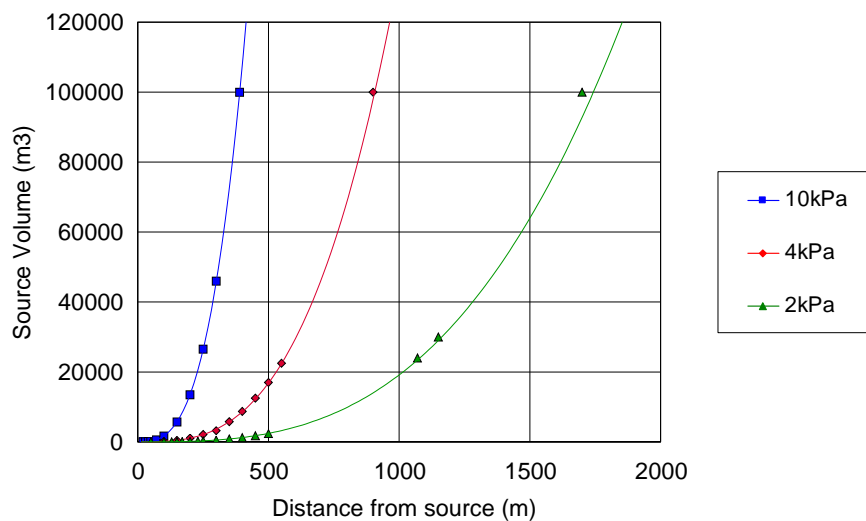
Figure D.18 Dependence of Overpressure on Cloud Volume
(TNO Multi-Energy Method)

The volume of the Buncefield cloud is difficult to estimate accurately, however given the size of the burned area and the estimates of the cloud height, a volume of up to 200,000 m^3 is not an unreasonable estimate. If a detonation occurred, not all of this would contribute to the generation of overpressure as some would be consumed before the transition and some would have a concentration outside the detonable limits. If, say, a volume of 100,000 m^3 underwent a detonation, overpressures of 4 kPa and 2 kPa would extend to about 900 m and 1700 m respectively. It should be noted that these distances are dependent on the cube root of the cloud volume, thus a doubling or halving of the cloud volume will only alter these distances by approximately 25%.

Table D.3 reproduces some representative values for overpressure damage from Baker et al [11]. It can be seen that this data suggests that there will be limited damage at overpressures below 2 kPa. It is recognised that there are uncertainties associated with the assessment of this type of building damage. However, given that there was fairly widespread damage within a radius of 2 km and sporadic damage to more than 4 km, it can be seen that the detonation scenario is not over-predicting the far field overpressure damage caused by the Buncefield explosion. Given that a detonation provides the most efficient means of generating overpressure energy from the combustion of unconfined vapour clouds (and delivering this as a single blast wave), this provides significant support to the detonation scenario.

Table D.3 Representative Overpressure Levels for Building Damage

Side-on Overpressure (kPa)	Description of Damage
0.3	Loud noise; sonic boom glass failure
0.7	Breakage of small windows under strain
1.0	Threshold for glass breakage
2.0	"Safe distance," probability of 0.95 of no serious damage beyond this value; some damage to house ceilings; 10% window glass broken.
3.0	Limited minor structural damage
3.5-7.0	Large and small windows usually shattered; occasional damage to window frames
5.0	Minor damage to house structures
8.0	Partial demolition of houses, made uninhabitable

It is also worth noting that the curves given in Figure D.18 would suggest that the overpressures 500 m from the 'centre' of the cloud would be between 4 and 10 kPa. This corresponds to the distance of the warehouse to the south of the Buncefield site from the point of initiation and is consistent with the level of damage observed.

D.8.   LACK OF HEARING DAMAGE IN WITNESSES

As described in Appendix A, it is understood that none of the witnesses suffered permanent damage to their hearing. The threshold for eardrum rupture is 35 kPa, with a 50% chance of rupture at 100 kPa. The lack of permanent hearing damage suggests that the overpressure where witnesses were outside would therefore need to be significantly less than 100 kPa.

The witnesses closest to the cloud boundary were those at the tanker loading bay being at least 40 m from the cloud edge. The Fluid Gravity simulation gives an overpressure of 70 kPa at a distance of 30 m from the cloud boundary. The Kingston simulations give 35 kPa at this distance and 29 kPa at 40 m.

Given the conservative nature of the Fluid Gravity simulations and the variability in how the detonation scenario could be realised, the lack of hearing damage to witnesses is not inconsistent with the detonation scenario.

D.9.   SUMMARY OF FINDINGS

The findings of this assessment of the potential for detonation to explain the Buncefield explosion can be summarised as follows:

1.   There is evidence from both experimental work and the incident record that indicates that a deflagration to detonation transition in the vapour cloud is credible.

2.   A detonation through the majority of the vapour cloud provides an explanation for the widespread pressure damage to items such as cars and instrumentation boxes.

3.   The detonation scenario that fits best with the evidence is one involving:

   a.   Ignition in the Pump House.

   b.   Flame acceleration in the tree line on Three Cherry Trees Lane.

   c.   Deflagration to detonation transition in the area of the junction of Buncefield Lane and Three Cherry Trees Lane.

4.   The evidence related to the arrival of overpressure provided by the CCTV records and witness statements does not contradict this proposed scenario.

5.   The modelling also shows that the net impulse imparted by the detonation to items within the cloud is in the direction opposite to the direction of propagation. This is consistent with the evidence found at Buncefield, where all directional indicators within the cloud pointed inwards to the approximately the same location. This pattern was also found at two other incidents reported as detonations.

6.   Modelling has also indicated that the detonation scenario would produce an extended (hundreds of milliseconds) period where the overpressure outside the cloud is above ambient. This would provide an explanation for the observations from the CCTV cameras that show that the rarefaction phase of the explosion did not begin until at least 300 ms after the arrival of the initial shock wave.

7.   Detonation modelling indicates a rapid decay in the magnitude of the overpressure with horizontal distance. This is consistent with the rapid change in the level of damage observed in cars located just inside and outside the cloud. It also provides pressure loadings on mid-field buildings that are consistent with the observed level of damage.

8.   The far field damage is consistent with the detonation scenario. Given that a detonation is the most efficient means of generating a single shock wave from the combustion of an open vapour cloud, this consistency (and lack of over-prediction) provides strong support for the proposition that a detonation occurred at Buncefield.

9. Though the damage to the Fuji building and Catherine House does indicate severe pressure loading, the damage to the Northgate building does not appear, from the analysis carried out, to be consistent with a detonation loading simulated to-date.

D.10. CONCLUSIONS

The Buncefield incident is unique in the amount of evidence that is available and therefore provides many measures against which any proposed scenario can be tested. The comparison of the evidence with a scenario involving a deflagration to detonation transition shows that it explains many aspects of the incident, including the directional indicators and the distribution of pressure damage, that cannot be explained by the 'deflagration only' scenario.

It is worth re-stating at this point that the reported detonations at Port Hudson and Ufa (discussed in Appendix H) both had similar patterns of directional indicators inside and outside the cloud as Buncefield. For example, Burgess & Zabetakis [12] stated in relation to the damage inside the Port Hudson cloud, *"We think that it is significant that the wind direction was everywhere opposite to the postulated direction of the detonation"*.

The only evidence that does not appear to be consistent with this scenario is the level of damage to the Northgate building. However, there is no known combustion mechanism that can explain the full range of the damage observed <u>and</u> give the loadings suggested as being the cause the damage on the Northgate building. There are also variations on the simple detonation scenario that could provide loadings that could be more consistent with the level of damage observed. Further work related to the explosion event should therefore include examination of some variations on the simple detonation scenario and the loading on the structure to determine the impact on the conclusions of the structural analysis.

Given the broad (if not complete) agreement with the evidence and the discrepancies between the evidence and the 'deflagration only' scenario, it is concluded that by far the most probable cause of the severe explosion at Buncefield is a deflagration to detonation transition, with the detonation propagating through a significant proportion of the cloud.

D.11. REFERENCES

1. Fundamentals Aspects of Unconfined Explosion, JA Nicholls, M Sichel, RS Fry, C Hu, DR Glass, R De Saro, K Kearney, Report on US Air Force research contract F08635-71-C-0083, 1974.

2. Estimating the Flammable Mass of a Vapour Cloud. John L Woodward, CCPS Concept Book, AIChE, 1998.

3. Liquid dispersal and vapour production during overfilling incidents, G Atkinson, S Gant, D Painter, L Shirvill and A Ungut, Hazards XX University of Manchester, UK, 14–17 April 2008 in IChemE Symposium Series 154

4. Concentration limits to the initiation of unconfined detonation in fueVair mixtures, DC Bull, Transactions of the Institute of Chemical Engineers, Volume 57, Number 4, Pages 219-2271979

5. Understanding vapour cloud explosions – an experimental study, RJ Harris and MJ Wickens, IGE comm. 1408, 1989.

6. Experimental observations of flame acceleration and transition to detonation following shock-flame interaction, G Thomas, R Bambrey and C Brown, Combust. Theory Modelling 5 (2001) 573-594.

7. Origins of the deflagration-to-detonation transition in gas-phase combustion, ES Oran and VN Gamezo, Combustion and Flame 148 (2007) 4–47.

8. Initiation of unconfined gas detonations in hydrocarbon-air mixtures by a sympathetic mechanism. Bull DC, Elsworth JE, McLeod MA, Hughes D, Progress in Astronautics and Aeronautics, Volume 75, Gas Dynamics of Detonations and Explosions, Pages 61-72, 1981

9. Present understanding of the explosion properties of flat vapour clouds, W Geiger, Heavy gas and risk assessment II: Proceedings of the second symposium, Ed S. Hartwig, Batelle Institute 1983.

10. TNO Yellow Book, 3rd Edition, CPR 14E: Methods for the Calculation of Physical Effects, Chapter 5, Committee for Prevention of Disasters, Netherlands, 1997.

11. Explosion Hazards and Evaluation, WE Baker, PS Westine, JJ Kulesz, RA Strehlow, Elsevier, 1983

12. Detonation of a flammable cloud following a propane pipeline break, DS Burgess and MG Zabetakis, US Bureau of Mines, Report of investigation 7752, US Department of the Interior, 1973.

A.1. ANNEXE 1 – KINGSTON CFD MODELLING

The modelling approach developed by Kingston CFD is described in this Annexe. This has included several stages from the initial tuning of the chemistry to obtain the right pressure peaks and detonation speed.

A.1.1. Governing Equations.

The governing equations for detonation (Euler equations) are as follows:

Continuity equation:

$$\frac{\partial \rho}{\partial t} = -\nabla(\rho V) \tag{-1}$$

Momentum conservation equation:

$$\frac{\partial \rho V}{\partial t} = -\nabla(\rho VV) - \nabla P \tag{-2}$$

Energy conservation equation:

$$\frac{\partial \rho E}{\partial t} = -\nabla(\rho EV) - \nabla(VP) \tag{-3}$$

Reaction progress equation:

$$\frac{\partial \rho \alpha}{\partial t} = -\nabla(\rho \alpha V) + \rho \omega \tag{-4}$$

Energy equation:

$$E = -\alpha \mathbb{Q} + \frac{P}{[\rho(\gamma - 1)]} + \frac{V^2}{2} \tag{-5}$$

Reaction equation:

$$\omega = A(1 - \alpha) EXP(-\frac{E_a}{RT}) \tag{-6}$$

Equation of state:

$$\frac{P}{\rho} = \frac{RT}{M} \tag{-7}$$

In the above equations P, V, E, ϱ, R, T, α and ω indicate the pressure, velocity, energy, density, gas constant, temperature, reaction progress variable and chemical reaction source term respectively.

A.1.2. Numerical Solution

The above equations are discretized using finite volume method. The explicit Euler scheme is used for time derivatives and the Van Leer scheme which is a total variation diminishing scheme is used for the shock capturing.

The Van Leer flux limited method can be expressed by the following formulation:

$$u_i^{n+1} = u_i^n - \lambda(\hat{f}_{i+\frac{1}{2}}^n - \hat{f}_{i-\frac{1}{2}}^n) \tag{-8}$$

$$\hat{f}_{i+\frac{1}{2}}^{n} = \frac{1+\eta_i^n}{2}\hat{f}_{i+\frac{1}{2}}^{L-W} + \frac{1-\eta_i^n}{2}\hat{f}_{i+\frac{1}{2}}^{B-W}$$

-9

$$u = \begin{bmatrix} \rho \\ \rho u \\ \rho e_T \end{bmatrix}$$

-10

$$f = \begin{bmatrix} \rho u \\ \rho u^2 + p \\ (\rho e_T + p)u \end{bmatrix}$$

-11

The courant number is kept under 0.1 to avoid large time steps during the solution. Further details about the scheme can be found in literature.

A.1.3. Chemistry

In general the chemical reaction of a hydrocarbon with air is as follows:

$$C_X H_Y + (X + \frac{Y}{4}) \times (O_2 + 3.76 N_2) \longrightarrow a CO_2 + b H_2 O + c N_2 + d CO + e HO + f NO + ...)$$
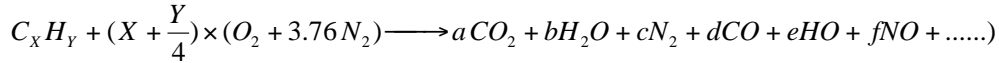
The actual combustion process involves hundreds of chain reactions for which detailed chemical kinetic schemes are available but extremely time consuming. Most detonation studies have hence only used one step chemistry which leads to conversion of reactants to products. Such assumption is accurate enough to predict the correct overpressure, velocity, temperature and the rest of detonation static parameters.

The one step chemistry is represented by a single step Arrhenius form of reaction in the form of equation 6, where A and E_a are the pre-exponential factor and activation energy for the reaction. These two values can be tuned to control the source term behaviour so the solver can capture the pressure and velocity time history in a vapour cloud detonation. Propane was used as the fuel.

Reference CJ calculations were firstly conducted as during the tuning process. This included both 1-D and 2-D for various grid resolutions. Table A.1 shows predicted pressure, temperature, shock and products velocities obtained from CJ calculations.

Table A.1 CJ values for Stoichiometric Propane-Air Detonation

Von-Neumann Spike	CJ Pressure	Temperature	Shock Velocity	Products Velocity
30 atm	17.5 atm	2800 K	1835 m/s	790 m/s

The above CJ predictions were conducted using an in-house code which has been validated against experimental results. By comparing the predictions during the tuning process, appropriate coefficients for the reaction were selected as shown below:

$$\omega = 6^9 \times (1 - \alpha) EXP(-\frac{12000}{T})$$

-12

D.12.4. Code developments

The detonation solver was developed within the frame of the open source CFD code OpenFOAM. The governing equations were implemented following the OpenFOAM coding style and the additional solver was added to the source code.

D.12.5. Initiation of the Detonation

To initiate the detonation, a line source of 3000 K and 20 bar was imposed on the left edge of the cloud.

APPENDIX E   POTENTIAL FOR ALTERNATIVE EXPLOSION MECHANISMS

E.1.   INTRODUCTION

There is a considerable amount of forensic evidence and indicators from the combustion event at Buncefield in the early morning of Sunday 11 December 2005. A theory explaining the damage caused by the event must be supported by the evidence gathered on and around the site, including:

- Directional indicators
  - o Direction of flame propagation
  - o Direction of broken or dislocated objects, e.g. net impulses imparted to standing objects are directed backwards (relative to the explosion propagation) across the whole cloud and towards the most likely ignition point
- Over pressure damage
  - o High (> 200 kPa) overpressures across the whole of the area of the cloud. The only exception is a small area (radius < 15 m) around the point of ignition where drag related damage is lower
  - o Extensive damage to the Fuji and Northgate buildings
  - o Crushing of barrels and instrument boxes across the site
  - o Extensive damage to vehicles in the car parks in front of the Fuji and Northgate buildings and between those two buildings
- Effects of over pressure on people located just beyond the vapour cloud, e.g. lack of hearing damage and physical displacement of the person, on the HOSL site and in its vicinity
- Closed Circuit TV footage from cameras located on the HOSL site and around the site
  - o Illumination
  - o Time of arrival of pressure waves
- Witness statements consistently describing an explosion event that lasts up to several seconds

The inference of events, such as time of arrival of the flame front or blast wave and what the flashes of light in the images from the cameras and CCTV footage actually represent is complex and requires careful interpretation. Appendix A sets out the factual assessment of the images without attempting such interpretation.

Witness statements are obviously subjective, but taken in conjunction with the other indicators consistently describe an explosion event lasting as long as several seconds

Two possible mechanisms, deflagration and detonation, are described in considerable detail in Appendix C and Appendix D, respectively, and will not be discussed further here.

Work in this appendix has been undertaken on the basis that neither standard deflagration nor detonation alone can fully explain the damage seen or are wholly supported by other forensic evidence.

This Appendix lists a number of alternative mechanisms. The merits of these mechanisms are discussed. At least one of the alternative mechanisms (Unsteady Deflagration Accelerated by

Forward Radiation from the Flame Front – See 1.2.6) appears to have the potential to explain the damage seen and in our opinion should be the subject of further work.

E.2.   DESCRIPTION OF CANDIDATE MECHANISMS

E.2.1. Mist Explosion

If the release of fuel had generated a flammable cloud of fuel mist or fuel mist and vapour rather than just a vapour cloud then there is the possibility that a mist explosion had occurred. Results from the experimental studies that have been undertaken on mist explosions are inconclusive, Bowen and Cameron (1999), but some of the results do indicate that a mist explosion can result in a more powerful explosion than the equivalent mass of fuel that has completely vaporised. From the postulated mechanism of how the vapour cloud was generated from the overfilling of Tank 912 it is difficult to see how a cloud containing fuel mist could have spread over the car park areas. The white mist seen on the CCTV records is thought to be a water mist or ice crystals rather than a fuel mist.

No satisfactory mechanism capable of generating such a mist – fine enough to persist for twenty minutes – could be found in the literature. The level of flame speed enhancement in such mists has been investigated, Bowen et al. (1997) and Ballal and Lefebvre (1981). Although significant, it falls far short of that required to explain the overpressures at Buncefield.

E.2.2. Multiple Detonations

In this case the cloud detonates in small fragments – punctuated by pauses. This could explain the high overpressures and low overall rate of spread. The question arises why should detonations fail and (more urgently) why should they restart? This process of re-initiation of detonation would have to occur in open areas to explain the symmetry of the overall explosion. The possibility of local detonation is not ruled out in the explanation explored in more detail in this section – see Section 1.2.8. Such detonations would have to die away within a few metres of the initiation point.

Zeldovich et al. (1987) showed numerically that the detonation wave speed could be reduced by introducing momentum and heat losses due to wall friction and cooling. Studies of unconfined detonations by Klein and Stewart (1993) and He and Calvin (1994) showed the speed of the detonation wave could be drastically reduced to such a degree as to quench the detonation wave. Ju and Law (2002) investigated quenching of detonation waves in particle-laden flows. The main findings of the modelling performed by Ju and Law (2002) were that the detonation wave can be quenched due to heat and momentum losses and that the smaller particles, for a fixed particle volume fraction, caused a larger a heat loss from the gas phase. The latter resulted in both a lower detonation speed and narrow detonation limit, Ju and Law (2002).

It is not clear whether it is possible to have another DDT or 'full-on' detonation after the detonation wave has been quenched or not.

Pintgen and Shepherd (2009) investigated a detonation wave exiting a round tube and entering an unconfined region. Under sub-critical conditions, the detonation wave is quenched, while in the super-critical case, the detonation wave is re-established and continue to propagate in the unconfined region. The conditions governing this are: mixture composition, thermodynamic conditions, detonation velocity at the tube exit, geometry of expansion and tube cross section.

E.2.3. Multiple Ignitions

There is an extensive drainage system underneath the car parks by the Fuji and Northgate buildings and along the two lanes. The possibility that flammable mixture could have entered

the drains underneath the car parks and the flame could propagate through the drains has been considered. However, this theory can be discarded on two points; (i) the drains underneath the car parks lead towards the West, e.g. away from the HOSL site, and (ii) the ductile drain covers were pushed inwards indicating that the pressure above ground exceeded that in the drains system.

Given a flammable vapour concentration in the car park drainage system then a possible scenario is as follows. An explosion in the above ground cloud would readily propagate through the grates into the drainage system and it is likely, at least in the initial stages of the explosion that the flame speeds in the drainage system (a confined geometry) would have been higher that that of the flame speed through the surface cloud. The result would be rapid propagation of the explosion through the drainage system and the creation of new ignition sources, as the flame propagates out of the grates, ahead of the flame propagating through the surface cloud. In terms of overpressure generation the net result of a number of near simultaneous ignition sources through the cloud would be the same as an explosion with one ignition source, but with much high flame speeds through the cloud. This multiple ignition source mechanism is not consistent with the abrasion pattern found on posts and tree trunks in the car parks that indicate a powerful explosion propagating in one direction right across the Northgate and Fuji building car parks. Also the drainage system in the car parks all run east/west, which is at ninety degrees to the direction of the high flame speed south/north as indicated by the abrasion damage and other direction indicators. Within the vapour cloud and around its periphery there were potentially a number of ignition sources that if resulted in near simultaneous ignitions could have also resulted in a similar effect to multiple ignitions from the drainage system.

Another possible additional ignition location was the emergency generator housed in an iso-container located to the South of the Northgate building.

The probability of near simultaneous ignitions occurring within the cloud would be very low and such a mechanism would not be consistent with a powerful explosion propagating in one direction across the car parks. For these reasons, a multiple ignition mechanism arising from propagation through the drains or from near simultaneous ignitions can be probably discounted. Also this mechanism is not supported by the uniform distribution pattern of overpressure indicators, you would expect to see some distribution pattern based on the arrangement of the various drainage systems.

E.2.4. Stratified Explosion

It has been suggested that an explosion could progress across the top of a very uniformly stratified cloud. This would generate turbulence that would mix air into the underlying rich gas mixture as well as promoting high flame speeds during a secondary explosion.

There are a number of factors that make this explanation untenable, e.g. most notably the radial symmetry of directional indicators around the ignition point. In practice this means that both primary and secondary combustion must start at the centre. The secondary explosion would have to go much faster than the primary, so there would have to be a long delay before the initiation of secondary combustion. This explanation does not seem credible given the number of obstacles, especially the hedgerows along Buncefield and Three Cherry Tree Lanes, which would distort the combustion driven flow.

Schultz and Shepherd (2000) and Shepherd (2009) highlighted that detonation waves behave very differently in stratified layers. The wave speed is different and so the wave front can be curved, at times so curved that the chemical reactions are decoupled from the shock front.

Schultz and Shepherd (2000) first discussed detonation diffraction as the wave exits a tube and enter an unconfined region. Schultz and Shepherd then considered the detonation wave

behaviour in the presence of fuel concentration gradient; the authors noted the similarity between the two situations. They found that a detonation wave propagating through a fluid with inhomogeneous fuel concentration would adjust to the local conditions, quench and then again undergo transition to detonation or fail completely.

Strehlow et al. (1972) found that the detonation wave system adapted more rapidly when the wave was propagating from a low sensitivity region to a high sensitivity region.

Thomas et al. (1991) argued that the interface between a detonation mixture and an inert gas is not perfect, e.g. sharp, and that pockets of shock-heated, but unburnt gas can be found between the frontal shock and the flame boundary. These pockets would explode, thus causing a secondary pressure pulse. Thomas et al. also found that detonation waves that enter a region with varying fuel concentration rapidly adjust its structure and speed to the local conditions.

The shock front of a detonation is intrinsically unstable with a quasi-periodic oscillation of the leading shock wave due to a set of weak shocks propagating transversally to the main shock.

This also holds true for deflagration too. In an internal combustion engine this is referred to as knocking, e.g. Lewis and van Elbe (1961) and Heywood (1988). Lewis and van Elbe (1961) state that the induction period could be as low as 10-4 s and that the combustion wave cannot travel across the cylinder in such a short time, thus leading to these violent combustion events. Heywood (1988) defined one type of engine knock as the violent combustion of pockets of fuel-air mixture, e.g. inhomogeneous fuel concentration in the cylinder, perhaps to the point of causing a detonation. This could result in severe damage to the engine.

The extension of the theory from a highly confined engine cylinder to a largely unconfined region, such as Buncefield, is not impossible. The theory of stratified explosion leading to such high overpressures as those experienced at the Fuji and Northgate buildings and the car parks in their vicinity is not a credible one as the conditions at Buncefield differ significantly from those in a hot cylinder, where the gases are undergoing strong compression by the moving piston.

E.2.5. Flame Acceleration due to Dust Particles

Gas explosions in fuel-air mixtures laden with particles can lead to significantly higher flame speeds and thus also higher over-pressures.

In the Buncefield case, it is not clear how many particles were suspended in the air ahead of the flame. The wind speed was low, Buncefield Major Incident Investigation Board (2008). However, CCTV footage shows that the propagation of vortical structures ahead of the flame front that lift dust off the ground. Thus, the turbulence generated by the vortices and the dust lifted off the ground could enhance the flame speed.

E.2.6. Unsteady Deflagration Accelerated by Forward Radiation from the Flame Front

The potential for thermal radiation to ignite suspended particulates ahead of the flame front and thereby accelerate flame spread was the topic of research in the 1980s, Moore and Weinberg (1981, 1983, 1987). They noted that the flame speed of a deflagration in some unconfined and uncongested explosions is of the order of a 100 m s-1. Moore and Weinberg's (1983, 1987) analysis concluded that forward radiation by particles or debris could have a significant effect on the flame speeds and provides a credible explanation of the severe damage caused by a deflagration of an essentially unconfined and uncongested flammable fuel-air clouds. This damage being well in excess than what would be expected of such an event. Moore and Weinberg (1983, 1987) argued that multiple ignition locations would greatly increase the flame area and thus the flame speed would be significantly increased. Experiments carried out by

Moore and Weinberg confirmed that the hypothesis were correct. What was of particular interest was that the lowest radiation flux, for ignition occurs are well below what can be expect from diffusion flames. The type and size of particle also played a significant role in the radiative heat transfer.

The evidence from Buncefield suggests that the process of flame acceleration by forward radiation may be fundamentally unstable. Instead of the flame spread progressing somewhat more rapidly at a steady rate, the burning could be episodic. The evidence for this is briefly reviewed below with some preliminary discussion of the fundamental physical processes that might be responsible for driving the instability.

Evidence on timings from CCTV, structural analysis and witness reports indicates that the total duration of the explosion was 1600 ms. Given the maximum radius of the cloud was 240 m this indicates an average velocity of 150 m s-1.

At first sight this appears inconsistent with the observation of very high (>200 kPa) overpressures across the whole area of the cloud. The inconsistency can be resolved if flame propagation is episodic, e.g. comprises short periods of intense combustion (which generate the high overpressures) punctuated by pauses (which lead to low average speeds).

Such a variation in burning rate can arise through the combination of two processes capable of heating particulates and associated gas ahead of the flame front:

1.   Thermal radiation

2.   Adiabatic compression

If forward radiation initiates combustion in suspended particulates the pressure will rise close to the flame front. If the particle density is sufficient, the resulting compression will initiate further ignition (in preheated particulates) further away from the flame front. This results in the initiation of ignition in an extended range. Still further out from the flame front, particulates and gas are not pre-heated sufficiently to be ignited by adiabatic compression. When the pressure subsides gas associated with these more distant particles simply cools and is left at a temperature well below that required for spontaneous ignition. There is an extended delay until forward radiation brings gas and particles to the temperature required for ignition and the next cycle of rapid combustion can start. The distance scale over, which the flame progresses in each cycle is determined by the range of thermal radiation i.e. the length scale of the burned cloud.

The episodic character of the explosion also explains how appropriate particulates could be numerous and suspended in the gas cloud. Since the average speed is sub-sonic, relatively strong shock waves progress ahead of the flame and these can disperse and fragment objects such as dried leaves.

E.2.7.   Unsteady Deflagration Without Radiative Effects

Analysis (interpretation) of the CCTV footage gives an indication of the time scales at which the events occur. The distances between the pump house, the cameras, buildings and other objects, are known from site observation. These data can be then be used to estimate the flame speed. The footage does not support a steadily increasing flame speed, but rather seems to suggest that it is an unstable process where the flame speeds up and slows down where the average speed is of the order of 150 m s-1.

Turbulence is generated where vapour is driven violently across the ground, however smooth the surface. The flow field induced by a violent localised explosion is poorly understood. Photographs and videos of bombs in dusty areas show that of the negative phase of the

explosion causes separation and mixing of vorticity (and associated debris) from the boundary layer into the main flow. It is not clear how significant this turbulence could be in promoting high flame speeds. The total surface area of contact is not very different to that in pipe arrays that cause a high level of flame acceleration. The difference is clearly that separation and a mixing process is required before any secondary phase of rapid combustion can take place in the main flow. This takes time and allows decay of turbulent kinetic energy.

Even if the level of turbulent kinetic energy remained high it is not clear whether the mixing process could occur rapidly enough to explain an average speed of 150 m s-1. The reasons for a pause in rapid combustion are also not clear - the flame might be expected to simply progress rapidly in the boundary layer.

Experimental investigation of the short and medium range flow induced by explosions would be useful – both in clarifying whether some simple fluid mechanical instability is possible and in providing insight into how debris is translated ahead of an explosion – which is in any case crucial to the understanding of the ignition of material by forward radiation from the flame front, see Section 1.2.6.

E.2.8. Cellular Flames

Assume a fuel-air mixture with quiescent, homogeneous, stoichiometric concentration ignited with no proximity to walls or other solid objects. The laminar flame will grow in a spherical fashion initially. However, the flame will soon become wrinkled due to hydrodynamic instabilities, e.g. Darrieus-Landau instabilities, inhomogeneous fuel concentration and differential diffusion. The cellular structure is stabilised by the increased gas velocity and reduced burning velocity in retarded areas and decreased gas velocity and increased burning velocity in advanced areas of the flame. Hence, the cellular combustion wave propagates at higher velocity than an unstable planar wave. At some point the flame will become turbulent, thus will experience an increase in the flame speed. It is not clear that the cellular flame structure persist when turbulent combustion commences; the flame would not remain cellular if it has to flow around obstacles, as this would destroy the cellular structure. In the Buncefield incident, the flame encountered a number of obstacles in the form of trees and shrubs lining Buncefield Lane and Three Cherry Trees Lane.

However, a study on cellular flame structure of lean premixed hydrogen flames indicate that the 3D cellular flame structure yields three to eight times increase in the flame speed compared to that predicted by 1D formulation of the thermo-diffusively unstable flames, Day et al. (2009). Day et al. (2009) also investigated the effect of turbulence on the flames. It is not inconceivable that this may have an effect in the deflagration of hydrocarbon-air mixtures. The length scales associated with the Buncefield site and its surroundings are considerably greater that those at which the numerical experiments were performed. This might or might not be relevant.

Bradley et al. (2001) examined the flame acceleration due to flame-induced instabilities. Bradley et al. found that the flame speed is dependent on the flame stretch rate in the initial stage, but proportional to t1/2 once the flame enters the unstable region and exhibits a cellular structure. It was also found that radiative heat losses by the flame to the surroundings became more significant as the flame radius grew. The effect of this increased heat loss was a reduction of the flame speed. Bradley et al. (2001) also highlighted that there was shortage of experimental data for large-scale explosions in the unstable regime.

Buckmaster et al. (2005) stressed that hydrodynamic and diffusive instabilities make flames highly dynamical structures which can exhibit both orderly and complex behaviour involving periodic and aperiodic pulsations, chaotic self-motion and fractal-like growth. The latter lead to self-fragmentation. Buckmaster et al. go on to say that these cellular flames could be highly fragmented, forming flame balls and allowing some unreacted fuel to escape the reaction zone.

E.3.   FACTORS POTENTIALLY AFFECTING COMBUSTION RATE

E.3.1.   Strong Ignition

The observed damage from forensic examination is consistent with an internal explosion in the pump house that housed the firewater pumps. There was also an internal explosion in the emergency generator cabin located on the south side of the Northgate building, though it is not possible to definitively say whether this occurred before an external explosion or as a result of an external explosion propagating into the cabin. The flames venting from an internal explosion in the pump house or generator cabin would have been a powerful ignition source for an external flammable atmosphere. However, it is clear that there was no direct initiation of a detonation. It is possible that the subsequent explosion in the generator cabin could have triggered a detonation.

The vapour concentration around the pump house may have been fuel rich, on the basis of dispersion studies and the clear evidence of prolonged burning of the vapour shown on the adjacent trees. So an explosion in the pump house may have initiated a flash fire or at worst a weak explosion in the surrounding vapour cloud. On the other hand the cloud around the generator cabin, taking into account the dispersion away from the source of release and the opportunity to mix with air during the dispersion process, was likely to have been well within the flammable range, possibly a near stoichiometric mixture. Under these circumstances an internal explosion would have initiated an explosion with initially a high flame speed. Experimental studies show, CCPS (1994) and Mannan (2005), however, that once the flame propagates away from the ignition source it decelerates unless this is some further mechanism, for example congestion in the surrounding vapour cloud, to sustain the high flame speeds.

There were also a number of empty tanks that showed signs of pressurisation following internal explosions. For example, Tank 910, located close to Tank 912 which was being overfilled, had an open manway and would have filled with fuel vapour to a depth of a few meters. The internal explosion displaced the roof of the tank (a portion travelled approximately 50 metres) and deformed the base. Failure of the roof/wall weld would have occurred at a pressure of a less than 5 kPa so a very rapid rise in the internal pressure could only have occurred because of jet ignition in through the open manway. The burning flow into the tank would eventually have been reversed, as gas inside was ignited. By this stage, however, it is likely that gas around the manway would have already ignited so the exploding tank would not have been effective in acting as a strong ignition source.

This theory is not supported by the forensic evidence and, hence is not a credible explanation on its own.

E.3.2.   Chemistry Effects

It is common practice to add various compounds to gasoline and other petrol products to achieve certain fuel characteristics. One commonly used additive is Methyl tert-Butyl Ether (MTBE), usually around 5 – 15 % by weight, which has several desirable effects on the gasoline; (i) it raises the Octane rating which prevents or minimises engine knock, and (ii) it has the potential to reduce the tailpipe emissions of carbon monoxide and hydrocarbons.

The petrol at Buncefield included a few percent of MTBE.

Pure MTBE can cause static electricity charge to build up as it falls through air. The compound can ignite flammable vapour when the electric static energy is discharged.

There may also have been other additives in the gasoline.

This is not a credible mechanism on its own, but could be important in conjunction some other phenomenon perhaps explain the damage caused by the combustion event.

E.3.3. Boundary layer effects in a flat cloud

Another possible feature of a shallow vapour cloud that could enhance the explosion strength, compared to a deeper cloud of similar volume, is the increased relative thickness of the ground boundary layer generated during an explosion. Turbulence is generated in the boundary layer and this is more likely to affect the overall turbulence of the vapour cloud and its burning velocity as the ratio of boundary depth to cloud depth increases.

E.3.4. Inhomogeneous Fuel Concentration in the Vapour Cloud

It is highly likely that the fuel concentration in the vapour cloud would not have been homogeneous horizontally. There could have been stratification and/or pockets of higher/lower fuel concentration. Significant variations in gas concentration might be part of the explanation for the discrepancy between high overpressures and low average flame speeds.

E.3.5. Internal Tank Explosion

Several tanks on the HOSL west site were empty at the time of the incident, tanks 904 & 910 in particular. At least one, tank 910 appears to have experienced an internal explosion due to vapour build up inside the tank via the open man-way and subsequent ignition, It has been suggested that this might have been responsible for the high overpressures. There are a number of reasons why this is not believed to have been part of the mechanism. First, the pattern of overpressure damage is not consistent with a localised source of overpressure in this location. A consistent level of damage (Fuji building and cars right across the car parks) is seen much further to the north than would be expected. Second, the structure of tank 910 is relatively weak so that the roof would be expected to fail at a relatively low pressure thus relieving any further pressure build up. If high internal overpressure had occurred one would expected damage to both the roof and the tank walls.

E.4.   CONCLUSIONS

A number of alternative mechanisms, in addition to the standard theories of deflagration and detonation, have been put forward. These mechanisms have been considered with reference to their ability to provide a credible explanation for the damage seen in the Buncefield incident.

The unsteady combustion with forward radiation appears to be consistent with the forensic evidence. Work by Moore and Weinberg (1983, 1987) has also suggested that high flame speeds are achievable in unconfined and uncongested vapour clouds by this means.

The mechanism of radiative ignition and some other mechanisms are recommended for further investigation.

It may also be that some of the mechanisms discussed here may be factors that caused combined effects with the standard deflagration and/or detonation mechanisms.

E.5.   REFERENCES

Ballal, D. R. and Lefebvre, A. H., Flame propagation in heterogeneous mixtures of fuel droplets, fuel vapour and air, 18th Symposium on Combustion, The Combustion Institute, Pittsburgh, PA, USA, pp 321-327, 1981.

Bowen, P. J., Bull, D. C., Prothero, A., and Rowson, J. J., Deflagration of hydrocarbon aerosol fuels, Combustion Science and Technology 130:25-47, 1997.

Bowen, P. J., and Cameron, L. R. J., Hydrocarbon aerosol explosion hazards: A review, Transactions of the IChemE 77 Part B:22-30, 1999.

Bradley, D., Cresswell, T. M., and Puttock, J. S., Flame acceleration due to flame-induced instabilities in large-scale explosions, Combustion and Flame 124:551-559, 2001.

Buckmaster, J., Clavin, P., Liñan, A., Matalon, M., Peters, N., Sivashinksy, G., and Williams, F. A., Combustion theory and modeling, Proceedings of the Combustion Institute 30:1-19, 2005.

Buncefield Major Incident Investigation Board, The Buncefield Incident 11 December: the final report of the Major Incident Investigation Board, 2008.

Centre for Chemical Process Safety (CCPS), Guidelines for evaluating the characteristics of vapour cloud explosions, American Institute of Chemical Engineers, 1994.

Day, M., Bell, J., Bremer, P.-T., Pascucci, V., Beckner, V., and Lijewski, M., Turbulence effects on cellular burning structures in lean premixed hydrogen flames, Combustion and Flame 156:1035-1045, 2009.

Fishburn, B., Slagg, N., and Lu, P., Blast effects from a pancake shaped fuel drop-air cloud detonation (theory and experiment), Journal of Hazardous Materials 5:65-75, 1981.

He, L., and Clavin, P. J., Journal of Fluid Mechanics 277:227-248, 1994.

Heywood, J. B., Internal Combustion Engine Fundamentals, McGraw-Hill Book Company, Singapore, 1988.

Ju, Y., and Law, C. K., Propagation and quenching of detonation waves in particle laden mixtures, Combustion and Flame 129:356-364, 2002.

Klein, R., and Stewart, D. S., SIAM Journal of Applied Mathematics 53:1401-1535, 1993.

Lewis, B., and Elbe, G. van, Combustion, Flames and Explosions of Gases, Academic Press Inc., New York, USA, 1961.

Mannan, S., Lees' Loss Prevention in the Process Industries, Hazard Identification, Assessment and Control (3rd edition), Volume 2, Chapter 17, Elsevier, 2005.

Moore, S. R., and Weinberg, F. J., High propagation rates of explosions in large volumes of gaseous mixtures, Nature 290:39-40, 1981.

Moore, S. R., and Weinberg, F. J., A study of the role of radiative ignition in the propagation of large explosions, Proceedings of the Royal Society of London A385:373-387, 1983.

Moore, S. R., and Weinberg, F. J., Further studies of the role of radiative ignition in the propagation of large explosions, Proceedings of the Royal Society of London A409:1-20, 1987.

Pintgen, F., and Shepherd, J. E., Detonation diffraction in gases, Combustion and Flame 156:665-677, 2009.

Schultz, E., and Shepherd, J., Detonation diffraction through a mixture gradient, Explosion Dynamics Laboratory Report No. FM00-1, 2000.

Shepherd, J. E., Detonation in gases, Proceedings of the Combustion Institute 32:83-98, 2009.

Thomas, G. O., Sutton, P., and Edwards, P. H., The behaviour of detonation waves at concentration gradients, Combustion and Flame 84:312-322, 1991.

Zeldovich, Ya. B., Gelfand, B. E., Kazhdan, Ya. M., and Frolov, S. M., Combustion, Explosion and Shock Waves 23:342-349, 1987.

APPENDIX F   ASSESSMENT OF STRUCTURAL DAMAGE

F.1.   BACKGROUND

This analysis was undertaken for the Buncefield Explosion Mechanism Working Group by the Head of Ordnance Risk Assessment from the Defence Ordnance Safety Group (DOSG) of the Ministry of Defence (MoD).

On the 11 December 2005, following an unplanned hydrocarbon fuel release, a major explosion occurred at the Buncefield Oil Storage and Transfer Depot, Hemel Hempstead. Investigations into the cause and nature of the explosion are ongoing.

This study aimed to employ explosion effects specialists within the DOSG risk assessment team to examine the damage levels caused to buildings in the vicinity of the fuel depot and to equate the levels of damage to known over-pressure criteria, military explosives quantities and explosives safety distances.

This work does not necessarily imply that the exact nature and behaviour of the explosion that took place at the Buncefield fuel depot was equivalent to or characteristic of that expected from detonation of a quantity of High Explosives (HE). The work was simply undertaken to generate data that could then be further used by the Buncefield Explosion Mechanism Working Group in better understanding and characterising the actual behaviour of the Buncefield explosion.

F.2.   INTRODUCTION

Following a joint discussion between DOSG and HSL personnel [B], a target list of appropriate structures for consideration was selected. These are shown in Table F.1 below. All distances were estimated from maps or site plans using storage Tank 912 as the origin of the source of the explosion. It is noted that other work-streams running in parallel to this study have indicated that the ignition of the cloud is likely to have occurred at a point North of Tank 912. This was not taken into account for this study.

Table F.1 Summary Table of Main Structures Considered in the Study

Building	Building Type	Distance from Source (m)
Fuji Building	Commercial, medium height (2 storey), medium strength concrete column frame, lightweight cladding	144 (to closest corner)
Northgate Building	Office, three storey, metal frame, reinforced concrete cladding with brick infill	135
3 COM and RO Buildings	Office, four storey, brick	234
RO Utilities Building	Single storey plant room, steel frame, brick built, corrugated metal roof	125
Fircones	Single storey domestic cottage, brick	252
Cottage	Single Storey domestic cottage, brick	234
Warehouses (North East)	Commercial, metal frame, light weight cladding, high rise	324
Warehouses (South)	Commercial, metal frame, light weight cladding, high rise	414
Far Field Domestic	UK housing estates	1050

The safety of the general public from military explosives and munitions is managed through the rigorous application of Quantity-Distance (QD) rules [A]. These rules equate tolerable levels of damage, and hence risk of fatality, to given safety distances for given quantities of explosives. There are many specific and complex QDs that are used by the MoD for various storage and transportation requirements but a key QD of relevance to this work is the "Inhabited Building Distance (IBD)". All further discussion refers only to the management and assessment of the blast effect from HEs and not high velocity fragmentation of debris.

IBD is the safety distance which is applied to the nearest public/privately owned or operated buildings or facilities beyond the MoD explosives site. In practice, this distance is usually predetermined by the nature of the military site and its surrounding locality such that the Net Explosive Quantity (NEQ) of explosives that can be safely stored is matched to the distance available to the nearest inhabited building i.e. the distance 'available' limits the storage quantity possible. For Mass Detonating, i.e. Hazard Division 1.1, explosives, the IBD equates to peak over-pressures at the inhabited buildings of 5 kPa. In its most common form it is applied using the equation;

$$D = 22.2Q^{1/3} \text{ (for Q>4500 kg)}$$

Where D = distance (m) and Q = quantity of explosives (kg)

At IBD, and hence 5 kPa over-pressure, the damage to domestic dwellings has been well characterised. This has been achieved through analysis of wartime building damage, specific testing undertaken by the MoD and international collaboration.

At IBD, the consequence expected is described as [A];

> "Unstrengthened will suffer minor damage, particularly to parts such as windows, door frames and chimneys. Partial collapse may occur in buildings where structural integrity relies on critical elements or the continuity of the structure."

F.2.2. Initial Approach

DOSG were given access to:

- The earlier accident investigation reports
- Layout diagrams of the Buncefield depot
- Maps of the surrounding area
- Photographic records of damage to buildings taken after the explosion
- A qualitative description of the damage to buildings and other structures including motor vehicles.
- Advantica were also in possession of an annotated map which showed, via pin-points, buildings for which there were known insurance claims completed or pending.

From this collective data it was possible to identify zones at which there was consistent IBD type damage to domestic dwellings. It is always the case that outliers occur in all data and these are typically discarded but areas where multiple cases of light damage occurred were identified.

Domestic housing estates exist to the North, West and South of the industrial area surrounding the Buncefield depot. There is no domestic housing to the East, the M1 motorway runs through the open area of land on the Eastern side.

Observation – There is a higher concentration of damage to domestic dwellings to the North and South of the depot compared to the West.

Selection of an appropriate distance for placing an IBD arc can be made:

Table F.2 IBD Distances Based Upon Far Field Damage to Domestic Dwellings

Case	IBD Location	Distance from assumed centre of explosion (m)
A	At a distance that equates to the closest edge of the clusters of multiple instances of minor damage to domestic dwelling.	1050
B	At a distance that equates to the mid-point zone of the clusters of multiple instances of minor damage to domestic dwelling.	1400

If it is assumed that there was a detonation of a quantity of Trinitrotoluene (TNT) at the location of Tank 912 on the original site and giving a peak side-on over-pressure of 5 kPa at each of the two distances in Table F.2 above, this would equate (using military TNT scaling tools) to quantities of 90000 kg TNT for Case A and 220000 kg TNT for Case B. Using the IBD equation given previously, quantities of 105000 kg and 250000 kg TNT respectively can be derived.

Observation - This suggests that the energy released in the fuel-air explosion was potentially very large in order to generate this much damage in the far field or an alternative mechanism is required to explain the levels of damage inflicted in the far-field.

However, if an HE event of this magnitude were to occur at the storage tank location, the levels of pressure experienced by the buildings on the adjacent industrial estates would be such that total demolition could be expected. This extreme level of damage was not seen. For example, the Northgate Building front face is estimated to be at 135 m from the source. At this distance from a 100 te TNT detonation, the over-pressure would be of the order of 124 kPa. This is greatly in excess of the structural withstand of this type of structure and would be entirely destroyed.

Observation – By back calculating the equivalent mass of explosives from basic IBD damage levels it overestimates the equivalent explosives mass to that suggested by damage in the close-in and mid-field.

The conclusions from this Initial Assessment are that the explosion event was driven by considerable energy, which is not unexpected given the chemical energy available within the fuel/air cloud of the scale that formed.

The minor damage to glazing, door frames, roofing materials, lightweight structures etc. can be associated with peak over-pressures of the order 5 kPa. This can be used to back calculate the TNT equivalence of energy required to generate this level of damage.

It is clear that using this approach, there is a significant over estimate of the quantity of the equivalent charge because the close-in and mid-field damage does not correspond to the quantities that the far-field damage suggests.

Alternatively, the explosion event generated a pressure-time history that is not consistent with a military high explosive pressure-time history and/or does not scale in the same way with distance as would TNT type detonation blast effects (inverse cube relationship).

F.2.3. Alternative Approach

Focus was then switched to the buildings located on, and closer to, the Buncefield storage depot site. By considering these buildings in turn, it became possible to relate the close-in damage to a quantity of military type explosives that would be capable of creating equivalent levels of damage. DOSGST2 has access to a variety of tools for predicting the blast effects from HE detonations ranging from simple look-up tables through empirically based software tools and spreadsheets through to full 3D hydrocode modelling of blast and materials failure. For this assessment, an empirical tool based upon the Kingery-Bulmash curves for TNT detonations [C] was used to investigate the relationships between peak and reflected pressures and corresponding damage levels at the various distances fro the Buncefield site.

Figure F.1 summarises the DOSG assessment of the typical pressures which would be required to cause the observed damage if this had been a TNT charge. The analysis suggests that this would equate to a HE charge of 7500 kg of TNT at the centre of Tank 912.

Observation – The close-in damage suggests an equivalent charge of 7500 kg TNT.

What was surprising is that there appears to be quite reproducible and consistent scaling with direction from the source of the explosion (Tank 912) and quite reliable scaling of pressure-related damage with distance. This suggests perhaps that the pressure decay with time and distance may be comparable to an HE type detonation even if the actual pressure-time history, i.e. the relative durations of the positive and negative phase pressures, was somewhat different to that which can be expected from HE charges.

Observation – There is reasonable symmetry in all directions to the damage around an assumed source of Tank 912. The pressure decay does approximate to that expected from a HE charge.

To go back to military explosives safety distances and their possible use for assisting with characterisation of damage levels, we can apply further QDs to the Buncefield scenario. Within the MoD regulations, buildings used for assembling or maintaining military munitions may be sited closer to one another than to buildings inhabited by members of the public. This is often due to the fact that small numbers of essential explosives workers can be exposed to a work place hazard greater than that to the public and also these buildings are often built to withstand or protect workers and assets from potential nearby explosions. These buildings are called Process Buildings and are afforded their own QD rule, Process Building Distance (PBD).

At PBD, the consequence expected is described as [A];

> "Buildings which are unstrengthened can be expected to suffer damage which is likely to cost above 30% of the total replacement cost to repair."

> "Serious injuries to personnel, which may result in death, are likely to occur due to fragments, debris, firebrands or other objects."

The PBD rule is;

$$D = 8Q^{1/3}$$

Where D = distance (m) and Q = quantity of explosives (kg)

If we use the 7500 kg quantity of TNT then this level of damage would be seen at distances of approximately 150 m. From Figure F.1, it can be seen that both the Fuji and Northgate building were sited at approximately this distance. Once again, the damage observed is consistent with that expected from a charge of this size.

This 'Alternative Approach' section appears to show that conventional explosion scaling may work quite well, showing reasonably consistent and correct pressure scaling for the mid-field buildings. However, It does not generate the required pressures to cause the far field damage to the residential areas.

Observation – An estimated charge size of 7500 kg TNT would not generate the far-field damage based on free field peak pressures.

F.2.4.   Rationalising the Close-In and Far-Field Damage Levels

It may also now be necessary to consider alternative mechanisms for the far-field damage observed. To create the degree of damage at distances of 1 km or more a charge size greater than 100 te of HE would be required based upon free-field pressures alone. This large charge size does not correlate well with the degree of damage seen on the depot site or in the mid-field. However, on the night/morning of the explosion the weather conditions were such that there was a strong inversion, the ground level conditions being cold and still. A temperature inversion is where the temperature, instead of falling, increases with height above the ground. With the colder and heavier air below, there is no tendency to form upward currents and turbulence is

suppressed. It is entirely likely that due to the inversion in the atmospheric conditions, blast/pressure reflections/bending may have occurred creating higher levels of damage than could normally have been expected. It is common for military explosives ranges to encounter greater restrictions on firing when inversions occur due to increased noise and disturbance to surrounding residential areas.

Observation – a likely explanation for the far-field damage is an atmospheric inversion which confined and focussed the energy released upwards from the explosion affecting structures out to greater distances than would have occurred otherwise.

F.2.5. Defence Estates Assessment of Glazing Damage to RO Building

To support the building damage assessment being performed by the ordnance risk assessment team, a request was placed with Technical Advisor (Specialist Structures) within Defence Estates (DE), who was asked to comment upon the damage levels at the RO building. TA(SS) is responsible for providing civil engineering expertise to MoD for the design and approval of structures which may be exposed to explosives effects, including blast over-pressure.

DE TA(SS) was asked to evaluate the glazing and window frame failure of the RO building and to comment on the possible pressures that this building may have been exposed to. The assessment concluded [D] that there was;

- Severe (80-100%) glazing pane damage to the east and north elevations with frame damage on the north elevation.
- Minimal damage to the perimeter masonry cladding.
- Minimal or no damage to the building structural frame.

From this, and given that the distance from Tank 912 to the nearest corner (North-East) of the RO Building is 218 m, an over-pressure of 20 kPa at this corner was said to be capable of generating the levels of damage at the RO building. This equates to a HE charge size of 20000 kg. The fact that the building front face is not 'normal' to the likely direction of the blast wave complicates the estimates of equivalent charge size but it is bounded by this figure as failure of masonry would be expected from this point upwards and often at lower pressures.

However, it was believed that equivalent glazing/frame damage was said to be possible down to 5000 kg. Therefore, a bracket of 5000-20000 kg can be put on the equivalent charge size for the Buncefield explosion, with most weight towards the upper figure. This is not inconsistent with Figure F.1.

Observation – A bracket of 5000-20000 kg TNT can be suggested as an HE explosion that could create the levels of damage to the glazing seen at the RO building.

F.2.6. Finite Element Modelling of the Northgate Building Front-Face Cladding

Weidlinger Associates Ltd were tasked [E] to specifically consider the failure of the front-face of the Northgate building (see Figure F.1 for an image of typical damage), The aim of the work was to investigate whether it was possible to back calculate the nature and intensity of the blast wave from the damage inflicted to the Reinforced Concrete (RC) cladding panels. These cladding panels were thought to be very amenable to this type of work. The panels consisted of a reinforced concrete structure, with a front lip on which brickwork sat. This type of panel is common in British commercial building design. There was also a reasonable amount of engineering detail available covering the make-up of the panel which was provided by the HSL.

One point of interest was the difference in behaviour of essentially three types of the same panel. From photographs it was clear to see that the uppermost row of panels had not only lost its brick facing but had also failed by bending inwards, midspan. All lower rows of panels had not failed in this manor due to the fact that these panels each butted up to a floor component preventing any bending inwards of the centre of the span. Further, there was a difference between the uppermost panels on the right hand side of the building, as looked at from the car park, compared to the left hand half of the building. The top most panels on the right hand side of the building had all failed in the manor as described above but the top most panels on the left half of the building had not. Research work by the HSL identified that the building had in fact been built in two stages at different times and whilst the design was essentially the same, the later half of the building had been built with higher strength of reinforcing. Details of these changes were available. These design factors, plus the very clear response of the panels to the explosion, make them very useful indicators of the nature and strength of the blast wave.

DOSGST2 had estimated that to create this level of damage to a brick clad, RC panel from an HE explosion, an event generating a peak side-on pressure of around 25 kPa at the range to the front face of the building would be required. At this pressure, brick cladding would be expected to fail and any weaker RC structures, such as cladding spans, would likely yield or fail. Lower pressure than this would not yield the concrete and much more would potentially see onset of failure in the actual major frame components of the structure.

The scope of the Weidlinger task was as follows;

i.   To generate Pressure-Impulse (PI) iso-damage curves for the specific RC cladding panels by using numerical modelling techniques.
ii. To generate various PI iso-damage curves for a variety of blast loading forms in order to assess the variability of the structural response to different types of blast (HE or vapour cloud explosion etc).

The primary intent of the DOSG study was to equate the damage observed at Buncefield to an estimated quantity of High Explosives. The scope of the Weidlinger task, however, was wider than this in that it aimed to try to determine what blast loadings could lead to the damage observed, especially the specific and characteristic difference observed between the upper 'strong' and 'weak' panels of the Northgate building. It is possible to do this because there are two key drivers that describe a blast load, peak pressure and impulse. A blast load is effectively pressure applied over a given period of time, if plotted this is termed the pressure-time history. In HE detonations the detonation shock front results in an initial, almost instantaneous pressure rise, therefore rapidly reaching a high peak-pressure. The decay back to ambient is typically slower and can involve a late phase which is below ambient pressure, the negative phase. However, not all explosions are detonations and depending upon the violence of the event and initial conditions, explosive loading can take the form of a very wide range of pressure-time histories. Damage is driven by a combination of the rate of initial pressure rise/magnitude of the peak pressure and also the total area under the pressure-time history graph, the impulse. The two extremes of load can be visualised as i) a very short duration but very intense shock driven pressure or ii) a long duration but typically lower pressure applied to structures for a significant period of time. Figure F.2 shows the unit load curves that could be expected for a vapour cloud explosion and a detonation.

It is possible for different combinations of peak pressure and impulse loadings to generate the same degree of damage but through different failure mechanisms or order of timings for mechanisms. This is termed Iso-damage and can be plotted as Iso-damage curves.

The Weidlinger work [E] first involved an engineering hand calculation to estimate the strength of the panels when resisting a statically applied uniform pressure on the external surface of the

panels. Assuming that the panels were undamaged/not cracked before the explosion, the uniform pressure required to crack the centre of the RC panel was approximately 13 kPa. This was valid for both the 'strong' and 'weak' panels. Once the concrete has failed, all the tension in the back of the panel would be carried by the reinforcing steel. Assuming mild steel was used, the reinforcing would yield at an applied pressure of 5.0 kPa for the 'weak' panel and 9.0 kPa for the 'strong' panel. These values are less than the pressure required to fail the concrete suggesting that the failure would be sudden but ductile under a constantly uniformly applied pressure loading.

The main part of the work conducted by Weidlinger, however, was conducted using structural analysis software called FLEX. FLEX is a non-linear explicit finite element code developed and used by Weidlinger to specifically address high severity loadings on military facilities and structures. Weidlinger have been working in partnership with the MoD for several years to develop advanced ways of simulating the response of structures to HE events.

The first sub task was to create a numerical representation of the 'weak' panel and to expose that to a loading generated by a charge of 100 te of TNT at 100 m stand-off. The details of the RC cladding panel model and assumptions are described in detail in Reference D. The panel was found to fail by cracking of the concrete at the midspan. The failure was said to be purely flexural failure and not shear failure at the supports or combined shear/flexural failure. This indicates a relatively long duration loading (longer than 70 ms). Figure F.3 shows three images taken from the model showing the failed panel.

Observation - The observed damage to the building requires flexural failure of the cladding. The modelling shows that very large HE explosions at the correct distance can give sufficiently long duration positive phases to result in flexural only type damage.

Step 2 of the work was then to evaluate the behaviour of the modelled panel to a variety of load pressure-time histories. It was not practical to re-run the high fidelity analysis as was conducted in Step 1 so an alternative approach was used using a coarser model taking advantage of the symmetry of the structure, the symmetry of the failure mode and the purely flexural nature of the failure mode. A single-degree-of-freedom (SDOF) methodology was applied whereby the dynamic behaviour of the structure was represented by a simple spring-mass-damper system. Having assessed and shown that the failure of the panel was flexural in nature, a pseudo-static load-deflection response of the panel could be assumed i.e. only valid for low intensity, long duration loading regime.

Instead of applying a blast load to the model a gradually ramped load is applied in order to determine a load-deflection response paying particular attention to the post-peak response. This required a displacement-controlled loading by application of a (numerically) controlled fluid filled bladder on the external face of the structure.

At this stage two FE models were created, one for each of the 'weak' and 'strong' panels. The ramped pseudo-static uniformly distributed pressure was applied to each model using the displacement-controlled method.

The results showed that the response is almost linear elastic, up to a deflection of approximately 6.5 mm at which point the back face of the concrete panel cracks. The tensile load on the back face is then immediately taken up by the reinforcing steel which immediately yields. As the steel yields it hardens up to its ultimate stress which occurs at a panel deflection of approximately 25 mm at which time the load-deflection curve plateaus.

The initial response of the 'weak' and 'strong' panels is similar but the plateau for the 'strong' panel is approximately 25% higher than that for the 'weak' panel.

Step 3 was to investigate four basic forms of loading to the panels. Given that different types of explosive event (e.g. vapour cloud deflagration versus HE detonation) could yield significantly different loading pressure-time histories (Figure F.2) it was felt that by determining which type of loading or equivalent magnitudes of respective loadings could generate the panel failure observed may assist in identifying the nature of the Buncefield explosion event. The loadings were forms representing i) a vapour cloud or gas explosion (finite rise time, a smooth peak and long venting dependent decay) ii) an idealised HE detonation (triangular load with zero rise time and linear decay), iii) a deflagration followed by detonation as the flame front reaches the Northgate building (long duration, low intensity load transitioning to a sharp pressure spike at the end of the loading) and iv) a partial detonation early on followed by an ongoing deflagration (initial sharp spike followed by a long duration, low intensity loading).

From these cases it was then possible to generate pressure-impulse diagrams and iso-damage curves. A total of 160000 loadcases were analysed. Each of the four load curves was scaled to give a range of peak-pressure/total-impulse combinations. The range of pressures considered was from 0 – 50 kPa. The range of impulse considered was 0 – 50 kPa.s. The parameter space was discretised on a grid of 200 pressures by 200 impulses to give a total of 40000 combinations.

Each of these scaled load curves was used as an input loading for each or the two panel types. The final permanent deflection was recorded. A contour plot of permanent deflection versus pressure and impulse was generated. By extracting discrete contours from each plot at specific deformation levels iso-damage curves were created. Figure F.4, Figure F.5 and Figure F.6 show key examples of the results of the iso-damage curves.

Once the iso-damage curves had been generated it was possible to compare directly the response of the observed and predicted responses of the two panels to each load type.

If it could be shown that the iso-damage curve representing a 200 mm permanent deflection of the 'weak' panel (its final observed state) actually crossed the iso-damage curve for minimal damage (assumed to be 30 mm deflection) to the 'strong' panel, the point at which the two curves crossed would represent an actual load curve which could produce the as-observed damage to the building.

Of the four assumed load types, the only one which produces crossing iso-damage curves is the assumed vapour cloud explosion load curve. The feature that causes these curves to cross is the curvature of the onset-of-damage curve along the pressure asymptote. Without this feature the iso-damage curves do not cross. It is due to the finite rise time associated with a vapour cloud explosion where there is no high-order detonation. Figure F.7 shows the only load curve which has been found to cause the observed structural response.

Observation - This means that the damage observed to the panels on the Northgate building must have been caused by loading consistent with a large scale deflagration of a vapour cloud without significant high-order detonation effects.

It is also interesting that the pressure asymptotes range from 14-18 kPa for both the 'weak' and 'strong' panels, a relatively specific range of pressures and the impulse asymptotes range from 1-4 kPa.s for the 'weak' panel and 2-10 kPa.s for the 'strong' panel, a relatively wide range. This means that the damage caused is very sensitive to the magnitude of peak pressure but much less sensitive to the magnitude of the impulse.

This primary conclusions of this work are that;

- The responses of the RC cladding panels used on the Northgate building are sensitive to the magnitude of the peak applied pressure and relatively insensitive to the applied impulse within the regimes considered.

- Pressure load curves which include relatively short duration, high intensity pressure spikes are unlikely to produce the different responses of the 'weak' and 'strong' RC panels. The difference in the response of the 'weak' and 'strong' panels tends to discount the possibility that there were high-order detonation effects, of a scale large enough to affect the whole of the Northgate building façade, in the Buncefield explosion.

- It was shown that a smooth blast loading curve wit a finite rise time and exponential decay, with the rise time being 30% of the overall duration and the decay being 70% of the duration, with a peak pressure of 15 to 20 kPa would produce the actual structural response observed.

F.3. REFERENCES

A - JSP 482 – MOD Explosives Regulations – Chapter 10 Quantity Distances and Licensing Criteria.

B - Explosion and Fire at the Buncefield Oil Storage and Transfer Depot, Hemel Hempstead, on 11 December 2005 – Blast Damage Assessment Report No EC/06/69, Draft 1, HSL, dated 2006.
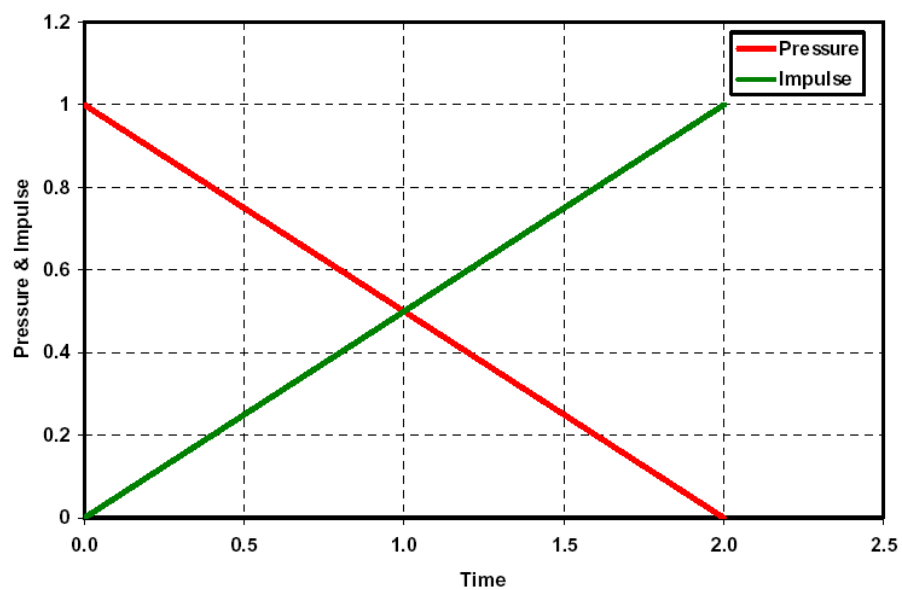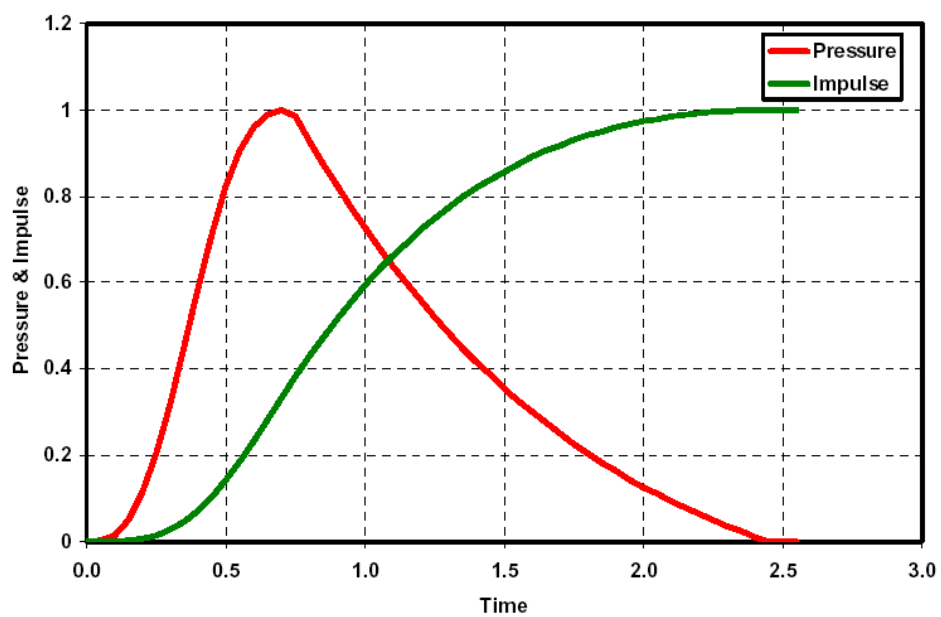
C – C N Kingery, G Bulmash, Air Blast Parameters from TNT spherical air burst and hemispherical surface burst; US Army Armament Research and Development Centre Ballistic Research Laboratory, 1984.

D – RO Building, Buncefield – Blast Damage Assessment, Letter from TPS Consultants to MoD Technical Advisor (Specialist Structures), dated 18 December 2008.

E – Characterising the Response of Reinforced Concrete Cladding Panels to Vapour Cloud Explosions – Wiedlinger Associates Ltd, Issue 1, DESO7021_090225_ V2.0, 4 June 2009.

Fircones
10.5kPa

Cottage
11.5kPa

Fuji Bld
23kPa

Warehouses
8kPa

Northgate
25kPa

Avica
7kPa

RO Bld
12kPa

RO Utilities Bld
30kPa

Control Room
9kPa

Warehouse
6kPa

Housing
<5kPa

912

=7500 kg TNT

252m
234m
144m
324m
135m
234m
125m
270m
414m
360m
460m
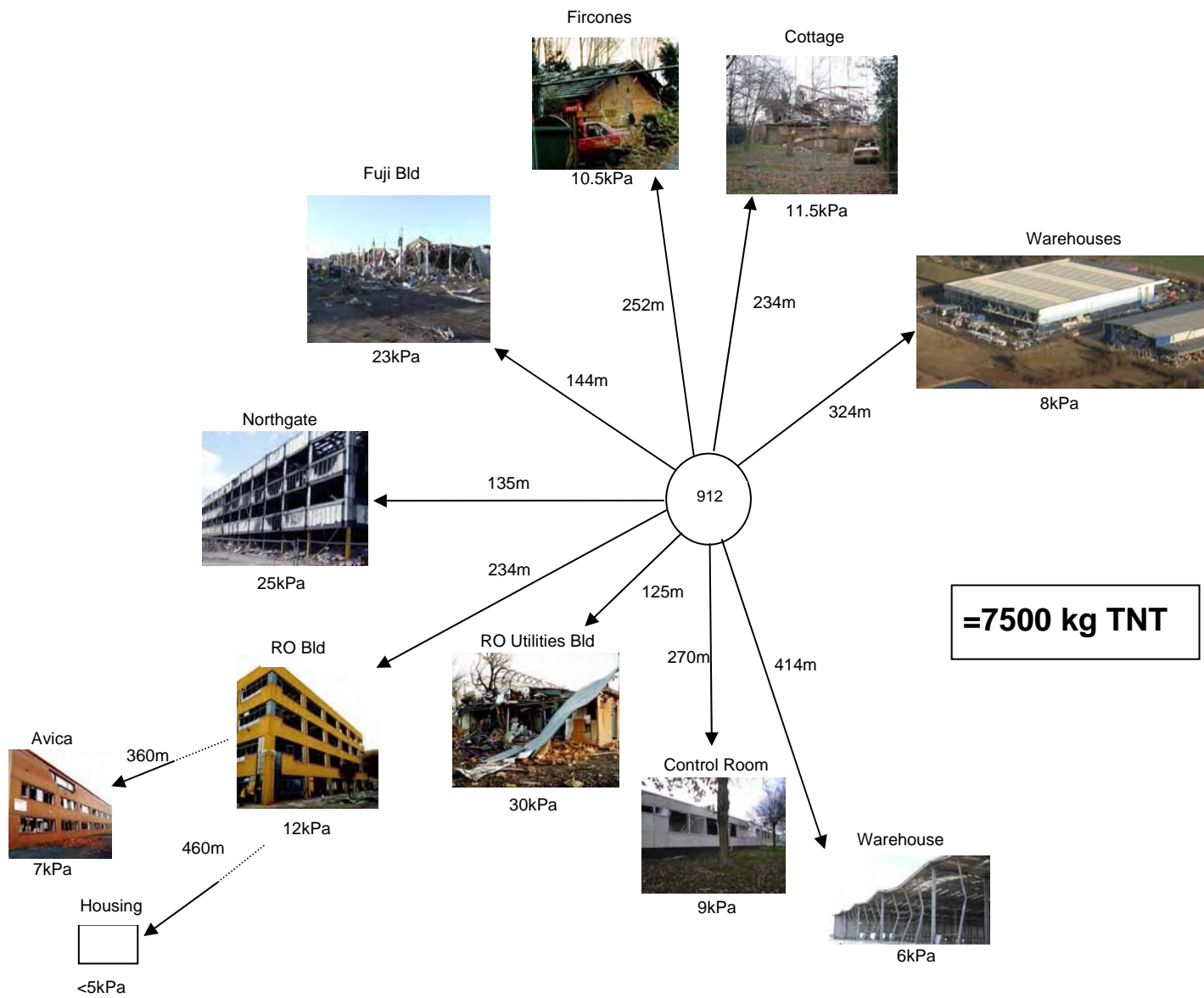
**Figure F.1** Buncefield Explosion Damage Pressure-Distance Relationships

Figure F.2 Unit Load Curves for a vapour cloud explosion (top) and a detonation (bottom)
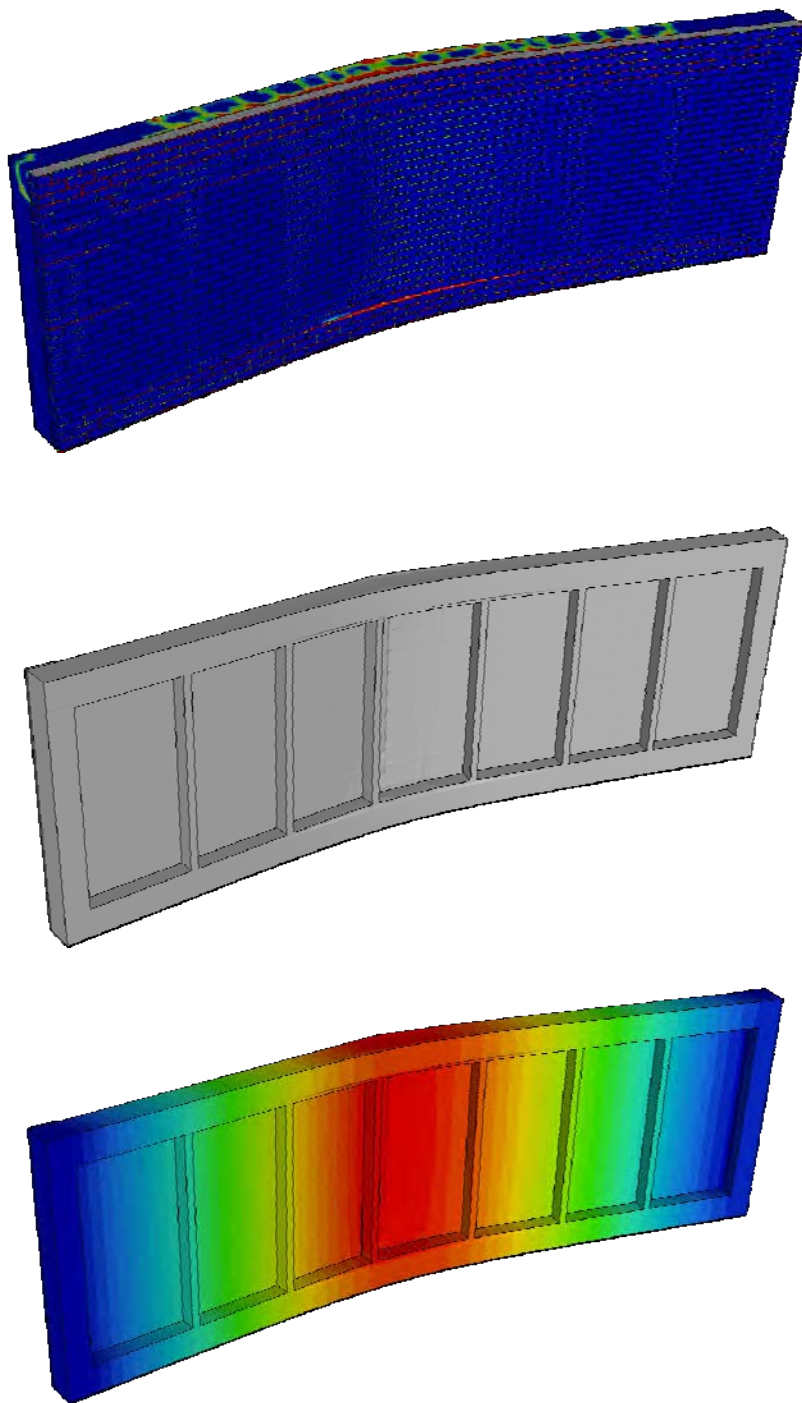
Figure F.3 Images from the FLEX Finite Element model, fine discretisation, showing the failure of the 'weak' RC Cladding Panel for a 100 te TNT detonation at 100 m stand-off
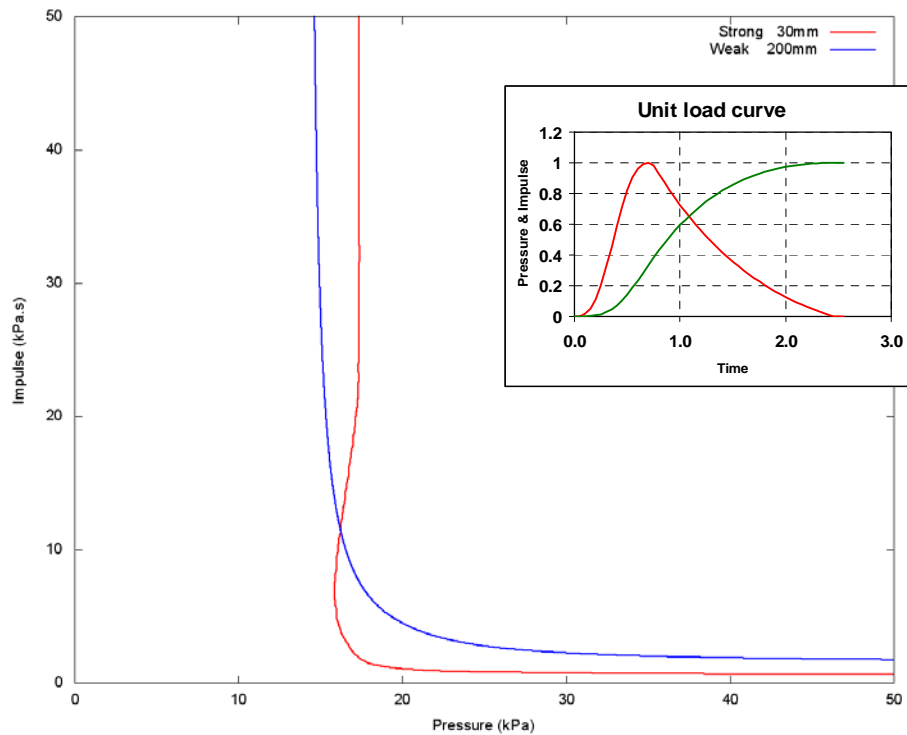
Figure F.4 Iso-damage curves predicted by SDOF model, applied loading as idealised vapour/dust explosion form (Assumed Blast Load A), showing onset of failure for strong panel and 200 mm permanent deflection for weak panel.
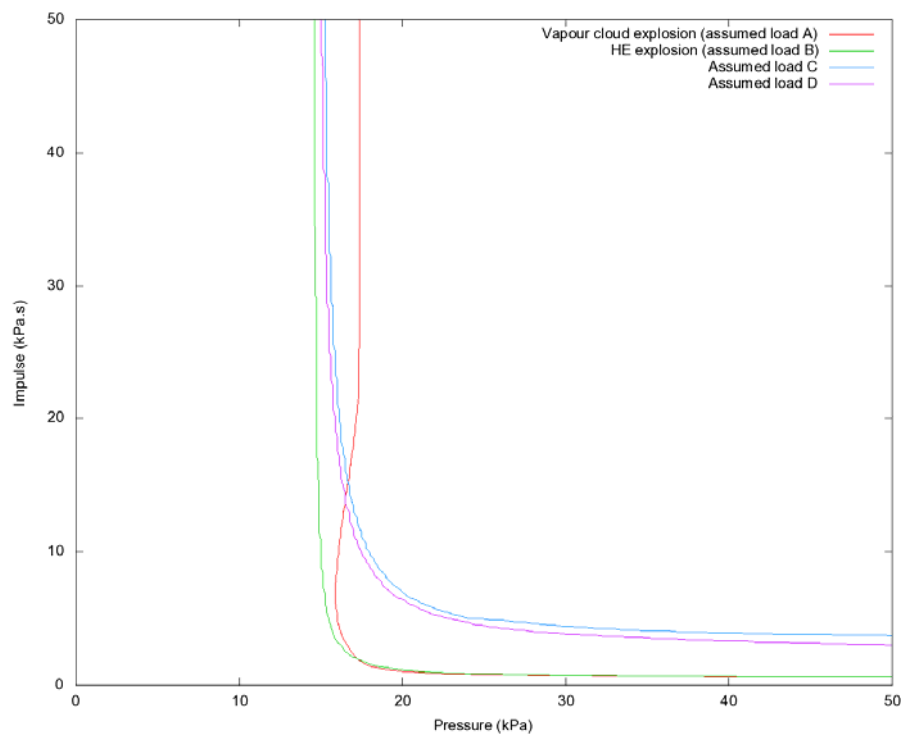
Figure F.5 Iso-damage curves predicted by SDOF model, applied loading as Assumed Blast Loads A to D, showing onset of failure for strong panel.
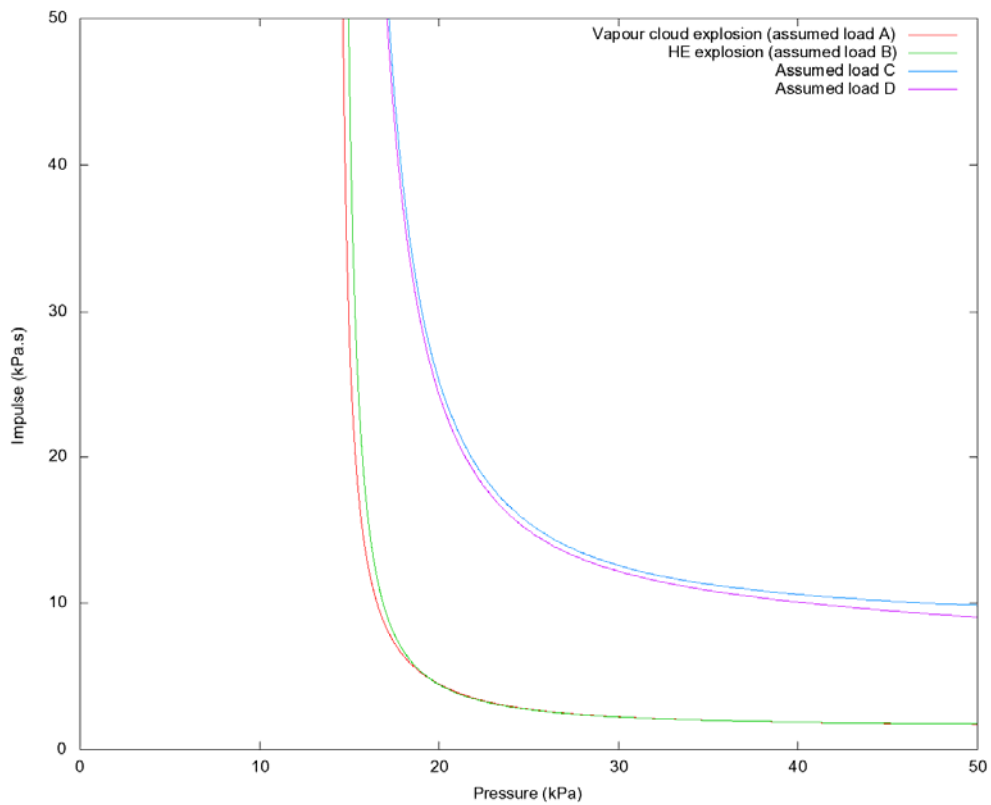
Figure F.6 Iso-damage curves predicted by SDOF model, applied loading as Assumed Blast Loads A to D, showing 200 mm deflection for weak panel.
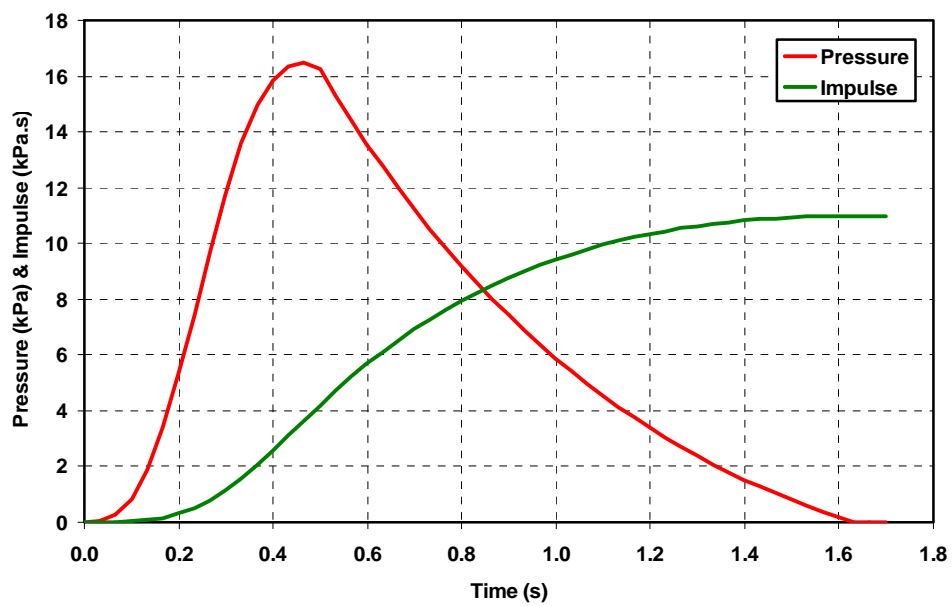
Figure F.7 The only load curve which has been found to cause the observed structural response.

APPENDIX G   REVIEW OF PREVIOUS SIMILAR ACCIDENTS

G.1.   INTRODUCTION

The purpose of this work is not to comprehensively review of all previous VCEs. A wider survey can be found in References 9.

Instead the review has focussed on 9 previous significant incidents for which detailed data is available. It is potentially significant in studying the Buncefield mechanism whether the key features of the explosion have been reported previously and in what circumstances.

The incidents examined are listed in Table G.1:

Table G.1 Incidents reviewed

	Date	Type of fuel/release
Buncefield	2005	Petrol - Tank overfill
Flixborough	1974	Cyclohexane – Process leak
Port Hudson	1970	Propane – Pipeline failure
Ufa	1989	LPG - Pipeline failure
Naples	1985	Petrol - Tank overfill
Saint Herblain	1991	Petrol - Process leak
Newark (NJ)	1983	Petrol - Tank overfill
Beek	1975	Propylene- Process leak
Texas City	2005	C5-C7 Process leak
Brenham	1992	C2-C4 Cavern overfill

The incidents are a mixture of overfills (4), pipeline failures (2) and process leaks (4).

Relevant details about the incidents are tabulated at the end of this appendix – under the following headings

Location/Date
Flammable substance
Release details (rate/time/total)
Circumstances of release
Extent of flammable cloud
Terrain
Location of ignition/explosion sequence
Directional evidence
Overpressure evidence

G.2.   DATA QUALITY

The quality of data that is available in these areas for the various incidents is very variable. In some cases there is considerable uncertainty in rate and/or duration of the loss of containment.

In others the extent of the flammable cloud was not fully established during investigation – generally because evidence of charring and sooting during the VCE was obliterated by subsequent spreading pool fires.

In all cases evidence has been reported that gives some idea of overpressures both inside and outside the cloud.

In about half the cases data on explosion directional indicators was reported i.e. the direction that posts, trees etc were broken by the blast. This provides a particularly clear basis on which to categorise explosions.

The assessment of the quality of data uncovered is unavoidably a subjective matter but a summary is given in Table G.3. The criteria on which the judgements have been made are given in Table G.2.

Table G.2 : Criteria used to judge quality of evidence available on VCEs:

	Excellent ➡	Poor
Extent of burning in cloud	Detailed evidence on extent of burned/scorched areas gathered during primary investigation. VCE and fire damage clearly distinguished. Good evidence on cloud depth.	Modelling of vapour flow (long after the incident) based on limited weather and release data. VCE footprint obliterated by subsequent fires
Overpressures in and around cloud	Multiple and varied examples of objects susceptible to overpressure e.g. light weight ductile enclosures. Good coverage of cloud. Interpretation supported by experiment.	Small number of generic indicators
Evidence on ignition, sequence and timings	CCTV Multiple, reliable indicators of ignition location and explosion sequence. Numerous, favourably-positioned witnesses: interviewed immediately.	No witnesses. Multiple possible ignitions sites
Directional evidence (on drag forces)	Multiple and varied examples of objects susceptible to drag e.g. lamp posts. High level of consistency.	No information recorded or accessible

Table G.3 Outcome of assessment of the quality of evidence available on VCEs:

		Excellent
		Good
		Moderate
		Poor

	Extent of burning in cloud	Overpressures in and around cloud	Evidence on ignition, sequence and timings	Directional evidence (on drag forces)
Buncefield	E	E	E	E
Flixborough	G	G	M	E
Port Hudson	E	M	M	E
Ufa	E	M	P	E
Naples	P	M	P	P
Saint Herblain	P	M	P	P
Newark (NJ)	P	M	P	P
Beek	G	M	P	M
Texas City	E	G	M	E
Brenham		M	M	P

G.3. RELEASE AND CLOUD VARIABLES

The incidents can be grouped in a number of useful ways (based on the circumstances that led to the explosion):

Type of substance

Terrain/congestion

Extent of flammable cloud

Duration of release

G.4. EXPLOSION CHARACTER

The incidents can also be grouped into those that:

Definitely resemble Buncefield in character

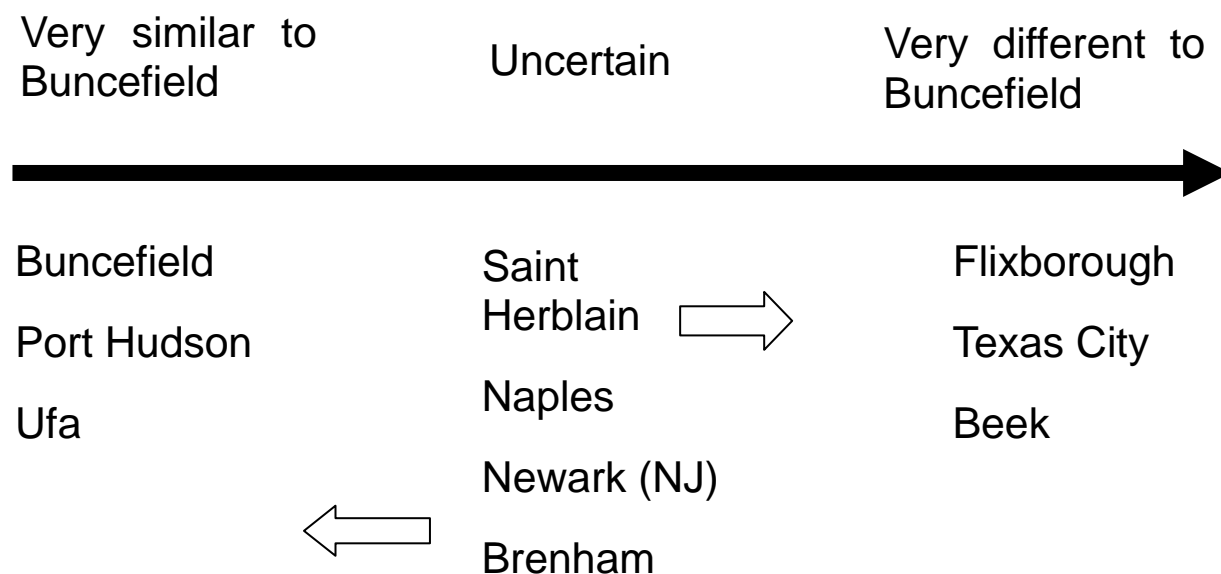Those that definitely do not resemble Buncefield in character

Those for which data are inconclusive.

The criteria used to make this judgement are derived from the observed explosion characterisitics and are shown in Table G.4 below:

Table G.4 Criteria used to determine the degree of similarity with Buncefield

Very similar to Buncefield	Very different
High overpressure over full extent of cloud	High overpressures in small (possibly congested) areas
Net impulse to posts, trees etc directed inwards (opposite to the direction of explosion propagation)	Net impulse to standing objects directed away from one or more areas of high overpressure/congestion.

The results of this grouping are shown below – detailed justification is provided in the data at the end of the Appendix and in the associated references

| Very similar to Buncefield | Uncertain | Very different to Buncefield |

Buncefield	Saint Herblain ⇨	Flixborough
Port Hudson	Naples	Texas City
Ufa	Newark (NJ)	Beek
	⇦ Brenham	

Figure G.1 Degree of similarity between incidents and Buncefield

The directional evidence from Port Hudson and Ufa clearly identifies them Buncefield–like incidents. Conversely Flixborough, Texas City and Beek definitely were not Buncefiled-like. There is insufficient evidence to be sure about the remaining incidents. The balance of non-directional evidence suggests that Port Herblain probably was not a Buncefield–like incident whereas Newark (NJ) and Brenham probably were.

G.5. CORRELATIONS BETWEEN RELEASE VARIABLES AND EXPLOSION TYPE

It is of interest to consider the correlations between these sets of inputs and outputs.

G.5.1. Fuel Type

The first variable is fuel type – See 0. There is too little data to make a detailed analysis but it is very clear that Buncefield type incidents are not exclusively associated with petrol or higher MW hydrocarbons generally.

This suggests that mechanistic analysis should focus attention on the physical circumstances of the cloud and terrain rather than the detailed composition of the fuel at Buncefield.
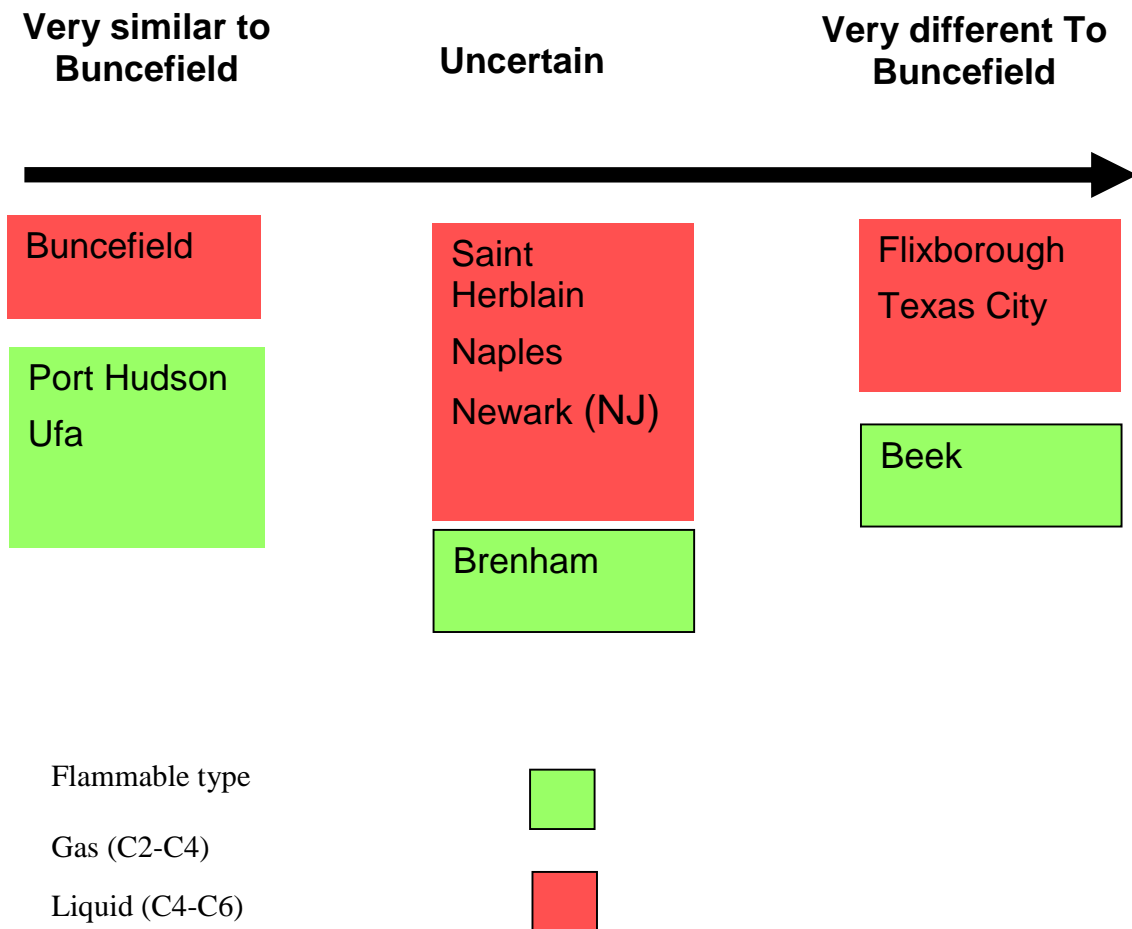
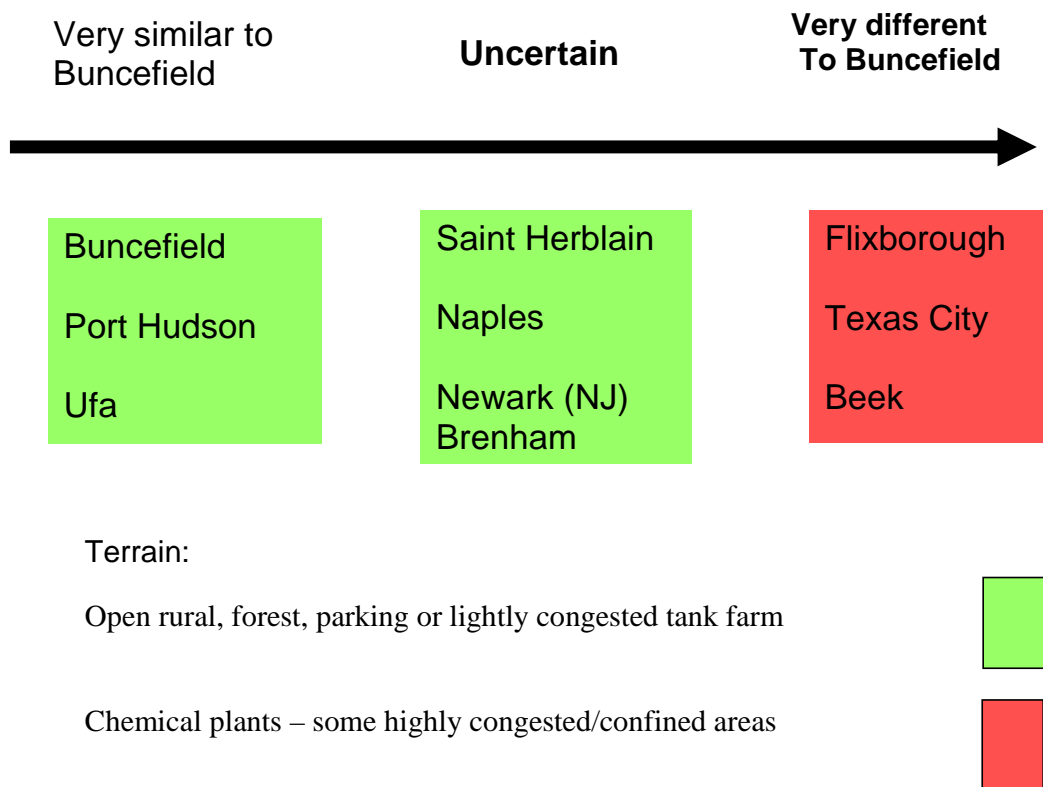**Figure G.2** Correlation of explosion type with flammable type

G.5.2. Terrain

There is a clear correlation between the type of terrain and the character of the explosion – Figure G.3. The explosions where high pressures are associated with high levels of confinement and congestion have all been at chemical plants – which is to be expected.

It appears that there is some other mechanism by which a severe explosion can propagate in other types of terrain. The three incidents at Buncefield, Port Hudson and Ufa cover a wide range of terrain types:

> Dense forest
> Sparse forest
> Arable land
> Tarmac parking
> Rough grassland
> Hedging/roads
> Tank farm

At Buncefield, in particular, it was possible to show that the severity of the explosion was maintained over at least the last four types of terrain.

Very similar to Buncefield | Uncertain | Very different To Buncefield

Buncefield	Saint Herblain	Flixborough
Port Hudson	Naples	Texas City
Ufa	Newark (NJ) Brenham	Beek

Terrain:

Open rural, forest, parking or lightly congested tank farm

Chemical plants – some highly congested/confined areas

Figure G.3

It is likely that an appropriately pre-mixed explosion in a heavily confined and congested area would always generate a VCE. This conclusion is supported by a considerable weight of experimental evidence.

On the other hand it is worth noting that there are examples of large ignited vapour clouds that produced large flash fires rather than VCEs. The incident at Donnellson [10] appears to have been one example. In this case the cloud covered 30-40 acres of woodland, a similar amount of farmland (cornfields) and a highway. The report on the incident makes no reference to overpressure damage, window breakage or any witness evidence of blast.

The circumstances of the leak, duration, cloud size and the terrain were rather similar to the Port Hudson but it seems there was no significant blast. It seems that whatever mechanism operated at Port Hudson did not apply at all in Donnellson.

This seriously challenges a hypothesis that ascribed the high overpressures at Port Hudson, Buncefield and Ufa to flame acceleration in dense vegetation. If this were the case why was flame acceleration not observed at Donnellson? It seems unreasonable to suppose that the most densely congested wooded areas at Donnellson were less efficient at driving flame acceleration than all of the open areas under the vapour clouds at Buncefield, Port Hudson and Ufa.

One potential difference between Donnellson and Port Hudson was the source and location of ignition. There is good evidence that the initial explosion at Port Hudson occurred in a storage building made from concrete blocks. The initial explosion would have been (weakly) confined,
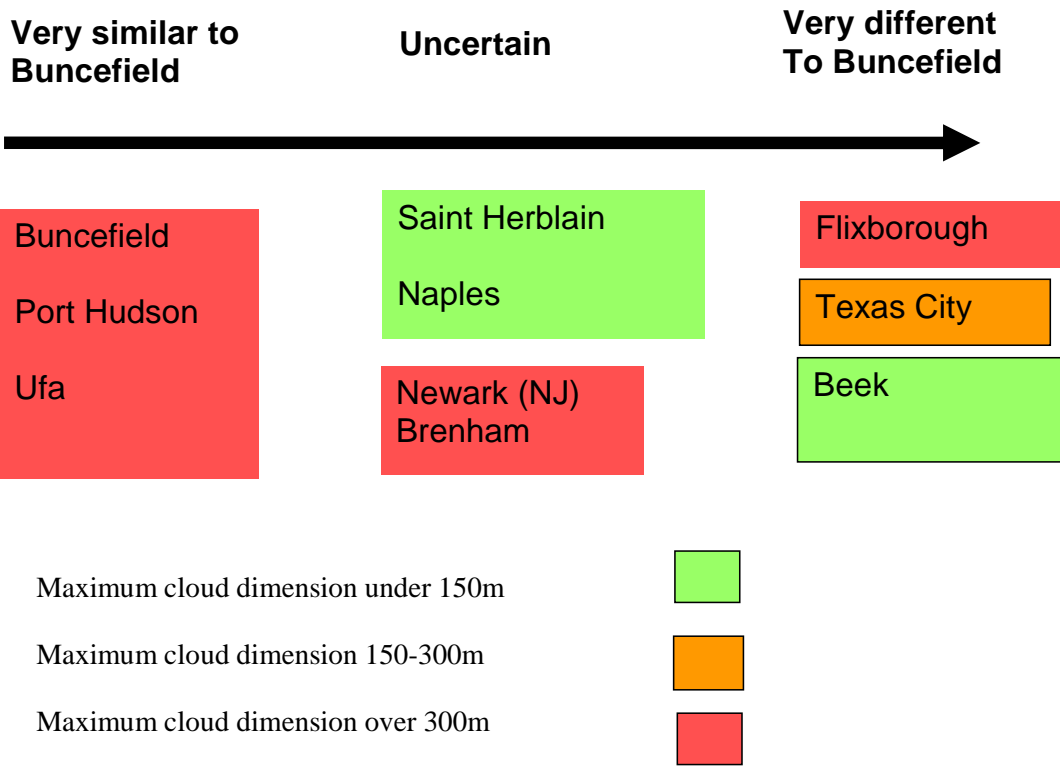
with a corresponding increase in the pressure. The original investigation report for the Port Hudson incident identified this as a potential mechanism of triggering detonation. No detailed evidence is available on the ignition at Donnellson.

On the other hand the Buncefield explosion started in a confined pump house with some congestion but this definitely did not lead to immediate detonation. Instead the only mechanism that could have led to detonation at Buncefield was flame acceleration in a hedgerow.

Without more detailed information about the vegetation at the various sites it is impossible to develop the analysis further but it is clear than flames propagating in woodland do not always undergo any significant flame acceleration at all – let alone to detonation.

G.5.3. Cloud size

There is no clear correlation between cloud size and explosion type – Figure G.4. The Flixborough cloud was quite large but there is no directional evidence in the open areas of blast effects other than those that can be ascribed to the shock wave from a powerful central explosion.

Very similar to Buncefield   **Uncertain**   **Very different To Buncefield**

Buncefield Port Hudson Ufa	Saint Herblain Naples	Flixborough
	Newark (NJ) Brenham	Texas City
		Beek

Maximum cloud dimension under 150m

Maximum cloud dimension 150-300m

Maximum cloud dimension over 300m

Figure G.4

A considerable amount of evidence is available from Buncefield on the area immediately surrounding the ignition point. The length of the area where the damage to vegetation is less than the rest of the area covered by the cloud is only approximately 15 m. This suggests that a Buncefield-like event could in principle occur in a rather small cloud - although such an event would probably not be investigated as a major accident. Accumulation of a substantial thickness of vapour in a small area (at least during a tank overfill) would also require vapour flow to be constrained.

Similarly significant explosions of the non-Buncefield type could occur in relatively small, congested areas.

Since both types of explosion appear possible in small and large clouds it is not surprising that the occurrence of well-documented major explosions does not correlate with cloud size.

G.5.4. Release duration

There is a correlation between release duration and explosion type – Figure G.5. The Buncefield–like explosions all occurred following extended releases. Dispersion of the heavy vapours over the most of the area of the cloud would have been by slow gravity currents. Flow speeds would have been low with the potential for very low (or zero) entrainment rates. Substantial volumes of gas would have been created with low concentration gradients in at least two-dimensions.

By contrast the vapour flow in the process releases at Flixborough, Beek etc. would have been more dynamic and non-uniform across a high proportion of the cloud.

It is possible that a high level of homogeneity in the cloud is a prerequisite for a Buncefield type explosion.

Very similar to Buncefield	Uncertain	Very different To Buncefield
Buncefield Port Hudson Ufa	Saint Herblain Naples Newark (NJ) Brenham	Flixborough Texas City Beek

Duration :
More than 15 minutes
Less than 2 minutes
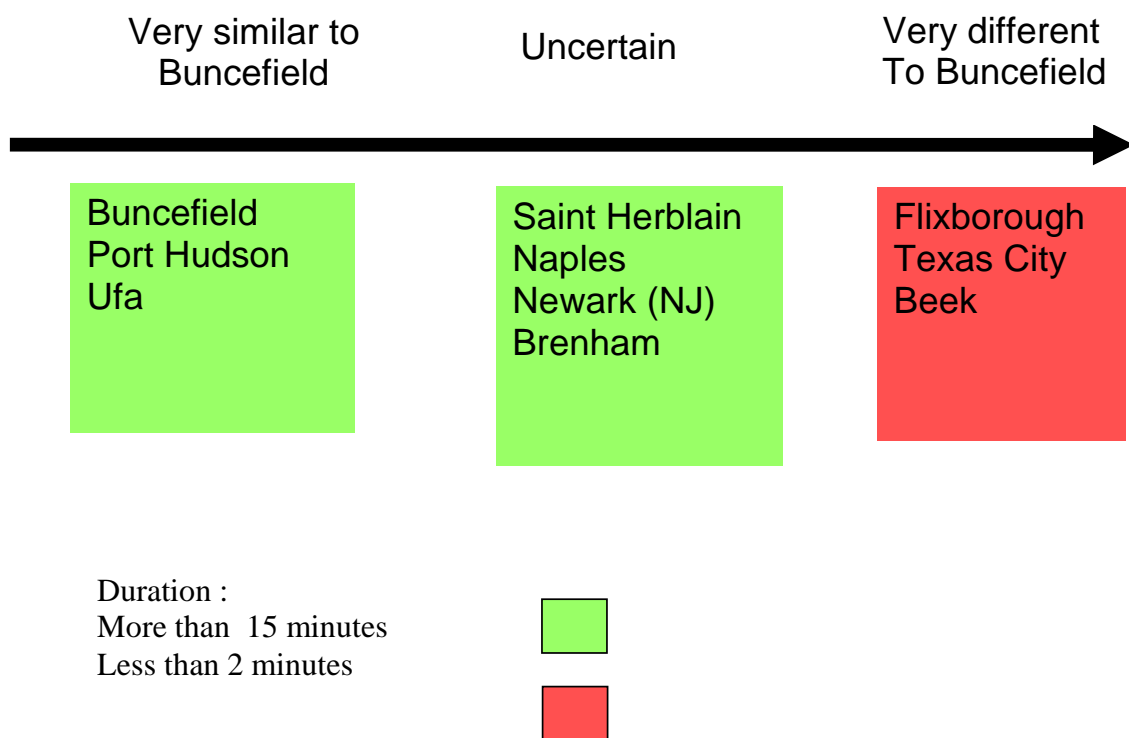
Figure G.5

G.6.   CONCLUSIONS

1. There have been a number of well-documented large VCEs that had similar characteristics to the Buncefield blast.
   - Net blast drag forces directed in the opposite direction to flame propagation
   - High overpressures over a wide area - not correlated with congestion.

2. There have been a number of well-documented large VCEs that were clearly of a different sort to the Buncefield blast.
   - Net blast drag forces directed away from one or more centres of congestion
   - High overpressures correlated with congestion.
3. The occurrence of a Buncefield-type explosion does not depend of the presence of high molecular weight hydrocarbons – there are examples with LPG.
4. The mechanism of explosion could be connected with the vegetation cover but the propagation of flame through extended areas of woodland does not necessarily generate significant overpressures.
5. Buncefield-like evens that have been reported in detail have been extended releases in which the cloud spread over a large area relatively slowly. On the other hand there is clear evidence from Buncefield that the explosion "got started" close to the point of ignition.

G.7.   INCIDENT DATA

Location/Date	Flixborough UK (1974) [11,12]
Flammable substance	Cyclohexane
Release details (rate/time/total)	Rate 2,500 - 5,000 kg/s Duration 20-40 seconds Total approx 100 tonnes
Circumstances of release	Failure of a section of 700 mm diameter temporary pipe (10 bar)
Extent of flammable cloud	Broad boomerang shape >300 m max length Likely to have been many tens of metres deep
Terrain	Heavily congested plant areas separated by open areas
Location of ignition/explosion sequence	Not definitively known
Directional evidence	Clear outward deflection of posts etc. consistent with a violent explosion centred above and point 50 m east of the release point
Overpressure evidence	Pressures at the edge of the cloud were approximately 1000 mbar declining with distance as would be expected for a TNT charge of 150-20 tonnes at an elevation of around 45 m [Ref 1]. There is disagreement about the magnitude of pressures within the cloud. Some authors have concluded that crushed tanks, drain covers etc. indicate very high pressures O(10 bar) within the cloud [Ref 2].
Discussion	The directional evidence is particularly clear and completely opposite to that at Buncefield. HSE's archive of photographs was reviewed as part of this project and a summary of the results is shown in Figure G.6. An album showing all the directional evidence on which this figure was based is available.
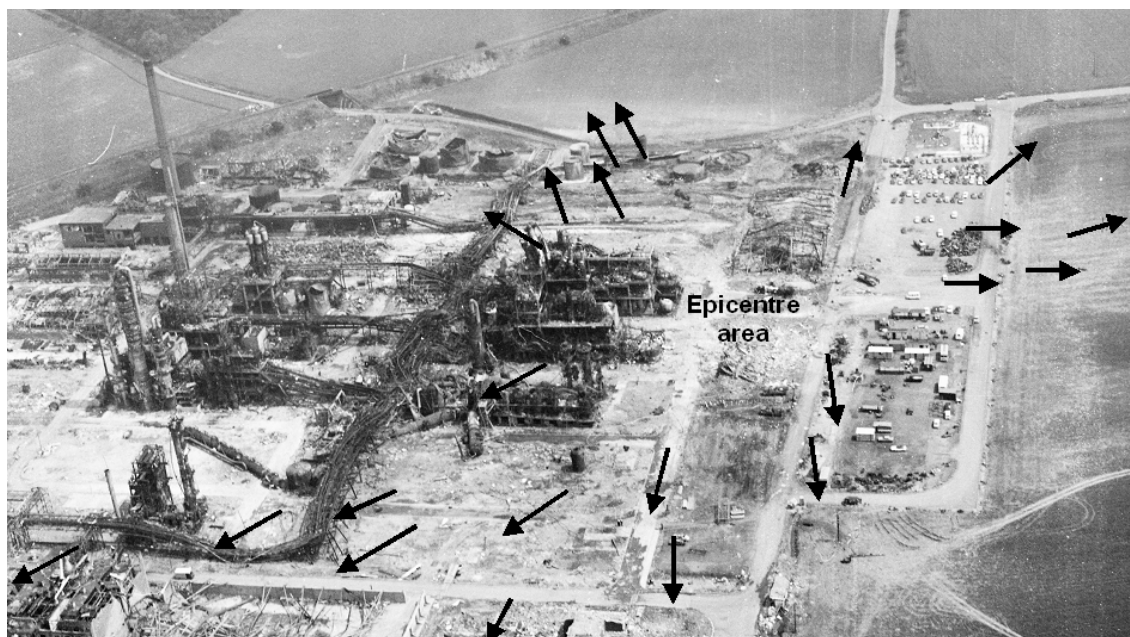
Figure G.6 Summary of direction indicators at Flixborough

Location/Date	**Port Hudson (December 1970)** (Bureau of Mines Investigation Report 7752)
Flammable substance	Propane
Release details (rate/time/total)	Rate ~80 l/s Time 24 minutes (prior to ignition) Total 120,000 litres
Circumstances of release	Pipeline failure (200 mm diam, 66 bar)
Extent of flammable cloud	See below - maximum length approx 500 m. The gas plume was made visible by water condensation – as at Buncefield.
Terrain	Gently rolling farmland and woods – rather similar to Buncefield. The accidents also occurred at the same time of year.
Location of ignition/explosion sequence	Ignition in concrete block warehouse (10 × 18 m) –similar to the ignition at Buncefield. Immediate illumination of the valley. No significant period flame propagation or acceleration observed by witnesses.

Directional evidence	All broken trees, utility poles etc. pointing towards the blast origin – on the western edge of the cloud. There were no failures in the opposite sense clearly indicating the drag forces were not caused by entrainment into the fire plume (which would have at least approximate radial symmetry). Directional damage at Port Hudson closely matched the observations at Buncefield .
Overpressure evidence	Damage to buildings, trees etc. within the cloud was severe and widespread – probably indiacting pressures of at least 1000 mbar over the area covered by the cloud. The character and distribution of damage strongly resembled that at Buncefield.
Discussion	The incident has long been assumed to have been a detonation on the basis of witness reports of the rapid burning rate in open country. The authors of the investigation report noted the difficulty in explaining the directional damage on the basis of fire-induced winds. The similarities between this incident and Buncefield are so striking that it is extremely unlikely that they could have radically different mechanisms. Much more detailed evidence is available from the Buncefield explosion – especially from CCTV records. Any conclusions about the mechanism at Buncefield will probably read across to the Port Hudson explosion.
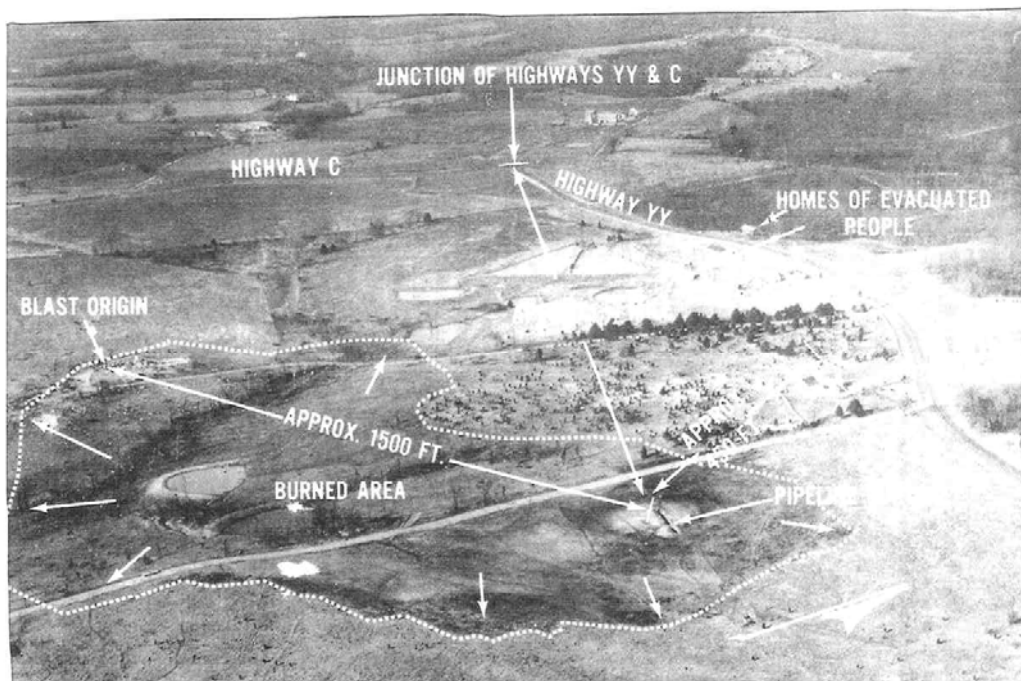
Figure G.7 The extent of the cloud in the Port Hudson Explosion

Location/Date	**Ufa – Ural Mountains (June 1989) [13]**
Flammable substance	LPG
Release details (rate/time/total)	Rate Order 1000 l/s Time approx 70 minutes (prior to ignition) Total 2000-10,000 tonnes
Circumstances of release	Pipeline failure (700 mm diameter 38 bar)
Extent of flammable cloud	2.5 km^2
Terrain	Steeply rolling woodland. Inhabitant 4-7 km away smelled hydrocarbons (presumably diluted below LFL)
Location of ignition/explosion sequence	Passing trains.
Directional evidence	Numerous trees pointing towards the blast origin.
Overpressure evidence	Trees felled over a huge area – indicating overpressures at least 1000 millibar. The only ductile damage reported was to trains - the description of damage is very reminiscent of damage to vehicles at Buncefield. " all of the 38 carriages were flattened not against each other like a pleat [as might occur in a collision] but as if they were clamped in a vice" Window broken at a range of 15 km
Discussion	The directional evidence at Ufa has been interpreted by Makhviladze [Ref 3] as a result of entrainment of air into a strong convection plume. This seems extremely unlikely to be the correct interpretation. The damage to trees clearly covers only areas where gas flow would have occurred – rather than all of those that would have been affected by entrainment into the updraft. Ref 3 shows that fairly high velocities (22 m/s) can be generated by updraft but this requires all gas to be concentrated very deep (30 m) layer near the point of release. Given the duration of the release and the steep slopes leading away from the release point this is unrealistic. In reality (as at Port Hudson and Buncefield) the gas would have been widely spread out in a relatively thin layer. Convection of burned gas would have been cellular with correspondingly weaker velocities.

		The sharp cut off in both pressure and thermal damage at the edge of the cloud (also observed at Port Hudson and Buncefield) clearly indicates that the damage was caused by blast rather than convection driven winds.
		The breaking of windows at 15 km from the site also indicates a severe blast – with the occurrence of high overpressures and correspondingly high drag forces.
		Gelfand who was part of the original investigation has another theory about what causes the characteristic inward breakage of trees [14].
		"Unusual forest fall was due to the character of the explosion. Along the edges of the disaster area the gas concentration decreased and detonated: there was an explosion. Inside the the gas cloud with practically 100% concentration there began intensive but not explosive burning"
		Again Gelfands explanation does not adequately explain the facts because of the lack of matching outward deflection of objects outside the cloud. The effect of a peripheral high intensity explosion would also not penetrate distances of up to 1 km back towards the origin of the explosion.

Location/Date	Naples (December 1985) [15]
Flammable substance	Petrol
Release details (rate/time/total)	Rate 130 kg/s Time approx 90 minutes (prior to ignition) Total 700 tonnes
Circumstances of release	Tank overfill (during ship to shore transfer) Low wind speed ~2 m/s
Extent of flammable cloud	Not reported – the subsequent tank farm fires (which lasted over a week) may have obliterated signs of original VCE. CFD modelling of cloud development has been done [Ref 4]
Terrain	Tank farm and associated plant – generally low congestion
Location of ignition/explosion sequence	Thought to be in the vicinity of a pumping station
Directional evidence	Not reported – probably largely obscured by fire damage
Overpressure evidence	A range of overpressure indicators were analysed – mostly outside the area thought to comprise the flammable cloud. Maximum indicated pressure 480 mbar. Windows broken to a range of 1 km. Seismic evidence suggested a TNT equivalence of 4.2 tonnes in the far field.
Discussion	The lack of directional evidence makes its difficult to judge whether this was the same type of event as Buncefield. Fire damage must also have made overpressures estimation problematic.

[15] Maremonti, M., Russo, G., Salzano, E. and Tufano, V. "Post accident analysis of vapour cloud explosions in fuel storage areas" Trans IChemE , Vol 77, Part B Novmeber 1999.

Location/Date	Saint Herblain (October 1991)
Flammable substance	Petrol
Release details (rate/time/total)	Rate ? Time approx 20 minutes (prior to ignition) Total ?
Circumstances of release	Leak on transfer line Low wind speed (<1 m/s)
Extent of flammable cloud	Not reported. Witness evidence suggests that the cloud volume was at least 23,000 m^3. A (water vapour) condensation aerosol made the cloud visible [Ref 5]. Cloud depth reported to be approximately 1.5 m.
Terrain	Tank farm and associated plant/ parking – generally low congestion
Location of ignition/explosion sequence	Not known
Directional evidence	Not reported.
Overpressure evidence	A range of overpressure indicators were analysed. Maximum indicated pressure 250 mbar. Windows broken to a range of 2 km.
Discussion	The lack of directional evidence makes its difficult to judge whether this was the same type of event as Buncefield. The effects of the explosion has been modelled by several methods i.e. TNT equivalence, Multi-energy method and CFD. The CFD combustion modelling suggested that high overpressures could be explained by flame acceleration in a row of closely parked tankers.

[16] Lechaudel, J.F., Mouilleau, Y. "Assessment of an accidental vapour cloud explosion" (1995) Loss Prevention and Safety Promotion in the Processs Industries ,Volume 1.

Location/Date	Newark New Jersey (January 1983)
Flammable substance	Petrol
Release details (rate/time/total)	Rate Of order 100 litres/s Time Of order 20 minutes Total 114 to 379 m^3
Circumstances of release	Tank overfill Wind very light
Extent of flammable cloud	Not known in detail. The cloud certainly travelled more than 300 m in some directions
Terrain	Tank farm, scrub land
Location of ignition/explosion sequence	Ignition thought to be at the incinerator of a drum finishing plant (300 m from the overfilled tank). Two smaller explosions were reported to have immediately preceded the main blast.
Directional evidence	Not recorded
Overpressure evidence	Flattened rail cars reported. Empty storage tanks 400-500 m distance destroyed or badly damaged. Tank trucks rolled over.
Discussion	The incident appears to have generated substantial overpressures in a lightly congested area. This matches what occurred at Buncefield, Port Hudson and Ufa but the lack of directional indicators and clear information on the extent of the cloud makes a definite conclusion impossible.

Location/Date	Beek (December 1985)
Flammable substance	Petrol
Release details (rate/time/total)	Rate order 40 kg/s Time approx 2 minutes (prior to ignition) Total approx 5 tonnes (of which 800 kg was thought to have exploded)
Circumstances of release	Process leak
Extent of flammable cloud	Extended between 30 and 90 m from source in different directions. The cloud depth was reported to have been between 3 and 3.5 m.
Terrain	Chemical works. Some highly congested plant areas
Location of ignition/explosion sequence	Ignition thought to have occurred at a cracker furnace.
Directional evidence	Not reported. Investigators "were able to show" that the focus of the blast was approximately at the centre of the cloud. But it is not clear whether this was based on directional information or variations in overpressure damage.
Overpressure evidence	A range of overpressure indicators were analysed. Maximum indicated pressure 1000 mbar (within the cloud). The most severe damage occurred where there were the highest concentrations of equipment e.g. pipe-tracks.
Discussion	The reported correlation of blast intensity with congestion is not similar to the observations at Buncefield.

Location/Date	Texas City (March 2005)
Flammable substance	Raffinate splitter hydrocarbons C5 –C7
Release details (rate/time/total)	Rate 268 l/s Time approx 107 seconds (prior to ignition) Total 28,700 litres These figures quoted in the CSB report appear inconsistent with the eyewitness observations of a full bore 6 m high geyser from the top of the 860 mm diameter stack (implies a flow rate of approx 6400 l/s).
Circumstances of release	Liquid flow from a vent stack
Extent of flammable cloud	18,600 m^2 . Maxim cloud dimension approximately 200 m. The CSB report includes an overhead photograph showing extent of blackening.
Terrain	Refinery – some areas of heavy congestion
Location of ignition/explosion sequence	Not known definitively. Could have been idling diesel truck heard racing in the cloud. However, this also occurred at Buncefield and definitely did not cause ignition.
Directional evidence	Detailed evidence presented in CSB report. Consistent with blast away from intense explosions in the most congested areas of the site. Several explosion foci. Definitely dissimilar to Buncefield.
Overpressure evidence	Overpressures of >1000 mbar within the congested regions.
Discussion	This appears to mirror the Beek incident. There was a rapid release for a short period (1.5 –2 minutes) before ignition occurred. Damage was focussed on congested areas of plant where there was enhancement of the turbulent burning velocity.

Location/Date	Brenham (April 1992) [20]
Flammable substance	Highly volatile liquids C2 –C4
Release details (rate/time/total)	Not known. Estimates from cloud size and explosive power are in the range 1000 to 10,000 barrels.
Circumstances of release	Overflow from a storage cavern
Extent of flammable cloud	~700,000 m^2 . Maxim cloud dimension approximately 1500 m.
Terrain	Open rural – with some significant gradients
Location of ignition/explosion sequence	Ignited by a car driving into the cloud. Descriptions from witnesses: "There were a series of explosions that sounded like thunder" "It was somewhat like a lightning storm" One witness reported feeling three distinct concussions.
Directional evidence	Not available
Overpressure evidence	Houses were destroyed over a mile from the edge of the cloud indicating high overpressures and a significant cloud depth. Around the gas station at the centre of the cloud buildings, fences and power lines were levelled. An overground storage tank was shifted on its concrete base.
Discussion	The severity of the damage indicates a powerful explosion. The area around the gas station appears uncongested but the extent of tree cover over the whole area covered by the cloud was not recorded.

G.8. REFERENCES

[1] Buncefield MIIB – Final Report

http://www.buncefieldinvestigation.gov.uk/reports/index.htm#final

[2] Atkinson, G.. and Gant, S., *Buncefield Investigation: Liquid flow and Vapour production* HSL Report FS/06/09

[3] Gant, S. and Atkinson, G., *Buncefield Investigation: Dispersion of the vapour cloud* HSL Report CM/06/13

[4] Atkinson, G., Blanchard, R. and Pritchard, D. *Buncefield Investigation: Likely Ignition Sources of the Flammable Vapour Cloud in and Around the Buncefield Oil Storage Depot on the 11th of December 2005.* HSL Report EC/06/66.

[5] Atkinson G., Gant S., Painter, D., Ungut A. and Shirvill,L. "Liquid dispersal and vapour production during overfilling incidents" (2008) IChemE Hazards XX Conference (UMIST).

[6] Dorofeev , S.B., Sidorov, V.P., Kusnetsov,M.S., Dvoinishnikhov,A.E., Alekseev,V.I. and Efimenko, A.A. *Airblast and heat radiation from fuel-rich mixture detonations,* Shock Waves (1996) Vol 6 pp21-28

[7] Glasstone , S and Dolan, P., (1980) The Effects of Nuclear Weapons (3rd Ed.) Castle House Publications.

[8] Tang, M.J. and Baker, Q.A. (1999) *A new set of blast curves from vapour explosion,* Process Safety Progress, Vol 18 No.3. p235-240.

[9] Lees, F.P. *Loss Prevention in the Process Industries (1996),* Pub. Butterworth-Heinemann.

[10] National Transport Safety Board Pipeline Accident Report: Donnellson, Iowa. August 4th 1978. Report No. NTSB-PAR-79-1.

[11] Sadee C., Samuels D.E., and O'Brien T.P. "The Characterisitics of the explosion of cyclohexane at the Nypro (UK) Flixborough plant on 1st June 1974."

[12] Gugan K., "Unconfined vapour cloud explosions" Institution of Chemical Engineers

[13] Makhviladze,G.M. and Yakush, S.E. "Large scale unconfined fires and explosions"

Proceedings of the Combustion Institute Volume 29, (2002) pp.195-210

[14] Gelfand, B. Private communication

[15] Maremonti, M., Russo, G., Salzano, E. and Tufano, V. "Post accident analysis of vapour cloud explosions in fuel storage areas" Trans IChemE , Vol 77, Part B Novmeber 1999.

[16] Lechaudel, J.F., Mouilleau, Y. "Assessment of an accidental vapour cloud explosion" (1995) Loss Prevention and Safety Promotion in the Processs Industries ,Volume 1.

[17] Bowen, P.J., Bull, D.C. , Prothero, A. and Rowson, J.J. *Deflagration of hydrocarbon aerosol fuels* Comb. Sci and Tech (1997), Vol 130, pp25-47.

[18] Ballal, D.R. and Lefebvre, A.H. (1981) Flame propagation in hetrogenous mixtures of fuel droplets, fuel vapour and air. 18th Symposium on Combustion. Pittsburgh: The Combustion Institute. p321-327.

[19] Lewis, B and von Elbe,G. *Combustion, Flames and Explosions of Gases, 3rd Ed (1987)* Academic Press.

[20] National Transport Safety Board Pipeline Accident Report: Brenham, Texas. April 7th 1992. Report No. NTSB-PAR-93-01.

APPENDIX H   MODELLING OF PANCAKE CLOUD DETONATIONS

H.1.   INTRODUCTION

This report provides the results of simulations of the detonation of a Propane/Air vapour cloud. Two scenarios are considered namely an open and an obstructed vapour cloud arrangement. This work was done by S.B.CARGILL AND A.M.MILNE of FLUID GRAVITY ENGINEERING LTD (FGE) under contract for the Steel Construction Institute.

FGE have been active for over 20 years in the field of modelling of explosions and detonations in condensed, multiphase and gaseous media. FGE were asked to undertake a short study to predict the consequences of a gaseous detonation (as opposed to an accelerating flame) within a geometry representative of the Buncefield cloud. FGE are not in a position to comment in detail on the likelihood of a detonation. Instead we will report the consequences of assuming a detonation to allow the review team to asses what aspects of these predictions may be consistent with the impressive array of evidence they have amassed.

Given the above constraints the agreed objective[3] for our study of the detonation scenario was to obtain solutions of the Euler equations to determine:

1. The pressure/time history of blast from an unobstructed cloud of interest (an idealised representation of the Buncefield cloud).
2. Determination of time integrated dynamic pressures within the cloud – related to net drag impulse experienced by fixed symmetric posts.
3. To determine the pressure field imposed on the face of an obstacle in the path of a detonation in a shallow cloud.

The cloud of interest for this work was stated to be a stoichiometric Propane/air mix detonated centrally. To meet the objectives two scenarios are considered, namely an open cloud and an obstructed cloud arrangement. We report the results of the required simulations below.

H.2.   SIMULATIONS

H.2.1. Modelling Methods

For the purposes of this report we assume that a full detonation of the vapour cloud occurs. To model the detonation within our hydrocode we use the Chapman-Jouget (CJ) theory. This assumes that the flow is one dimensional and the front of the detonation is a jump discontinuity with infinite reaction rate. Figure H.1 shows the typical structure of the pressure pulse assuming CJ theory in a closed tube. Here P_{CJ} represents the CJ pressure of the mixture. The pressure decays from the CJ value to a constant level. This underlying shape is always the same and is simply stretched as the detonation wave propagates.

---

[3] Atkinson, G., Jan 2009, *"Characterisation of open and obstructed pancake cloud Detonations"* , Emailed Modelling Schedule
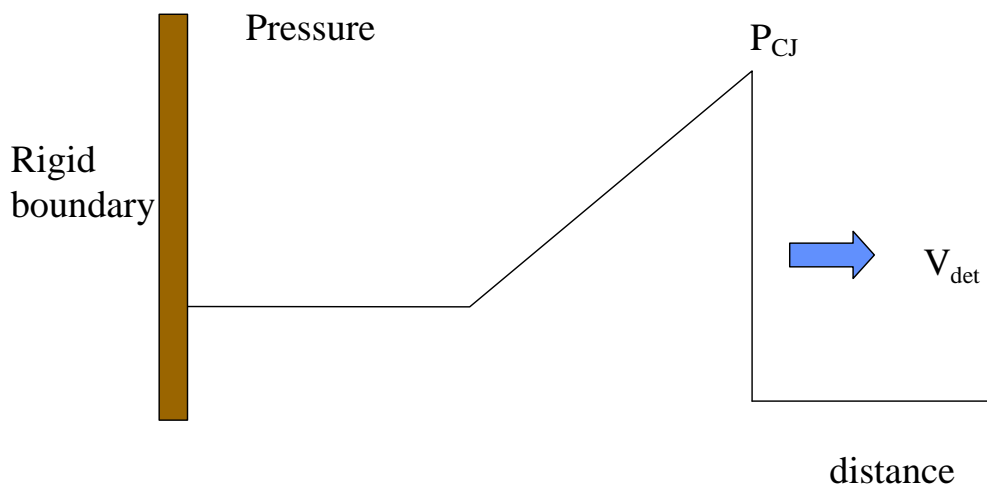
Figure H.1 Pressure-Distance Profile for a typical Detonation Propagation

Using CJ theory it is possible to calculate the detonation pressure (CJ pressure) and the detonation velocity for a known mixture. For this work we agreed to assume a stoichiometric mixture of Propane and air as being representative of a generic gaseous detonation. Using any from a selection of equilibrium chemistry thermodynamic codes[4,5] we can calculate the relevant detonation properties of the mixture.

For the Propane/Air Stoichiometric mixture it was calculated that a detonation velocity of $V_{det} = 1801$ m/s was predicted with a detonation pressure of $P_{CJ} = 17.4$ atm. Using these parameters a simple programmed burn detonation model is used within the hydrocode to simulate the detonation of the Propane/Air mixture.

The following sections discuss the results of the two simulations representing the detonation of both an open and obstructed Propane/Air detonation.

H.2.2. Scenario 1 – Open Pancake Cloud

In scenario 1 we perform a simulation of the detonation of an unobstructed propane/air stoichiometric cylindrically symmetric cloud of radius 200 m and height 3 m. Time histories of a wide range of variables are recorded at several locations within the model as described in Figure H.2. Note that recordings are taken both within the cloud itself and beyond the edge of the cloud. The detonation is assumed to be initiated at the centre of the cloud.

---

[4] Fried, L.E., 1998, *"CHEETAH 2.0"*, Lawrence Livermore National Laboratory

[5] Morley, C., *"Gaseq, Chemical equilibria in perfect gases"*
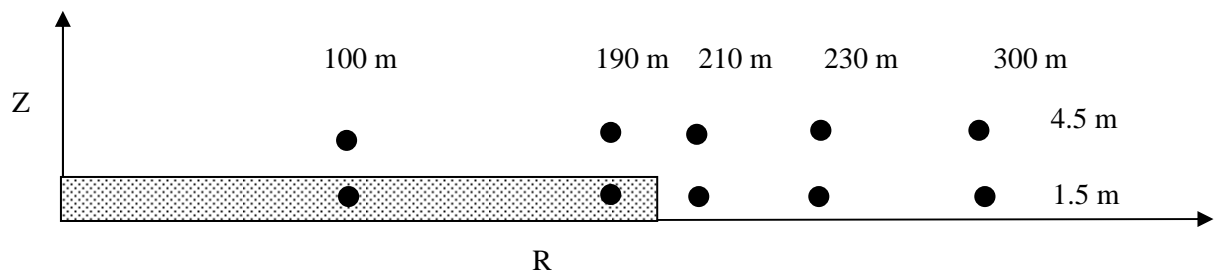
Figure H.2 Scenario 1 Arrangement

Figure H.3 shows a snapshot of the computational domain 0.05 s after detonation showing both the radial velocity and the pressure. In the pressure snapshot we see the typical detonation behaviour of the high CJ pressure at the detonation front followed by the resulting rarefaction wave. This structure results in the radial velocity becoming negative behind the shock front as the cloud recovers from the rapid expansion caused by the detonation.
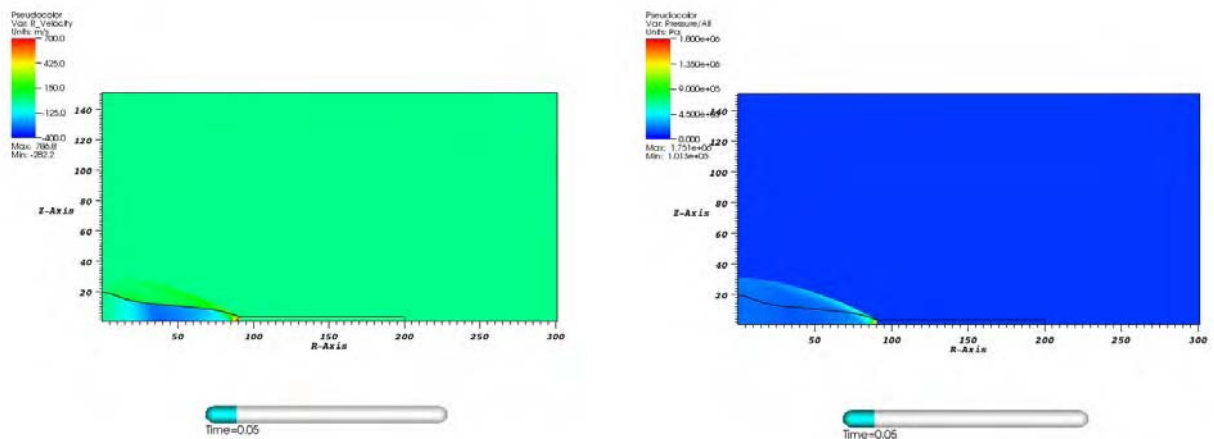
Figure H.3 Pressure and radial Velocity 0.05 s after Detonation – Scenario 1

Figure H.4 shows snapshots 0.15 s after detonation. Here we see that the detonation of the vapour cloud is now complete. The pressure wave is now shown to advance into the area surrounding the vapour cloud. Here we note that the magnitude of the pressure wave quickly diminishes as we move away from the cloud. The snapshot of radial velocity shows that large portions of the cloud still remain with a large negative velocity.
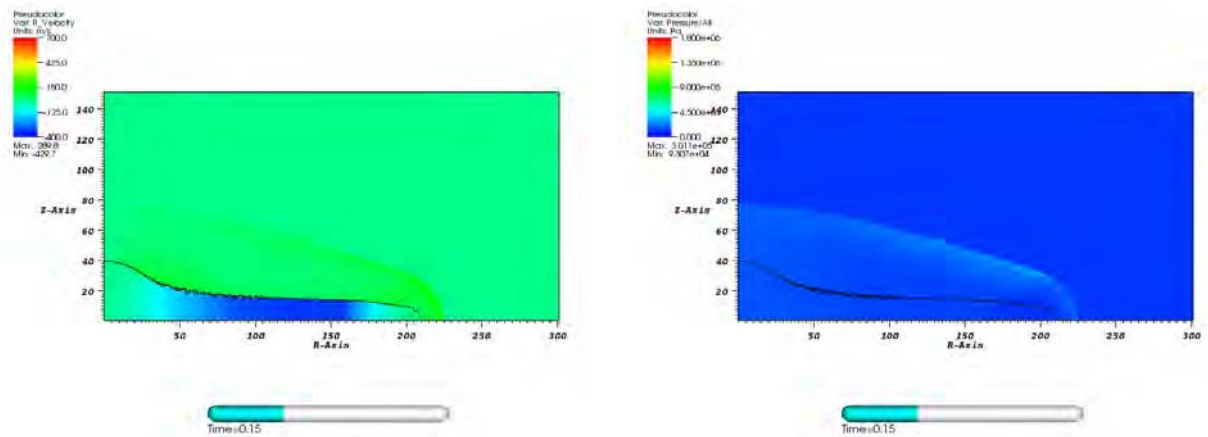
Figure H.4 Pressure and radial Velocity 0.15 s after Detonation – Scenario 1

In discussions preceding this work the customer identified the negative velocities occurring within the vapour cloud were of particular interest. To aid in the analysis Figure H.5 highlights the radial velocities at a time 0.15 s after detonation where red areas show positive radial velocity and blue areas show negative radial velocities.
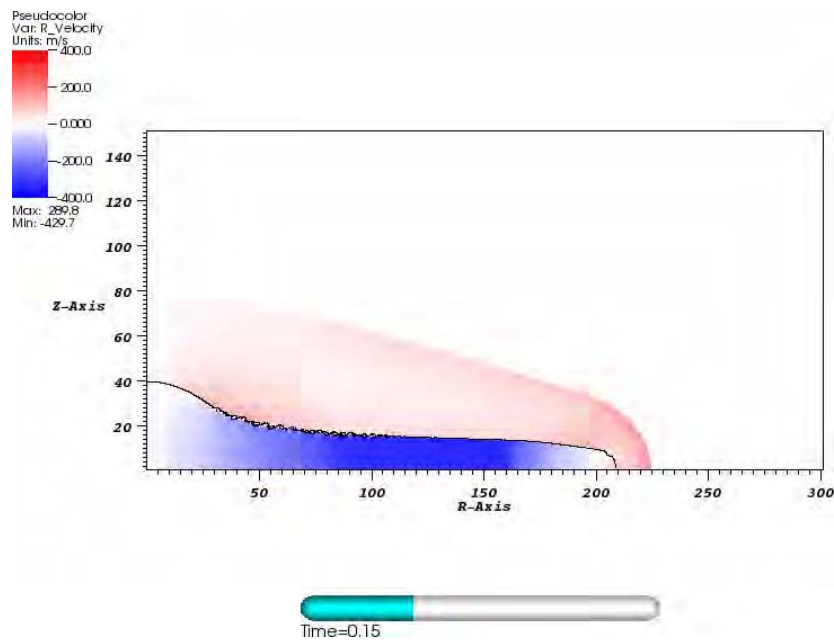
Figure H.5 Radial Velocity Direction – Scenario 1

The above figures only show results at specific times in the calculation. It is useful to also consider the evolution of the behaviour at specific points within the calculation. Figure H.6 shows the behaviour of the pressure, impulse and radial velocity at a radius of 100 m at mid height within the cloud. Here we see that at this location within the vapour cloud after a short positive velocity the cloud experiences a prolonged negative velocity phase.
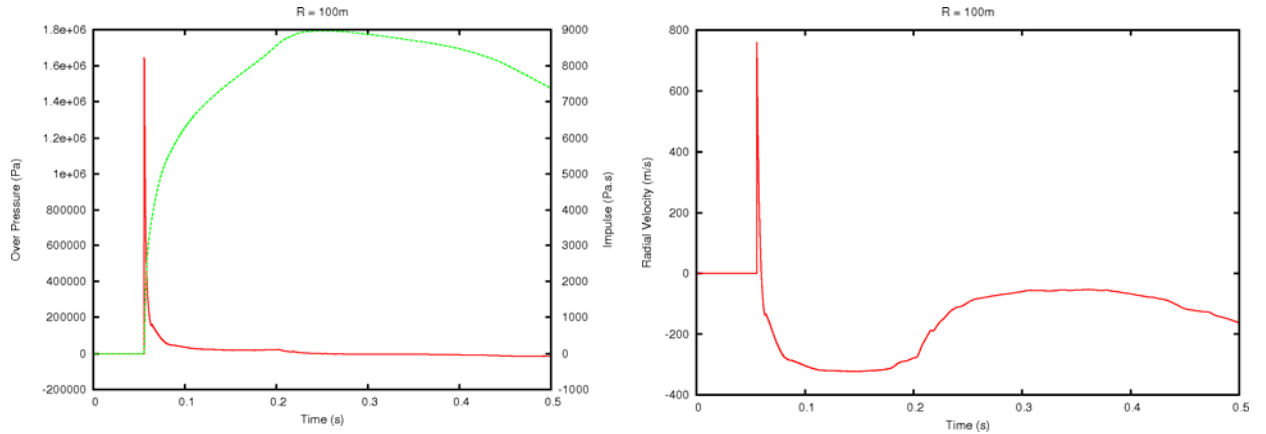
Figure H.6 Pressure/Impulse and Velocity Time Histories at a Radius of 100 m –
Scenario 1

Figure H.7 plots the same variables at a radius of 230 m which is located 30 m beyond the edge of the cloud. Here we see that both the pressure and impulse loading found here is greatly reduced from that seen within the cloud itself. Also the radial velocities at this point remain positive throughout.
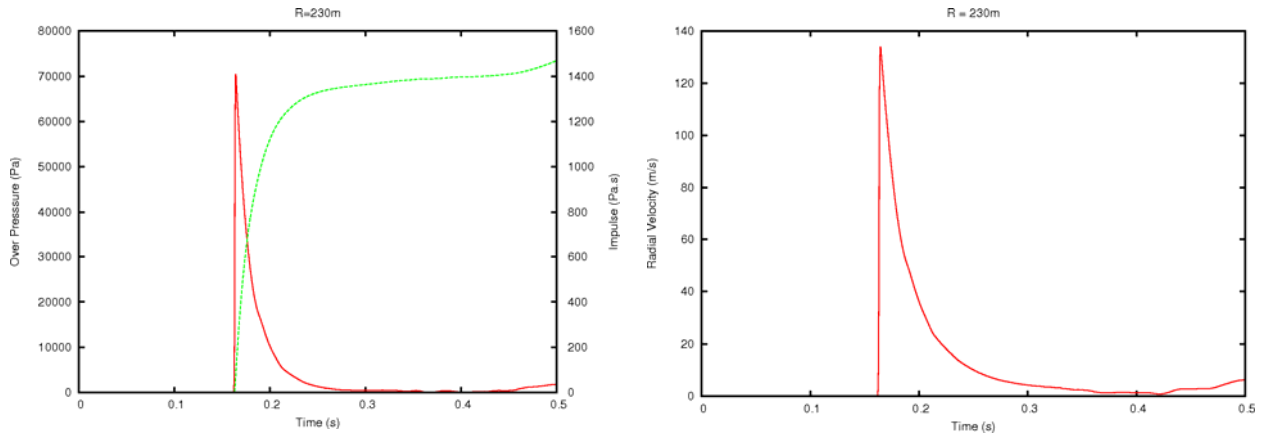
Figure H.7 Pressure and Velocity Time Histories at a Radius of 230 m – Scenario 1

The data recorded at each of the locations described in Figure H.2 are available electronically. This data is in raw text files enabling easy visualisation using any graphical plotting tool. Within the wide range of variables recorded was the dynamic pressure ($\frac{1}{2}\rho v^2$) and its integral (impulse) at each of the required locations, where ρ is the density of the gas and v its velocity. The dynamic pressure can be used to assess the deflection experienced by a small object within a fluid flow. Figure H.8 shows the dynamic pressure and impulse at a radius of 100 m. Here we see that the initial detonation produces an initial high peak dynamic pressure however the resulting cumulative impulse is influenced mainly by the long negative velocity phase as shown in Figure H.6.

163
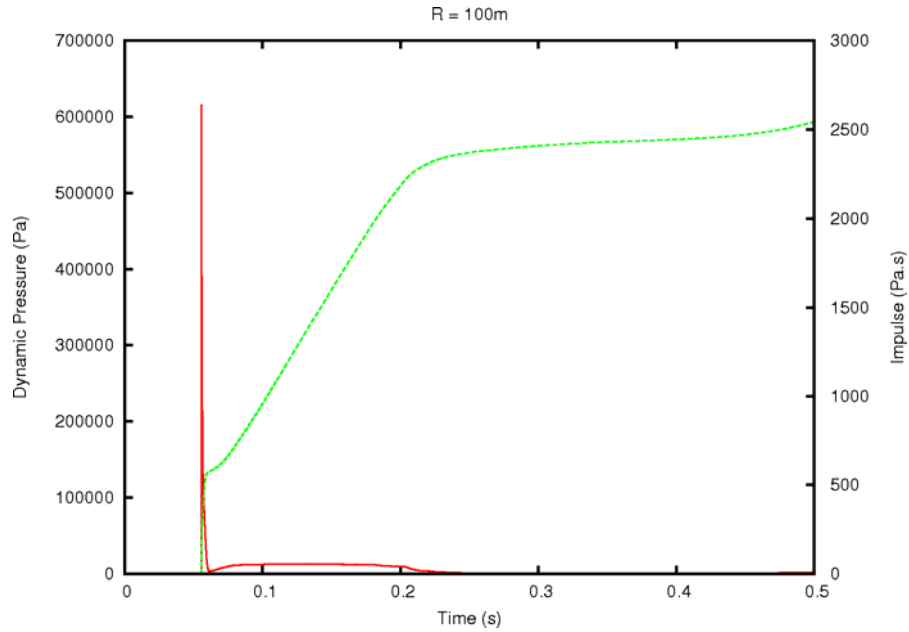
Figure H.8 Dynamic Pressure and Impulse Time Histories at a
Radius of 100 m – Scenario 1

Figure H.9 shows the corresponding plot at a radius of 230 m at a location outside the vapour
cloud.

At this location where no sustained negative velocity flows were found we see that the dynamic
pressure and impulse found are significantly lower than those found within the cloud.
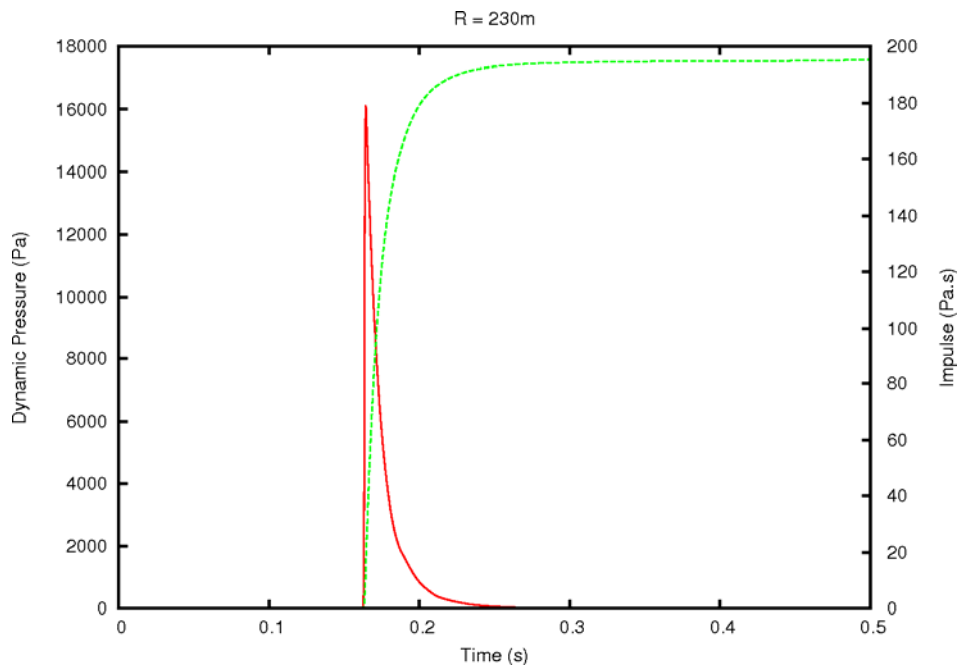
Figure H.9 Dynamic Pressure and Impulse Time Histories at a
Radius of 230 m – Scenario 1

As noted earlier the direction of the fluid flow is of particular importance to the customer. As a
result plots of a variant of the dynamic pressure were requested that take into account the

direction of the fluid flow. Here the dynamic pressure is taken to be ½ ρ(t) .U(t).│U(t)│ and the cumulative impulse as ∫½ ρ U│U│dt.

Figure H.10 shows these variables at a radius of 100 m. Here we see that the initial detonation results in a large positive dynamic pressure however it is the subsequent prolonged negative phase which dominates the cumulative impulse. At a radius of 230 m we see no difference in the dynamic pressures found since the radial velocity remains positive at this location and thus Figure H.9 shows the same result.
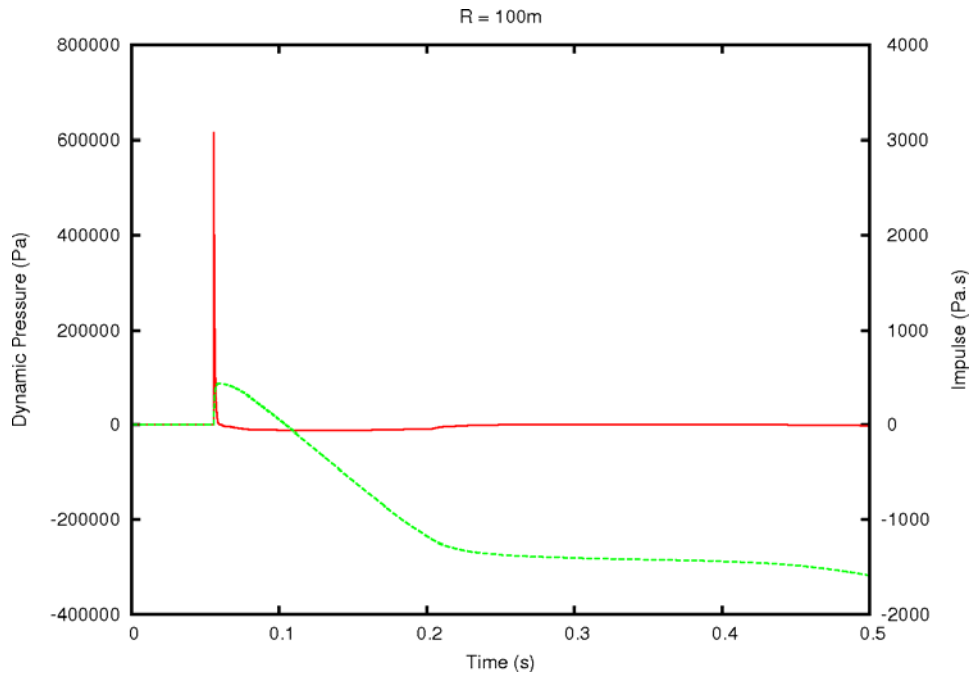
Figure H.10 Velocity Direction Dependant Dynamic Pressure and Impulse Time Histories at a Radius of 100 m – Scenario 1

For these calculations it is important to consider the effects of the vapour cloud detonation over a wide area. To do this we can plot the peak pressures found throughout the model. Figure H.11 plots contours of the peak pressures found in the model up to a time of 0.5 s after detonation. Here we see that within the vapour cloud the peak pressure found is the CJ pressure of the detonation model used. Beyond the vapour cloud however the peak pressures found in the air fall off quite dramatically. The black line shows the locations of the edge of the detonation products at 0.5 s.
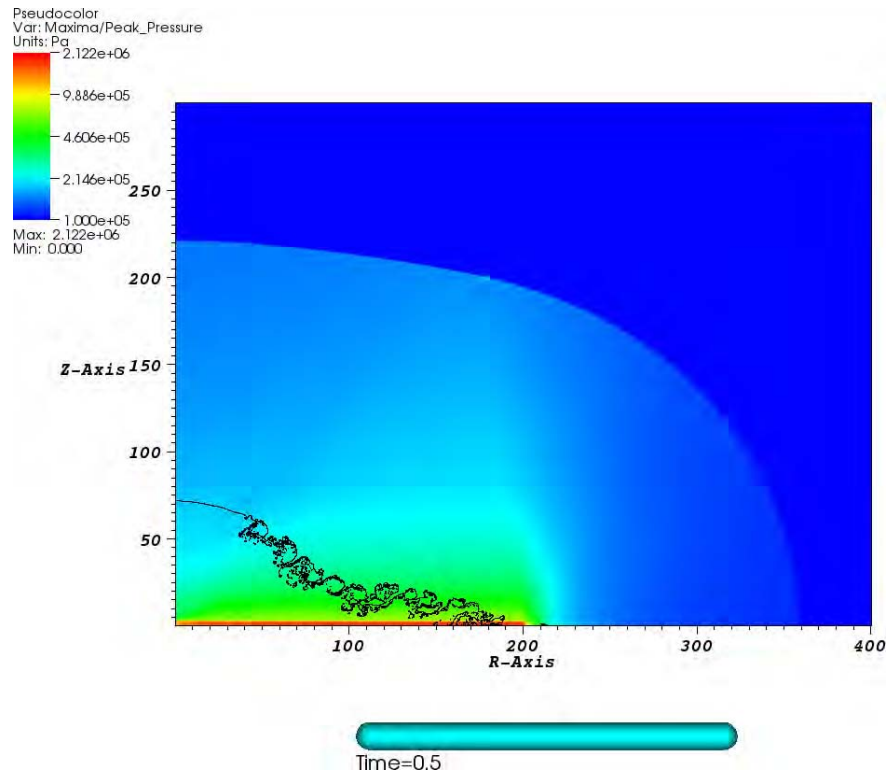
Figure H.11 Contours of Peak Pressure – Scenario 1

It is useful to consider in more detail the fall in peak pressures found as we move beyond the vapour cloud. Figure H.12 plots the peak pressures found in the model at various radii at a height of 1.5 m, the mid height of the cloud. As expected within the cloud the peak pressures found are constant, corresponding to the detonation pressure. Beyond the edge of the vapour cloud, at 200 m, the peak pressures found diminish rapidly. This result implies a highly localised area of damage as a result of a detonation of the vapour cloud. In fact this indicates that the damage area would largely be limited to the area occupied by the vapour cloud.
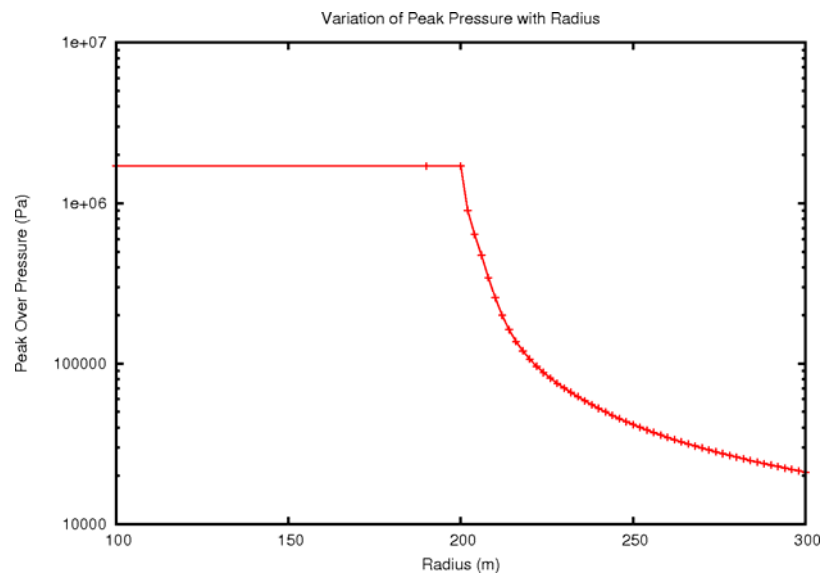
Figure H.12 Peak Pressure Variation with Radius – Scenario 1

Figure H.13 shows the corresponding peak impulse found throughout the model. Here we find that although the impulse found diminishes as we move from the vapour cloud. This decrease with distance however is not as rapid as that seen in the peak pressures.
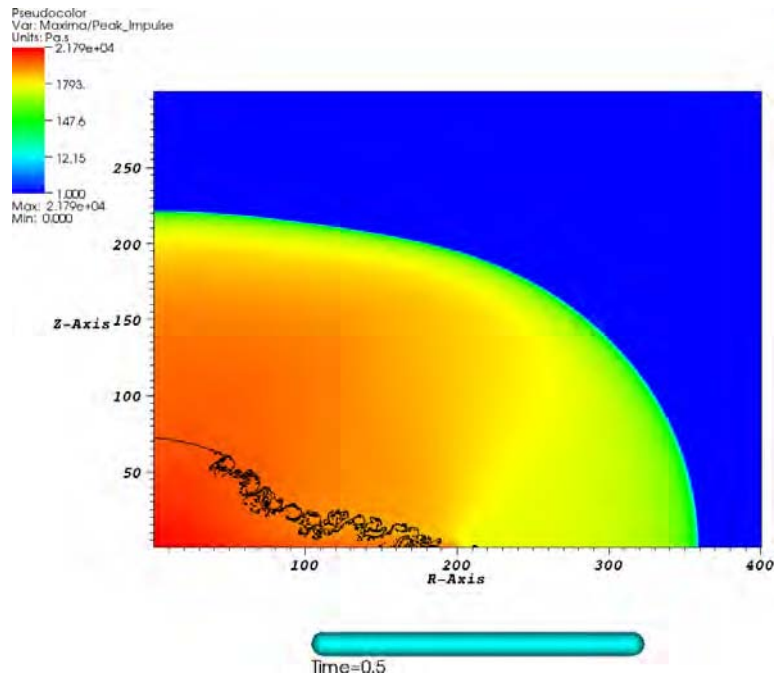
Figure H.13 Contours of Peak Impulse – Scenario 1

Figure H.14 shows the peak dynamic pressures found in the model up to a time of 0.5 s after detonation. Again we see that the high levels of dynamic pressure area are in those areas occupied by the vapour cloud.
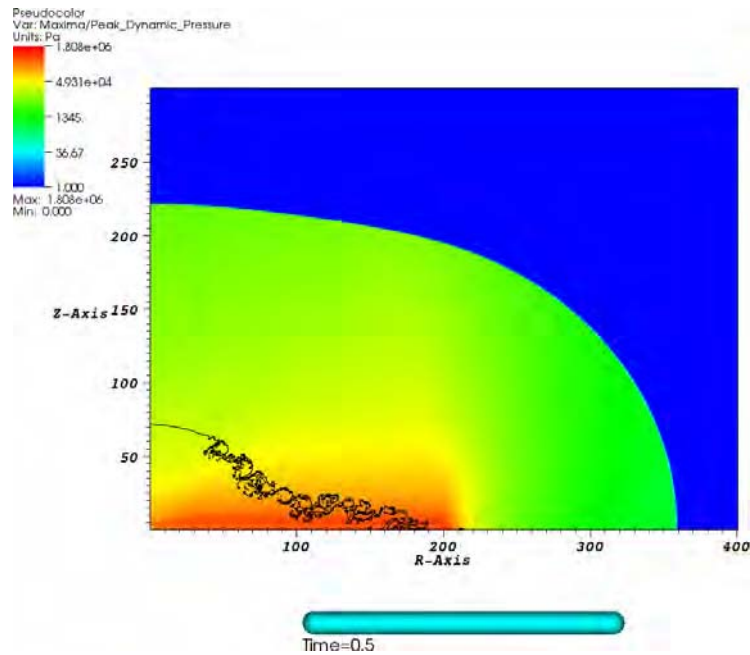
Figure H.14 Contours of Peak Dynamic Pressure – Scenario 1

Finally Figure H.15 shows the peak dynamic pressure impulse found in the model. Again we see that the areas containing high values are largely limited to those close to the original location of the vapour cloud.
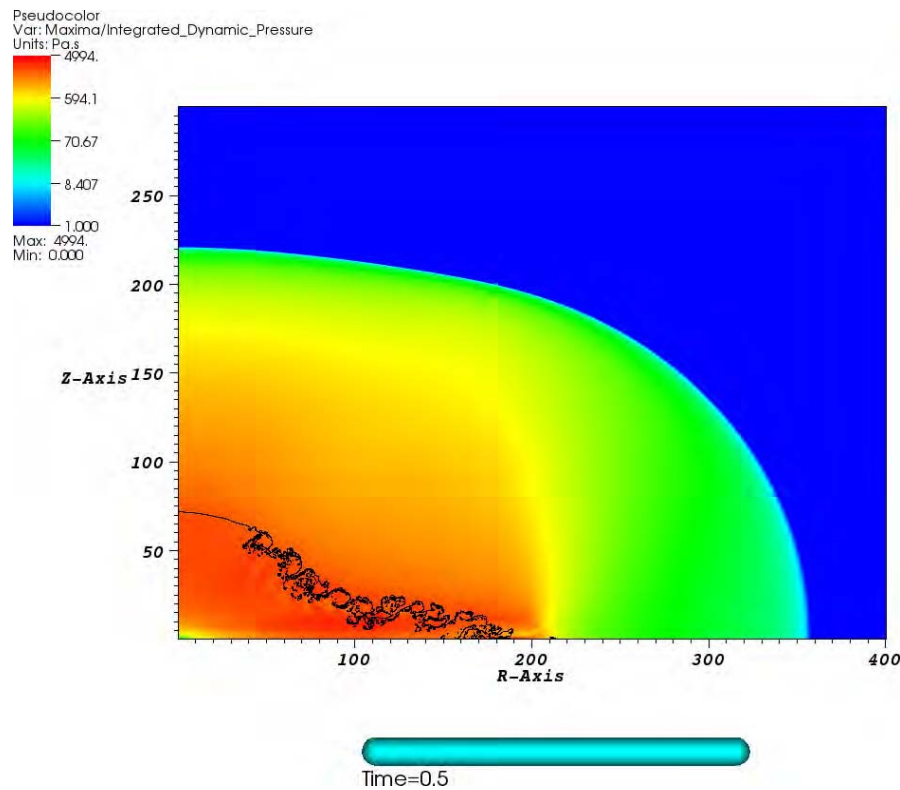
Figure H.15 Contours of Dynamic Impulse – Scenario 1

In this section we have shown the typical behaviour resulting from the detonation of an unobstructed vapour cloud. Within the vapour cloud we have seen that very high loadings will be found. However the levels of loading are found to diminish rapidly as we move away from the original location of the vapour cloud. Within the vapour cloud we also see significant phases of negative radial velocity for a sustained period of time. From discussions with the customer it was noted that this result was significant. As such the time histories recorded in this simulation have been stored on a CD enclosed with this report for further analysis by any interested parties.

H.2.3. Scenario 2 – Obstructed Pancake Cloud

In scenario 2 we perform a simulation of the detonation of a cylindrical propane/air cloud of radius 200 m and height 3 m. Here the cloud will be obstructed by a rigid obstacle (height and width 13 m) positioned as sketched in Figure H.16. Again time histories will be recorded at various locations within the model as shown in the figure.
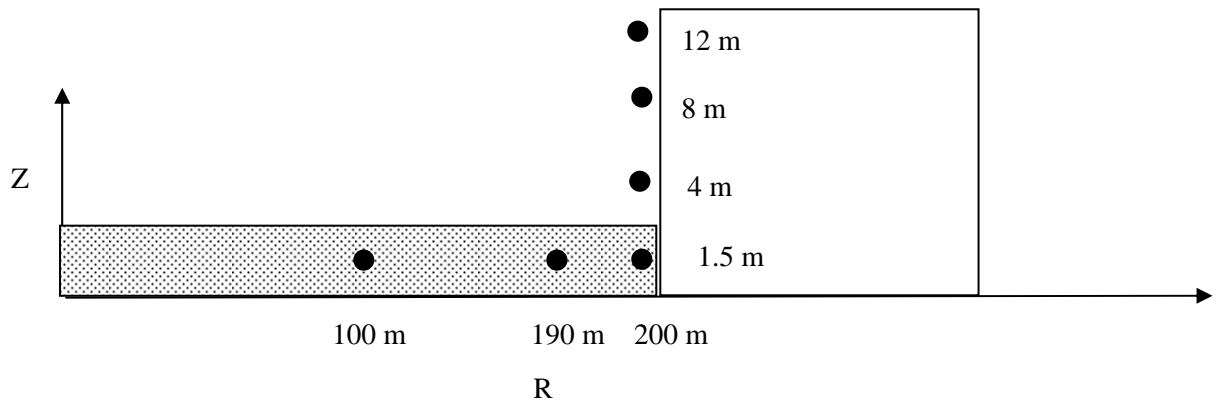
Figure H.16 Scenario 2 Arrangement

The obstacle in this scenario is arranged to be rigid throughout the calculation and is not allowed move. The same propane/air stoichiometric mixture detonation model as used in scenario 1 is employed here. Figure H.17 shows the resulting snapshot 0.15 s after detonation of both the pressure and radial velocity. At this stage the detonation is complete and the pressure wave has reflected from the obstacle. We of course also see the diffraction of the pressure wave over the top of the obstacle. As in scenario 1 within the vapour cloud we see significant areas which are showing a negative radial velocity. We also see the effect of the reflection from the obstacle at approximately 150 m in these figures.
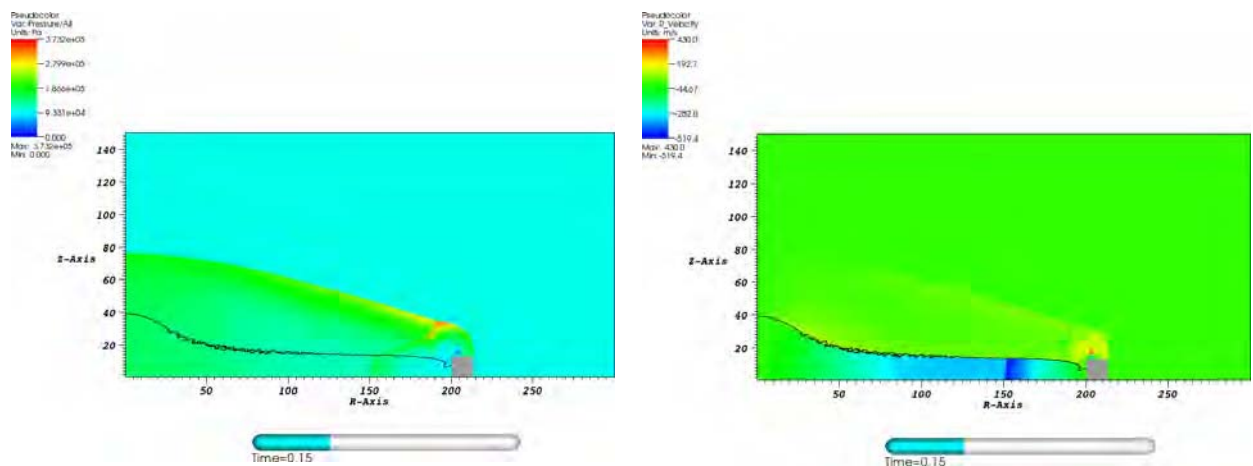
Figure H.17 Pressure and Radial Velocity 0.15 s after Detonation – Scenario 2

As in scenario 1 we plot the radial velocity at 0.15 s highlighting the direction component. In addition to the shock reflection from the obstacle we see significant velocities occurring near the corner of the obstacle. These high velocities here will of course enhance the dynamic pressures at these locations.
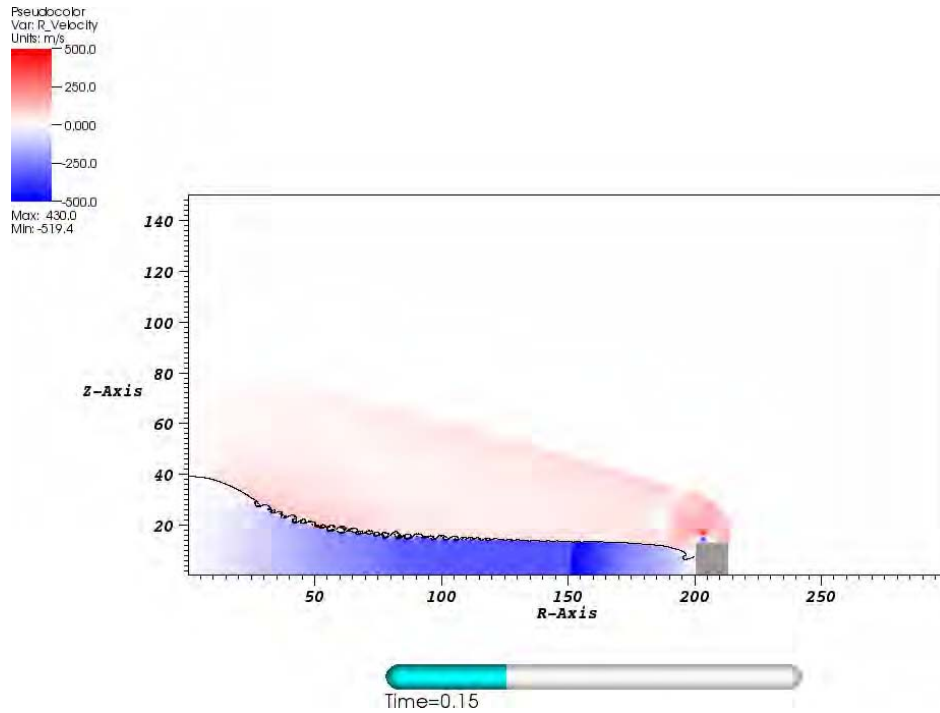
Figure H.18 Radial Velocity Direction – Scenario 2

Figure H.19 plots the time histories of pressure, impulse and radial velocity at a radius of 100 m and a height of 1.5 m. At this location we see very little difference to those found from scenario 1, shown in Figure H.6. The only significant difference occurs at approximately 0.2 s as the reflection from the obstacle passes this point.
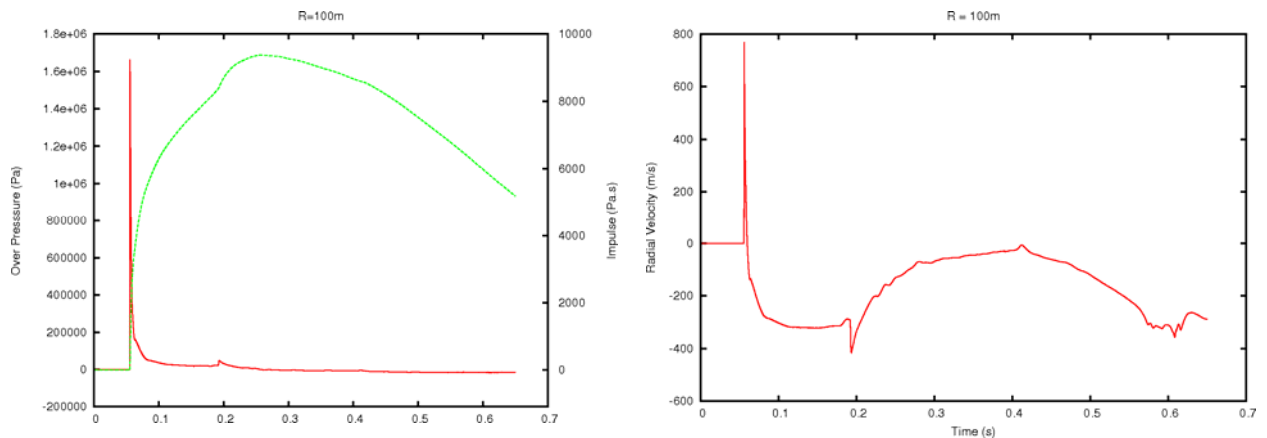

Figure H.19 Pressure/Impulse and Velocity Time Histories at a Radius of 100 m – Scenario 2

For this scenario the main aim is to calculate the loads experienced by the obstacle as a result of the detonation. As such Figure H.20 shows the pressure time histories at various heights on the face of the obstacle. Here we see that at a height of 1.5 (within the vapour cloud) the peak pressure found is approximately double the detonation pressure, as one would expect from a reflection from a solid obstacle as used in this simulation. As we move up the obstacle the pressures diminish quickly as we move outside the original vapour cloud as seen in scenario 1.
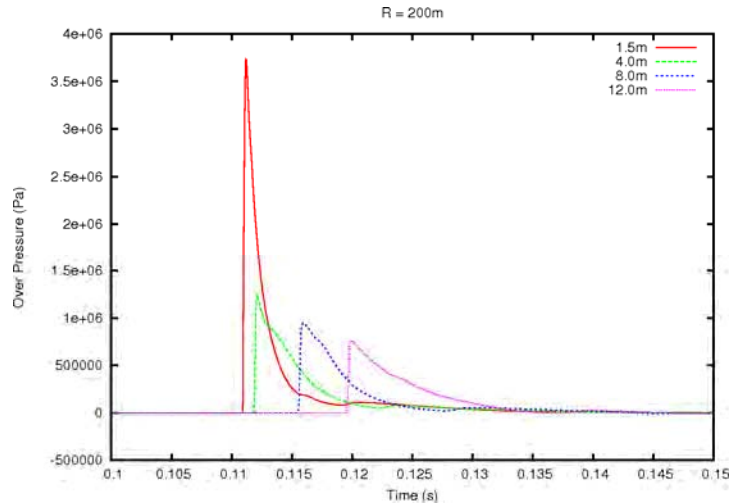
Figure H.20 Pressure Time Histories on Obstacle

An important result when considering the effect of a blast on an obstacle is the impulse loading experienced by the obstacle. Figure H.21 shows the impulse recorded at various heights on the obstacle. During this study it became clear that a corresponding structural analysis on the obstacle was to be performed (by Weidlinger Associates Ltd.) using the results of this simulation. We have performed many similar types of analysis with Weidlinger which indicated that many more measuring locations would be required. Conversations with Weidlinger have indicated that only simple models are being used at this stage. As such the results from this calculation should be sufficient for their needs. More detailed structural modelling would require a more complete set of loading curves from a more detailed model.
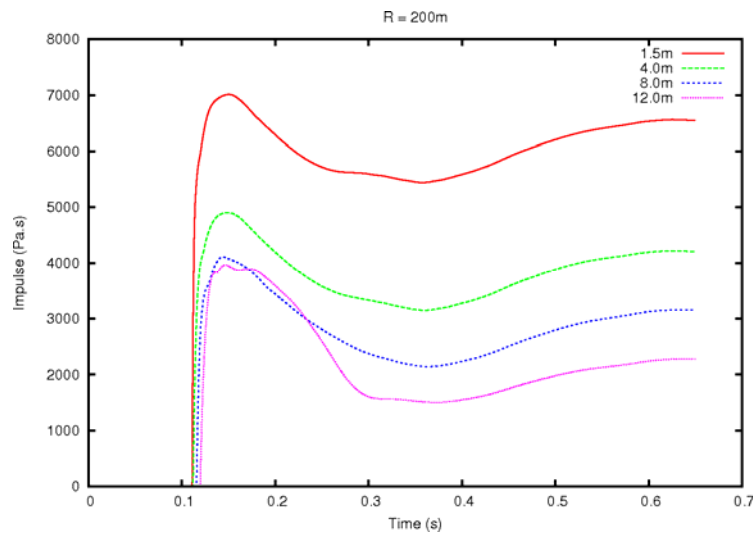
Figure H.21 Impulse Time Histories on Obstacle

Figure H.22 shows the peak pressure contours found throughout the computational domain. Here we see a similar rapid fall in peak pressures out with the vapour cloud as found in scenario 1. Figure H.23 looks at the peak pressures found around the rigid obstacle. The reflection from the obstacle enhances the peak pressures found close to the obstacle as one would expect. Conversely loadings found behind the obstacle are naturally lower than in the unobstructed scenario.

171
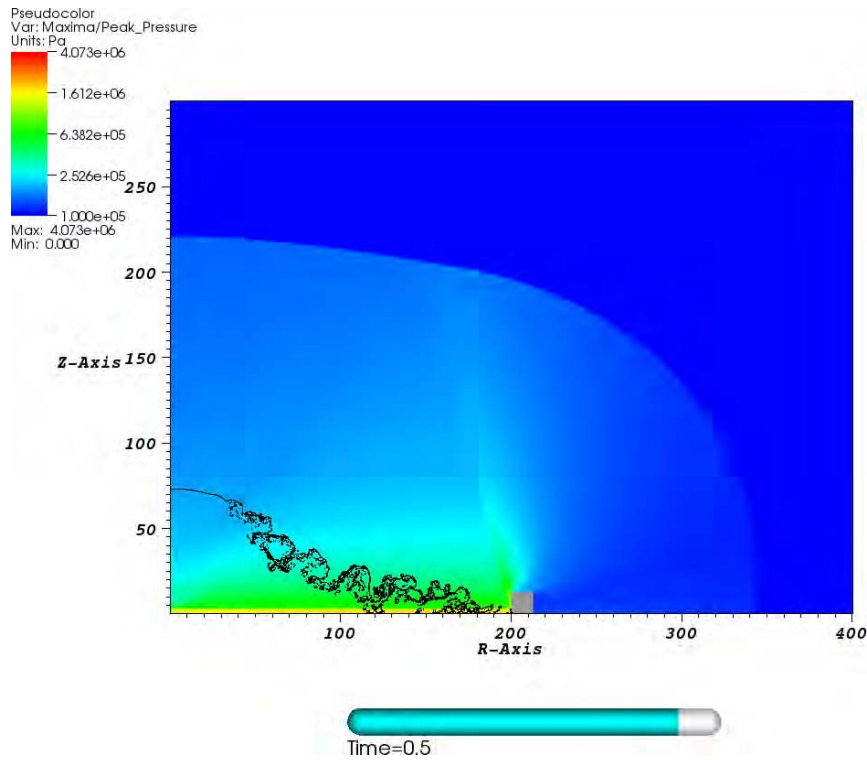
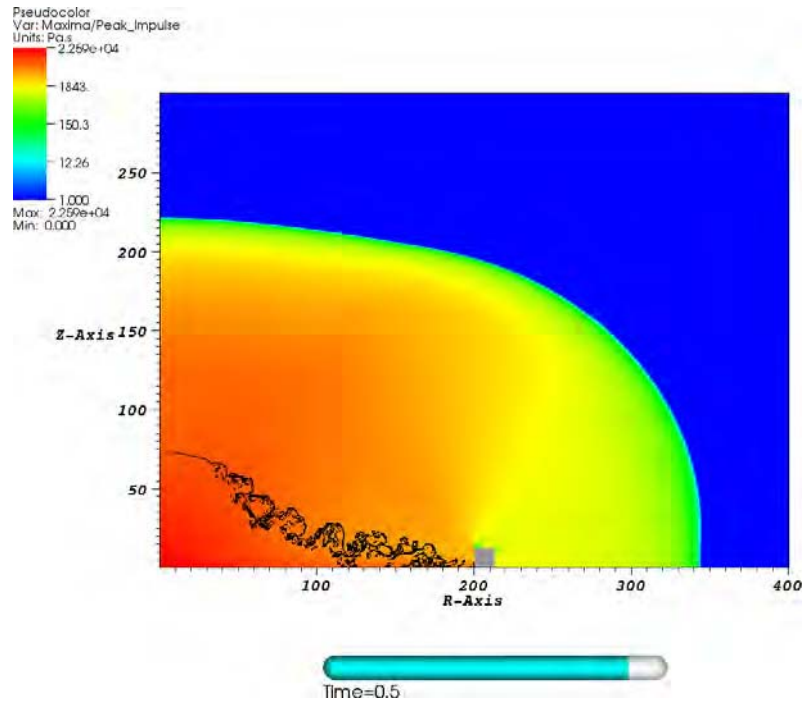**Figure H.22** Contours of Peak Pressure – Scenario 2
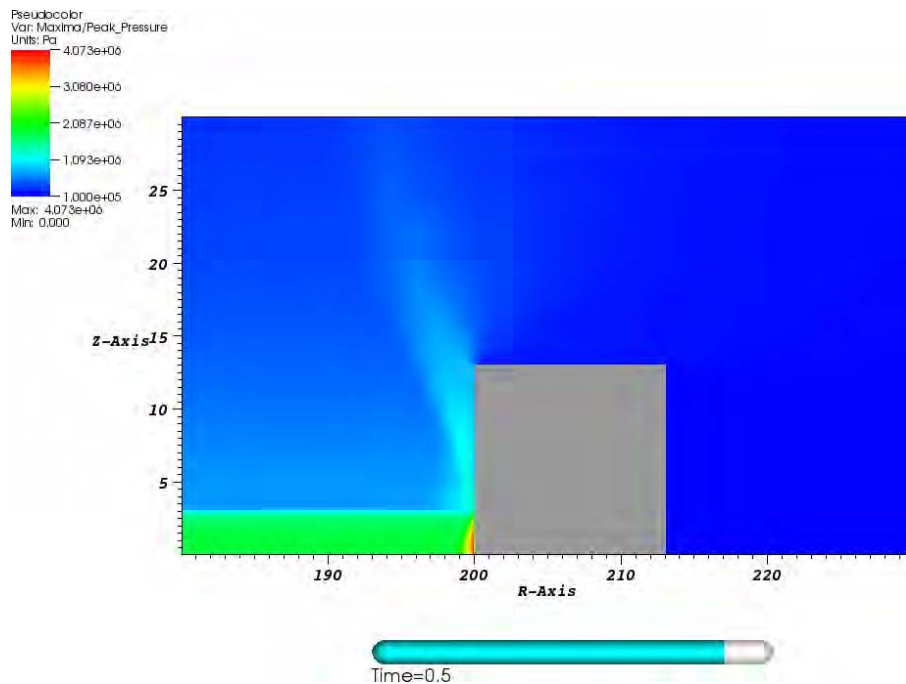
Figure H.23 Contours of Peak Pressure Close to Obstacle – Scenario 2

These figures clearly show the complex flow resulting from the interaction of the detonating cloud with the obstacle. What looks like an oblique rearward facing shock originating from near the base of the obstacle can clearly be seen. This requires some extra discussion. When we plot contours of peaks we lose information regarding the timing of the event. The feature is in fact the locus of a triple point associated with the wave reflection. This can be seen in Figure H.24 below which shows the evolution of the wave interactions in terms of Mach number contours.
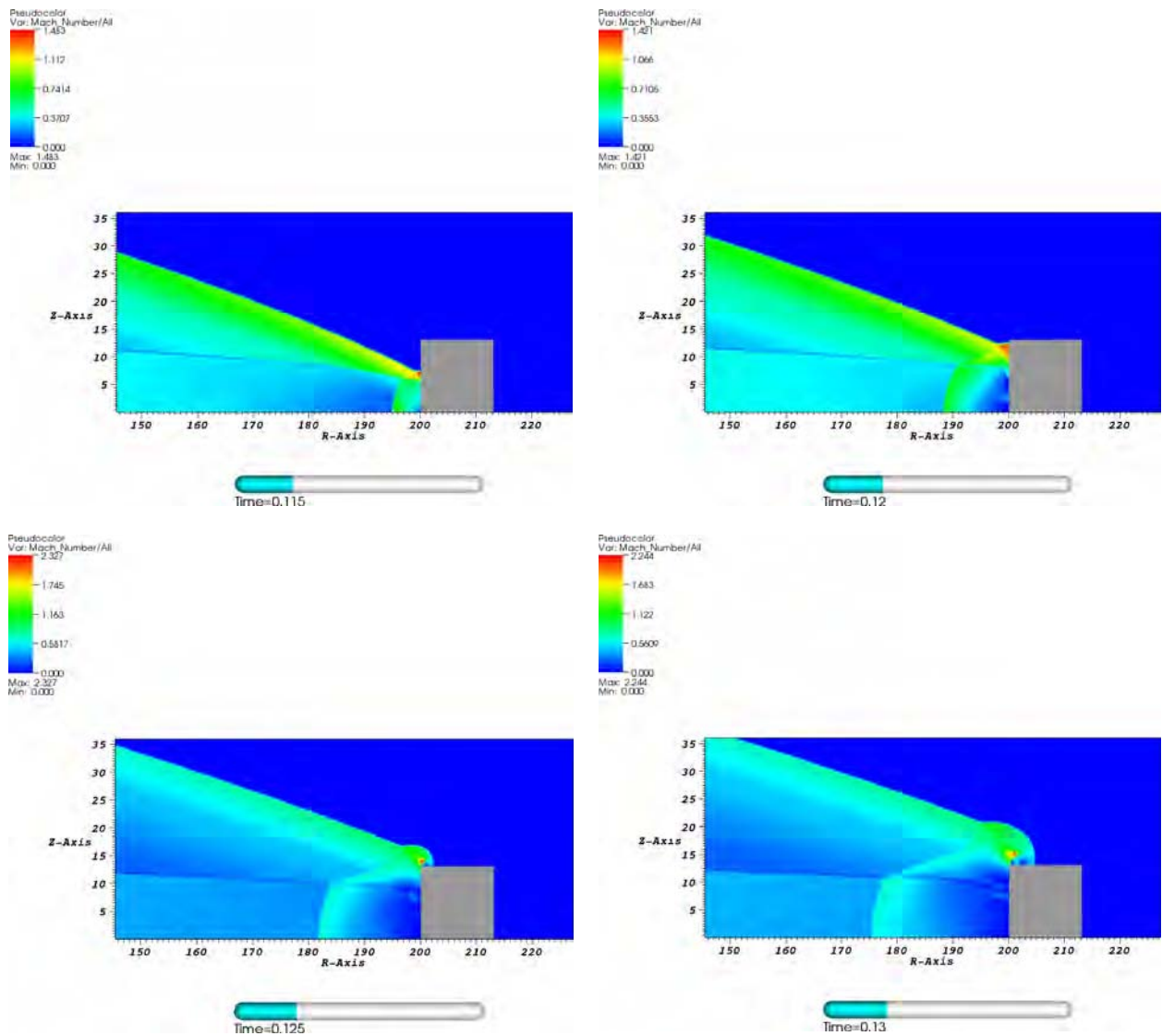
Figure H.24 Contours of Mach Number – Scenario 2

Figure H.25 shows the peak impulse contours found throughout the computational domain. As in scenario 1 we find that although the impulse recorded diminishes as we move away from the vapour cloud although the fall is not as rapid as that seen in the peak pressures.
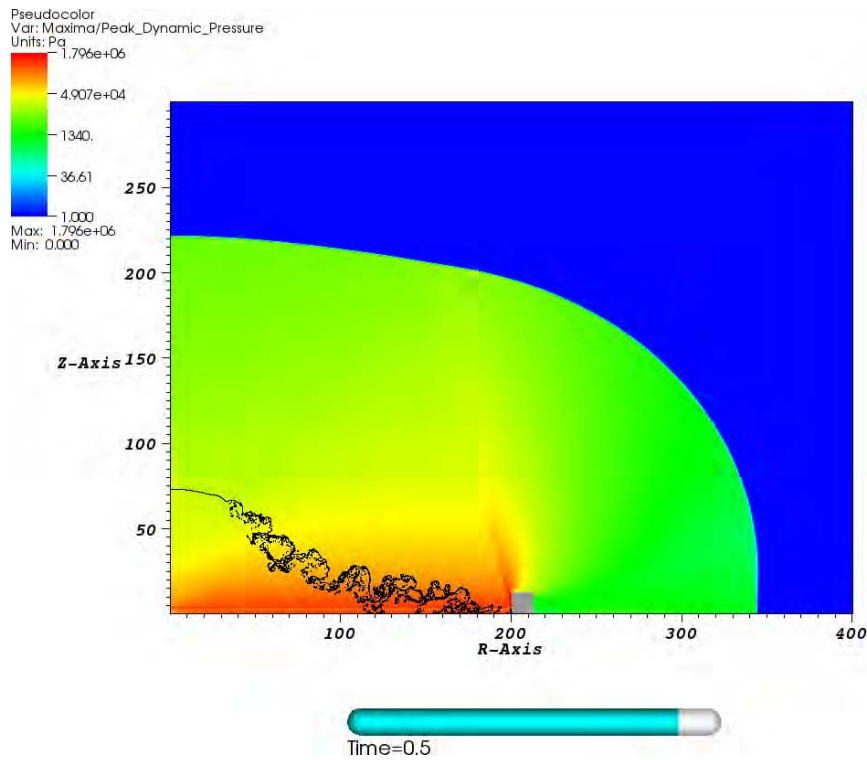
Figure H.25 Contours of Peak Impulse – Scenario 2

Figure H.26 plots the dynamic pressure and impulse at a radius of 100 m. As expected we see very little difference to the result found from scenario 1 at this location.
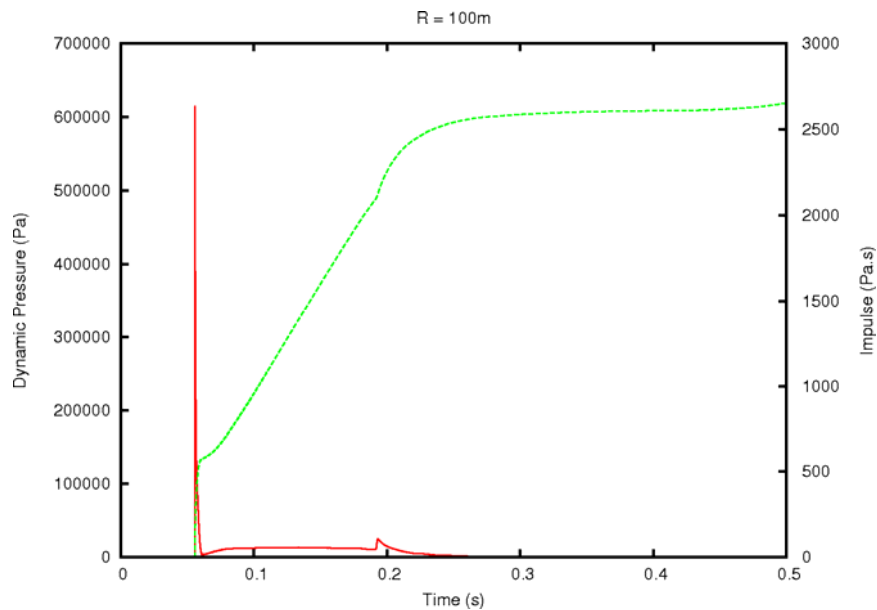
Figure H.26 Dynamic Pressure and Impulse Time Histories at a Radius of 100 m – Scenario 2

We next consider the dynamic pressures experienced throughout the model. Figure H.27 shows the contours of peak dynamic pressures found through the model up to 0.5 s after detonation. Once again we clearly see the rearward facing feature associated with the obstacle. It is important to note that the associated triple-shock forces the flow to be vertical near to the obstacle as opposed to being predominantly horizontal in or near the cloud.

Figure H.27 Contours of Peak Dynamic Pressure – Scenario 2

Figure H.28 shows the integrated dynamic pressure (the impulse) located in the model. Here we see that as expected high velocities around the corner of the obstacle serves to increase the loadings found here.
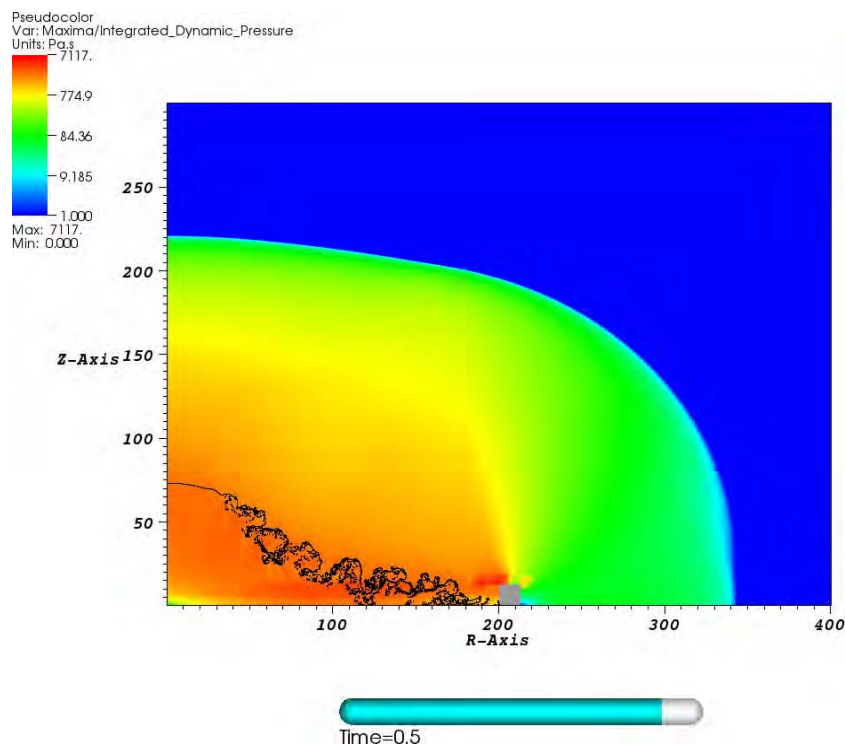

Figure H.28 Contours of Dynamic Impulse – Scenario 2

175

Figure H.29 plots the dynamic pressure recorded on the face of the obstacle at various heights. As noted above, this is due to vertical flow near the obstacle since the normal component of the flow is zero at this boundary. Here we see that close to the base of the obstacle the peak dynamic pressure is significantly lower than at locations higher up the obstacle. At the base of the obstacle the fluid flow understandably stagnates in the corner resulting in these lower dynamic pressures. Higher on the obstacle the rapidly expanding detonation products lead to higher velocities here resulting in the higher peak dynamic pressures found.
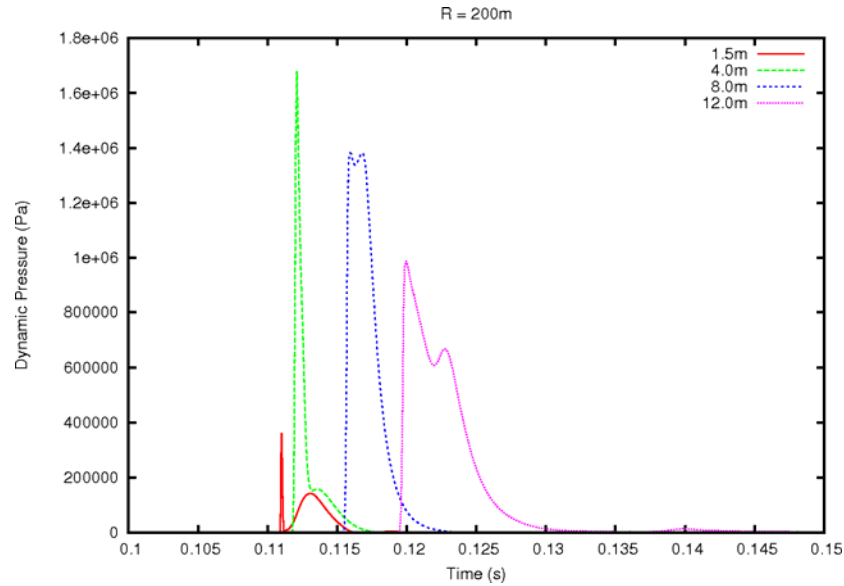

Figure H.29 Dynamic Pressure Time Histories on Obstacle

Figure H.30 shows the integral of these dynamic pressure time histories on the face of the obstacle. Here we see that the impulse found increases significantly as we move higher up the obstacle.
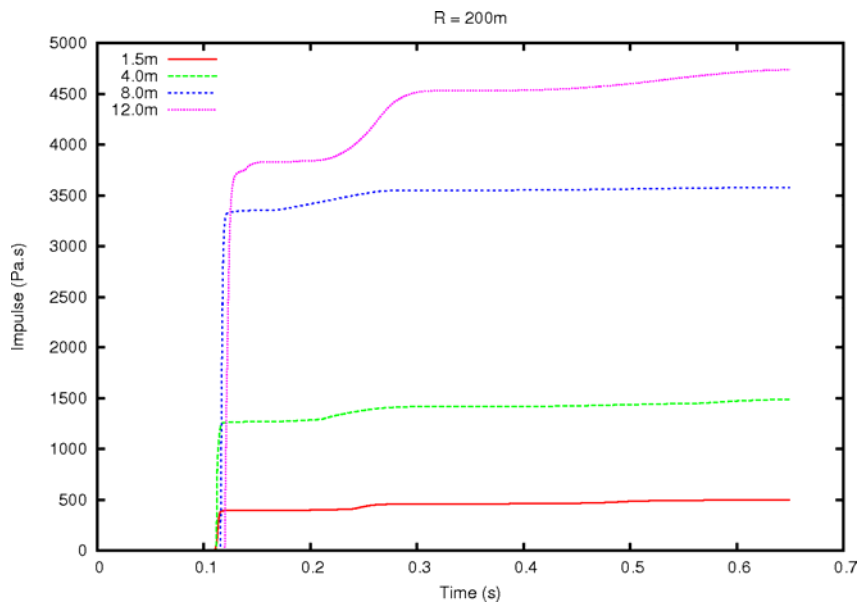

Figure H.30 Dynamic Pressure Impulse Time Histories on Obstacle

Figure H.31 plots the peak dynamic pressures found around the obstacle. Here we see that the highest values are found immediately above the original location of the vapour cloud (3 m) close to the obstacle. At this location the expanding gases are forced along the face of the rigid obstacle resulting in higher velocities and the corresponding dynamic pressures.
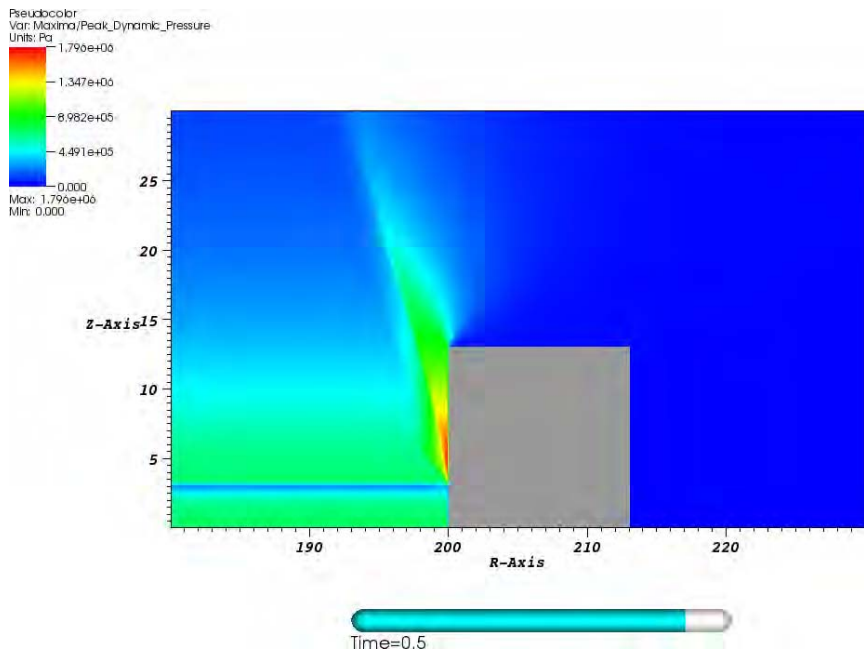
Figure H.31 Contours of Peak Dynamic Pressure – Scenario 2

Figure H.32 shows the corresponding integral of the dynamic pressure at points close to the obstacle. Here we see that continuing velocities around the edges of the obstacle lead to high levels of dynamic impulse. At the base of the obstacle we see significantly lower levels of dynamic impulse due to the stagnating fluid flows in this area.
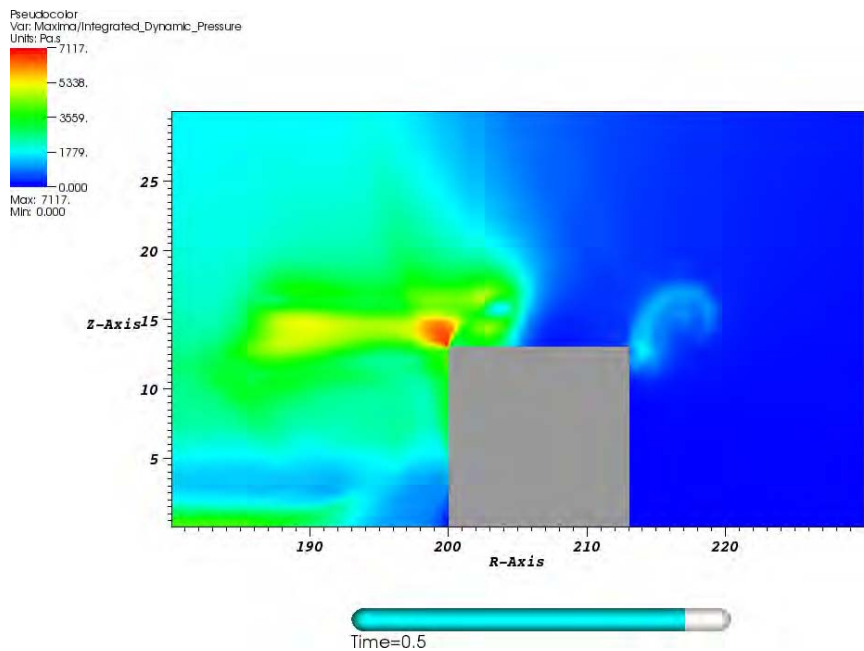
Figure H.32 Contours of Dynamic Impulse – Scenario 2

In the obstructed pancake vapour cloud detonation considered in this section we have seen that at locations some distance from the obstacle the loadings found are very similar to those found in scenario 1. Close to the obstacle however the pressure loadings have been found to be significantly higher than those in the unobstructed scenario as one would expect. Close to the base of the obstacle however dynamic pressures have are significantly reduced with a corresponding increase found higher up the obstacle.

A wide range of variables have been recorded at each of the locations highlighted in Figure H.16.

H.3. DISCUSSION

In this report we have considered the resulting conditions found following the detonation of a stoichiometric Propane/Air vapour cloud as a generic example potentially relevant to the Buncefield explosion. An initial calculation of an unobstructed pancake cloud showed that significant negative radial velocity phases occur within the vapour cloud. This negative velocity phase results in significant levels of sustained dynamic pressure. The resulting integral of the dynamic pressure is considerably enhanced by this phase of the fluid flow. These dynamic pressure predictions can, in principle, be used to estimate the deflection of small obstacles responding to this flowfield.

A subsequent simulation placed a rigid 13×13 m obstacle at the end of the vapour cloud. Here we found that pressure loadings were significantly enhanced on the face of the obstacle. For resolved objects within the model it is these pressures which need to be used to predict deformation. For completeness we also report dynamic pressures in this scenario. Care should be taken in interpreting their relevance in loading studies. For rigid obstacles they do not provide a load but if significant deformation occurs at the time of high flow speed this will influence the development of the deformation. The lower velocities at the base of the obstacle results in much reduced levels of dynamic loading below 5 m. Above this point we see that the dynamic loading increases to similar levels as those seen within the unobstructed vapour cloud.

Buncefield Explosion Mechanism Phase 1

Volumes 1 and 2

The Buncefield explosion (11 December 2005) resulted in tremendous damage to the outlying area and huge fires involving 23 large oil fuel tanks. One important aspect of the incident was the severity of the explosion, which would not have been anticipated in any major hazard assessment of the oil storage depot before the incident. The Buncefield Major Incident Investigation Board (MIIB) invited explosion experts from academia and industry to form an Advisory Group to advise on the work that would be required to explain the severity of the Buncefield explosion. This MIIB Advisory Group carried out a preliminary assessment of the forensic evidence obtained following the incident and of the results of experiments carried out by the Health and Safety Laboratory – HSL. The objectives of this assessment were:

- to determine whether a sequence of events could be identified that would explain why such severe explosion pressures were generated; and
- if this was not possible, to recommend to the Board what further actions would be required to explain the explosion severity.

The Advisory Group attempted to explain the explosion event at Buncefield using deflagration, detonation or a combination of both. It also examined other possible means of flame acceleration. However, it was not possible to identify a single scenario that could explain all aspects within the time available.The Advisory Group therefore recommended that a joint industry research project be initiated that would, in its first phase, have the objectives of completing the assessment started by the Advisory Group and, on the basis of this, of defining the requirements for further research. The research undertaken, both experimental and theoretical, and has lead to a better understanding of likely explosion mechanisms and explanation of the observed damage.

Environment and Spatial Planning
Ministry of Housing, Spatial Planning and the Environment

StatoilHydro

UKpia

energy INSTITUTE

RR718

www.hse.gov.uk